CANARIUM SCHWEINFURTHII RESIN AS AN ORGANIC BINDER FOR CARBONIZED BRIQUETTES

Kivumbi Bernard

A Dissertation Submitted in Partial Fulfilment of the Requirements for the Degree of Doctor of Philosophy in Sustainable Energy Science and Engineering of the Nelson Mandela African Institution of Science and Technology

Arusha, Tanzania

July, 2022

ABSTRACT

Charcoal is the predominant fuel used in many developing countries for domestic and commercial purposes. Transport and handling of charcoal produces fines amounting to 10-20% by weight. The fines can be turned into lumps of charcoal by briquetting using suitable binders. This study investigated the use of *Canarium Schweinfurthii* resin as a binder for production of carbonized briquettes from charcoal fines. The binder and charcoal fines were characterized through proximate analysis, ultimate analysis, higher heating value (HHV), and SEM. Four briquette samples (B25, B30, B35, and B40) with a ratio of charcoal fines: binder of 3:1, 7:3, 13:7, and 3:2, respectively were produced at a compaction pressure of 5.92-7.96 MPa. The physical properties of briquettes determined were bulk density, impact resistance index (IRI), compressive strength (CS), splitting tensile strength (STS), water resistance index (WRI), and morphology. The chemical properties of briquettes determined were proximate analysis, ultimate analysis, HHV, and energy density. The physical properties of briquettes were analysed using Design Expert. One-way ANOVA and Fisher's LSD were used to analyse the chemical properties of briquettes. The phases of the Water Boiling Test (WBT) considered were Cold Start High Power, Hot Start High Power and Simmer phases. Ignition properties, combustion properties, gas temperature, water temperature, ambient temperature, emissions, and WBT performance metrics were investigated using the Laboratory Emission Monitoring System. The ignition properties included ignition time, flame and incandescence. The combustion properties included smoke, flame, soot, and ash. The emissions measured were $PM_{2.5}$, SO_2, NO_x, C_xH_y, CO, and CO_2. The WBT performance metrics evaluated were time to boil, burning rate, thermal efficiency, specific fuel consumption, firepower, total emissions, specific emissions, emissions per MJ, and emissions rate. The ash from charcoal fines was analysed using x-ray diffraction. The briquettes had a bulk density of 0.770-1.036 g/cm^3, IRI of 2.90-73.33, CS of 2.25-10.94 MPa, STS of 0.09-0.42 MPa, WRI of 99.26-99.29, and an HHV of 29.7-31.3 MJ/kg. The ignition time was 6.47-7.01 min, time to boil was 14.7-41.9 min, burning rate was 1.1-8.2 g/min, thermal efficiency was 21.79-54.61%, specific fuel consumption was 21.7-70.1 g/L, and firepower of 535.9-4123.2 W. The ash was found to contain $CaCO_3$ (76.6 wt%), CaO (13.1 wt%) and amorphous compounds (10.3 wt%). Design Expert predicted briquette B40 with the optimum physical properties. The produced briquettes can be used as an alternative source of fuel to wood fuel since they exhibit similar combustion properties.

DECLARATION

I, Kivumbi Bernard do hereby declare to the senate of Nelson Mandela African Institution of Science and Technology that this dissertation is my own original work and that it has neither been submitted nor being concurrently submitted for degree award in any other institution.

Kivumbi Bernard

Name and Signature of the Candidate Date

The above declaration is confirmed by:

Dr. Thomas T. Kivevele

Name and signature of Supervisor 1 Date

Dr. Yusufu A. C. Jande

Name and Signature of Supervisor 2 Date

Prof. John B. Kirabira

Name and Signature of Supervisor 3 Date

COPYRIGHT

CERTIFICATION

The undersigned certify that they have read and hereby recommend for acceptance by the Nelson Mandela African Institution of Science and Technology a dissertation titled "*Canarium Schweinfurthii Resin as an Organic Binder for Carbonized Briquettes*" in Partial Fulfillment of the Requirements for the Degree of Doctor of Philosophy in Sustainable Energy Science and Engineering of the Nelson Mandela African Institution of Science and Technology.

Dr. Thomas T. Kivevele

Name and signature of Supervisor 1 Date

Dr. Yusufu A. C. Jande

Name and Signature of Supervisor 2 Date

Prof. John B. Kirabira

Name and Signature of Supervisor 3 Date

ACKNOWLEDGEMENTS

I am indebted to Wise-Futures centre for giving me the scholarship opportunity to pursue PhD studies in Sustainable Energy Science and Engineering at the Nelson Mandela African Institution of Science and Technology, NM-AIST, Arusha Tanzania. I am grateful to Gulu University for granting me the study-leave to pursue PhD studies.

I wish to extend my heartfelt thanks to my supervisors Dr. Thomas T. Kivevele, Dr. Yusufu Abeid Chande Jande, and Prof. John Baptist Kirabira for their generous guidance and support towards the success of this research. Their intellectual positive criticism of the research contributed to its enormous improvement throughout its course.

I extend my sincere gratitude to all the technicians at the laboratories of NM-AIST, Arusha Technical College (Arusha, Tanzania), College of Engineering, Design, Art and Technology, Makerere University (Kampala, Uganda) and Centre for Research in Energy and Energy Conservation (CREEC), Makerere University for the technical support towards the success of this research.

I am indebted to my father, Mr. Paul Ssonko (RIP) and my ailing mother, Miss Teddy Nalubega for nurturing me to become who I am today. May his soul rest in eternal peace and may the Almighty continue to protect her. Also, special thanks to my dear wife, Jackline Auma for the moral support and looking after the family diligently during the times I was busy with studies in Arusha, Tanzania.

I also appreciate the academic staff at NM-AIST for the knowledge they imparted unto me and nonteaching staff at NM-AIST that made the smooth running of the research possible. I am grateful to my masters and PhD colleagues, workmates, relatives and friends for the moral support and sharing of ideas that led to the success of the research.
May the Almighty reward you abundantly.

DEDICATION

To my father, Mr. Paul Ssonko (RIP) and my ailing mother, Miss Teddy Nalubega. Also to my dear wife, Jackline Auma , and my two children: Andrea Maria Nakirijja and Adonai Paul Ssonko.

TABLE OF CONTENTS

LIST OF TABLES

LIST OF FIGURES

LIST OF APPENDICES

LIST OFABBREVIATIONAND SYMBOLS

Δt_c	Time to Boil
Δt_c^T	Temperature Corrected Time to Boil
Δt_h^T	Temperature Corrected Time to Boil
CB_c	Hood Carbon Balance
CB_h	Hood Carbon Balance
CB_s	Hood Carbon Balance
C_c	Mass of Char With Dish After Test
CE_c	Total Carbon in Exhaust
CC_c	Exhaust Carbon Concentration
CC_h	Exhaust Carbon Concentration
CC_s	Exhaust Carbon Concentration
C_h	Mass of Char With Dish After Test
CE_h	Total Carbon in Exhaust
C_s	Mass of Charcoal and Container After Test
CE_s	Time at Start of Simmer Phase
C_s	Total Carbon in Exhaust
$E_{CO_{2c}}$	CO_2 Emission Per Water Boiled
$E_{CO_{2h}}$	CO_2 Emission Per Water Boiled
$E_{CO_{2s}}$	CO_2 Emission Per Water Simmered
E_{CO_c}	CO Emission Per Water Boiled
E_{CO_h}	CO Emission Per Water Boiled
E_{CO_s}	CO Emission Per Water Simmered
$EF_{CO_{2c}}$	CO_2 Emission Factor
$EF_{CO_{2h}}$	CO_2 Emission Factor
$EF_{CO_{2s}}$	Co_2 Emission Factor
EF_{CO_c}	CO Emission Factor
EF_{CO_h}	CO Emission Factor
EF_{CO_s}	CO Emission Factor
EF_{PM_c}	PM Emission Factor
EF_{PM_h}	PM Emission Factor

EF_{PM_s}	PM Emission Factor
EF_{PM_s}	PM Emission Factor
E_{PM_c}	PM Emission Per Water Boiled
E_{PM_s}	PM Emission Per Water Simmered
f_{cd}	Equivalent Dry Wood Consumed
f_{ce}	Dry Fuel Consumed Estimated From Emissions
f_{cf}	Mass of Fuel After Test
f_{ci}	Mass of Fuel Before Test
f_{cm}	Fuel Consumed, Moist
f_{hd}	Equivalent Dry Wood Consumed
f_{he}	Dry Fuel Consumed Estimated From Emissions
f_{hf}	Mass of Fuel After Test
f_{hi}	Mass of Fuel Before Test
f_{hm}	Fuel Consumed, Moist
FP_c	Firepower
FP_h	Firepower
FP_s	Firepower
f_{sd}	Equivalent Dry Wood Consumed
f_{se}	Dry Fuel Consumed Estimated from Emissions
$T1_{si}$	Starting Water Temperature ($T1_{si} = T1_{hf}$)
t_{si}	Time at End of Simmer Phase
f_{sf}	Mass of Unburned Fuel Remaining After Test
f_{sm}	Fuel Consumed, Moist
h_c	Thermal Efficiency
h_h	Thermal Efficiency
h_s	Thermal Efficiency
$m_{CO_{2c}}$	Co_2 Mass Produced
$m_{CO_{2h}}$	CO_2 Mass Produced
$m_{CO_{2s}}$	Co_2 Mass Produced
m_{CO_c}	Co Mass Produced
m_{CO_h}	CO Mass Produced
m_{CO_s}	CO Mass Produced

m_{PM_c}	PM Mass Produced
m_{PM_h}	PM Mass Produced
m_{PM_s}	PM Mass Produced
N_2O	Dinitrogen Oxide
$P1_{cf}$	Mass of Pot with Water After Test
$P1_{ci}$	Mass of Pot with Water Before Test
$P1_{hf}$	Mass of Pot with Water After Test
$P1_{hi}$	Mass of Pot with Water Before Test
$P1_{sf}$	Mass of Pot with Water After Test
$P1_{sf}$	Mass of Charcoal and Container After Test
$P1_{si}$	Starting Mass of Pot with Water before Test
P_{atm}	Atmospheric Pressure
r_{cb}	Burning Rate
r_{hb}	Burning Rate
r_{sb}	Burning Rate
SC_c	Specific Fuel Consumption
SC_c^T	Temperature-Corrected Specific Fuel Consumption
SC_h	Specific Fuel Consumption
SC_h^T	Temperature-Corrected Specific Fuel Consumption
SC_s	Specific Fuel Consumption
SE_c^T	Temperature-Corrected Specific Energy Consumption
SE_h^T	Temperature-Corrected Specific Energy Consumption
SE_s	Specific Energy Consumption
$T1_{cf}$	Water Temperature at End of Test
$T1_{ci}$	Water Temperature at Start of Test
$T1_{hf}$	Water Temperature at End of Test
$T1_{hi}$	Water Temperature at Start of Test
$T1_{sf}$	Water Temperature at End of Test
$T1_{si}$	Water Temperature at Start of Test
$T1_{si}$	Water Temperature at End of Test
T_a	Ambient Temperature
T_b	Local Boiling Point of Water

T_{cd}	Average duct temperature
t_{cf}	Time at End of Test
t_{ci}	Time at Start of Test
T_{hd}	Average Duct Temperature
t_{hf}	Time at End of Test
t_{hi}	Time at Start of Test
T_{sd}	Average Duct Temperature
t_{si}	Mass of Unburned Fuel Remaining After Test
V_c	Total Exhaust Flow
V_h	Total Exhaust Flow
V_s	Total Exhaust Flow
w_{cr}	Effective Mass of Water Boiled
w_{cv}	Water Vaporized
w_{hr}	Effective Mass of Water Boiled
w_{hv}	Water Vaporized
w_{sr}	Effective Mass of Water Simmered
w_{sv}	Water Vaporized
ΔC_c	Change in Char During Test
ΔC_h	Change in Char During Test
ΔC_s	Change in Char During Test
Δt_c	Time to Boil
Δt_h	Time to Boil
Δt_s	Time to Boil
ANOVA	Analysis of Variance
ASTM	American Society for Testing and Materials
AVG	Average
C	Carbon
CO_2	Carbon Dioxide
CO_{2b}	Background CO_2 Concentration
CO_{2c}	Average CO_2 concentration
CO_{2h}	Average CO_2 Concentration
CO_{2s}	Average CO_2 Concentration

CO_b	Background CO Concentration
CO_c	Average CO concentration
CO_h	Average CO concentration
CO_s	Average CO Concentration
CharFracC	Char Carbon Fraction
CO	Carbon Monoxide
CREEC	Centre for Research in Energy and Energy Conservation
CSHP	Cold Start High Power
Diff	Difference
DTG	Differential Thermogravimetric
EHV	Effective Calorific Value
FC	Fixed Carbon
FuelFracC	Fuel Carbon Fraction
GHGs	Greenhouse Gases
H	Hydrogen
HHV	higher heating value
HSHP	Hot Start High Power
Int	Intensity
IRI	Impact Resistance Index
IWA	International Workshop Agreement
k	Mass of Charcoal Container
LCL	Lower Critical Limit
LEMS	Laboratory Emission Monitroing System
LHV_{char}	Lower Heating Value of char
LHV	Lower Heating Value
LHV	Lower heating value
LSD	Least Significance Difference
MC_{wet}	Moisture Content (wet basis)
MC	Moisture Content
Mtoe	Mega Tonnes of Oil Equivalent
N	Nitrogen
NO_2	Nitrogen Dioxide
NO_x	Nitrogen oxides

NO	Nitrogen monoxide
O	Oxygen
PM_b	Background particulate matter concentration
PM_c	Average Particulate Matter Concentration
PM_h	Average PM concentration
PM_s	Average PM Concentration
P1	Dry mass of empty pot
PEMS	Portable Emission Monitoring System
PM	Particulate Matter
Prob	Probability
PVA	polyvinyl acetate
Q	Hood flow rate
S	Sulphur
SO_2	Sulphur Dioxide
SO_3	Sulphur Trioxide
SE	Square Error
SEM	Scanning Electron Microscopy
STD	Standard Deviation
TDR	Turn Down Ratio
TG	Thermogravimetric
UCL	Upper Critical Limit
VM	Volatile Matter
WBT	Water Boiling Test
WHO	World Health Organization
WRI	Water Resistance Index
XRD/XRF	X-Ray Diffraction/X-Ray Fluorescence

CHAPTER ONE

INTRODUCTION

1.1 Background of the Problem

Biomass follows coal and oil as the world's third largest energy source. Biomass continues to meet a major fraction of the energy demand in rural areas of most developing countries and its potential is estimated at 1250 Mtoe of primary energy. This is about 14% of the world's annual energy consumption (Sugumaran & Seshadri, 2010). A number of countries in the world are implementing policies towards decreasing greenhouse gas emissions, to secure and diversify the supply of energy (Heinimö & Junginger, 2009).

Charcoal is the predominant fuel used in many developing countries for domestic and commercial purposes. Transport and handling of charcoal produces fines about to 10-20% by weight (Rousset *et al.,* 2011). Charcoal fines are also obtained from the production of charcoal from sustainably managed planted eucalyptus forests or from the steel industry, a major consumer of charcoal (Rousset *et al*., 2011). The fines can be turned into lumps of charcoal by briquetting using suitable binders. Biochar from pyrolysis of biomass waste can also be used in production of briquettes (Fadhil, 2020). For transport, handling, and storage, briquettes with high density and mechanical strength are prefered. High density reduces transport and storage costs while high compressive strength, i.e. >2.56 MPa prevents breakages (Okot *et al*., 2018).

Oleoresins are complex mixtures of acidic and neutral diterpenes together with a more or less important fraction of volatile compounds (monoterpenes and sesquiterpenes). Industrial processing by steam distillation converts the crude oleoresin into gum turpentine (volatile compounds) and gum rosin (diterpenes). Both gums in turn are further processed into chemical industrial products such as food gums, coatings, adhesives, cleaners, printing inks, disinfectants, pharmaceuticals, fragrances and flavouring (Rezzi *et al*., 2005). Diterpene (C_{20}) resin acids are the major components of rosin (da Silva Rodrigues-Correˆa *et al*., 2013). Yadav *et al*. (2014) reported that diterpenoids and triterpenoids are not steam volatile and they are obtained from plants, tree gums and resins. Bhattacharya *et al*. (1989) classified resin under organic binders.

Natural and synthetic resins (e.g. acrylic, phenolic, formaldehyde) (Drobíková *et al*., 2015) have been used in several studies for production of briquettes. Thoms *et al*. (1999) studied physical characteristics of cold cured anthracite/coke breeze briquettes prepared from a coal tar acid resin. Briquettes with excellent properties such as mechanical strength, thermal degradation, and water-proofing characteristics were produced. Benk (2010) studied briquette binders using air blown coal

tar pitch and phenolic resins as raw materials. The optimum amount of air blown coal tar pitch was 50% w/w in the blended binder. Briquettes cured at 200°C for 2 h had a tensile strength of 50.45 MN/m^2. When the cured briquettes were carbonized at temperatures of 470°C, 670°C and 950°C, their strength increased with temperature up to 71.85 MPa. Sotannde *et al*. (2010) produced charcoal briquettes from neem wood residues using starch and gum arabic (gum extract from *Acacia senegal L*.) as binders. The briquettes were analysed for fixed carbon, volatile matter, ash content and heating value. The results showed that gum arabic bonded briquettes with a blending ratio of charcoal: binder of 10:3 had better physical and combustion qualities than starch bonded briquettes with a blending ratio of charcoal: binder of 5:1.

The *Canarium Schweinfurthii* tree is found throughout tropical Africa in rainforest, gallery forest, and transitional forest from Senegal to Cameroon and extending to Ethiopia, Tanzania and Angola (Kuete, 2017). The essential oil of African Elemi resin from Uganda contains monoterpenes mainly α −phellandrene, α −terpineol, β −linalool, γ −terpinene, p −cymene, sabinene, carvenone and 6-camphenone (Nagawa *et al*., 2015). The terpenoids α −phellandrene, p −cymene, and γ −terpinene are classified under monoterpenoid hydrocarbons while α −terpineol, β − linalool, carvenone, and 6-camphenone are classified under oxygenated monoterpenoids (Šiler & Mišić, 2016). Yousuf *et al*. (2011) isolated 3α-Hydroxytirucalla-8,24-dien-21-oic (epielemadienolic) acid, a triterpene derivative from *Canarium Schweinfurthii* Engl. resin. The GC-MS of *Canarium Schweinfurthii* gum obtained by Ameh (2018) revealed the following phytoconstituents; Stearic acid, 1-penta-decanecarboxylic acid, 2-(hydroxymethyl)-2-nitropropane-1,3-diol, Nonacosane, 1-piperoylpiperidine, dihex-5-en-2-yl phthalate, Stigmasta-5,22-dien-3-ol, 9-octadecenoic acid, methyl ester, and Oleic acid. Thus, this study characterized the charcoal fines, *Canarium Schweinfurthii* resin as an alternative binder and also determined the physical and chemical properties of carbonized briquettes produced from charcoal fines using the resin as binder. The carbonized briquettes were tested on an improved cookstove using the Laboratory Emission Monitoring System (LEMS) to assess their suitability for cooking as well as the resulting emissions.

1.2 Statement of the Problem

Charcoal fines are a byproduct of transport and utilization of charcoal. The charcoal fines can be recycled through production of briquettes using binders. Binders are classified into three groups namely; organic, inorganic, and compound binders. Starch and molasses are the most common organic binders used for briquette production. Starch is used as food while the molasses are used as animal feed and as fermentation sources for ethyl alcohol and other chemicals. The inorganic

binders mainly used for production of briquettes are lime and clay. The inorganic binders have high ash content.

Natural resins e.g., gum arabica and synthetic resins e.g., coal tar pitch, coal tar acid, and phenolic have been used as binders for production of briquettes (Benk, 2010; Sotannde *et al*., 2016; Thoms *et al*., 1999). In Uganda, *Canarium Schweinfurthii* resin is currently used as an incense by the local people and on religious ceremonies (Nagawa *et al*., 2015). *Canarium Schweinfurthii* resin, being a natural resin has potential for application as an organic binder. There is limited information on use of the resin as a binder for briquette production thus, the need to investigate its potential. This study aimed at production of carbonized briquettes using *Canarium Schweinfurthii* resin as binder as well as testing for ignition and emissions resulting from their utilisation.

1.3 Rationale of the Study

Charcoal is the predominant fuel used in many developing countries for domestic and commercial purposes. Transport and handling of charcoal produces fines about to 10-20% by weight (Rousset *et al.,* 2011). Charcoal fines are also obtained from the production of charcoal from sustainably managed planted eucalyptus forests or from the steel industry, a major consumer of charcoal (Rousset *et al*., 2011). The fines can be turned into lumps of charcoal by briquetting using suitable binders. Biochar from pyrolysis of biomass waste can also be used in production of briquettes (Fadhil, 2020). For transport, handling, and storage, briquettes with high density and mechanical strength are prefered. High density reduces transport and storage costs while high compressive strength, i.e. >2.56 MPa prevents breakages (Okot *et al*., 2018). There is limited information on use of the resin as a binder for briquette production thus, the need to investigate its potential. This study aimed at production of carbonized briquettes using Canarium Schweinfurthii resin as binder as well as testing for ignition and emissions resulting from their utilisation

1.4 Research Objectives

1.4.1 General Objective

To evaluate carbonized briquettes produced from charcoal fines using *Canarium Schweinfurthii* resin as binder.

1.4.2 Specific Objectives

The specific objectives of the study were to:

(i) Assess the properties of charcoal fines, and *Canarium Schweinfurthii* resin.

(ii) Investigate the physical and chemical properties of carbonized briquettes produced from charcoal fines using *Canarium Schweinfurthii* resin as a binder.

(iii) Analyse the ignition, combustion and emissions of the produced carbonized briquettes.

1.5 Research Questions

(i) What are the physical and chemical properties of charcoal fines, and binder?

(ii) How does the mixing ratio of charcoal fines and binder as well as compaction pressure affect the performance of the carbonized briquettes?

(iii) What is the ignition and combustion performance of the carbonized briquettes?

(iv) To what extent do the emissions from combustion of carbonized briquettes conform with the standards?

1.6 Significance of the Study

(i) The research provided baseline information on the use of *Canarium Schweinfurthii* resin as a binder for production of carbonized briquettes.

(ii) Analysis of the products of combustion provided information towards safe utilisation of the developed carbonized briquettes.

(iii) Production of briquettes contributes to the economy, in terms of income, tax revenue and employment.

1.7 Delineation of the Study

The research was limited to investigation of *Canarium Schweinfurthii* resin as a binder for production of carbonized briquettes using charcoal fines. Furthermore, the study assessed the emissions resulting from use of carbonized briquettes.

CHAPTER TWO

LITERATURE REVIEW

2.1 Biomass, Biofuels and Bioenergy

Biomass is an organic material which has stored sunlight in the form of chemical energy e.g. herbaceous plant matter, wood, crop and forest residues, and dung. Biofuels are solid, liquid or gaseous fuels produced from biomass. Bioenergy means any usable energy obtained from biofuels (Tilli, 2003). Table 1 shows the proximate analysis (moisture, volatile matter, fixed carbon, ash) of selected biomass (feedstock) and biofuels (carbonized feedstock and briquettes). Table 2 shows the ultimate analysis as well as the higher heating values (HHV) of the feedstock and biofuels. From Table 2, the HHV of the feedstock (uncarbonized) is 12.6-18.89 MJ/kg while the HHV of the feedstook (carbonized) is 14.3-29.10 MJ/kg. Ward *et al*. (2014) produced carbonized briquettes from human waste and reported an HHV of 21-25 MJ/kg. Lubwama and Yiga (2017) reported that high ash content reduces heating value, increases thermal resistance to heat transfer, and leads to generation of slag deposits which requires frequent equipment maintenance.

Table 1: Proximate analysis of selected feedstock and briquettes; FS-UC (feedstock- uncarbonized), FS-C (feedstock-carbonized), B-C (briquettes-carbonized)

Feedstock	Proximate analysis (FS-UC)				Proximate analysis (FS-C)				Proximate analysis (B-C)				Reference
	Moisture (%)	VM (%)	FC (%)	Ash (%)	Moisture (%)	VM (%)	FC (%)	Ash (%)	Moisture (%)	VM (%)	FC (%)	Ash (%)	
Low rank coals (1)	17.6	30.4	34.7	17.3	1.1	10.2	68.7	20	n.a	n.a	n.a	n.a	
Low rank coals (2)	18.4	33.7	38.3	9.6	2	11.8	74.6	11.6	n.a	n.a	n.a	n.a	
Sawdust	9.8	77.7	9.6	2.9	3.8	27.1	60.7	7.9	n.a	n.a	n.a	n.a	Blesa *et al.* (2001)
Straw	9.6	68.3	14.2	7.9	2.9	20.8	60.5	15.8	n.a	n.a	n.a	n.a	
Olive stone	10.2	70.5	17.2	2.1	3.2	19.5	74.1	3.3	n.a	n.a	n.a	n.a	
Almond shell	9.2	70.4	18	2.4	1.2	24.8	72.6	1.4	n.a	n.a	n.a	n.a	
Water hyacinth	n.a	n.a	n.a	n.a	n.a	n.a	n.a	n.a	18.1	47.4	15	19.5	Carnaje *et al.* (2018)
Hazelnut shells	0	72	21	7	n.a	n.a	n.a	n.a	n.a	n.a	n.a	n.a	Haykiri-Acma and Yaman (2010)
Brown seaweed	5	63.3	9.2	22.5	0	21.9	18.3	59.8	n.a	n.a	n.a	n.a	Haykiri-Acma *et al.* (2013)
Groundnut shells	9.2	67.7	19.3	3.8	n.a	n.a	n.a	n.a	6.7-7.3	20-28	48-55	17-22.5	Lubwama and Yiga (2017)
Bagasse	22.5	62.7	12.2	2.5	n.a	n.a	n.a	n.a	6-6.8	32-37	48-52	11-12.5	
Durian peel	n.a	n.a	n.a	n.a	n.a	n.a	n.a	n.a	0.01	3.94	78	18.18	Nuriana *et al.* (2014)
Municipal waste	8.69	69.76	10.78	10.77	n.a	n.a	n.a	n.a	5.88	63.94	15.8	14.39	Prasityousil and

Feedstock	Proximate analysis (FS-UC)				Proximate analysis (FS-C)				Proximate analysis (B-C)				Reference
	Moisture (%)	VM (%)	FC (%)	Ash (%)	Moisture (%)	VM (%)	FC (%)	Ash (%)	Moisture (%)	VM (%)	FC (%)	Ash (%)	
composting													Muenjina (2013)
Sawdust	6.74	67.43	19.71	6.12	n.a	n.a	n.a	n.a	n.a	n.a	n.a	n.a	
Cassava rhizome waste	11.79	59.65	24.43	4.13	7.23	46.39	32.9	13.48	n.a	n.a	n.a	n.a	Sen and Annachhatre (2016)
Sugarcane bagasse fly ash	n.a	n.a	n.a	n.a	30-70	n.a	34	62	9.19	5.464	48.6	34.74	Teixeira *et al.* (2010)
Human waste	n.a	n.a	n.a	n.a	n.a	n.a	49	20	n.a	n.a	n.a	n.a	Ward *et al.* (2014)

n.a-not available, VM (volatile matter), FC (fixed carbon)

Table 2: Ultimate analysis and higher heating value (HHV) of selected feedstock and briquettes; feedstock- uncarbonized (FS-UC), feedstock-carbonized (FS-C), briquettes-carbonized (B-C)

Feedstock	Ultimate analysis (FS-UC)					HHV (FS-UC)	Ultimate analysis (FS-C)					HHV (FS-C)	HHV (B-C)	Reference
	C (%)	H (%)	N (%)	S (%)	O (%)	MJ/kg	C (%)	H (%)	N (%)	S (%)	O (%)	MJ/kg	MJ/kg	
Palm kernel shell	n.a	n.a	n.a	n.a	n.a	n.a	81.4	1.6	1.8	0.16		27.51-28.1		Bazargan *et al.* (2014)
Hazelnut shells	54.8	6.7	1	0.1	37.4	18.89	n.a	n.a	n.a	n.a	n.a	n.a	n.a	Haykiri-Acma and Yaman (2010)
Brown seaweed	42.7	6.5	4.2	1.7	44.6	12.6	84.8	2	4.2	4.8	4.2	14.3	n.a	Haykiri-Acma *et al.* (2013)
Palm empty fruit branches	48.8	6.3	0.7	0.2	36.7	16.38								
Rice husk	n.a	n.a	n.a	n.a	n.a	n.a	35.9-36.6	2.36-2.42	0.41-0.45	0.08-0.16	n.a	18.43-24.16		Jamradloedluk and Wiriyaumpaiwong (2007)
Rice straw	n.a	n.a	n.a	n.a	n.a	n.a	49.4-51.8	3.43-3.64	0.77-0.82	0.17-0.19	n.a	21.37-24.98		
Water hyacinth	n.a	n.a	n.a	n.a	n.a	n.a	23.5-24.2	2.08-2.13	0.70-0.73	0.32-0.38	n.a	17.04-22.04		
Bagasse	n.a	n.a	n.a	n.a	n.a	n.a	65.3-66.4	3.53-3.78	0.35-0.40	0.13-0.22	n.a	22.64-29.10		
Human waste	n.a	n.a	n.a	n.a	n.a	n.a	58.23	6.1	5.19	0.43	10.05	25.57	21-25	Ward *et al.* (2014)

2.2 Fundamental Aspects of Briquetting

2.2.1 Overview

Briquetting is one of the agglomeration/ densification technologies which increases the density of residues for energy production. Briquetting utilizes raw materials such as loose biomass, waste from wood industries, and other combustible waste products (Grover & Mishra, 1996). The diameter of a briquette is 50-80 mm (Tilli, 2003). Prasityousil and Muenjina (2013) produced carbonized briquettes from municipal waste composting char and sawdust char and the cylindrical briquettes had an outside diameter of 3.8 cm, inside diameter of 1.3 cm and height of 15 cm. Teixeira *et al.* (2010) produced carbonized briquettes from sugarcane bagasse fly ash having a diameter of 30 mm. Figure 1 shows the different types of briquettes.

(a) (b) (c) (d)

Figure 1: (a) Carbonized briquettes with a hole at the centre (Suhartini *et al.*, 2011), (b) carbonized honey comb briquette with multiple holes (Ferguson, 2012), (c) carbonized briquette without a hole (Carnaje *et al.*, 2018), (d) uncarbonized straw briquette with a hole at the centre (Ferguson, 2012)

2.2.2 Properties of Solids Important to Densification

According to Grover and Mishra (1996), the properties of solids that are important to densification are:

(i) Flow ability and cohesiveness (binders and lubricants can impart these characteristics for compaction)

(ii) Surface forces (important to agglomeration for strength)

(iii) Particle size (too fine a particle means higher cohesion, causing poor flow)

(iv) Hardness (too hard a particle leads to difficulties in agglomeration)

(v) Adhesiveness

(vi) Particle size distribution (sufficient fines are needed to cement larger particles together for a stronger unit).

2.2.3 Compaction Characteristics of Biomass and their Significance

(i) Particle size

Generally, biomass material of 10-20% powdery component (< 4 mesh) with 6-8 mm size gives the best results. The packing dynamics is improved due to the different size particles which also contributes to high static strength. Fine and powdered particles of size less than 1 mm are not suitable for a screw extruder since they are less dense, more cohesive, non-free flowing entities. (Grover & Mishra, 1996). Bazargan *et al.* (2014) did a study on compaction of palm kernel shell biochars for application as solid fuel and considered the following particle sizes; S_1 >3000 µm, 700 < S_2<3000 µm, 300< S_3<700 µm and S_4<300 µm. The results showed that particle size S_4<300 µm had the highest splitting tensile strength. Blesa *et al.* (2001) did a study on effect of the pyrolysis process on the physicochemical and mechanical properties of smokeless fuel briquettes and the particle size of the pyrolysed materials considered were: coals (0.5–0.25 mm), sawdust (<1 mm), olive stone (<0.83 mm). Prasityousil and Muenjina (2013) produced carbonized briquettes from municipal waste composting char and sawdust char using an ASTM sieve no. 4 (pore size 4.75 mm).

(ii) Moisture

When the feed moisture content is 8-10 %, the briquettes will have 6-8% moisture, will be strong and free of cracks and the briquetting process is smooth. Moreover, water acts as a film type binder by strengthening the bonding in briquettes. For organic and cellular products, water helps in promoting bonding by van der Waals' forces by increasing the true area of contact of the particles (Grover & Mishra, 1996). From Table 1, the moisture content of uncarbonized feedstock is 5-22.5%, carbonized feedstock is 0-70% and for carbonized briquettes is 0.01-18.1%. Teixeira *et al.* (2010) produced carbonized briquettes from sugarcane bagasse fly ash and reported that moisture content of the feedstock was 30-70%. However, the feedstock was passed through a filter press or belt press extruder to reduce the moisture and final drying was done using a gas washer to achieve the recommended moisture content for briquette production.

(iii) Temperature of Biomass

Variation of the temperature of biomass affects the briquette moisture stability, density, and crushing strength. High pressure conditions cause the moisture in the biomass to form steam which

then hydrolyses the lignin and hemicellulose parts of biomass into lower lignin products, molecular carbohydrates, sugar polymers and other derivatives which provide a bonding effect "in situ". The die temperature should be in the range of 280-290°C (Grover & Mishra, 1996). Maize cob briquettes densified between 20-80°C showed that at a temperature of 80°C, the produced briquettes had high density and durability/ mechanical strength (Kpalo *et al.,* 2020a).

(iv) Temperature of the Die

This is important for medium pressure compaction with a heating device and no binder is necessary (Grover & Mishra, 1996). The die temperature facilitates the release of components such as cellulose, lignin, and hemicellulose and the lignin acts as binder (Kpalo *et al.,* 2020a). The screw type briquetting machine can be operated with less power leading to a longer life of the die. Furthermore, the surface of the briquette is partially carbonized/torrefied to a dark brown colour making the briquette resistant to atmospheric moisture during storage. The temperature should be in the range 280-290°C (Grover & Mishra, 1996).

(v) External Additives

Addition of coal and charcoal in very fine form improves the heating value and combustibility of the briquettes. About 10-20% char fines can be used in briquetting without impairing their quality. In addition, only screw pressed briquettes can be carbonized (Grover & Mishra, 1996). From Table 1, it can be noted that briquettes are made from a single feedstock or blending different feedstock. This is mainly done to supplement different feedstock due to scarcity and to ensure sustainability as well as enhance the HHV of the resulting briquettes. Lubwama *et al.* (2020) did a study on effects and interactions of the agricultural waste residues and binder type on physical properties and calorific values of carbonized briquettes. Experiments with cassava starch binder and wheat starch binder showed that the physical properties of the developed briquettes were affected significantly by the carbonized agricultural residue used and binder type. Also, calorific values of groundnut shell and bagasse briquettes were found to be significantly affected by the agricultural residue type.

2.2.4 Types of Binders

Briquetting at low pressure requires a binding agent to aid in the formation of bonds between the biomass particles. The binders are classified into organic, inorganic and compound binders (Zhang *et al*., 2018).

(i) Organic Binders

These are classified into four types, namely; biomass binders, tar pitch and petroleum bitumen binders, lignosulphonate binders and polymer binders. Biomass binders include; agricultural waste, forestry biomass, aquatic plants, Tar pitch and petroleum bitumen binders include; petroleum bitumen, coal tar, coal tar pitch, tar residue, lignin liquor. Lignosulphonate binders include; lignin derivative, paper mill, lignin liquor. Polymer binders include starch and polyvinyl acetate (PVA). The advantages of organic binders are; good bonding, good combustion performance, high drop test strength, high crush strength, low ash. The disadvantages of organic binders are; high price, decompose easily and burn when heated (mechanical strength and thermal stability of organic binder briquettes are poor) (Zhang *et al.,* 2018).

(ii) Inorganic Binders

They are classified into three types, namely; industrial binders, civilian binders and environmental protection binders. Industrial binders include; clay, limestone, bentonite, cement. Civilian binders include; clay and limestone. Environmental protection binders include; calcium oxide, limestone, iron oxide, magnesium oxide. The merits of inorganic binders include; low cost, strong adhesion, abundant resource, non-pollution, excellent thermal stability, and good hydrophilicity. The demerit of inorganic binders is the increased amount of ash (Zhang *et al.,* 2018).

(iii) Compound Binders

They are composed of at least two binders each performing a different role. The merits of compound binders are; improve the quality of briquettes, reduce the amount of inorganic binder, reduce the cost of organic binder and better performance of briquettes (Zhang *et al.,* 2018).

2.2.5 Binding Mechanisms of Densification

The behaviour of biomass as a fuel is influenced by its chemical and physical properties. Chemical properties include proximate analysis, ultimate analysis, and HHV. Physical properties include bulk density, moisture content, void volume, and thermal properties. The binding mechanisms under high pressure are divided into attractive forces between solid particles, adhesion and cohesion forces, and interlocking bonds (Grover & Mishra, 1996). Two hypotheses of briquette forming mechanisms have been proposed namely; non-binder briquetting mechanism, and cold-press briquetting mechanism with binder (Zhang *et al.,* 2018).

(i) Non-Binder Briquetting Mechanism

The hypotheses have been proposed for lignite and include; bituminous/ humic acid hypothesis, capillary hypothesis, colloid hypothesis, and adhesion molecules hypothesis (Zhang *et al.*, 2018).

Bituminous/ Humic Acid Hypothesis

Young lignite is easy to briquette due to its high content of humic acid and asphaltine. In addition, the asphaltine will soften and become a plastic substance in the temperature range of 70–90°C. Asphaltine and humic acid thus act as its own binder. Furthermore, pitch in lignite acts as binder, which holds coal particles together under the action of external force and suitable temperature. Also, the free humic acid in lignite has strong polarity and colloid properties, which could hold coal particles together during briquetting. The limitation of the hypothesis is that, pulverized coal used for briquetting is still very good after the extraction of humic acid, and the resulting briquettes have high strength (Zhang *et al.*, 2018).

Capillary Hypothesis

It postulates that there is a large number of hydrated capillary precocities in lignite. During briquetting under an applied pressure, the capillaries will crush; the water is squeezed out from the capillaries, and covers the surface of the coal particles to form a water film. Consequently, the water film will fill the voids between coal particles, and become the interaction force between molecules. When the pressure is released, the capillary regains a little dilation, some water will return into the capillaries, and the rest will remain on the surface of coal particles to form the crescent shape because of the effect of surface tension. Finally, the coal grains are bonded into a solid lump under the action of capillary force. The limitation of the hypothesis is that the formability of European lignite is better than Yunnan lignite, although they were formed at the same time. In addition, the capillary force disappears when lignite is dried but the lignite can still shape under high pressure, and the briquette strength is high (Zhang *et al.*, 2018).

Colloid Hypothesis

This hypothesis postulates that lignite comprises solid and liquid colloidal material. The solid material consists of tiny granular humic acid which comes together and produces intermolecular cohesion under the action of external force. Since these cohesions possess charge, it makes the solution contact with crystal molecules, combining to form jellylike colloidal particles. The intermolecular cohesion varies with the coal rank and coal's property. Coal particles are bonded together under pressure by means of Van der Waals force or molecular adhesive force. The smaller

the particle size, the larger is the specific surface area and increased bonding of binder resulting in greater strength of the briquette. The limitation of the hypothesis is that some non-colloid materials such as metal powder and salt crystals are also easy to shape. In addition, lignite is not a crystalline polymer with a regular molecular structure thus, it is not sufficient to explain lignite shaping only by colloid hypothesis (Zhang *et al.,* 2018).

Adhesion Molecules Hypothesis

It postulates that the bonding force of particles is due to water forced from primary capillary pores and filled in the gap between particles under pressure. The water between the particles produces a surface tension resulting in the formation of secondary capillary adsorption force. As a result, Van der Waals and capillary force bond the coal particles together. The molecular adhesive force is a result of coal particles coming close to each other. However, the hypothesis can't explain non-binder lignite briquetting of north-east Inner Mongolia and Yunnan (Zhang *et al.,* 2018).

(ii) The Cold-Press Briquetting Mechanism with Binder

The hypotheses of briquetting mechanism with binder are mainly proposed for lignite, anthracite, and bituminous coal. They include; soaking and bridging, mechanic and chemical bonding force, and the minimal contact angle and maximum bonding power.

Soaking and Bridging Mechanism

The quality of briquette is directly influenced by the soaking and bonding between coal particles and binder. Materials with high viscosity such as organic solvents and asphalt are used as binder. When the pores and surface of the coal particles are covered with binder, solid bridge is formed at the coal particle contact point. The viscosity, water content, and components of tar have significant effects on caking property and wetting degree when tar is used as binder. The viscosity of bitumen affects the compressive strength of briquette, and the content of coke-forming components affects the thermal stability of briquette. Briquettes prepared with corn starch binder and silicon-containing binder showed that silicon-oxygen bonds formed between silica acid gel particles after the curing reaction have the effect on connection bridge (negative ion connection bridge), which can connect the gel particles and coal particles into a complex net structure (Fig. 2 and 3) (Zhang *et al.,* 2018).

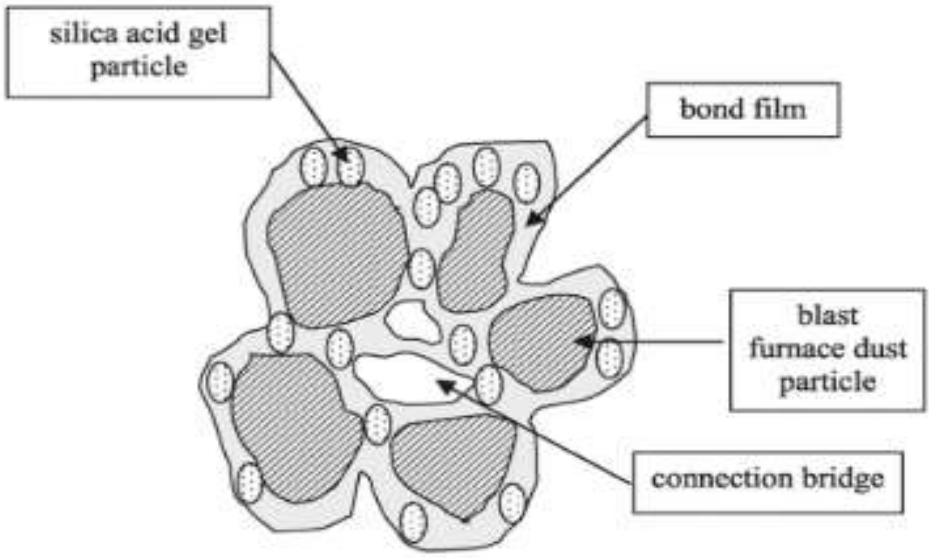

Figure 2: The bonding mechanism of sodium silicate (Zhang *et al.*, 2018)

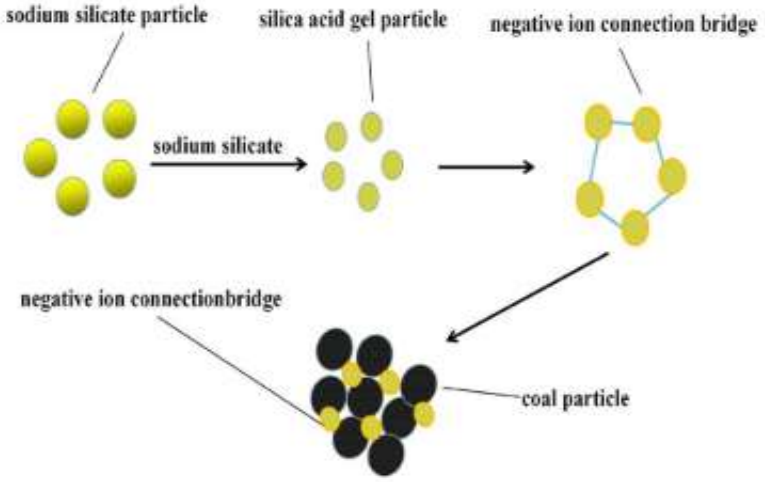

Figure 3: The bonding mechanism of sodium silicate (Zhang *et al.*, 2018)

The Mechanic and Chemical Bonding Force

This postulates that the interaction between coal particles and binder is a complex process, including wetting, mass transfer as well as combination of both factors. The adhesive strength between binder and coal particles is comprehensive. Mechanical power plays a major role for nonpolar coal particles in briquetting process. During pressing of the briquette, the binder/adhesive penetrates the pores and the cured briquettes, as a result of mechanical bonding, have improved strength. The strength of briquette is influenced by the curing conditions and water content. During the drying process, with the reduction of water from coal particles, the distance between the coal particles is reduced, the friction between the coal particles is increased, and briquette strength is increased (Zhang *et al.*, 2018).

Adding inorganic adhesives to coal with a certain amount of water and applying an external force, results in relative slip between the minerals and the binders in coal particles, leading to simultaneous increase in attraction and repulsion as a result of the decrease of the distance between coal particles. Attraction is mainly capillary forces, covalent, and ionic bonding forces on the contact surface. The crushing strength of the briquette is higher when the attractive force is greater than the repulsive force. According to solvent solubility parameter close principle, as solvents to dissolve coating finishing agents, organic binder has strong affinity for coal particles. A covalent or hydrogen bond forms when binder molecules with active groups share a pair of electrons with coal's active groups. Figure 4 shows the hydroxyl groups on the surface of kaolin. The hydroxyl groups could combine with functional groups on coal surface to produce hydrogen bond, which contributes to briquetting. In addition, the organic binder can penetrate into coal's small cell, mesh force is generated in the interface after drying and solidifying, which improves the briquetting strength (Zhang *et al.*, 2018).

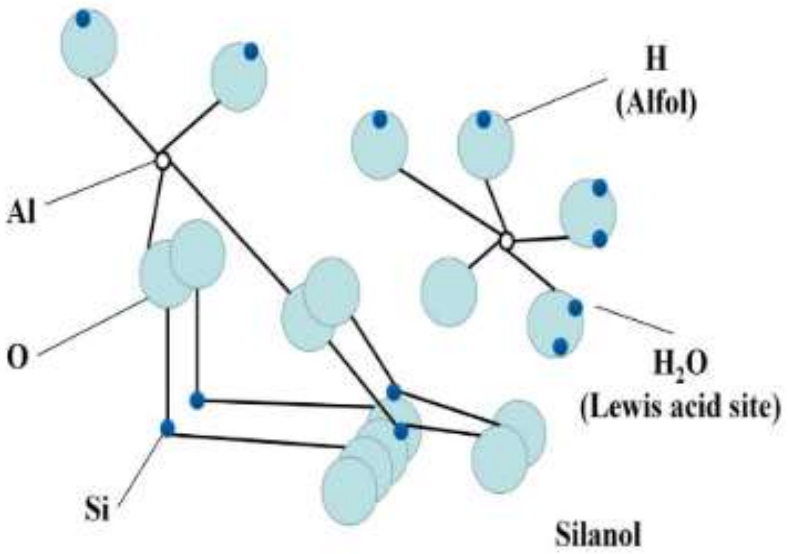

Figure 4: The hydroxyl groups on the surface of kaolin (Zhang *et al.*, 2018)

The texture of briquettes and the briquetting forming mechanism was analysed by means of an Optical microscope and Thermogravimetric analysis (Zhang *et al.*, 2018). The results showed that the addition of inorganic components assist in absorbing organic components, and then form chemical bonds with the coal particles, as shown in Fig. 5. The generation of a continuous gel-phase is important to promote the thermal stability of the briquette through the agglomeration of coal particles.

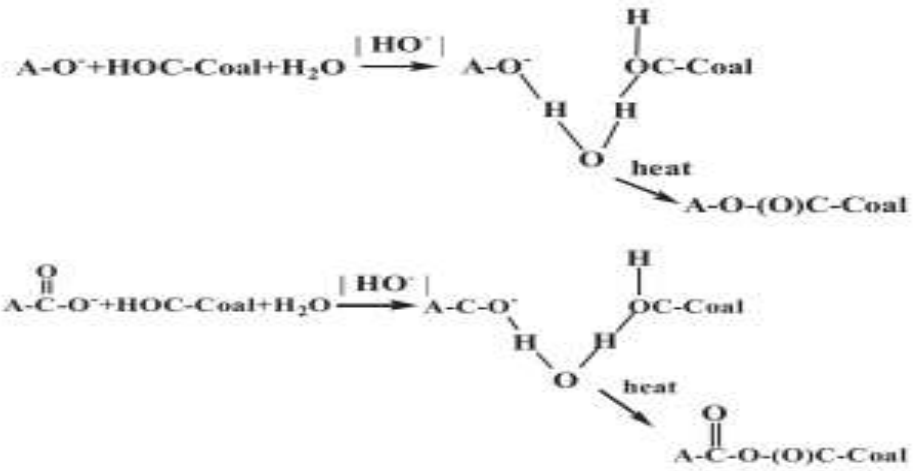

Figure 5: The chemical bond between binder and coal particles (Zhang *et al.*, 2018)

The bonding mechanism of corn starch is shown in Fig. 6. Corn starch can improve the briquette strength at room temperature and after drying as a result of the expansibility after absorbing water, viscosity and compatibility after gelatinization. After 200°C, corn starch gradually transforms into a continuous solid connection bridge, which connects the blast furnace dust particles closely. When the temperature is above 1000°C, the solid connection bridge disappears gradually and strength of the briquettes decreases (Zhang *et al.*, 2018).

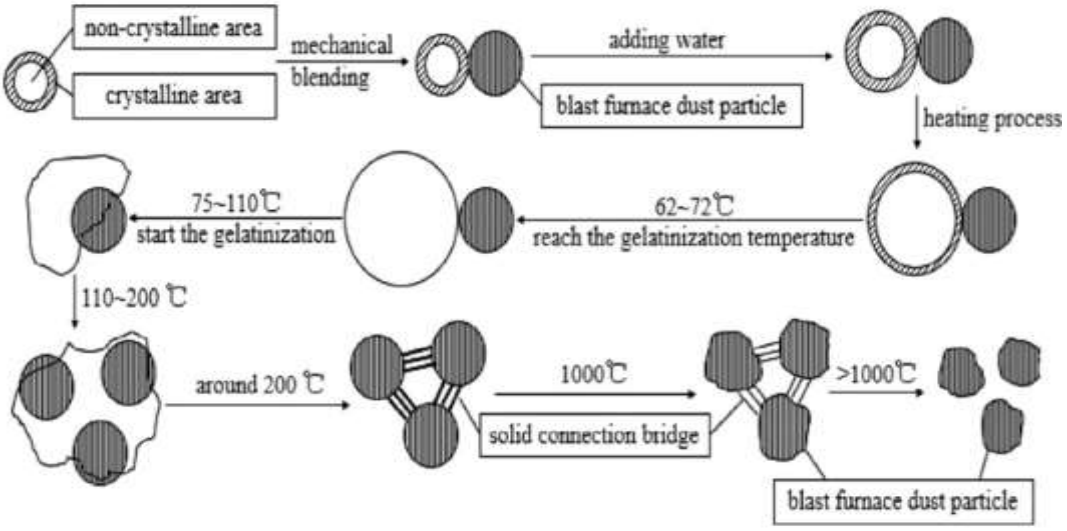

Figure 6: The bonding mechanism of corn starch (Zhang *et al.*, 2018)

The Minimal Contact Angle and Maximum Bonding Power

This hypothesis compares the wetting property of coal to the compressive strength of briquettes. The higher the degree of coalification, the higher the compressive strength of briquettes, because of the difference of the properties of wetting of coal. With the increase of coalification of the coals, the contact angle between coal and the binder decreases, the energy of adhesion and the degree of

wetting of coal increases. Thus, the compressive strength of briquettes increases. The relation between the compressive strength and the critical surface tension of wetting of coal has been investigated (Zhang *et al.,* 2018). The results showed that the higher the critical surface tension, the higher the degree of wetting of coal and hence the compressive strength of briquettes increases. With the increase of the hydrophobic group, the contact angle between coal and the starch binder increases, the wettability of coal particle, the compressive strength of briquette and adhesive performance of briquette decrease (Zhang *et al.,* 2018).

2.2.6 Briquetting Technology

Briquetting technologies are classified into low pressure compaction with a binder, medium pressure compaction with a heating device and high pressure compaction. Solid particles are the starting materials in all these compaction techniques. Briquetting and extrusion both represent compaction i.e., the pressing together of particles in a confined volume (Fagbemi *et al.,* 2014; Grover & Mishra, 1996). Initially, when pressure is applied during compaction, it will lead to some non-permanent elastic deformation of the sample that lasts only as long as the force is applied. As the pressure increases, permanent plastic deformation begins to occur. Bonding arising from the diffusion of molecules from one particle to the next and the formation of solid bridges is more probable under higher pressures. Therefore, high pressures (and temperatures) cause better connection at the points of contact resulting in denser and durable products. Furthermore, higher pressures are known to decrease sample porosity (Bazargan *et al.,* 2014). Table 3 shows the feedstock, binder, binder concentration, compaction pressure, compressive strength, splitting tensile strength, bulk density, impact resistance index, and water resistance index of various carbonized briquettes. Briquetting technology includes screw press extruder, mechanical piston press, hydraulic piston press, roller press, and manual press (Kpalo *et al.,* 2020a).

(i) Screw Press Extruder

It consists of a die and screw extruder. There are three types of screw presses namely; cylindrical screw press with heated dies, conical screw press, and one without externally heated dies. In the screw extruder, the biomass is continuously fed into a screw, which forces the material into a heated cylindrical die to the point where lignin flow occurs (Kpalo *et al.*, 2020a). Figure 7 shows a screw extruder.

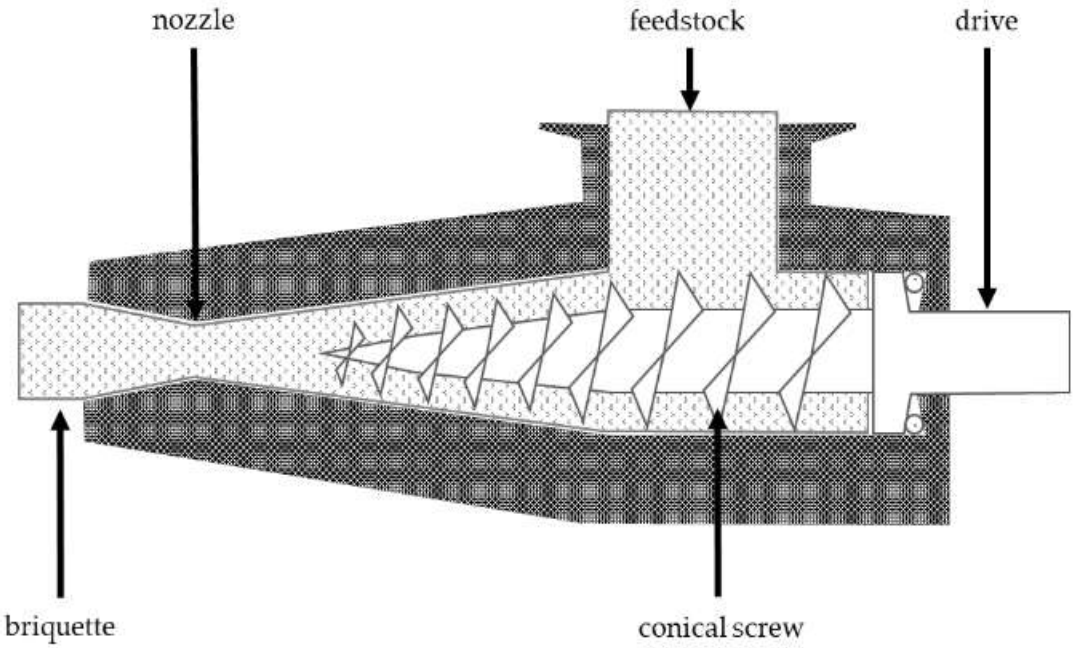

Figure 7: Screw extruder (Kpalo *et al.*, 2020a)

Table 3: Feedstock, binder, binder concentration (BC), compaction pressure (CP), compressive strength (CS), splitting tensile strength (STS), bulk density (ρ), impact resistance index (IRI), and water resistance index (WRI) of selected carbonized briquettes

Feedstock	Binder	BC (%)	CP (MPa)	CS (kPa)	STS (kPa)	ρ (g/cm^3)	IRI	WRI	Reference
Palm kernel shell	Cassava starch	10	20-100	n.a	17-38	0.288-0.747	167	<50%	Bazargan *et al.* (2014)
Low rank coals and biomass (sawdust, straw, olive stone and almond shell)	humates	15	125	1250-5000		n.a	150-700	95%	Blesa *et al.* (2001)
Water hyacinth	molasses	20-40	0.827	390-1910		0.84-0.89	n.a	n.a	Carnaje *et al.* (2018)
Rubber seed shell	cassava starch	25	n.a	1080	284	6.48	n.a	n.a	Fagbemi *et al.* (2014)
hazelnut shells	molasses and pyrolytic liquid	10-15	5-10	8100	n.a	n.a	n.a	n.a	Haykiri-Acma and Yaman (2010)
Brown seaweed	sulfite liquor, molasses and linobind	2-10	187	35 400-10 8700	n.a	n.a	20-100	11-31s	Haykiri-Acma *et al.* (2013)
Rice straw, bagasse and water hyacinth	cassava starch	22.22	n.a	264-2609	n.a	0.578-0.925	n.a	n.a	Jamradloedluk and Wiriyaumpaiwong (2007)
Groundnut shells and bagasse	Cassava & wheat starch	2.91-8.25	≤7	n.a	n.a	0.2-1.0	44-97.5	n.a	Lubwama and Yiga (2017)
Durian peel	starch	10	n.a	146.5- 151	n.a	0.99	n.a	n.a	Nuriana *et al.* (2014)

Feedstock	Binder	BC (%)	CP (MPa)	CS (kPa)	STS (kPa)	ρ (g/cm^3)	IRI	WRI	Reference
Municipal waste composting char and sawdust char	slop waste	10-20	n.a	1250-2000	n.a	0.85-1.24	n.a	136 min	Prasityousil and Muenjina (2013)
Cassava rhizome waste	molasses, starch gel, concentrated slop, Cassava pulp and soybean residue	0-40	n.a	851 – 1494	n.a	0.69-0.91	153.7-416.7	n.a	Sen and Annachhatre (2016)
Sugarcane bagasse fly ash	Cassava starch	8	69.43	n.a	n.a	1.12	n.a	n.a	Teixeira *et al*. (2010)
Human waste	molasses, lime, corn starch and wheat starch	3-20	9.65	>375	n.a	n.a	10-700	n.a	Ward *et al.* (2014)

*n. a -not available

(ii) Mechanical Piston Press

This consists of a ram (piston) and a die and it is driven by an electric motor. Biomass feedstock is compressed in a die by a reciprocating ram with a very high compaction pressure to obtain a briquette. The machine develops a compression pressure of about 196.1 MPa and is typically used for large scale production in the range 200–2500 kg/h. The density of the produced briquettes is 1000 -1200 kg/m^3 (Kpalo *et al.,* 2020a). Figure 8 shows a piston press.

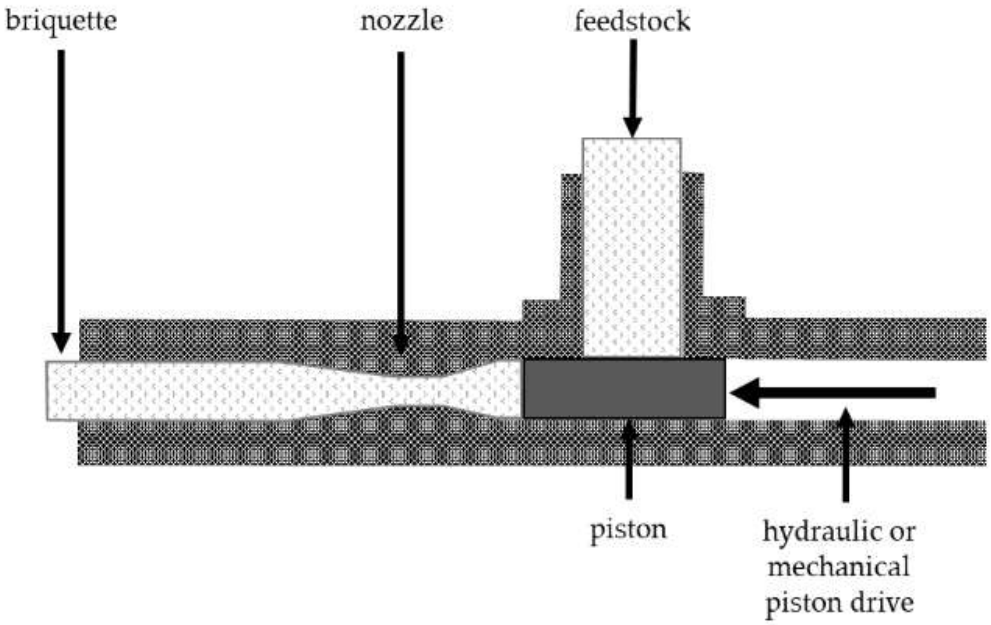

Figure 8: Piston press (Kpalo *et al.*, 2020a)

(iii) Hydraulic Piston Press

It's mode of operation is similar to the mechanical piston press except that the energy to the piston is exerted by a cylinder operated by a hydraulic system. The briquetting pressure in the hydraulic system is normally limited to 30 MPa. The piston head can exert a higher pressure when it is of a smaller diameter than the hydraulic cylinder, but the gearing up of pressure in commercial applications is modest. These machines have production capacities of 50–400 kg/h and can tolerate moisture content greater than 15% which is common for mechanical piston presses. The bulk density of the produced briquettes is lower than 1000 kg/m^3 due to limited pressure. In addition, the briquettes have a uniform shape and size, typically using 40 × 40 mm cylinders, and the quality of the product is much higher compared to mechanical presses (Kpalo *et al.,* 2020a).

(iv) Roller Press

This technology is used to produce pillow-shaped briquettes. It comprises two cylindrical rollers of the same diameter, rotating in opposite direction on parallel axes. The rollers are positioned

with a small gap between them and the distance from each other depends on factors such as the binder used, type of biomass, moisture content, and particle size. During operation, the raw material is fed into the press and forced through the gap between the rollers on one side. It is then pressed into a die forming the densified product, on the opposite side. The bulk density of the briquettes is in the range 450-550 kg/m^3 (Kpalo *et al.*, 2020a). Figure 9 shows a roller press.

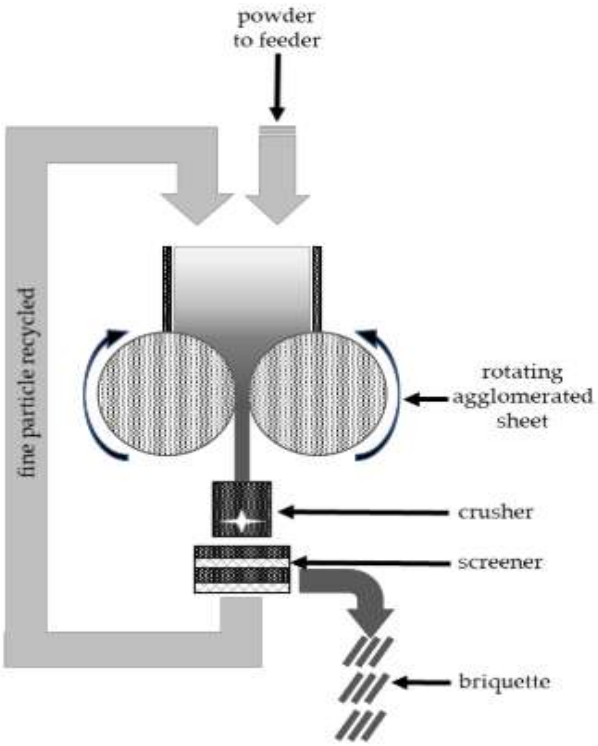

Figure 9: Roller press (Kpalo *et al.*, 2020a)

(v) Manual Press

These include piston or screw presses which are operated manually and hardly use electricity. Manual presses are designed for the purpose of briquette making or adapted from existing implements used for other purposes e.g., the manual clay brick making press can be used to make briquettes from both carbonized and uncarbonized biomass feedstock. Another common example is the Washington University (WU)-presser. The press is made from both metal and wood with the latter being the most common. These machines operate with very minimal pressure and the feedstock requires binder. The advantages of a manual press include; low capital, low operating costs, low level of skill to operate. The disadvantage of a manual press is the low production capacity of about 5 kg/h (Kpalo *et al.*, 2020a). Figure 10 shows a manual press.

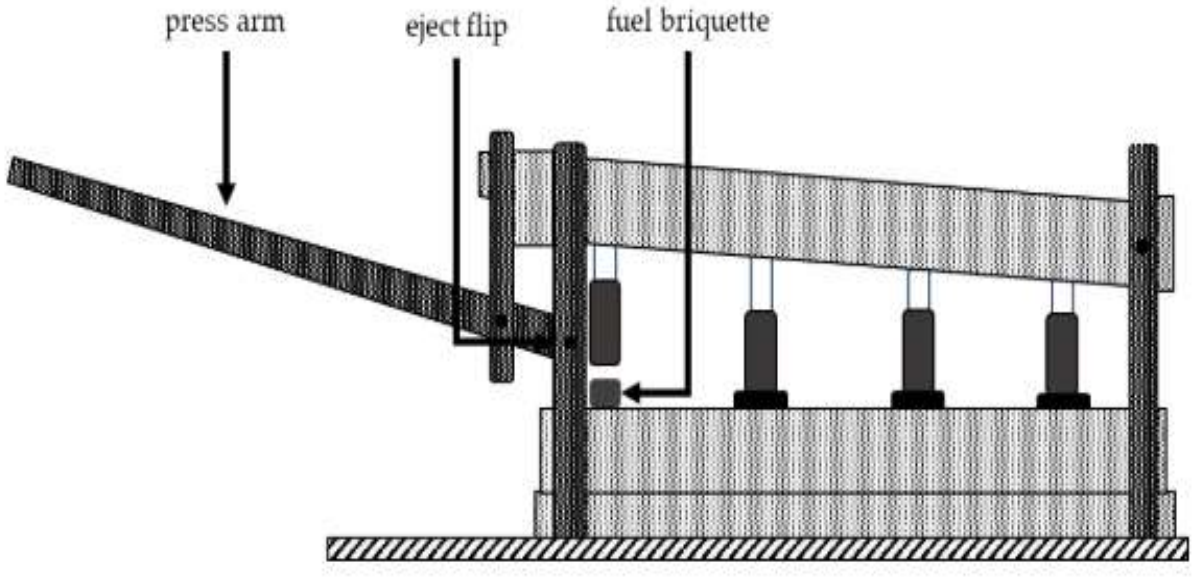

Figure 10: Manual press (WU-presser) (Kpalo *et al.*, 2020a)

2.3 Ignition of Carbonized Briquettes

Ignition can be defined as a rapid transition process by which an exothermic oxidation reaction and self-supported combustion is initiated (Moqbel *et al*., 2010). The steps of solids ignition include an increase in solids temperature, decomposition of the solid phase, escape of volatiles from the solid surface, diffusion of pyrolyzed species from the solid surface into the gas phase, diffusion of oxygen to the reaction sites on the solid surface followed by gaseous reactions and heterogeneous reactions at the solid surface (Moqbel *et al*., 2010). In auto-ignition, a reaction mixture will ignite spontaneously without the presence of an external ignition source. This occurs at the auto-ignition temperature needed to supply the activation energy. Induced ignition is caused by an ignition source (e.g. spark, flame, hot surface) which supplies the minimum ignition energy (Lackner, 2011). Ignition temperature depends on volatile matter, particle size, sample size, bed height, heating rate, oxygen concentration, and pressure (Pandey & Dhakal, 2013). Ignition temperature is reduced with increasing pressure and oxygen concentration (Lackner, 2011). In briquette making, a hole at the centre of the fuel improves the combustion characteristics of the briquette through rapid drying, easy ignition and highly efficient burning due to the draft and insulated combustion chamber that the hole creates (Romallosa & Kraft, 2017). Carnaje *et al.* (2018) did a study on charcoal briquettes from water hyacinth (*Eichhornia crassipes*) using molasses as binder and the following volumes of kerosene were applied as ignition agent: 5 mL, 10 mL, and 15 mL. The results showed that ignition time was 2.22-3.3 min. Rotich (1998) did a study on carbonization and briquetting of sawdust for use in domestic cookers using starch as binder with paraffin/wood chips/pieces of paper as ignition agents. The results showed that ignition time was between 7-10 min. Onchieku *et al.* (2012) studied optimum parameters for the production

of charcoal briquettes from bagasse using clay as binder. Molasses were used as a filler and ignition enhancer. Results showed that the ignition time was 4.4-7.35 min.

Chirchir *et al.* (2013) did a study on effect of binder types and amount on physical and combustion characteristics of rice husk-bagasse-charcoal dust composite briquettes using three binders (molasses, cow dung and clay) with paraffin as ignition agent. The ignition time depended on the amount and type of binder with the following results; molasses (7.5-14 min), clay (15-25 min) and cow dung (10-15 min). Onuegbu *et al.* (2011) did a study on ignition time and Water Boiling Test of bio-coal and biomass briquette blends with cassava starch as binder using elephant grass (*pennisetum purpurem)* and spear grass (*imperata cylindrica*) as ignition agent. The results showed that ignition time was 0.33-3.1 min and increased proportionally to the plant material (volatile matter). Onuegbu *et al.* (2010) ignited coal briquettes using a cigarette lighter and the time required to ignite the briquettes was recorded as the ignition time. Gesase *et al.* (2019) performed ignition tests on briquettes by pouring bioethanol gel on a briquette sample placed in a beaker to allow infiltration of the gel into the briquette thus, the successful ignition was achieved using 15-20 ml of bioethanol gel with ignition time of 2.06-2.72 min.

2.4 Combustion Products and Pollutants

Combustion is described as self-sustained, exothermic reaction between fuel and oxidizer (Moqbel *et al*., 2010). The combustion behaviour of biomass is affected by the following factors: (a) the geometrical shape of the fuel, the porosity, and the tendency of the fuel to undergo fragmentation. The external surface area of the fuel particle determines the rate of initial devolatilization as well as the subsequent progress of the flame front into the particle and combustion of the char formed. These determine the burning rate and consequently the temperature in the combustion chamber, (b) the supply of air and operating conditions especially the fuel load which determines the air/fuel ratio, and (c) the chemical composition-C, N, ash content and volatile content (Mitchell *et al*., 2016).

Control of pollutant emissions is a major factor in the design of modern combustion systems. Pollutants of concern include particulate matter (PM), such as soot, fly ash, metal fumes, various aerosols; carbon monoxide; oxides of nitrogen, NO_x, which consist of NO and NO_2; the sulphur oxides, SO_2 and SO_3; unburned and partially burned hydrocarbons, such as aldehydes; and greenhouse gases such as N_2O, but particularly CO_2 (Chen *et al*., 2016; Khlifi *et al*., 2019; Turns, 2000). Primary pollutants (emitted directly from the source) and secondary pollutants (those formed via reactions involving primary pollutants in the atmosphere) affect the environment and human health in the following ways; soiling and deterioration of materials, harm to vegetation,

potential increase of morbidity (sickness) and mortality in humans, altered properties of the atmosphere and precipitation (Chen *et al*., 2016; Turns, 2000).

2.5 Water Boiling Test (WBT)

The WBT comprises three phases i.e., Cold Start High Power (CSHP), Hot Start High Power (HSHP), and Simmer phases (Clean cooking alliance, 2014). Figure 11 shows the temperature profile during the WBT.

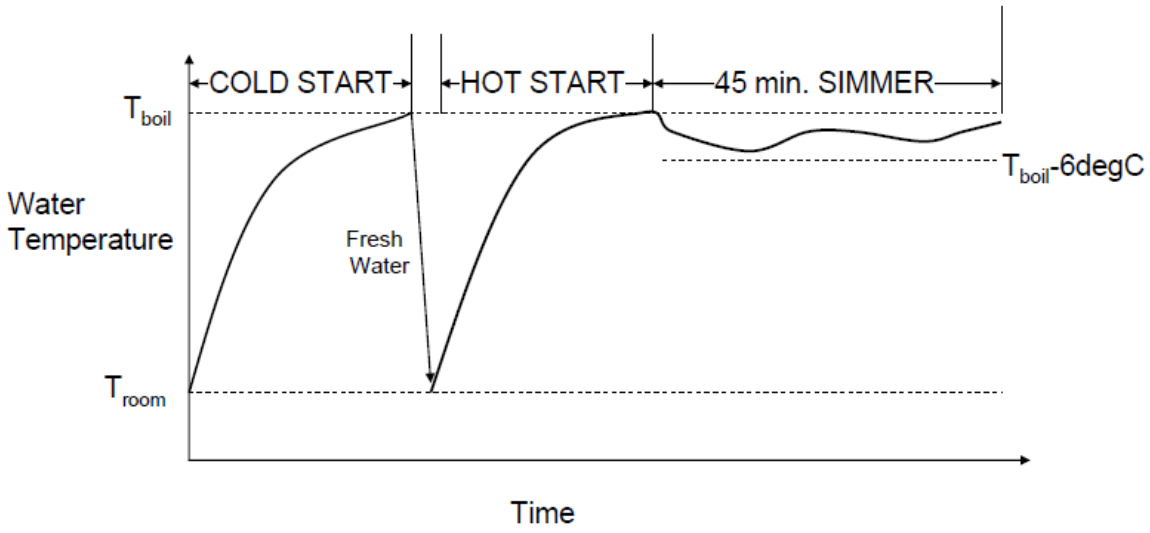

Figure 11: Temperature profile during the WBT (Clean cooking alliance, 2014)

2.5.1 Cold Start High Power (CSHP) Phase

The tester begins with the stove at room temperature and uses a pre-weighed bundle of fuel to boil a measured quantity of water in a standard pot. The tester then replaces the boiled water with a fresh pot of ambient-temperature water for the HSHP phase.

2.5.2 Hot Start High Power (HSHP) Phase

The HSHP phase is performed after the CSHP phase while the stove is still hot. The tester uses a pre-weighed bundle of fuel to boil a measured quantity of water in a standard pot. Repeating the test with a hot stove, results in identifying performance differences between a stove when it is cold and when it is hot. This is particularly important for stoves with high thermal mass, since these stoves may be kept warm in practice.

2.5.3 Simmer Phase

It provides the amount of fuel to simmer a measured amount of water at just below boiling point for 45 min. This phase simulates the long cooking of legumes or pulses common throughout much of the world.

2.5.4 Emissions Testing

This basic testing protocol includes optional instructions for measuring carbon dioxide (CO_2), carbon monoxide (CO), and particulate matter (PM) concentrations in the stove's exhaust and other pollutants.

2.5.5 Water Boil Test Performance Metrics

The subscripts, 'c', 'h', and 's' are used to represent the CSHP, HSHP and Simmer phases respectively (Clean cooking alliance, 2014).

(i) Cold Start High Power (CSHP) Phase

Higher Heating Value, HHV (kJ/Kg)

This is also known as gross calorific value. It is the theoretical maximum amount of energy that can be extracted from the combustion of the moisture-free fuel if it is completely combusted and the combustion products are cooled to room temperature such that the water produced by the reaction of the fuel-bound hydrogen is condensed to the liquid phase.

Lower Heating Value, LHV (kJ/Kg)

Also known as net heating value. This is the theoretical maximum amount of energy that can be extracted from the combustion of the moisture-free fuel if it is completely combusted and the combustion products are cooled to room temperature but the water produced by the reaction of the fuel-bound hydrogen remains in the gas phase. The LHV typically differs from HHV by 1.32 MJ/kg for wood fuels.

Moisture Content, MC_{wet} (%)

This is the percentage of wood moisture on a wet basis, as shown in Equation 1.

$$MC_{wet} = \frac{m_{fuel,wet} - m_{fuel,dry}}{m_{fuel,wet}} \quad (1)$$

Effective Calorific Value, EHV (kJ/kg)

It accounts for the energy required to heat and evaporate the moisture present in the fuel. The EHV is not actually used in any WBT calculations. It is computed using Equation 2.

$$\boldsymbol{EHV = LHV \times (1 - MC_{wet}) - MC_{wet} \times \Delta h_{H_2O}} \quad (2)$$

Where, Δh_{H_2O} is change in specific enthalpy of water shown in Equation 3

$$\Delta \boldsymbol{h_{H_2O}} = \boldsymbol{h_{H_2O(gas),T_b}} - \boldsymbol{h_{H_2O(liquid),T_{fuel,i}}} \quad (3)$$

The specific enthalpy of the liquid water at the initial temperature ($T_{fuel,i}$) and the water vapour at the local boiling temperature (T_b) is found from a steam table (Thermopedia, 2011). A reasonable approximation is given in Equation 4:

$$\Delta \boldsymbol{h_{H_2O}} = \Delta \boldsymbol{h_{H_2O,fg}} + \boldsymbol{h_{H_2O(liquid),T_b}} - \boldsymbol{h_{H_2O(liquid),T_{fuel,i}}} = \Delta \boldsymbol{h_{H_2O,fg}} + \boldsymbol{C_{p,H_2O}}\left(\boldsymbol{T_b} - \boldsymbol{T_{fuel,i}}\right) \quad (4)$$

The specific heat capacity of liquid water, C_{p,H_2O} is 4.186 kJ/kg-K, and the specific enthalpy of vaporization of water, $\Delta h_{H_2O,fg}$ is 2260 kJ/kg. Hence, EHV is computed from Equation 5.

$$\boldsymbol{EHV} = \boldsymbol{LHV} \times (\mathbf{1} - \boldsymbol{MC_{wet}}) - \boldsymbol{MC_{wet}}\left[\mathbf{4.186}\left(\boldsymbol{T_b} - \boldsymbol{T_{fuel,i}}\right) + \mathbf{2260}\right] \quad (5)$$

Fuel Consumed (moist), f_{cm} (g)

This is the mass of wood used to heat the water to boiling point. It is computed as shown in Equation 6, where $\boldsymbol{f_{ci}}$ is the pre-weighed bundle of wood, and $\boldsymbol{f_{cf}}$ is the wood remaining at the end of the test phase.

$$\boldsymbol{f_{cm}} = \boldsymbol{f_{ci}} - \boldsymbol{f_{cf}} \quad (6)$$

Net Change in Char during the Test, ΔC_c (g)

This is the mass of char produced during the test, calculated as shown in Equation 7 where, k is the mass of an empty pre-weighed container in which the hot char is placed and C_c is total weight of the char and the container.

$$\Delta C_c = C_c - k \quad (7)$$

Mass of Water Vaporized, w_{cv} (g)

This is the amount of water lost through evaporation during the test. It is obtained using Equation 8. Where, $P1_{ci}$ is the initial weight of pot and water, and $P1_{cf}$ is the final weight of pot and water.

$$\boldsymbol{w_{cv}} = \boldsymbol{P1_{ci}} - \boldsymbol{P1_{cf}} \quad (8)$$

Effective Mass of Water Boiled, w_{cr} (g)

This is the water remaining at end of the test. It is a measure of the amount of water heated to boiling. It is computed as shown in Equation 9 where $P1_{cf}$ is the final weight of pot and water, and $P1$ is the weight of the pot.

$$\boldsymbol{w_{cr} = P1_{cf} - P1} \quad (9)$$

Time to Boil, Δt_c (min)

This is the difference between start, t_{ci} and finish, t_{cf} times as shown in Equation 10.

$$\boldsymbol{\Delta t_c = t_{cf} - t_{ci}} \quad (10)$$

Temperature-Corrected Time to Boil, Δt_c^T (min)

It is the same as Equation 10, but adjusts the result to a standard 75ºC temperature change (25-100ºC). The results are thus standardized and a comparison can be made between tests that may have used water with higher or lower initial temperatures as shown in Equation 11.

$$\boldsymbol{\Delta t_c^T = \Delta t_c \times \frac{75}{T1_{cf} - T1_{ci}}} \quad (11)$$

Equivalent Dry Fuel Consumed, f_{cd} (g)

It adjusts the amount of dry fuel that was burned in order to account for two factors: (a) the energy that was needed to remove the moisture in the fuel and (b) the amount of char remaining unburned. The mass of dry fuel consumed is the moist fuel consumed, f_{cm} minus the mass of water in the fuel as shown in Equation 12.

$$\boldsymbol{dry\ fuel = f_{cm} \times (1 - MC_{wet})} \quad (12)$$

The energy that was needed to remove the moisture in the fuel ($\Delta E_{H_2O,c}$) is obtained from Equation 13.

$$\boldsymbol{\Delta E_{H_2O,c} = m_{H_2O,c}\left[C_{p,H_2O}(T_b - T_{fuel,i}) + \Delta h_{H_2O,fg}\right]} \quad (13)$$

In similar fashion to Equation 5,

$$\boldsymbol{T_{fuel,i} \approx T_a} \quad (14)$$

The mass of water in the fuel is: $\boldsymbol{m_{H_2O,c} = f_{cm} \times MC_{wet}}$ (15)

Thus:

$$\Delta E_{H_2O,c} = f_{cm} \times MC_{wet}[4.186(T_b - T_a) + 2260] \quad (16)$$

The fuel required to remove the moisture in the fuel is computed as shown in Equation 17.

$$\boldsymbol{fuel\ to\ evaporate\ water = \frac{\Delta E_{H_2O,c}}{LHV}} \quad (17)$$

The fuel energy stored in the char remaining, $\Delta E_{char,c}$ is computed as shown in Equation 18 where ΔC_c is the mass of char and LHV_{char} is the energy content of the char.

$$\boldsymbol{\Delta E_{char,c} = \Delta C_c \times LHV_{char}} \quad (18)$$

The equivalent amount of unburned fuel remaining in the form of char is calculated as shown in Equation 19.

$$\boldsymbol{fuel\ in\ char = \frac{\Delta E_{char,c}}{LHV}} \quad (19)$$

Hence:

$$\boldsymbol{f_{cd} = dry\ fuel - fuel\ to\ evaporate\ water - fuel\ in\ char} \quad (20)$$

Substituting Equations: 12, 16, 17, 18 and 19 into Equation 20 gives:

$$f_{cd} = f_{cm} \times (1 - MC_{wet}) - \frac{f_{cm} \times MC_{wet}[4.186(T_b - T_a) + 2260]}{LHV} - \frac{\Delta C_c \times LHV_{char}}{LHV} \quad (21)$$

$$\boldsymbol{f_{cd} = \frac{f_{cm}\{LHV(1-MC_{wet}) - MC_{wet}[4.186(T_b - T_a) + 2{,}260]\} - \Delta C_c \times LHV_{char}}{LHV}} \quad (22)$$

Thermal Efficiency, h_c (%)

This is a ratio of the work done by heating and evaporating water to the energy consumed by burning fuel. It is computed using Equation 23.

$$\boldsymbol{h_c = \frac{\Delta E_{H_2O,heat} + \Delta E_{H_2O,evap}}{E_{released,c}}} \quad (23)$$

The energy to heat the water, $\Delta E_{H_2O,heat}$ is computed as shown in Equation 24 where, m_{H_2O} is the mass of water, C_{p,H_2O} is the specific heat capacity, ΔT is the change in temperature.

$$\Delta E_{H_2O,heat} = m_{H_2O} \times C_{p,H_2O} \times \Delta T$$

$$\Delta E_{H_2O,heat} = (P1_{ci} - P1) \times 4.186 \times (T1_{cf} - T1_{ci}) \quad (24)$$

The energy to evaporate the water, $\Delta E_{H_2O,evap}$ is obtained from Equation 25 where w_{cv} is the mass of water evaporated.

$$\Delta E_{H_2O,evap} = w_{cv} \times \Delta h_{H_2O,fg}$$

$$\Delta E_{H_2O,evap} = w_{cv} \times 2260 \quad (25)$$

The energy consumed, $E_{released,c}$ is obtained from Equation 26 where, f_{cd} is the equivalent mass of dry fuel consumed.

$$E_{released,c} = f_{cd} \times LHV \quad (26)$$

Thus:

$$h_c = \frac{4.186(P1_{ci} - P1)(T1_{cf} - T1_{ci}) + w_{cv} \times 2260}{f_{cd} \times LHV} \quad (27)$$

Burning Rate, r_{cb} (g/min)

This is a measure of the rate of fuel consumption while bringing water to a boil. It is calculated as shown in Equation 28 where, f_{cd} is equivalent dry fuel consumed, and Δt_c is the time of the test.

$$r_{cb} = \frac{f_{cd}}{\Delta t_c} \quad (28)$$

Specific Fuel Consumption, SC_c (g /L)

Specific consumption can be defined for any number of cooking tasks and should be considered "the fuel required to produce a unit output" whether the output is cooked beans, boiled water, or loaves of bread. For the CSHP, it is a measure of the amount of wood required to produce one litre (or kilo) of boiling water starting with cold stove. It is obtained from Equation 29.

$$SC_c = \frac{f_{cd}}{w_{cr}} \quad (29)$$

Temperature-Corrected Specific Fuel Consumption, SC_c^T (g /L)

This corrects specific consumption to account for differences in initial water temperatures. It enables comparison of stoves tested on different days or in different environmental conditions. The correction is a simple factor that "normalizes" the temperature change observed in test

conditions to a "standard" temperature change of 75ºC (25-100ºC). It is obtained from Equation 30.

$$\boldsymbol{SC_c^T = SC_c \times \frac{75}{(T1_{cf} - T1_{ci})}} \quad (30)$$

Temperature-Corrected Specific Energy Consumption, SE_c^T (kJ /L)

This is a measure of the amount of fuel energy required to produce one litre (or kilo) of boiling water starting with cold stove. This is computed as shown in Equation 31.

$$\boldsymbol{SE_c^T = SC_c^T \times \frac{LHV}{1000}} \quad (31)$$

Firepower, FP_c (W)

This is the fuel energy consumed to boil the water divided by the time to boil, Δt_c as shown in Equation 32. It tells the average power output of the stove during the High Power test. By using f_{cd} in this calculation, the remaining char and the fuel moisture content are both accounted.

$$\boldsymbol{FP_c = \frac{f_{cd} \times LHV}{\Delta t_c \times 60}} \quad (32)$$

Total Exhaust Flow, V_c (m^3)

The total exhaust flow, V_c is the volumetric flow rate through the hood, Q multiplied by the time of the test period, Δt_c as shown in Equation 33.

$$\boldsymbol{V_c = Q \times \frac{\Delta t_c}{60}} \quad (33)$$

Exhaust Carbon Concentration, CC_c (ppm)

This is the average concentration of carbon atoms in the stove exhaust which accounts for the carbon atoms present in the CO_2, CO, and PM as shown in Equation 34.

$$\boldsymbol{CC_c = CO_{2carbon,c} + CO_{carbon,c} + PM_{carbon,c}} \quad (34)$$

One molecule of CO_2 contains one carbon atom. Thus, the concentration of carbon from CO_2 [ppm_v] is the same as the concentration of CO_2. The CO_2 concentration, $CO_{2carbon,c}$ is computed as shown in Equation 35, where CO_{2c} is the concentration measured during the test, and CO_{2b} is the background concentration.

$$\boldsymbol{CO_{2carbon,c} = CO_{2c} - CO_{2b}} \quad (35)$$

The CO carbon concentration, $CO_{carbon,c}$ is calculated using Equation 36.

$$\boldsymbol{CO_{carbon,c} = CO_c - CO_b} \quad (36)$$

The PM is measured as a mass concentration $\left[\frac{\mu g}{m^3}\right]$. It is assumed that the PM is 80% carbon by mass, so the PM mass carbon concentration is computed as shown in Equation 37.

$$\boldsymbol{PM_{carbon,c}\left[\frac{\mu g}{m^3}\right] = 0.8\,(PM_c - PM_b)} \quad (37)$$

To convert the mass concentration $\left[\frac{\mu g}{m^3}\right]$ to $[ppm_v]$ the following steps are followed. The mass concentration of a gas is the mass of the gas per unit volume. The parts per million by volume of a gas is the volume fraction of space that the gas occupies multiplied by 1 000 000 as shown in Equation 38.

$$\boldsymbol{Conc_{carbon}\left[\frac{g}{m^3}\right] = \frac{m_{gas}}{V_{total}} \qquad Conc_{carbon}\,[ppm_v] = \frac{V_{gas}}{V_{total}} \times 10^6} \quad (38)$$

To convert from $\left[\frac{g}{m^3}\right]$ to $[\boldsymbol{ppm_v}]$, the ideal gas law is used to convert $\boldsymbol{m_{gas}}$ to $\boldsymbol{V_{gas}}$ as shown in Equation 39.

$$\boldsymbol{P_{total}V_{gas} = n_{gas}RT} \quad (39)$$

The number of moles of the gas, $\boldsymbol{n_{gas}}$ is computed as shown in Equation 40 where, $\boldsymbol{m_{gas}}$ is the mass of the gas, and $\boldsymbol{MW_{gas}}$ is the molecular weight.

$$\boldsymbol{n_{gas} = \frac{m_{gas}}{MW_{gas}}} \quad (40)$$

Substituting Equation 40 into Equation 39 gives:

$$\boldsymbol{P_{total}V_{gas} = \frac{m_{gas}}{MW_{gas}}RT}$$

Thus:

$$\boldsymbol{V_{gas} = \frac{m_{gas}\,RT}{MW_{gas}\,P_{total}}} \quad (41)$$

Where temperature of the gas, $T = T_{cd} + 273.15\ K$; universal gas constant, $R = 0.008314\ \left[\frac{kJ}{mol-K}\right]$; $MW_{gas} = MW_{carbon} = 12\ g/mol$; atmospheric pressure, $P_{total} = P_{atm}\ [kPa]$

$$\boldsymbol{V_{gas} = \frac{m_{gas} \times 0.008314 \times (T_{cd} + 273.15)}{12 \times P_{atm}}} \quad (42)$$

Then, substitute Equation 42 into the Equation 38 to give:

$$\boldsymbol{PM_{carbon,c}\,[ppm_v] = \frac{\frac{m_{gas}\times 0.008314\times(T_{cd}+273.15)}{12\times P_{atm}}}{V_{total}} \times 10^6}$$

$$PM_{carbon,c}\,[ppm_v] = \frac{m_{gas}}{V_{total}} \times \frac{0.008314\times(T_{cd}+273.15)}{12\times P_{atm}} \times 10^6 \quad (43)$$

Combining Eq. 37 and 38 gives,

$$\left(\frac{m_{gas}}{V_{total}}\right)\left[\frac{g}{m^3}\right] = \frac{PM_{carbon,c}\left[\frac{\mu g}{m^3}\right]}{10^6\left[\frac{\mu g}{g}\right]} = \frac{0.8\,(PM_c - PM_b)}{10^6}\left[\frac{g}{m^3}\right] \quad (44)$$

Thus:

$$\boldsymbol{PM_{carbon,c}[ppm_v] = \frac{0.8\,(PM_c - PM_b)}{10^6} \times \frac{0.008314\times(T_d+273.15)}{12\times P_{atm}} \times 10^6}$$

$$\boldsymbol{PM_{carbon,c}[ppm_v] = \frac{(PM_c - PM_b)\times 0.008314\times(T_d+273.15)}{15\times P_{atm}}} \quad (45)$$

Putting it all together results in Equation 46.

$$\boldsymbol{CC_c = (CO_{2c} - CO_{2b}) + (CO_c - CO_b) + \frac{(PM_c - PM_b)\times 0.008314\times(T_{cd}+273.15)}{15\times P_{atm}}} \quad (46)$$

Total Carbon in Exhaust, CE_c (g/m^3)

It is the mass concentration of carbon in the exhaust. It is calculated by using the ideal gas law to convert the volumetric exhaust carbon concentration [ppm_v] (CC_c calculated above) to a mass concentration. In the calculation of CC_c , it is shown that the volumetric concentration [ppm_v] is related to the mass concentration (g/m^3) by the formula:

$$Conc_{carbon}[ppm_v] = Conc_{carbon}\left[\frac{g}{m^3}\right] \times \frac{0.008314 \times (T_{cd} + 273.15) \times 10^6}{12 \times P_{atm}}$$

Rearranging,

$$Conc_{carbon}\left[\frac{g}{m^3}\right] = \frac{Conc_{carbon}[ppm_v]}{\frac{0.008314 \times (T_{cd} + 273.15) \times 10^6}{12 \times P_{atm}}}$$

$$\boldsymbol{CE_c = \frac{CC_c \times 12\times P_{atm}\times 10^{-6}}{0.008314\times (T_{cd}+273.15)}} \quad (47)$$

Dry Fuel Consumed Estimated from Emissions, f_{ce} (g)

This is the estimate of dry fuel consumed based on the total carbon mass collected in the emission hood as shown in Equation 48. The total carbon mass is the product of mass concentration, CE_c and the total volume collected, V_c . $FuelFracC$ is the fuel carbon fraction.

$$\boldsymbol{f_{ce}\ [g_{fuel}] = \frac{CE_c\ \left[\frac{g_{carbon}}{m^3}\right] \times V_c\ [m^3]}{FuelFracC\left[\frac{g_{carbon}}{g_{fuel}}\right]}}$$

(48)

Hood Carbon Balance, CB_c (%)

This is the ratio of carbon collected in the emission hood to carbon consumed. The carbon balance is equivalent to the ratio of burned fuel collected in the emission hood to fuel consumed.

$$Carbon\ Balance = \frac{carbon\ emission\ collected}{total\ carbon\ consumed}$$

$$= \frac{(dry\ fuel\ collected\ in\ emission) \times (carbon\ fraction\ of\ fuel)}{(dry\ fuel\ \ consumed) \times (carbon\ fraction\ of\ fuel)}$$

$$= \frac{dry\ fuel\ collected\ in\ emissions}{dry\ fuel\ \ consumed} \qquad (49)$$

The dry fuel collected in the emissions is the quantity, f_{ce} calculated in Equation 48. The dry fuel consumed is determined by weighing the fuel and char before and after the test period. The dry fuel consumed is the moist fuel consumed minus the mass of moisture in the fuel minus the mass of fuel remaining in the form of char as shown in Equation 50.

$$dry\ fuel\ \ consumed = f_{cm}(1 - MC_{wet}) - \frac{\Delta C_c \times CharFracC}{FuelFracC} \qquad (50)$$

Thus:

$$\boldsymbol{CB_c = \frac{f_{ce}}{f_{cm}(1 - MC_{wet}) - \frac{\Delta C_c \times CharFracC}{FuelFracC}}} \qquad (51)$$

The value of CB_c is formatted as a percent in WBT_data-calclulation_sheet_4.2.3.xls (Aprovecho Research Center, 2020). The carbon balance indicates what fraction of the stove emissions are captured by the hood.

CO_2 emission Factor, $EF_{CO_{2c}}$ (g/ kg)

This is the average grams of CO_2 emitted per kilogram of fuel burned. It is calculated from the ratio of CO_2 concentration to carbon concentration as shown in Equation 52.

$$\frac{\boldsymbol{Conc_{CO_2}\,[ppm_v]}}{\boldsymbol{Conc_{Carbon}\,[ppm_v]}} = \frac{(\boldsymbol{CO_{2c} - CO_{2b}})}{\boldsymbol{CC_c}} \tag{52}$$

$$\boldsymbol{Conc_{Carbon}\,[ppm_v]} = \frac{\boldsymbol{n_{gas}}}{\boldsymbol{n_{Total}}} \times \boldsymbol{10^6} \tag{53}$$

Hence, the volumetric concentration ratio of two gases is equivalent to the molar ratio as shown in Equation 54.

$$\frac{Conc_{CO_2}\,[ppm_v]}{Conc_{carbon}\,[ppm_v]} = \frac{\frac{n_{CO_2}}{n_{Total}}\times 10^6}{\frac{n_{Carbon}}{n_{Total}}\times 10^6} = \frac{n_{CO_{2c}}}{n_{carbon,c}} \tag{54}$$

From Equation 54, the moles of CO_2, $n_{CO_{2c}}$ is converted to grams of CO_2, m_{CO_2} as shown in Equation 55. The moles of carbon, $n_{carbon,c}$ is converted to kilograms of fuel, m_{fuel} as shown in Equation 56.

$$m_{CO_2}\left[g_{CO_2}\right] = n_{CO_{2c}}\left[mol_{CO_2}\right] \times \frac{44\,[g_{CO_2}]}{1\,[mol_{CO_2}]} \tag{55}$$

$$m_{fuel}\,[kg] = n_{carbon,c}\,[mol_{carbon}] \times \frac{12\,[g_{carbon}]}{1\,[mol_{carbon}]} \times \frac{1\,[g_{fuel}]}{FuelFracC\,[g_{carbon}]} \times \frac{1\,[kg_{fuel}]}{1000\,[g_{fuel}]} \tag{56}$$

Putting it all together:

$$EF_{CO_{2c}}\frac{[g_{CO_2}]}{[kg_{fuel}]} = \frac{m_{CO_2}\,[g_{CO_2}]}{m_{fuel}\,[kg]}$$

$$= \frac{n_{CO_{2c}}\,[mol_{CO_2}]\times 44\left[\frac{g_{CO_2}}{mol_{CO_2}}\right]}{n_{carbon,c}\,[mol_{carbon}]\times 12\left[\frac{g_{carbon}}{mol_{carbon}}\right]\times\frac{1\,[g_{fuel}]}{FuelFracC\,[g_{carbon}]}\times\frac{1\,[kg_{fuel}]}{1000\,[g_{fuel}]}} \tag{57}$$

From Equation 52 and 54,

$$\frac{n_{CO_{2c}}\,[mol_{CO_2}]}{n_{carbon,c}\,[mol_{carbon}]} = \frac{(CO_{2c} - CO_{2b})}{CC_c} \tag{58}$$

Hence:

$$EF_{CO_{2c}} = \frac{(CO_{2c} - CO_{2b})}{CC_c} \times \frac{44}{12} \times FuelFracC \times 1000 \tag{59}$$

CO Emission Factor,EF_{COc} (g/ kg)

This is the average grams of CO emitted per kilogram of fuel burned calculated as shown in Equation 60.

$$EF_{CO_c} = \frac{(CO_c - CO_b)}{CC_c} \times \frac{28}{12} \times FuelFracC \times 1000 \quad (60)$$

Particulate Matter emission Factor, EF_{PM_c} (mg/ kg)

This is the average grams of PM emitted per kilogram of fuel burned. The PM concentration is a mass concentration with units $\mu g/m^3$. If the ratio of the mass concentration of PM to the mass concentration of carbon is considered, then:

$$\frac{(PM_c - PM_b)\left[\frac{\mu g_{PM}}{m^3_{air}}\right]}{CE_c\left[\frac{g_{carbon}}{m^3_{air}}\right]} = \frac{(PM_c - PM_b)}{CE_c}\left[\frac{\mu g_{PM}}{g_{carbon}}\right] \quad (61)$$

The numerator of Equation 61 can be converted from micrograms to grams of PM as shown in Equation 62.

$$m_{PM}\,[g_{PM}] = \frac{m_{PM}\,[\mu g_{PM}]}{1\,000\,000\left[\frac{\mu g_{PM}}{g_{PM}}\right]} \quad (62)$$

The denominator of Equation 61 can be converted from grams of carbon to kilograms as shown in Equation 63.

$$m_{fuel}\left[kg_{fuel}\right] = \frac{m_{carbon}\,[g_{carbon}]}{FuelFracC\left[\frac{g_{carbon}}{g_{fuel}}\right]\times 1000\left[\frac{g_{fuel}}{kg_{fuel}}\right]} \quad (63)$$

Putting it all together results in Equation 64:

$$EF_{PM_c} = \frac{m_{PM}\,[g_{PM}]}{m_{fuel}\,[kg_{fuel}]} = \frac{(PM_c - PM_b)\times FuelFracC\times 1000}{CE_c\times 1\,000\,000} \quad (64)$$

CO_2 Mass Produced, $m_{CO_{2c}}$ (g)

This is the total mass of CO_2 emitted during the test phase calculated as shown in Equation 65.

$$m_{CO_{2c}} = EF_{CO_{2c}} \times \left[f_{cm}(1 - MC_{wet}) - \Delta C_c \times \frac{charFracC}{fuelFracC}\right] \times \frac{1}{1000} \quad (65)$$

CO Mass Produced, m_{CO_c} (g)

This is the total mass of CO emitted during the test phase calculated as shown in Equation 66.

$$m_{CO_c} = EF_{CO_c} \times \left[f_{cm}(1 - MC_{wet}) - \Delta C_c \times \frac{CharFracC}{fuelFracC}\right] \times \frac{1}{1000} \quad (66)$$

Particulate Matter Mass Produced,m_{PM_c} (g)

This is the total mass of PM emitted during the test phase calculated as shown in Equation 67.

$$m_{PM_c} = EF_{PM_c} \times \left[f_{cm}(1 - MC_{wet}) - \Delta C_c \times \frac{CharFracC}{fuelFracC}\right] \times \frac{1}{1000} \quad (67)$$

CO_2 Emission per Water Boiled, $E_{CO_{2c}}$ (g/ L)

It is calculated as shown in Equation 68 where $m_{CO_{2c}}$ is the total mass of CO_2 emitted, and w_{cr} is the effective mass of water boiled.

$$E_{CO_{2c}}\left[\frac{g_{CO_2}}{L_{H_2O}}\right] = \frac{m_{CO_{2c}}[g_{CO_2}]}{w_{cr}[g_{H_2O}]} \times 1000 \left[\frac{g_{H_2O}}{L_{H_2O}}\right] \quad (68)$$

CO Emission per Water Boiled, E_{CO_c} (g/L)

It is obtained using Equation 69 where m_{CO_c} is the total mass of CO emitted, and w_{cr} is the effective mass of water boiled.

$$E_{CO_c}\left[\frac{g_{CO}}{L_{H_2O}}\right] = \frac{m_{CO_c}[g_{CO}]}{w_{cr}[g_{H_2O}]} \times 1000 \left[\frac{g_{H_2O}}{L_{H_2O}}\right] \quad (69)$$

Emission per Water Boiled, E_{PM_c} (g/L)

It is computed using Equation 70 where m_{PM_c} is the total mass of PM emitted, and w_{cr} is the effective mass of water boiled.

$$E_{PM_c}\left[\frac{g_{PM}}{L_{H_2O}}\right] = \frac{m_{PM_c}[g_{PM}]}{w_{cr}[g_{H_2O}]} \times 1000 \left[\frac{g_{H_2O}}{L_{H_2O}}\right] \quad (70)$$

(ii) Hot Start High Power (HSHP) phase

In this test, measurements and calculations are identical to the CSHP phase except that the char remaining is not extracted and weighed. The char remaining is assumed to be the same as the char remaining from the CSHP phase.

Fuel Consumed (Moist), f_{hm} (g)

$$f_{hm} = f_{hi} - f_{hf} \quad (71)$$

change in char during the test, ΔC_h (g)

$$\Delta C_h = \Delta C_c \quad (72)$$

mass of water vaporized, w_{hv} (g)

$$\boldsymbol{w_{hv} = P1_{hi} - P1_{hf}} \quad (73)$$

Effective mass of water boiled, w_{hr} (g)

$$\boldsymbol{w_{hr} = P1_{hf} - P1} \quad (74)$$

Time to boil, Δt_h (min)

$$\boldsymbol{\Delta t_h = t_{hf} - t_{hi}} \quad (75)$$

Temperature-Corrected Time to Boil, Δt_h^T (min)

$$\boldsymbol{\Delta t_h^T = \Delta t_h \times \frac{75}{T1_{hf} - T1_{hi}}} \quad (76)$$

Equivalent Dry Fuel Consumed, f_{hd} (g)

$$\boldsymbol{f_{hd} = \frac{f_{hm}\{LHV(1 - MC_{wet}) - MC_{wet}[4.186(T_b - T_a) + 2260]\} - \Delta C_h \times LHV_{char}}{LHV}} \quad (77)$$

Thermal efficiency, h_h (%)

$$\boldsymbol{h_h = \frac{4.186(P1_{hi} - P1)(T1_{hf} - T1_{hi}) + w_{hv} \times 2260}{f_{hd} \times LHV}} \quad (78)$$

Burning Rate, r_{hb} (g/min)

$$\boldsymbol{r_{hb} = \frac{f_{hd}}{\Delta t_h}} \quad (79)$$

Specific Fuel Consumption, SC_h (g /L)

$$\boldsymbol{SC_h = \frac{f_{hd}}{w_{hr}}} \quad (80)$$

Temperature- corrected specific fuel consumption, SC_h^T (g /L)

$$\boldsymbol{SC_h^T = SC_h \times \frac{75}{(T1_{hf} - T1_{hi})}} \quad (81)$$

Temperature- Corrected Specific Energy Consumption, SE_h^T (Kj/L)

$$\boldsymbol{SE_h^T = SC_h^T \times \frac{LHV}{1000}} \quad (82)$$

Firepower, FP_h (W)

$$\boldsymbol{FP_h = \frac{f_{hd} \times LHV}{\Delta t_h \times 60}} \quad (83)$$

Total exhaust flow, V_h (m^3)

$$\boldsymbol{V_h = Q \times \frac{\Delta t_h}{60}} \quad (84)$$

Exhaust Carbon Concentration, CC_h (ppm)

$$\boldsymbol{CC_h = (CO_{2h} - CO_{2b}) + (CO_h - CO_b) + \frac{(PM_h - PM_b) \times 0.008314 \times (T_{hd} + 273.15)}{15 \times P_{atm}}} \quad (85)$$

Total Carbon in Exhaust, CE_h (g/m^3)

$$\boldsymbol{CE_h = \frac{CC_h \times 12 \times P_{atm} \times 10^{-6}}{0.008314 \times (T_{hd} + 273.15)}} \quad (86)$$

Dry Fuel Consumed Estimated from Emissions, f_{he} (g)

$$\boldsymbol{f_{he} = \frac{C_h \times V_h}{FuelFracC}} \quad (87)$$

Hood Carbon Balance, CB_h (%)

$$\boldsymbol{CB_h = \frac{f_{he}}{f_{hm}(1 - MC_{wet}) - \frac{\Delta C_h \times CharFracC}{FuelFracC}}} \quad (88)$$

CO_2 Emission Factor, $EF_{CO_{2h}}$ (g/ g)

$$EF_{CO_{2h}} = \frac{(CO_{2h} - CO_{2b})}{CC_h} \times \frac{44}{12} \times FuelFracC \times 1000 \quad (89)$$

CO Emission Factor,EF_{CO_h} (g/ g)

$$EF_{CO_h} = \frac{(CO_h - CO_b)}{CC_h} \times \frac{28}{12} \times FuelFracC \times 1000 \quad (90)$$

PM Emission Factor, EF_{PM_h} (g/ g)

$$EF_{PM_h} = \frac{(PM_h - PM_b) \times FuelFracC \times 1000}{CE_h \times 1{,}000{,}000} \quad (91)$$

CO_2 Mass Produced, $m_{CO_{2h}}$ (g)

$$m_{CO_{2h}} = EF_{CO_{2h}} \times \left[f_{hm}(1 - MC_{wet}) - \Delta C_h \times \frac{CharFracC}{fuelFracC} \right] \times \frac{1}{1000} \quad (92)$$

CO Mass Produced, m_{CO_h} (g)

$$m_{CO_h} = EF_{CO_h} \times \left[f_{hm}(1 - MC_{wet}) - \Delta C_h \times \frac{CharFracC}{fuelFracC}\right] \times \frac{1}{1000} \quad (93)$$

Particulate Matter Mass Produced,$m_{PM,h}$ (g)

$$m_{PM,h} = EF_{PM,h} \times \left[f_{hm}(1 - MC_{wet}) - \Delta C_h \times \frac{CharFracC}{fuelFracC}\right] \times \frac{1}{1000} \quad (94)$$

CO_2 Emission per Water Boiled, $E_{CO_{2h}}$ (g/ L)

$$E_{CO_{2h}} = \frac{m_{CO_{2h}}}{w_{hr}} \times 1000 \quad (95)$$

CO Emission per Water Boiled, E_{CO_h} (g/ L)

$$E_{CO_h} = \frac{m_{CO_h}}{w_{hr}} \times 1000 \quad (96)$$

Particulate Matter Emission per Water Boiled, E_{PM_h} (g/ L)

$$E_{PM_h} = \frac{m_{PM_h}}{w_{hr}} \times 1000 \quad (97)$$

(iii) Variables For Low Power (Simmering) Phase

The assumption made in this test is based on the amount of char present at the start of the Simmer phase. At the end of the HSHP phase, when the water comes to a boil, it is quickly weighed without disturbing the char and then the fire is tended to maintain the water within a few degrees of boiling for 45 min. There will be char remaining in the stove from the wood that was used to bring the water to a boil during the Hot Start. Removing that char from the stove, weighing it, and relighting it disturbs the fire and may result in the water temperature dropping too far below boiling. Therefore, the recommended procedure is to assume that the char present at the start of the Simmer phase is the same as the char that was measured after the CSHP test (ΔC_c). While this is not entirely accurate, the error introduced by this assumption should be minimal – especially if the tester(s) followed an identical procedure in the CSHP and HSHP phases.

Fuel Consumed (Moist), f_{sm} (g)

$$f_{sm} = f_{si} - f_{sf} \quad (98)$$

Change in Char during the Test, ΔC_s (g)

$$\Delta C_s = C_s - k \quad (99)$$

Mass of Water Vaporized, w_{sv} (g)

$$w_{sv} = P1_{si} - P1_{sf} \quad (100)$$

Effective Mass of Water Simmered, w_{sr} (g)

$$w_{sr} = P1_{sf} - P1 \quad (101)$$

Time to Boil, Δt_s (min)

$$\Delta t_s = t_{sf} - t_{si} \quad (102)$$

Equivalent Dry Fuel Consumed, f_{sd} (g)

$$f_{sd} = \frac{f_{sm}\{LHV(1-MC_{wet}) - MC_{wet}[4.186(T_b - T_a) + 2260]\} - \Delta C_s \times LHV_{char}}{LHV} \quad (103)$$

Thermal Efficiency, h_s (%)

$$h_s = \frac{4.186(T1_{sf} - T1_{si})(P1_{si} - P1 + w_{sr})/2 + w_{sv} \times 2260}{f_{sd} \times LHV} \quad (104)$$

The thermal efficiency should not be used to evaluate the Low power stove performance. Instead, the Turn down ratio and the IWA Low power specific fuel consumption should be used.

Burning Rate, r_{sb} (g/min)

$$r_{sb} = \frac{f_{sd}}{\Delta t_s} \quad (105)$$

Specific Fuel Consumption, SC_s (g /L)

$$SC_s = \frac{f_{sd}}{w_{sr}} \quad (106)$$

The specific consumption in the Simmer phase (SC_s) indicates the mass of fuel required to maintain each litre (or kilo) of water three degrees below boiling temperature. The same is true for other indicators, like burning rate and firepower.

Specific Energy Consumption, (kJ /L)

$$SE_s = SC_S \times \frac{LHV}{1000} \quad (107)$$

Firepower, FP_s (W)

$$\boldsymbol{FP_s = \frac{f_{sd} \times LHV}{\Delta t_s \times 60}} \quad (108)$$

Turn Down Ratio, TDR

This is the ratio of average High firepower, FP_c to average Low firepower, FP_s as shown in Equation 109. It represents the degree to which the firepower of the stove can be controlled by the user.

$$TDR = \frac{FP_c}{FP_s} \quad (109)$$

Total Exhaust Flow, V_s (m^3)

$$\boldsymbol{V_s = Q \times \frac{\Delta t_s}{60}} \quad (110)$$

Exhaust Carbon Concentration, CC_s (ppm)

$$\boldsymbol{CC_s = (CO_{2s} - CO_{2b}) + (CO_s - CO_b) + \frac{(PM_s - PM_b) \times 0.008314 \times (T_{sd} + 273.15)}{15 \times P_{atm}}} \quad (111)$$

Total Carbon in Exhaust, CE_s (g/m^3)

$$\boldsymbol{CE_s = \frac{CC_s \times 12 \times P_{atm} \times 10^{-6}}{0.008314 \times (T_{sd} + 273.15)}} \quad (112)$$

Dry Fuel Consumed Estimated from Emissions, f_{se} (g)

$$\boldsymbol{f_{se} = \frac{C_s \times V_s}{FuelFracC}} \quad (113)$$

Hood Carbon Balance, CB_s (%)

$$\boldsymbol{CB_s = \frac{f_{se}}{f_{sm}(1 - MC_{wet}) - \frac{\Delta C_s \times CharFracC}{FuelFracC}}} \quad (114)$$

CO_2 Emission Factor, $EF_{CO_{2s}}$ (g/ g)

$$EF_{CO_{2s}} = \frac{(CO_{2s} - CO_{2b})}{CC_s} \times \frac{44}{12} \times FuelFracC \times 1000 \quad (115)$$

CO Emission Factor, EF_{CO_s} (g/ g)

$$EF_{CO_s} = \frac{(CO_s - CO_b)}{CC_s} \times \frac{28}{12} \times FuelFracC \times 1000 \quad (116)$$

PM Emission Factor, EF_{PM_s} (g/ g)

$$EF_{PM_s} = \frac{(PM_s - PM_b) \times FuelFracC \times 1000}{C_s \times 1{,}000{,}000} \quad (117)$$

CO_2 Mass Produced, $m_{CO_{2s}}$ (g)

$$m_{CO_{2s}} = EF_{CO_{2s}} \times \left[f_{sm}(1 - MC_{wet}) - \Delta C_s \times \frac{charFracC}{FuelFracC} \right] \times \frac{1}{1000} \quad (118)$$

CO Mass Produced, m_{CO_s} (g)

$$m_{CO_s} = EF_{CO_s} \times \left[f_{sm}(1 - MC_{wet}) - \Delta C_s \times \frac{charFracC}{FuelFracC} \right] \times \frac{1}{1000} \quad (119)$$

Particulate Matter Mass Produced, m_{PM_s} (g)

$$m_{PM_s} = EF_{PM_s} \times \left[f_{sm}(1 - MC_{wet}) - \Delta C_s \times \frac{charFracC}{FuelFracC} \right] \times \frac{1}{1000} \quad (120)$$

CO_2 Emission per Water Simmered, $E_{CO_{2s}}$ (g/ L)

$$E_{CO_{2s}} = \frac{m_{CO_{2s}}}{w_{sr}} \times 1000 \quad (121)$$

CO Emission Per Water Simmered, E_{CO_s} (g/ L)

$$E_{CO_s} = \frac{m_{CO_s}}{w_{sr}} \times 1000 \quad (122)$$

PM Emission per Water Simmered, E_{PM_s} (g/ L)

$$E_{PM_s} = \frac{m_{PMs}}{w_{sr}} \times 1000 \quad (123)$$

(iv) International Workshop Agreement (IWA) performance metrics

High Power Thermal Efficiency (%)

If the Hot Start phase is omitted, then the Cold Start efficiency is reported as shown in Equation 124.

$$High\ power\ thermal\ efficiency = h_c \quad (124)$$

If the Hot Start phase is not omitted, then the average of the Cold Start efficiency, h_c and Hot Start efficiency, h_h is reported as shown in Equation 125.

$$High\ power\ thermal\ efficiency = \frac{h_c + h_h}{2} \quad (125)$$

Low Power Specific Fuel Consumption (MJ/min/L)

It is the energy consumed per litre of water Simmered per minute. It is calculated according to Equation126.

$$Low\ power\ specific\ fuel\ consumption = \frac{f_{sd} \times LHV}{w_{sr} \times \Delta t_s \times 1000} \quad (126)$$

High Power CO (g/MJ)

This metric is the CO emission per unit of energy delivered to the cooking pot.

$$High\ power\ CO = \frac{CO\ emission\ [g]}{Energy\ delivered\ to\ pot\ [MJ]} \quad (127)$$

$$Energy\ delivered\ to\ pot\ [MJ] = h_c \times f_{cd}[g] \times LHV\left[\frac{kJ}{Kg}\right] \times \frac{1}{1000}\left[\frac{MJ}{kJ}\right] \times \frac{1}{1000}\left[\frac{kg}{g}\right] \quad (128)$$

If the Hot Start phase is omitted, then the metric is calculated for the Cold Start.

$$High\ power\ CO = \frac{m_{CO_c} \times 1000000}{h_c \times f_{cd} \times LHV} \quad (129)$$

If the Hot Start phase is not omitted, then the metric is calculated for the Cold Start and Hot Start and the average of the two is reported.

$$High\ power\ CO = \frac{\frac{m_{CO_c} \times 1000000}{h_c \times f_{cd} \times LHV} + \frac{m_{CO_h} \times 1000000}{h_h \times f_{hd} \times LHV}}{2} = \frac{1000000}{LHV \times 2} \times \left(\frac{m_{CO_c}}{h_c \times f_{cd}} + \frac{m_{CO_h}}{h_h \times f_{hd}}\right) \quad (130)$$

High Power PM (mg/MJ)

This is the PM emission per unit of energy delivered to the cooking pot as shown in Equation 131.

$$High\ power\ PM\left[\frac{mg}{MJ}\right] = \frac{PM\ emissions\ [mg]}{Energy\ delivered\ to\ pot\ [MJ]} \quad (131)$$

If the Hot Start phase is omitted, then the metric is calculated for the Cold Start as shown in Equation 132.

$$High\ power\ PM = \frac{m_{PM_c} \times 10^9}{h_c \times f_{cd} \times LHV} \quad (132)$$

If the Hot Start phase is not omitted, then the metric is calculated for the Cold Start and Hot Start and the average of the two is reported as shown in Equation 133.

$$High\ power\ PM = \frac{\frac{m_{PM_c} \times 10^9}{h_c \times f_{cd} \times LHV} + \frac{m_{PM_h} \times 10^9}{h_h \times f_{hd} \times LHV}}{2} = \frac{10^9}{LHV \times 2} \times \left(\frac{m_{PM_c}}{h_c \times f_{cd}} + \frac{m_{PM_h}}{h_h \times f_{hd}}\right) \quad (133)$$

Low Power PM (mg/min/L)

It is the PM emission per litre of water Simmered per minute as shown in Equation 134. By normalizing for the amount of water and the time of Simmer, this metric can be used to compare stove performance even when the amount of water and length of the Simmer is different between stoves.

$$Low\ power\ PM = \frac{m_{PM_S}}{\Delta t_s \times w_{sr}} \times 1000000 \quad (134)$$

Indoor CO Emissions (g/min)

This metric reports the High Power or Low Power CO emission rate into the kitchen, whichever is greater as shown in Equation 135.

$$Indoor\ CO\ Emissions = \max(ER_{co,high}, ER_{co,low}) \quad (135)$$

If the Hot Start phase is omitted, then the High Power emission rate is calculated for the Cold Start.

$$ER_{co,high} = \frac{m_{CO,indoor,c}}{\Delta t_c} \quad (136)$$

Where, $m_{CO,indoor,c}$ is the total mass of CO emitted into the kitchen during the test period. If the Hot Start phase is not omitted, then the High Power emission rate is calculated for the Cold Start and Hot Start and the average of the two is reported as shown in Equation 137.

$$ER_{co,high} = \frac{\frac{m_{CO,indoor,c}}{\Delta t_c} + \frac{m_{CO,indoor,h}}{\Delta t_h}}{2} \quad (137)$$

The Low Power emission rate is calculated from the Simmer period.

$$ER_{co,low} = \frac{m_{CO,indoor,s}}{\Delta t_s} \quad (138)$$

For non-chimney stoves that vent 100% of emissions into the kitchen, the total mass emitted into the kitchen is equal to the total mass emitted from the stove ($m_{CO,indoor,c} = m_{CO_c}$, $m_{CO,indoor,h} = m_{CO_h}$, $m_{CO,indoor,s} = m_{CO_s}$). For other stoves that vent outdoors, the fugitive emissions into the kitchen must be measured separately from the total emissions and the formula in WBT_data-calclulation_sheet_4.2.3.xls (Aprovecho Research Center, 2020) corrected accordingly.

Indoor Particulate Matter Emissions (mg/min)

This metric reports the High Power or Low Power $PM_{2.5}$ emission rate into the kitchen, whichever is greater as shown in Equation 139.

$$Indoor\ PM\ emissions = \max(ER_{PM,high}, ER_{PM,low}) \quad (139)$$

It is computed in the same manner as the indoor CO emissions except a factor of 1000 is added to convert grams to milligrams. If the Hot Start phase is omitted, then the High Power emission rate is calculated for the Cold Start.

$$ER_{PM,high} = \frac{m_{PM,indoor,c}}{\Delta t_c} \times 1000 \quad (140)$$

Where, $m_{PM,indoor,c}$ is the total mass of PM emitted into the kitchen during the test period. If the Hot Start phase is not omitted, then the High Power emission rate is calculated for the Cold Start and Hot Start and the average of the two is reported.

$$ER_{PM,high} = \frac{\frac{m_{PM,indoor,c}}{\Delta t_c} \times 1000 + \frac{m_{PM,indoor,h}}{\Delta t_h} \times 1000}{2} \quad (141)$$

The Low Power emission rate is calculated from the Simmer period:

$$ER_{PM,low} = \frac{m_{PM,indoor,s}}{\Delta t_s} \times 1000 \quad (142)$$

For non-chimney stoves that vent 100% of emissions into the kitchen, the total mass emitted into the kitchen is equivalent to the total mass emitted from the stove ($m_{PM,indoor,c} = m_{PM_c}$, $m_{PM,indoor,h} = m_{PM_h}$, $m_{PM,indoor,s} = m_{PM_s}$). For other stoves that vent outdoors, the fugitive emissions into the kitchen must be measured separately from the total emissions and the formula in WBT_data-calclulation_sheet_4.2.3.xls (Aprovecho Research Center, 2020) corrected accordingly.

2.6 Conclusion

Binders have been used for production of briquettes in the range of 2-40%. The organic binders reported for production of briquettes are; starch, molasses, humates, slop waste, pyrolytic liquid, sulfite liquor, cow dung and soybean residue. Starch and molasses are the most common binders used. Starch is used as food while the molasses may be in limited supply from the sugarcane industry. The inorganic binders mainly used for production of briquettes are lime and clay. The inorganic binders have high ash content. In addition, some studies combine more than two binders (compound binders) in the production of briquettes. However, very few studies have been done on the production of carbonized briquettes using natural resins. The compressive strength of the briquettes is 146.5-108700 kPa while the splitting tensile strength is 17-284 kPa. The ignition agents mentioned in different studies include; molasses, elephant grass, spear grass, kerosene

(paraffin), bioethanol gel, cigarette lighter. The ignition times reported are 0.33-25 min. In addition, some of the binders also act as ignition enhancers e.g. molasses contain volatile matter which acts as ignition enhancer.

CHAPTER THREE

MATERIALS AND METHODS

3.1 Conceptual Framework

Figure 12 shows the conceptual framework followed to execute the research.

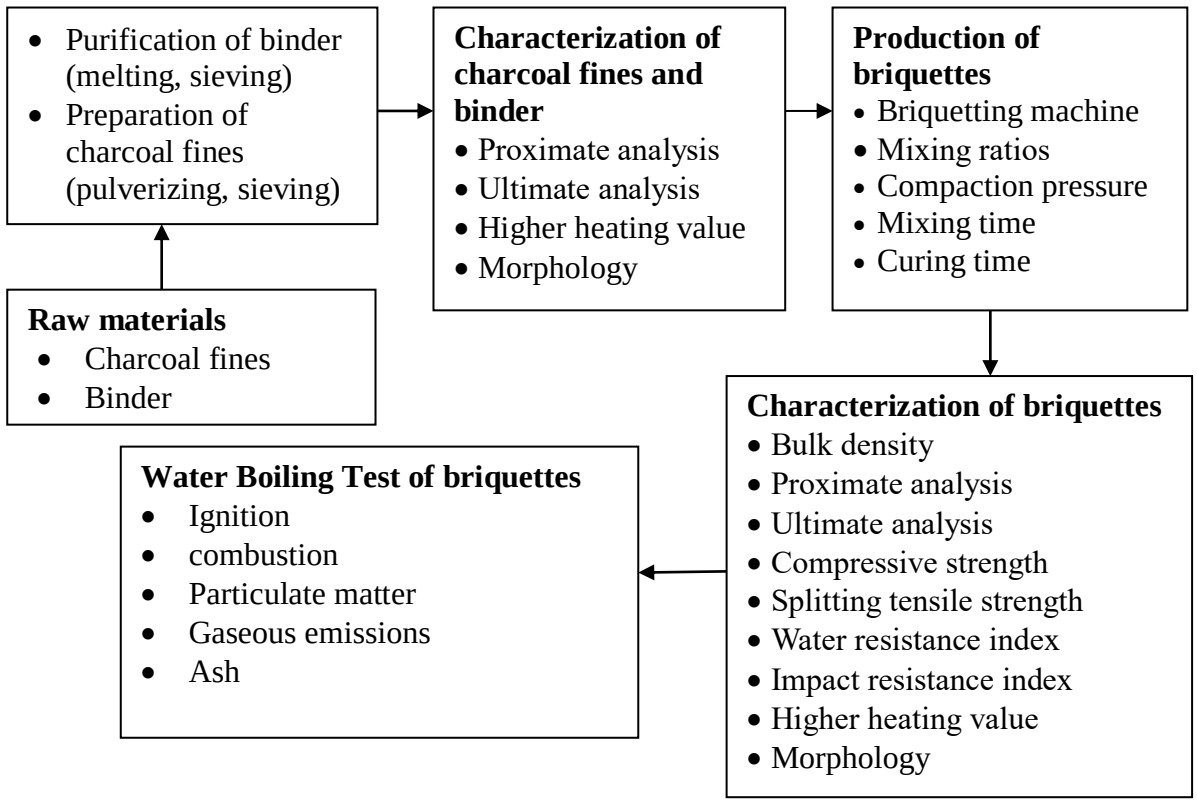

Figure 12: Conceptual framework

3.2 Purification of the *Canarium schweinfurthii* Resin (Binder)

The crude *Canarium schweinfurthii* resin mixed with impurities of bark was obtained from St. Balikuddembe (Owino) market in Kampala, Uganda. The crude resin was heated in a pan placed on a Hotplate Stirrer (Corning, PC 420D) to a boiling point of about 163°C (Appendix 1) measured with an Infrared Thermometer (Wintact, WT900). The melted crude resin was sieved with a 1.99 mm square wire mesh to remove the impurities of bark and the purified resin (gum rosin) was collected in a pan and allowed to cool to room temperature and solidify. Figure 13 shows the preparation of the binder.

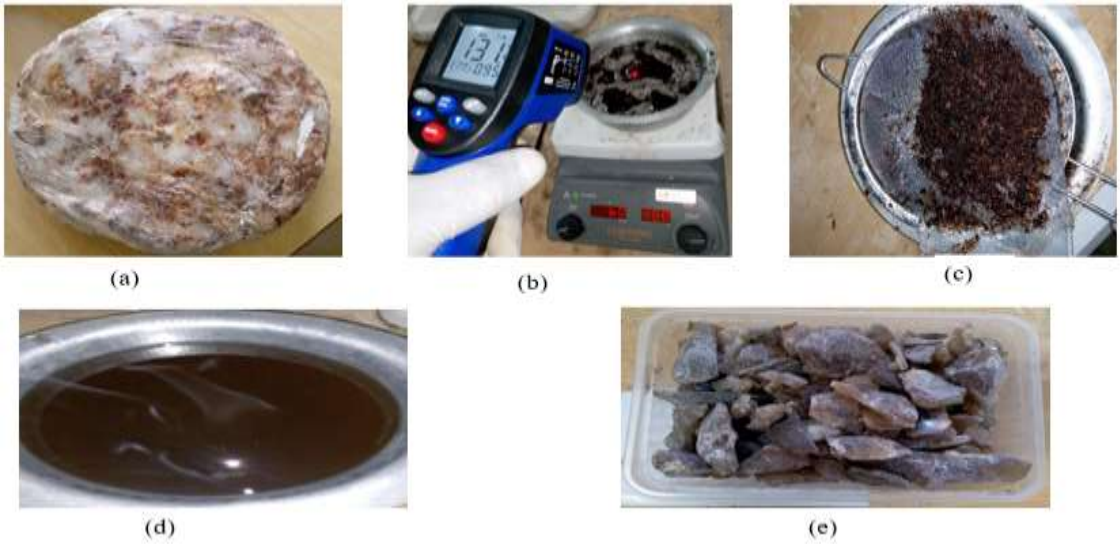

Figure 13: Binder preparation: (a) as-received, (b) melting/boiling, (c) sieving, (d) liquid binder (e) solid binder

3.3 Preparation of the Charcoal Fines

Due to poor handling, the charcoal fines (by-product of charcoal made from carbonized wood) sourced from consumers were mixed with sand making it difficult to sieve thus, lumps of wood charcoal were purchased from the retailers, pulverized, and sieved to obtain a representative sample. A sack of charcoal was obtained from Tengeru market in Arusha, Tanzania. The charcoal was pulverized using a Sealing Type Swinging Pulveriser (DXF-20D) to obtain fine particles. The ground charcoal was sieved using a 355 μm sieve placed on an Electromagnetic sieve shaker (ES-04) to obtain fines recommended for the production of high strength briquettes (Bazargan *et al*., 2014). The sieved material was stirred thoroughly to produce a homogeneous mixture. Figure 14 shows the procedure for preparation of charcoal fines.

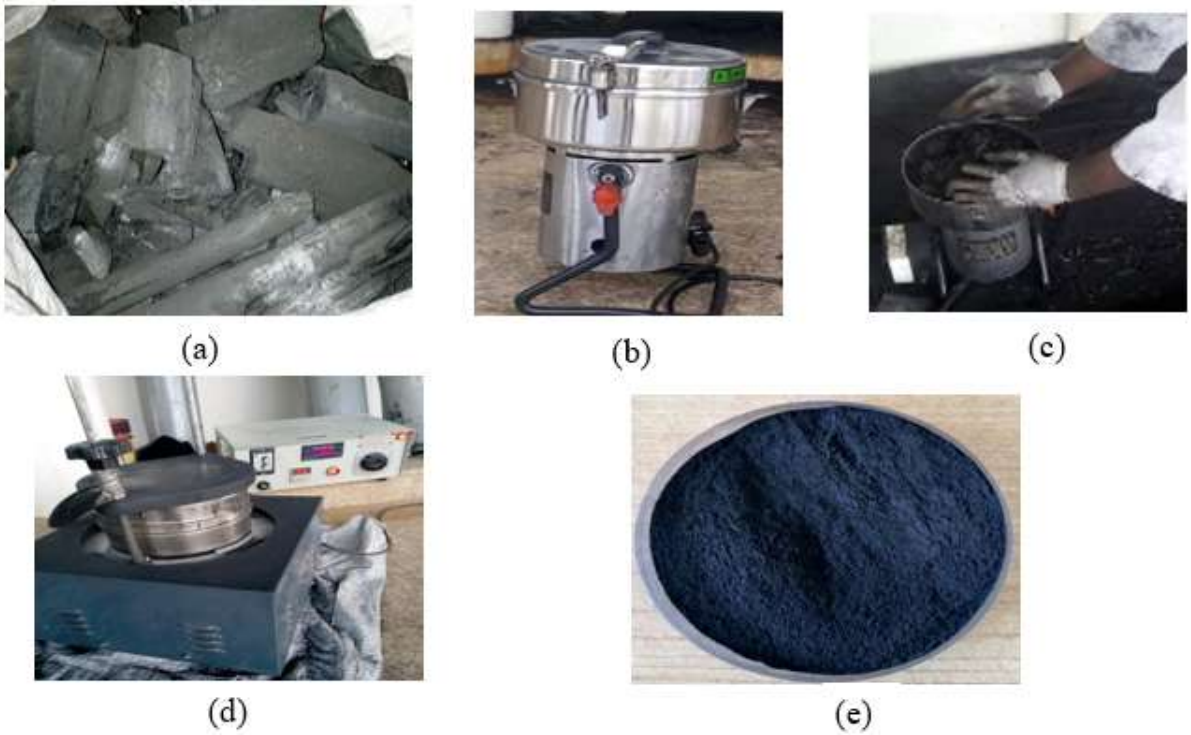

Figure 14: Preparation of charcoal fines: (a) lumps of charcoal, (b) Sealing Type Swinging Pulveriser (c) loading the lumps of charcoal in the pulveriser, (d) Electromagnetic sieve shaker, (e) charcoal fines

3.4 Characterization of Charcoal Fines and *Canarium schweinfurthii* Resin (Binder)

The equipment used for characterization is shown in Appendix 2. Proximate analysis was done using a Thermogravimetric Analyser (Eltra Thermostep) to determine the moisture, volatiles, fixed carbon, and ash content of charcoal fines and binder according to the American Society for Testing and Materials (ASTM E1131-08) standard (ASTM, 2014a). This was done in a nitrogen atmosphere followed by an oxidising atmosphere and the experiment was conducted at Nelson Mandela African Institution of Science and Technology (NM-AIST). The moisture content in the charcoal fines was classified under highly volatile matter as recommended by the ASTM E1131-08 standard (ASTM, 2014a). The TG (Thermogravimetric) and DTG (Differential Thermogravimetric) thermograms from proximate analysis were also analysed. The ultimate analysis was done at NM-AIST using the Elemental Analyser (Flash, 2000) to determine the elemental composition of the binder and charcoal fines following the ASTM D3176-15 standard (American Society for Testing and Materials [ASTM], 2015). The higher heating value (HHV) of the binder and charcoal fines was determined at NM-AIST using the Bomb Calorimeter (IKA, C2000) according to the ASTM D5865-13 standard (ASTM, 2013). Three replicates were considered. The morphology of the charcoal fines and binder was examined at Busitema University, Faculty of Engineering using Scanning Electron Microscopy (SEM) (Vega 3 Tescan). An accelerating voltage of 20.0 kV was used.

3.5 Physical and Chemical Properties of Carbonized Briquettes

3.5.1 Production of Carbonized Briquettes

The production of briquettes was conducted at NM-AIST Laboratory as shown in Fig. 15. The charcoal fines and solid binder (*Canarium Schweinfurthii* resin) were weighed using an Analytical Balance (Explorer, EX 124) with an accuracy of ± 0.0001 g. Below the binder concentration of 25 wt%, the resulting briquettes disintegrated during ejection from the die and their strength was undesirable. Above the binder concentration of 40 wt%, the produced briquettes become stronger. Moreover, it is logical to use a small quantity of binder for production of briquettes as this is economical (Sen *et al*., 2016). The binder concentrations of 25, 30, 35 and 40 wt% were considered to form four briquette samples (B25, B30, B35 and B40) with the following ratio of charcoal fines: Binder, respectively; 3:1, 7:3, 13:7, 3:2. The binder was first melted in a pan on a Hotplate Stirrer (Stuart, CB162) set at 400℃. Charcoal fines were then added and the mixture stirred manually for 4-5 min to obtain a homogeneous mixture before pouring it into the die of the briquetting machine. The pouring temperature of the mixture was 125-134℃ (Appendix 3), recorded using an Infrared Thermometer (Wintact, WT900). After pouring in the die, the mixture was compressed for 5 min (Sotannde *et al*., 2010) using a 20 ton hydraulic jack. The compaction pressure after 5 min was 5.92-7.96 MPa (Appendix 4) recorded with a Pressure Gauge (Nuoha Fina, EN887-1). The cured briquettes were then ejected from the die and stored at room temperature.

Figure 15: Production of briquettes: (a) melting binder, (b) mixing binder/charcoal fines, (c) compaction, (d) sample briquettes

3.5.2 Physical and Chemical Properties of the Carbonized Briquettes

(i) Physical Properties

Bulk Density

The mass of briquette was measured using an Analytical Balance (Explorer, EX124). The dimensions (height, outside diameter, inside diameter) of the cylindrical briquette to determine volume were measured using a Vernier Caliper (HVC01200) with an accuracy of 0.05 mm. The ASTM 2395-14 standard was followed (ASTM, 2014b). Five replicates were considered. The density, ρ (g/cm^3) was computed using Equation 143.

$$\rho = \frac{m}{\frac{\pi}{4}(d_1^2 - d_2^2)h} \quad (143)$$

where d_1-Outside diameter (cm), d_2-Inside diameter (cm), h- Height (cm), m-mass (g)

Impact Resistance Index (IRI)

The IRI was determined by repeatedly dropping the briquettes from a height of 2 m onto a tiled floor until they fractured (Bazargan *et al*., 2014). Five replicates were considered. The IRI was computed according to Equation144.

$$IRI = \frac{n_d}{n_p} \times 100 \quad (144)$$

where n_d -Average number of drops, n_p - Average number of pieces

Compressive and Splitting Tensile Strength

The dimensions (height, outside diameter, inside diameter) of the cylindrical briquette were measured using a Vernier Caliper (HVC01200) with an accuracy of 0.05 mm. The compressive and splitting tensile forces of the briquette were determined using a 300 kN (Testometric, FS300AT) and 25 kN (Testometric, M500-25) materials testing machines, following the ASTM C39/C39M-17b and ASTM C496/C496M-11 standards, respectively (ASTM, 2011, 2017). For compressive and splitting tensile forces, the flat and curved surfaces of the briquette sample, respectively were placed between horizontal metal plates of the machine as shown in Fig. 16 and Appendices 14 and 15. This was followed by applying an increasing load at a rate of 0.5 mm/min until the briquette failed by cracking or breaking. Three replicates were considered. The compressive strength (F) and splitting tensile strength (T) were calculated using Equation 145 and 146, respectively (Gilvari *et al*., 2019).

$$F = \frac{P}{\frac{\pi}{4}(d_1^2 - d_2^2)} \quad (145)$$

$$T = \frac{2P}{\pi d_1 h} \quad (146)$$

where d_1-Outside diameter (mm), d_2-Inside diameter (mm), h-Height (mm), P-Load (N)

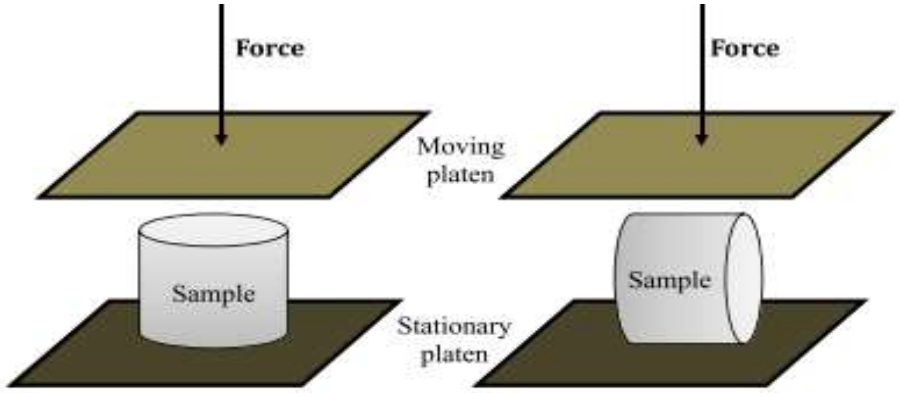

(a) (b)

Figure 16: (a) compressive strength (b) splitting tensile strength (Bazargan *et al*., 2014)

Water Resistance Index (WRI)

A weighed briquette was immersed in tap-water contained in a beaker at room temperature for 30 min (Bazargan *et al*., 2014) as shown in Fig. 17. It was then withdrawn, wiped to remove surface moisture, and reweighed. Five replicates were considered. The percentage of water absorbed was calculated using Equation 147 while the WRI was computed according to Equation 148 (Kpalo *et al*., 2020b).

$$\%water\ absorbed = \frac{w_2 - w_1}{w_1} \times 100 \quad (147)$$

Where $\boldsymbol{w}_1$- weight of briquette before immersion (g), $\boldsymbol{w}_2$- weight of briquette after immersion (g).

$$WRI = 100 - \%water\ absorbed \quad (148)$$

Figure 17: Water resistance index; briquettes immersed in water contained in a beaker

Morphology of the Briquettes

The experiment was carried out at Busitema University, Faculty of Engineering. The morphology of the briquettes was examined using SEM (Vega 3 Tescan) shown in Appendix 2d. An accelerating voltage of 20.0 kV was used.

(ii) Chemical Properties

Proximate Analysis, Ultimate Analysis, Higher Heating Value, and Energy Density

The equipment used for characterization is shown in Appendix 2. Sample briquettes were pulverized using a Planetary Ball Mill (Retsch PM100) to obtain a homogeneous mixture for proximate analysis, ultimate analysis, higher heating value, and energy density. Proximate analysis, ultimate analysis and higher heating value of the briquettes were determined using the same procedure used for characterization of the *Canarium Schweinfurthii* resin and charcoal fines. The TG and DTG thermograms from proximate analysis were also analysed. The energy density was calculated by multiplying the density with the HHV of the briquettes (Kambo & Dutta, 2014). Three replicates were considered.

3.5.3 Statistics of Proximate Analysis, Ultimate Analysis and HHV of Briquettes

The data for proximate analysis, ultimate analysis and HHV obtained from simple random sampling of the briquettes were subjected to a one-way Analysis of Variance (ANOVA) and Fisher's Least Significance Difference (LSD) using OriginPro 9 software to determine the significant differences between the various treatments of the briquettes. All significance tests in this study were conducted with $P < 0.05$. For ANOVA, the following hypothesis was tested; Null Hypothesis: The means of all levels are equal, Alternative Hypothesis: the means of one or more levels are different.

3.5.4 Effect of Binder Concentration and Compaction Pressure on Physical Properties of Briquettes

The two factors considered were binder concentration (A) and compaction pressure (B). The responses were the physical properties i.e., Bulk density (ρ), Impact resistance index (IRI), compressive strength (F), splitting tensile strength (T), and water resistance index (WRI). Design Expert software was used to analyse the effect of binder concentration and compaction pressure on physical properties of the briquettes. The experimental data for the responses was considered in three replicates.

3.6 Water Boiling Test of the Carbonized Briquettes

3.6.1 Experimental Setup

The research was carried out at the Centre for Research in Energy and Energy Conservation (CREEC), Makerere University. The experiment was conducted using the Laboratory Emission Monitroing System (LEMS) as shown in Appendix 5 and Fig. 18, according to the ISO 19867-1 standard (Aprovecho Research Center, 2018). The schematic diagram in Fig. 18 was drawn using Microsoft Visio. A blower (Dayton, 1TDU2) on the LEMS was used to push the air/exhaust through the system. The hood face velocity was less than 0.25 m/s measured with a hot wire anemometer (TPI, SP565) while the blower is running (Aprovecho Research Center, 2018).

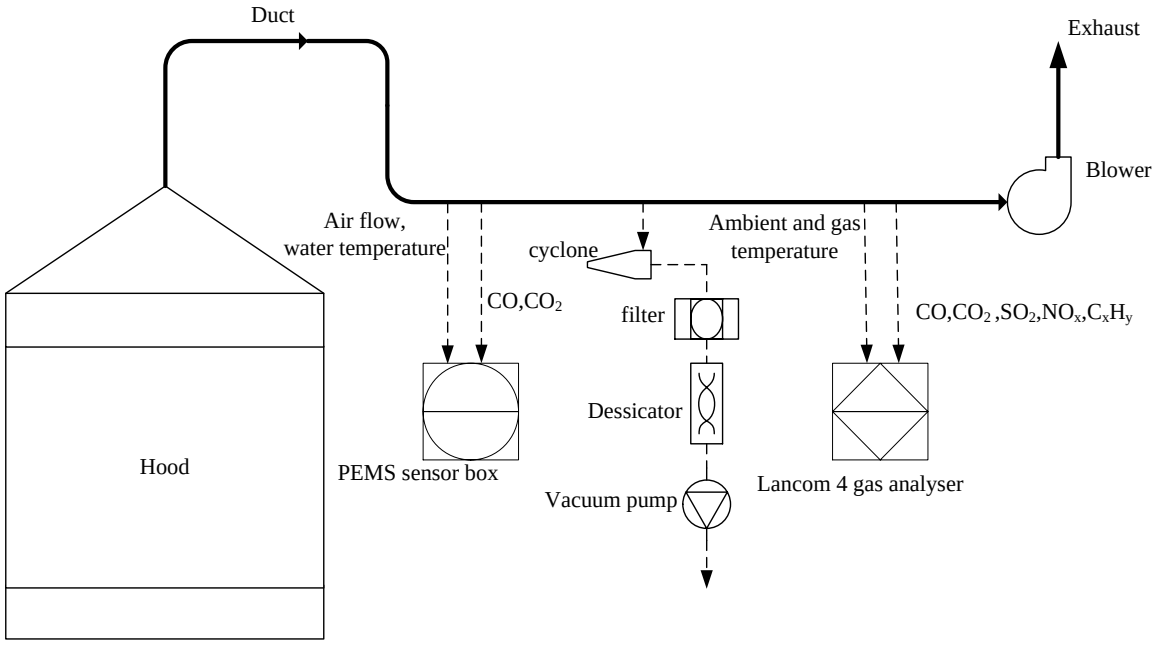

Figure 18: Schematic diagram of the Laboratory Emission Monitoring System

3.6.2 Ignition of Briquettes

A natural draft cookstove (Burn) shown in Fig. 19a was selected for the experiment and its weight measured using an electric weighing scale (Hiweigh, WPS). The four briquette samples (B25, B30, B35, B40) were placed inturn in the combustion chamber of the cookstove. Four briquettes were loaded on the cookstove. The stove was reweighed to determine the weight of the samples and placed under the hood of the LEMS. The bioethanol gel used for ignition of the briquettes was 5% of the briquette weight according to the ISO 19867-1 standard (ISO, 2018). The bioethanol gel was weighed on the ash tray of the cookstove using the electric weighing scale (Hiweigh, WPS). The ash tray with the bioethanol gel was lighted with a match and then placed into the ash chamber

of the cookstove to ignite the briquettes. Three replicates were considered and the time taken for the bioethanol gel to burn to completion was recorded as the ignition time using a stopwatch.

Figure 19: (a) Cookstove (Burn), (b) Weighing water, (c) gas analyser (PEMS, 2000) , (d) gas analyser (Ametek Land, lancom 4), (e) Filter holder, (f) Drying the filter paper, (g) furnace, (h) XRD/XRF analyser

3.6.3 Combustion

The local boiling point was determined empirically according to the WBT 4.2.3 protocol (Clean cooking alliance, 2014) and found to be 95℃ at an altitude of 1240 m (Wikipedia, 2021) were the experiment was carried out. The WBT 4.2.2 and 4.2.3 protocols were considered during the combustion experiment (Clean cooking alliance, 2014). The phases of the WBT considered were Cold Start High Power (CSHP), Hot Start High Power (HSHP) and Simmer phases. An electric weighing scale (Hiweigh, WPS) was used to measure 2.5 kg (2.5 L) of water in a pot as shown in Fig. 19b. A thermocouple (26AWG K type, chromel, Alumel) with 260 PTFE insulation was placed 5 cm from the bottom of the pot (Clean cooking alliance, 2013) to measure the temperature of the water. The thermocouple was connected to a Portable Emission Monitoring System (PEMS) sensor box (PEMS, 2000) shown in Fig. 19c and the water temperature was monitored from a computer using the PEMS software. After ignition, the pot with water was placed on the cookstove and the water temperature (T_{water}) was recorded with the PEMS software. The gas temperature (T_{gas}) and ambient temperature ($T_{ambient}$) were recorded with the gas analyser (Ametek Land, lancom 4) shown in Fig. 19d. During combustion of the briquettes, smoke, flame, soot, and ash from the burning briquettes were monitored.

3.6.4 Gaseous Emissions and Particulate Matter During the Water Boiling Test

Gaseous emissions and PM were measured during ignition, CSHP, HSHP, and Simmer phases. The gaseous emissions measured by the gas analyser (Ametek Land, Lancom 4) included CO, CO_2, SO_2, NO_x, and C_xH_y while the PEMS sensor box was used to record CO and CO_2 for evaluation of WBT performance metrics. For PM measurement, the electronic weighing scale (Citrizon, CX265) was first calibrated using a 500 mg class 1 weight (Troemner, 7026-1W). A filter paper (HI-Q, FPAE-102) was then weighed using the calibrated electronic weighing scale considering three replicates. The filter paper was placed in a filter holder (ILPH-102) shown in Fig. 19e and fixed on the LEMS. A vacuum pump (Gast, 71R655-V10-C222TX) was used to push the exhaust from the duct through the filter at a speed of 16.7 Lpm. The PM collected by the filter paper was 2.5 µm while the larger PM (>2.5 µm) was collected with a cyclone (URG-2000-30EHS). After the experiment, the filter paper was removed from the filter holder and placed in a dessicator (Igloo, FR320) as shown in Fig. 19f to absorb the moisture from the collected $PM_{2.5}$. The temperature and relative humidity inside the dessicator were monitored using a white digital indoor-outdoor temperature and humidity gauge (AcuRite, 00611A3).

After drying, the filter paper was reweighed to deterrmine the amount of $PM_{2.5}$ captured. The WBT performance metrics were analysed using the excel workbook titled WBT_data-calclulation_sheet_4.2.3.xls (Appendix 6) (Aprovecho Research Center, 2020). A sample of charcoal fines was heated in a box furnace (Cole-Parmer, CBFL516C) as shown in Fig. 19g at a temperature of 600℃ to obtain ash following the ASTM D1102 standard. The ash and charcoal fines were then sieved with a 150 µm sieve to obtain a sample which was analysed using a portable X-ray diffraction/X-ray fluorescence (XRD/XRF) analyser (Olympus, Terra II) shown in Fig. 19h to determine its chemical composition. The XRD data was analysed using XPowder software and the experiment was conducted at NM-AIST Laboratory. The XRD plots were drawn using OriginPro 9 software.

CHAPTER FOUR

RESULTS AND DISCUSSION

4.1 Characterization of the *Canarium Schweinfurthii* Resin (Binder) and Charcoal Fines

4.1.1 Thermogravimetric and Differential Thermogravimetric Thermograms from Proximate Analysis

Appendices 7, 8 show the TG and DTG data while Fig. 20a, b shows the TG and DTG thermograms for charcoal fines and binder, respectively. Figure 20c shows the temperature profile of the TG and DTG analysis. The first weight loss at around 105℃ was due to removal of the highly volatile matter as a result of dehydration in association with the degradation of thermally unstable organic constituents below 200℃ (Haykiri-Acma *et al*., 2013) and the corresponding peak on the DTG thermogram was 0.003 g/min for charcoal fines. The second weight loss for heating the sample from 105-915℃ and cooling to 750℃ was attributed to removal of medium volatile matter and the corresponding peaks on the DTG thermograms were 0.012 g/min and 0.188 g/min for charcoal fines and binder, respectively. The third weight loss for heating the sample at around 750℃ was due to char combustion as reported by Zhu *et al*. (2019) and the corresponding peak on the DTG thermogram was 0.009 g/min for charcoal fines. On the contrary, heating the binder to 915℃ resulted in complete devolatilization and there was negligible mass of the sample remaining after that temperature as shown by the TG thermogram thus, there was no char combustion. This is due to the fact that the binder contains terpenoids which are highly volatile. The residual mass was ash as reported by Wu *et al*. (2018) for the charcoal fines and negligible mass was observed for the binder as shown by the TG thermograms.

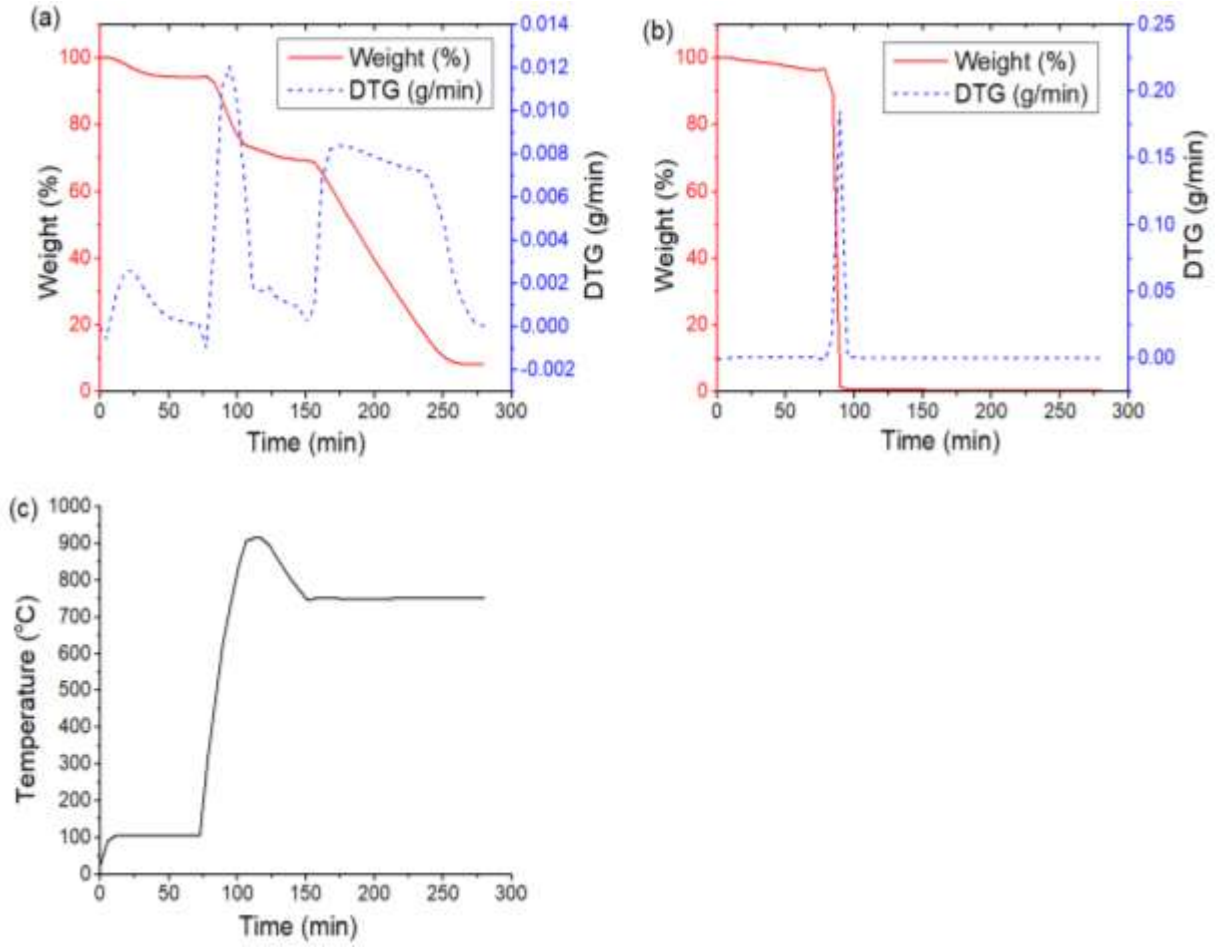

Figure 20: (a) & (b); TG and DTG thermograms for charcoal fines and binder, respectively, (c) temperature profile during TG and DTG analysis

4.1.2 Proximate Analysis of Binder and Charcoal Fines

The proximate analysis results of the charcoal fines and binder are shown in Table 4 and Appendix 9. It was observed that the charcoal fines contained a significant amount of medium volatile matter which is attributed to the inefficient local methods of pyrolysis of wood to produce charcoal. The binder had a high percentage of medium volatile matter since it contains terpenoids which are highly volatile. The zero amount of ash in the binder implies that the heating value of the binder is not affected by the ash as reported by Samadi *et al.* (2019). Hu *et al*. (2015) produced biochar pellets using organic binders (lignin and starch) and reported that the biochar pellets had higher volatile matter, but lower ash content and fixed carbon similar to this study. Pereira *et al*. (2012) also reported volatile matter in charcoal produced from six Eucalyptus clones in a laboratory kiln.

4.1.3 Ultimate Analysis, and Higher Heating Value of Binder and Charcoal Fines

The ultimate analysis, and HHV results of the charcoal fines and binder are shown in Table 4, and Appendices 10, 11. The nitrogen found in the charcoal fines is attributed to the fuel-N incorporated mainly in pyrrolic and pyridinic structures (Glarborg *et al*., 2003). The nitrogen in the *Canarium*

Schweinfurthii resin was also identified by Ameh (2018) using GC-MS. The hydrogen and oxygen in charcoal fines is attributed to the medium volatile matter in the raw material as noted from the proximate analysis. Idris *et al*. (2015) produced charcoal from oil palm biomass with a heating value of 23-25 MJ/kg while Pereira *et al*. (2012) produced charcoal from Eucalyptus clones with a heating value of 29.60-31.89 MJ/kg and these results are close to the heating value of 28.11 MJ/kg for charcoal fines obtained in this study. Zhao *et al*. (2012) reported that terpenoids are extremely flammable, with high heating value, for instance, α-pinene has a heating value of 45 MJ/kg which is close to the value of 40.17 MJ/kg obtained in this study for the *Canarium Schweinfurthii* resin containing a mixture of terpenoids.

Table 4: Proximate analysis, ultimate analysis, and HHV of binder and charcoal fines

Sample	Proximate analysis (wt %, as received)				Ultimate analysis (wt%, db*)					HHV (MJ/k)
	Highly volatile matter	Medium volatile matter	Ash	Fixed Carbon	C	H	N	O	S	
Charcoal fines	6.06	21.95	7.69	64.30	71.73	2.17	1.72	6.91	ND*	28.11
Binder	4.71	95.30	0	0	81.04	10.84	1.11	6.29	ND*	40.17

*db-dry basis

*ND-Not Detected

4.1.4 Morphology of Binder and Charcoal Fines

Figure 21a, b shows the SEM micrographs for binder and charcoal fines. Figure 21a shows that the solid binder exhibited a smooth appearance with some regions having dendrites and a pore. Figure 21b shows that the charcoal fines exhibited regions with a fibrous and porous structure (Gani & Naruse, 2007) while other regions were amorphous. This could be attributed to the volatile matter (Raju *et al*., 2014) in the charcoal fines as shown from the proximate analysis results in Table 4.

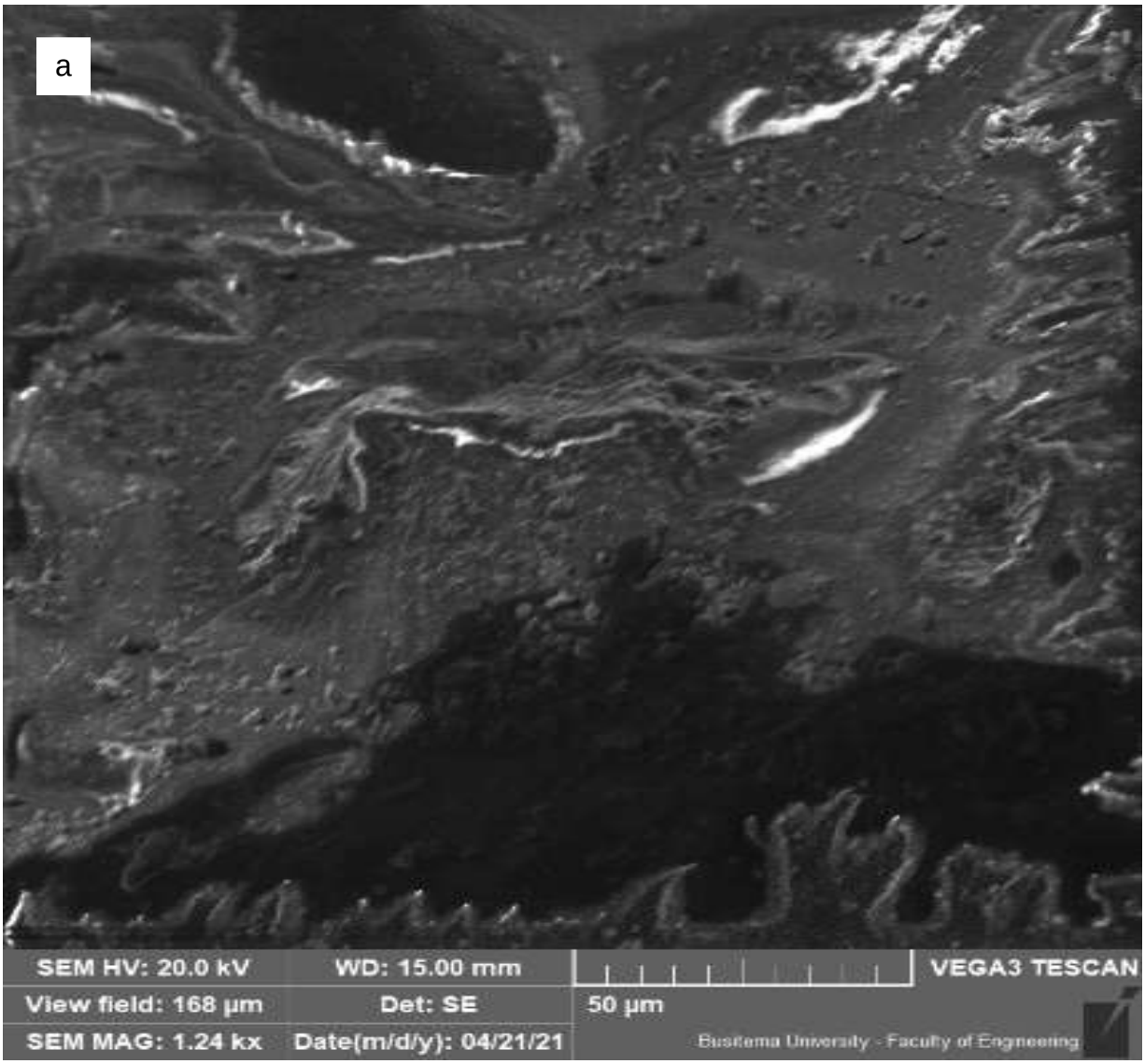
a
SEM HV: 20.0 kV
WD: 15.00 mm
VEGA3 TESCAN
View field: 168 µm
Det: SE
50 µm
SEM MAG: 1.24 kx
Date(m/d/y): 04/21/21
Bustema University - Faculty of Engineering

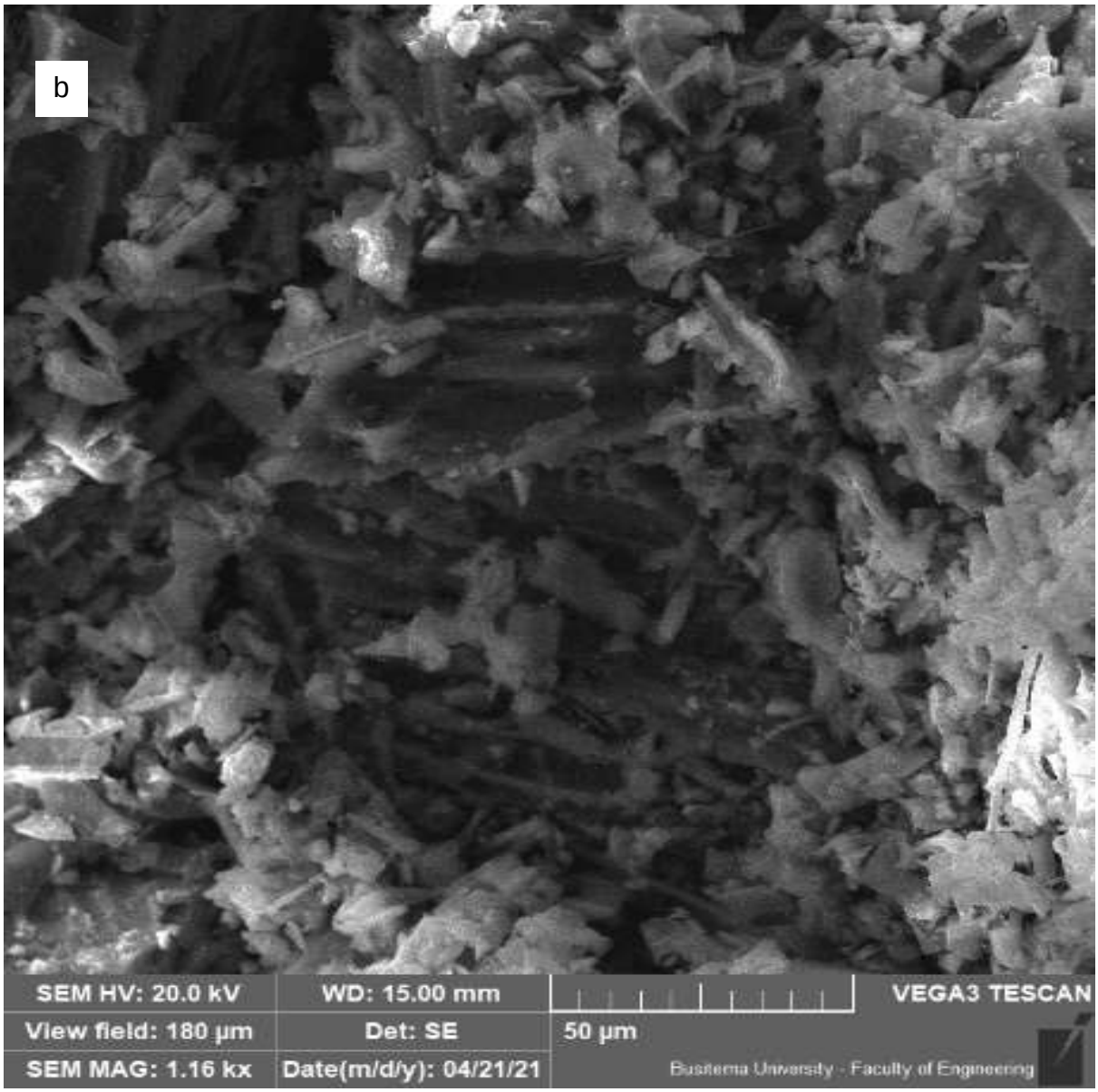

Figure 21: SEM micrographs; (a) Binder, (b) charcoal fines

4.2 Physical Properties of the Carbonized Briquettes

4.2.1 Bulk density

Appendix 12 shows the results for the outside diameter (d_1), inside diameter (d_2), height (h), volume (V), mass (m), and density ($\boldsymbol{\rho}$) of briquettes. It was observed that the bulk density increased with increasing binder concentration (Fig. 22) since the same amount of charcoal fines were used, and there was a slight increase in volume while the mass of briquette increased greatly as more binder was added (Appendix 12). The bulk density was 0.770, 0.877, 0.951, 1.036 g/cm^3 for briquettes B25, B30, B35 and B40 respectively. Kpalo *et al*. (2020a) reported that briquettes can be produced with binders with a density ≥1.0 g/cm^3. Using other binders, the density of

briquettes obtained by other researchers as detailed in Table 3 was in the range of 0.2-1.24 g/cm^3 and this is comparable to the values (0.770-1.036 g/cm^3) obtained in this study.

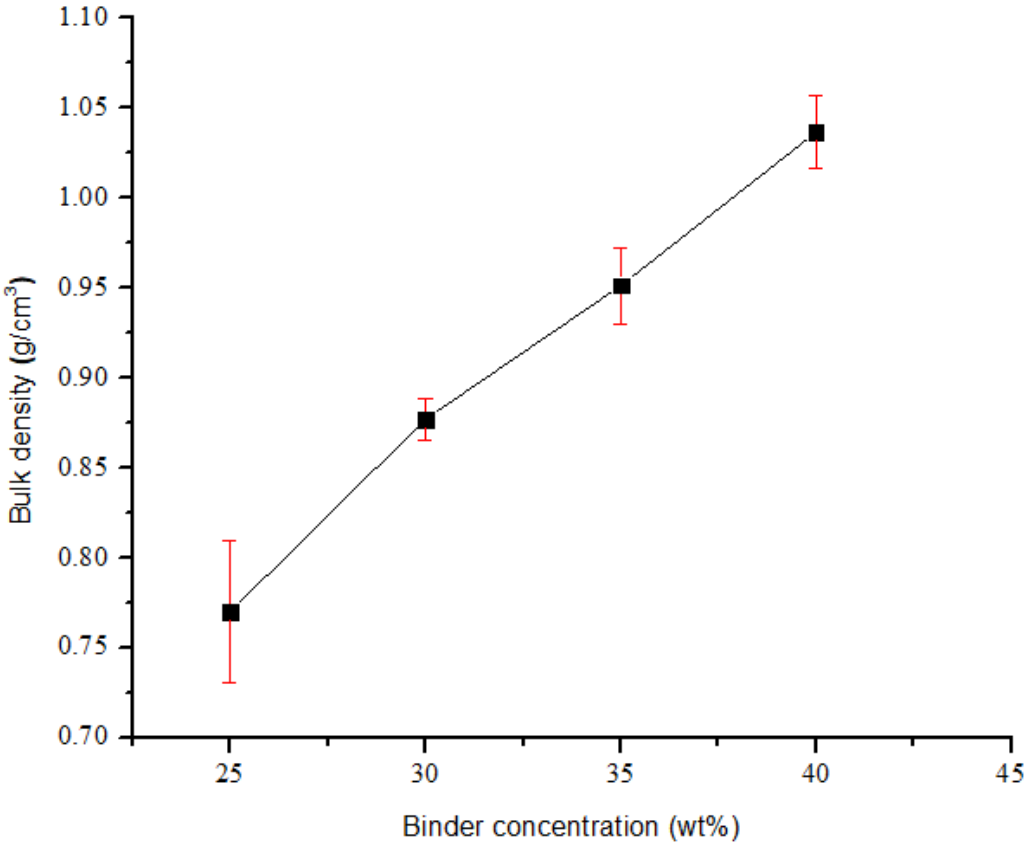

Figure 22: Bulk density versus binder concentration

4.2.2 Impact Resistance Index (IRI)

The IRI of the briquettes is shown in Fig. 23 and Appendix 13. It was observed that the IRI increased with binder concentration due to improved bond performance (Zhang *et al*., 2018). Briquette B25 broke into 30-40 pieces on the first time of impact with IRI of 2.90. Briquette B30 broke into 4-13 pieces on the first/second time of impact with IRI of 16.97. Briquettes B35 and B40 broke into 2-4 pieces on the first/second time of impact with IRI of 60.00 and 73.33, respectively. These results concurred with the findings reported previously by Sen *et al*. (2016) that as the density of the briquettes increases, the IRI also increases. Briquettes B35 and B40 passed the recommended IRI value of 50 (Bazargan *et al*., 2014).

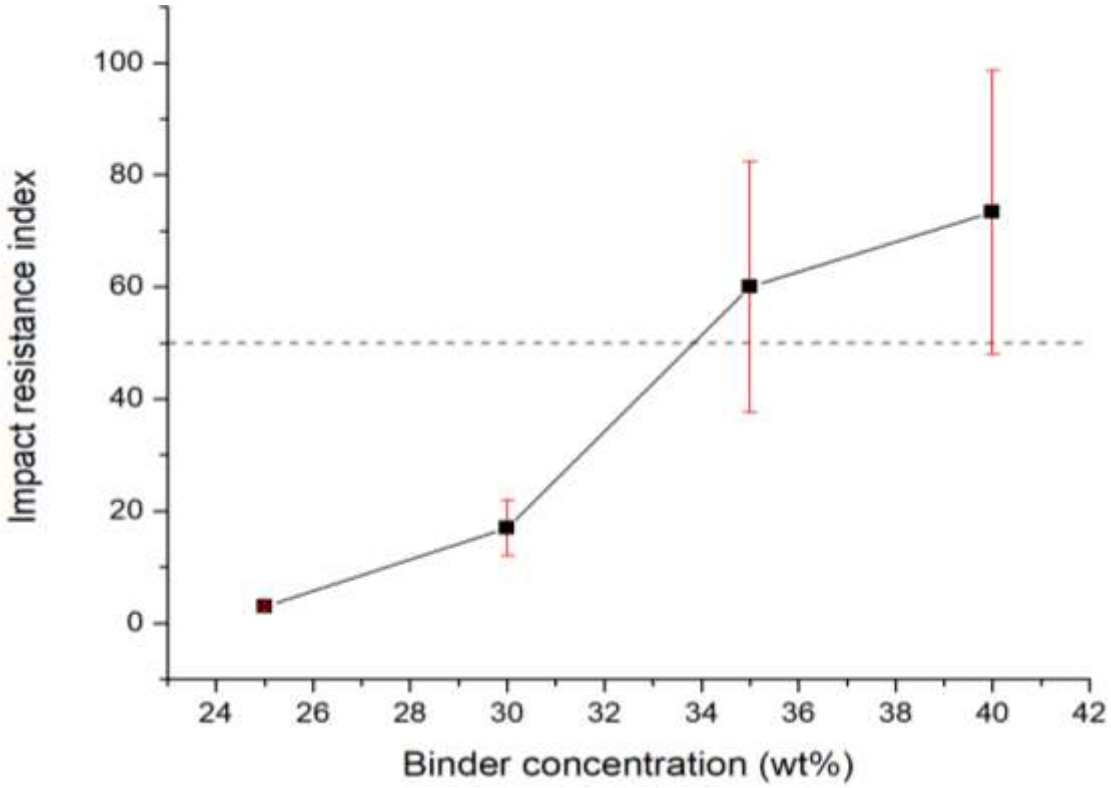

Figure 23: Impact resistance index (IRI) versus binder concentration (wt%)

4.2.3 Compressive and Splitting Tensile Strength

The compressive and splitting tensile strength results are shown in Fig. 24a, b and Appendix 14-19. The compressive strength was 2.25, 3.93, 8.06 and 10.94 MPa for briquettes B25, B30, B35 and B40, respectively. The splitting tensile strength was 0.09, 0.21, 0.32 and 0.42 MPa for briquettes B25, B30, B35 and B40, respectively. Generally, the compressive and splitting tensile strengths increased with increasing binder concentration due to improved bond performance (Zhang *et al.,* 2018). In addition, compressive strength was greater than the splitting tensile strength as reported by Gilvari *et al*. (2019). Bazargan *et al*. (2014) reported splitting tensile strengths of 0.017-0.035 MPa for briquettes with 30-40% moisture content produced using 10 wt% cassava starch as binder and those results are less than the ones (0.09-0.42 MPa) obtained in this study. According to Turkish Standard (TS)12055, Class I briquettes should have a compressive strength greater than 13 MPa, while Class II briquettes should withstand a compressive strength not lower than 10 MPa (Haykiri-Acma *et al*., 2013). Thus, briquette B40 met the Class II standard while briquette B35 was close to Class II standard. Briquettes B25 and B30 were below the TS. For compressive strength, all the briquettes met the recommended minimum value of 0.375 MPa reported for commercial charcoal briquettes (Ward *et al*., 2014).

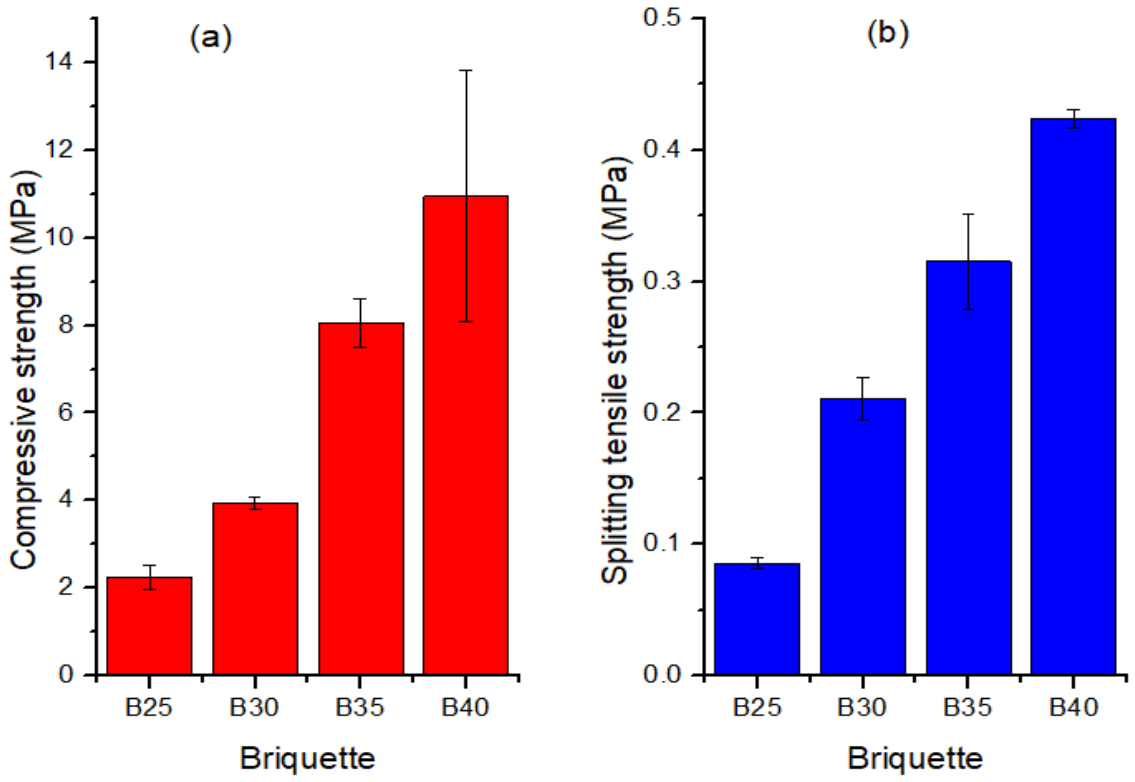

Figure 24: (a) Compressive strength, (b) splitting tensile strength

4.2.4 Water Resistance Index (WRI)

The WRI results are shown in Fig. 25 and Appendix 20. It was observed that the WRI for all the briquettes was between 99.26-99.29 % which met the recommended WRI of 95 % (Gilvari *et al*., 2019). The high WRI is attributed to the binder used which contains terpenoids that are insoluble in water. Bhattacharya *et al*. (1989) reported that *Canarium Schweinfurthii* resin is an organic binder that is hydrophobic thus, the binder coated the charcoal fines making the briquettes impervious to water. Thoms *et al*. (1999) produced cold cured anthracite/coke breeze briquettes using coal tar acid resin and the briquettes had excellent water-proofing characteristics similar to the ones in this study. Fichan *et al*. (1999) reported that at 25℃, water solubility of terpenes showed low solubility (0.037-0.22 mmol/L), whereas oxygenated monoterpenes exhibited 20 times higher solubility (2-20 mmol/L) and this agrees with the WRI results for the briquettes in this study made with *Canarium Schweinfurthii* resin containing terpenoids. Furthermore, briquettes B25 and B30 were loosely bound thus, some particles broke from the briquettes during the experiment and this could partly explain their low WRI. Bazargan *et al*. (2014) produced briquettes from palm kernel shell biochars using starch as binder and obtained a WRI below 50% implying that the briquettes were less resistant to water absorption compared to this study. Haykiri-Acma *et al*. (2013) produced biobriquettes from carbonized brown seaweed using molasses,

sulphide liquor, and linobind as binders and the WRI revealed that the times for disintegration in water were between 11-31 s which is less than the time considered in this study.

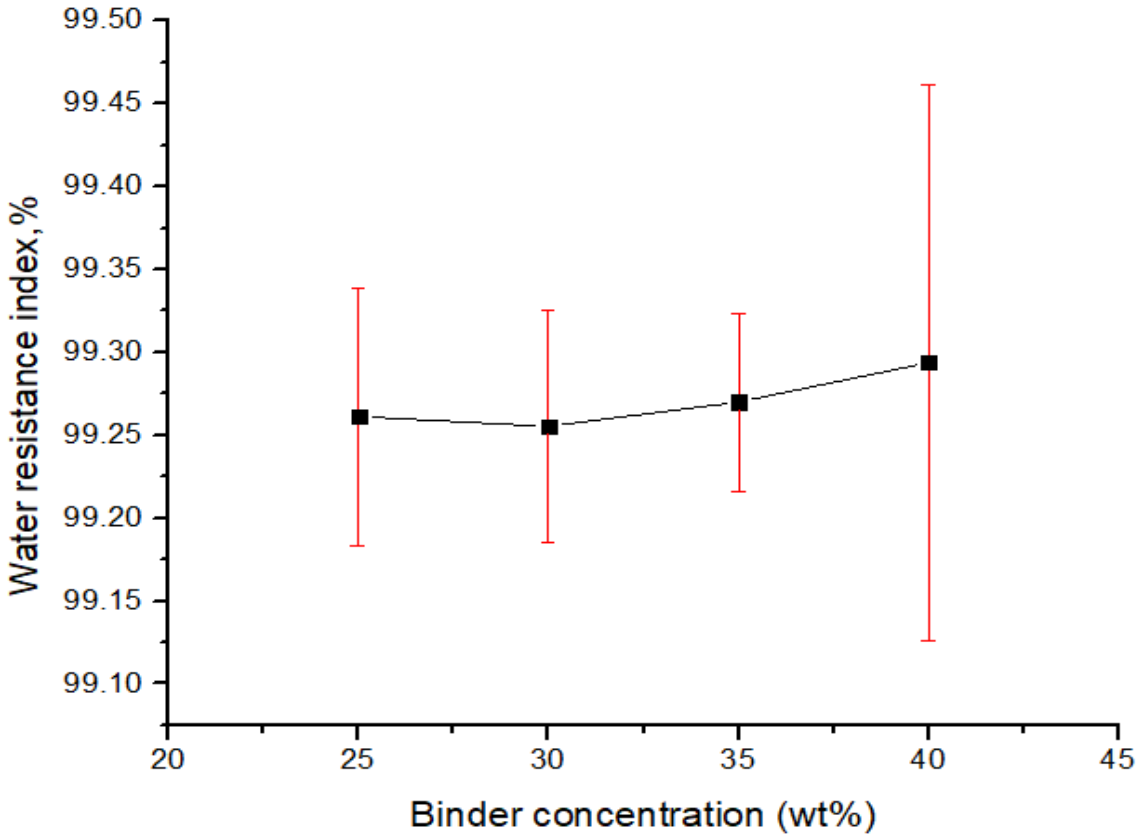

Figure 25: Water resistance index versus binder concentration

4.2.5 Morphology of Briquettes

Figure 26a-d shows the SEM micrographs for briquettes B25, B30, B35 and B40. The charcoal fines were coated with the binder during mixing. In addition, there was agglomeration of the mixture resulting in the granular appearance (Blesa *et al*., 2001). The compaction of the granules in the briquetting machine resulted in a porous structure which enhances burning efficiency of the briquettes since it provides more paths for airflow allowing more oxygen and air to circulate inside of the briquettes (Carnaje *et al*., 2018). The soaking and bridging mechanism for briquettes made from coal and binder postulates that coal particles were wetted by binder and then particles were bonded together through "binder bridge" (Zhang *et al*., 2018). The same mechanism applies to the charcoal fines and binder in this study. Huang and Hao (2012) analysed gasification briquettes prepared with Shenmu bituminous coal using SEM. The results showed that the cured binder plays a role of "bridge bond" among coal particles which applies to the briquettes in this study. Mixing of the charcoal fines with binder at high temperature and the resulting compaction at high pressure resulted in diffusion of molecules at the point of contact from one particle to another, thus forming solid bridges (Okot *et al*., 2018). Hu *et al*. (2015) reported that the bonding forces involved in the

biochar pellets densified with lignin mainly related to the attraction and cohesion forces that include hydrogen bonds, Van Der Waals forces, and mechanical interlock. Similar bonding forces are possible for briquettes produced in this study.

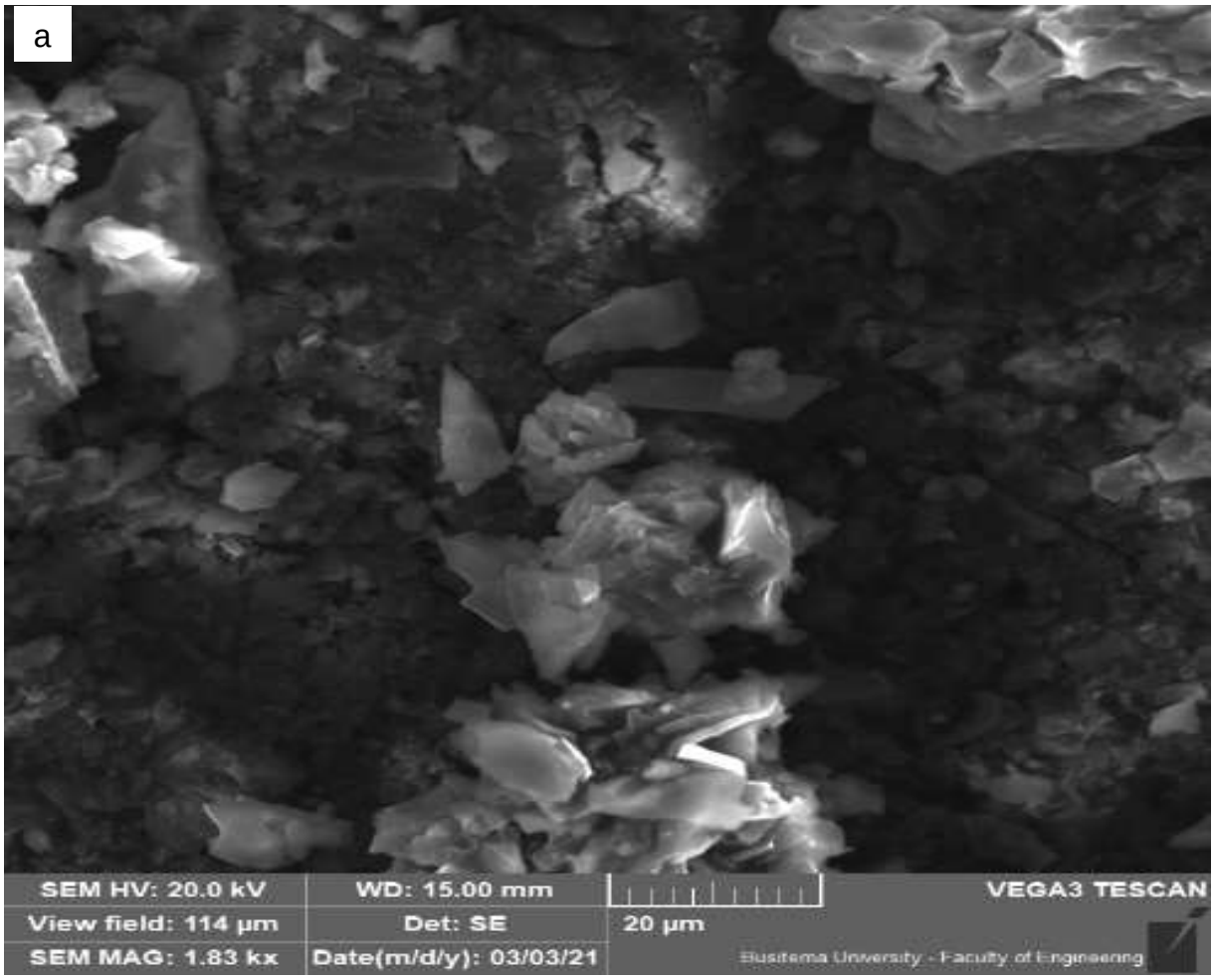

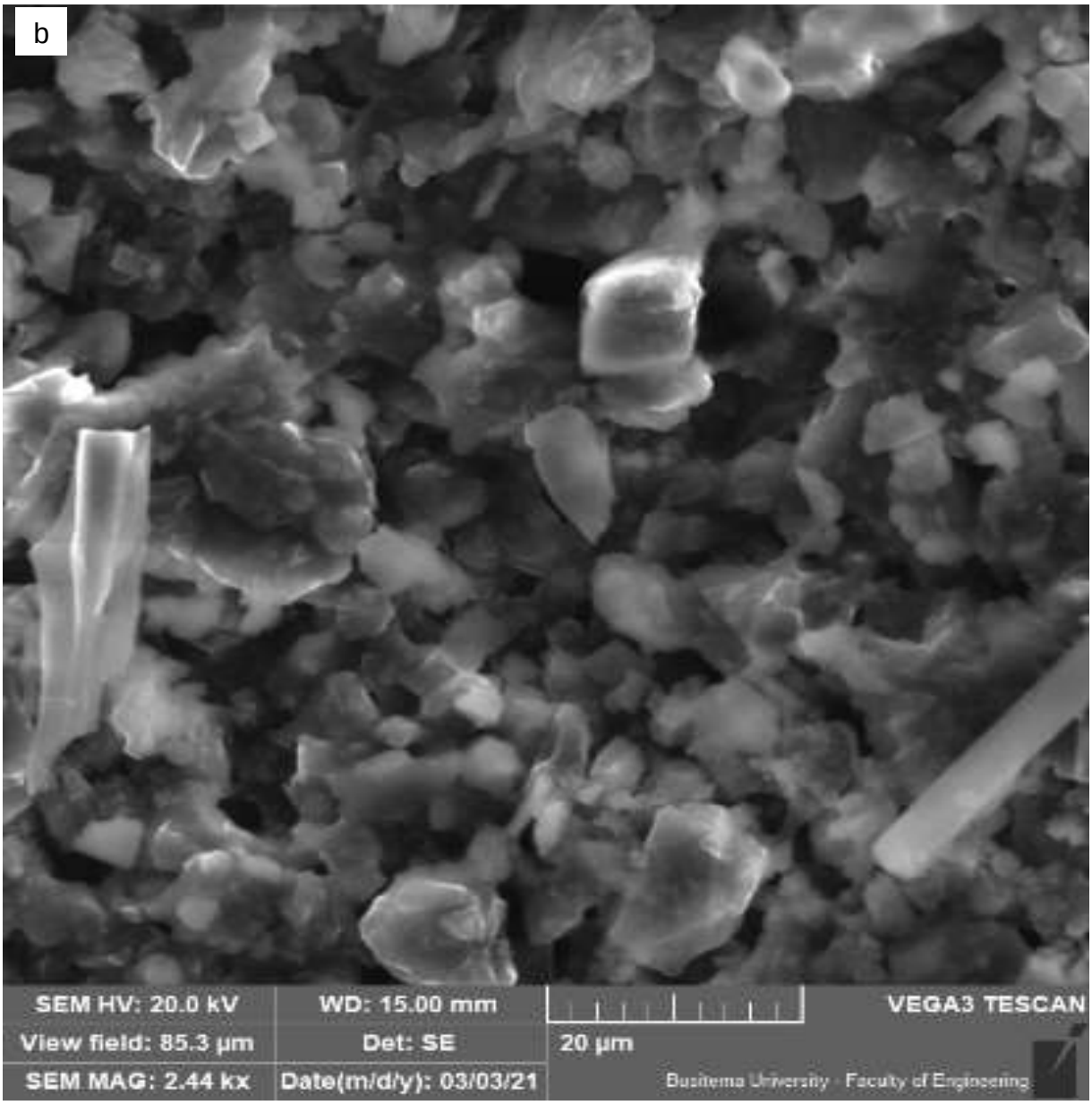
b
SEM HV: 20.0 kV
WD: 15.00 mm
VEGA3 TESCAN
View field: 85.3 µm
Det: SE
20 µm
SEM MAG: 2.44 kx
Date(m/d/y): 03/03/21
Busitema University - Faculty of Engineering

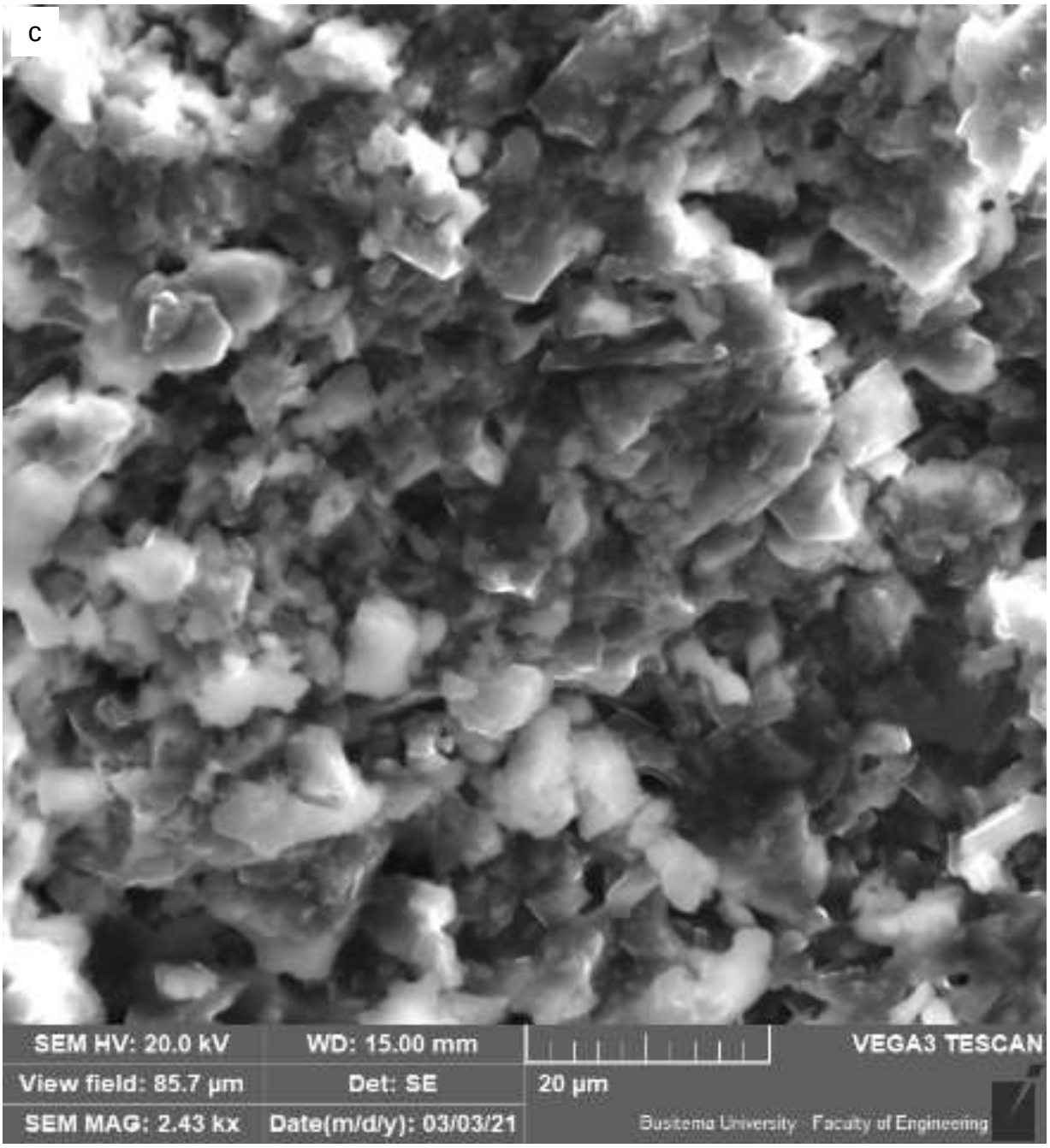
c
SEM HV: 20.0 kV
WD: 15.00 mm
VEGA3 TESCAN
View field: 85.7 µm
Det: SE
20 µm
SEM MAG: 2.43 kx
Date(m/d/y): 03/03/21
Bustema University - Faculty of Engineering

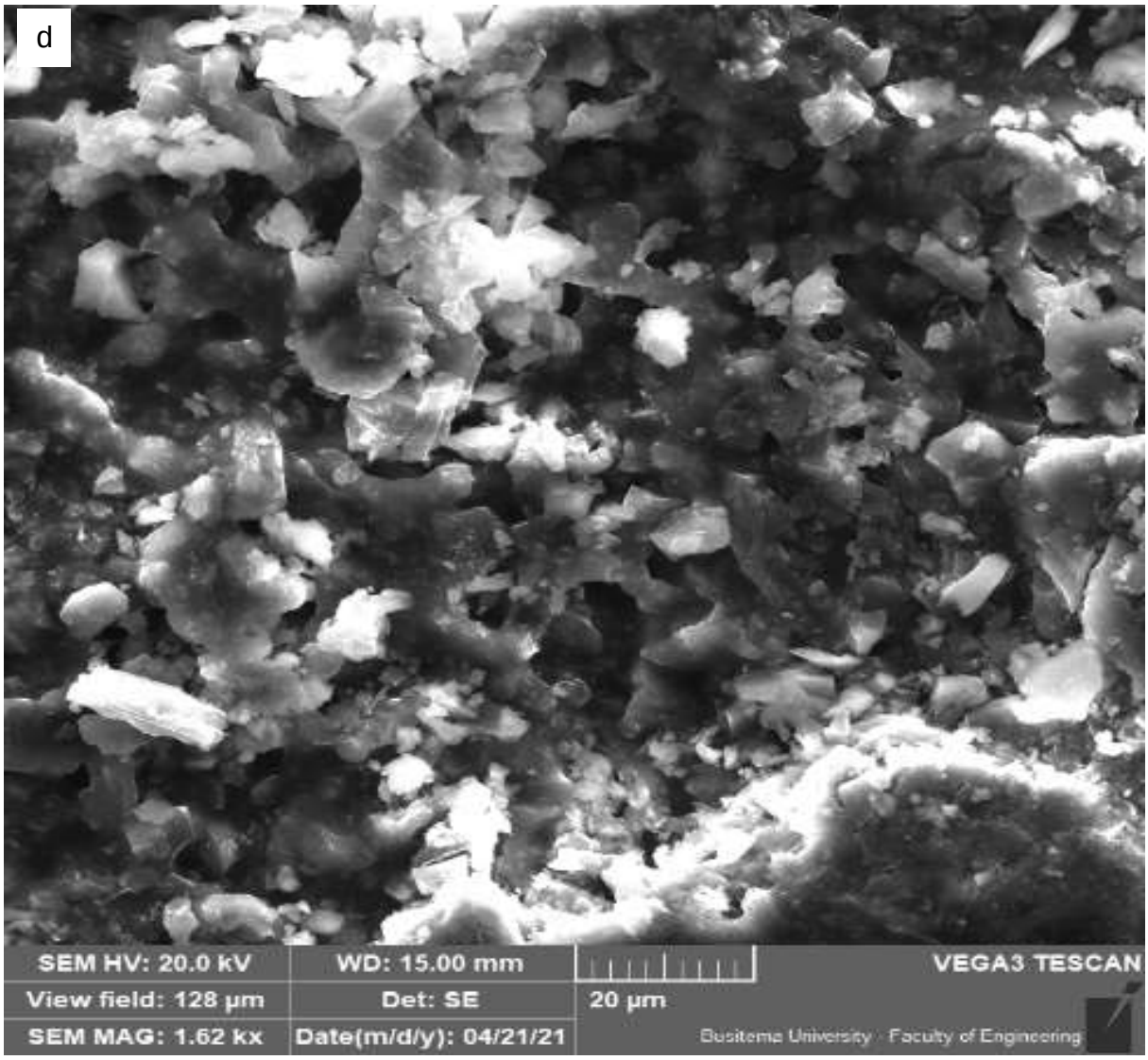

Figure 26: SEM micrographs of briquettes; (a) B25, (b) B30, (c) B35, (d) B40

4.3 Chemical Properties of the Carbonized Briquettes

4.3.1 Thermogravimetric and Differential Thermogravimetric Thermograms from Proximate Analysis

Figure 27a-d shows the TG and DTG thermograms while Appendices 21-24 show the TG and DTG data for the briquettes. The TG and DTG analysis followed the same temperature profile shown in Fig. 20c. The first weight loss at around 105℃ was due to release of the highly volatile matter (Hu *et al*., 2015) and the corresponding peaks on the DTG thermograms were 0.0025 g/min for all the briquette samples. The second weight loss on heating the sample from 105-915℃ and cooling back to 750℃ was due to release of medium volatile matter (Kivevele & Huan, 2013) and the corresponding peaks on the DTG thermograms were 0.05 g/min, 0.0425 g/min, 0.0575 g/min, 0.0775 g/min for briquettes B25, B30, B35 and B40, respectively. The third weight loss for heating the sample at around 750℃ was due to char combustion (Mitchell *et al*., 2016) and the

corresponding peaks on the DTG thermograms were approximately 0.0075 g/min for all the briquette samples. The residual mass was ash for all the briquette samples as shown in Table 6.

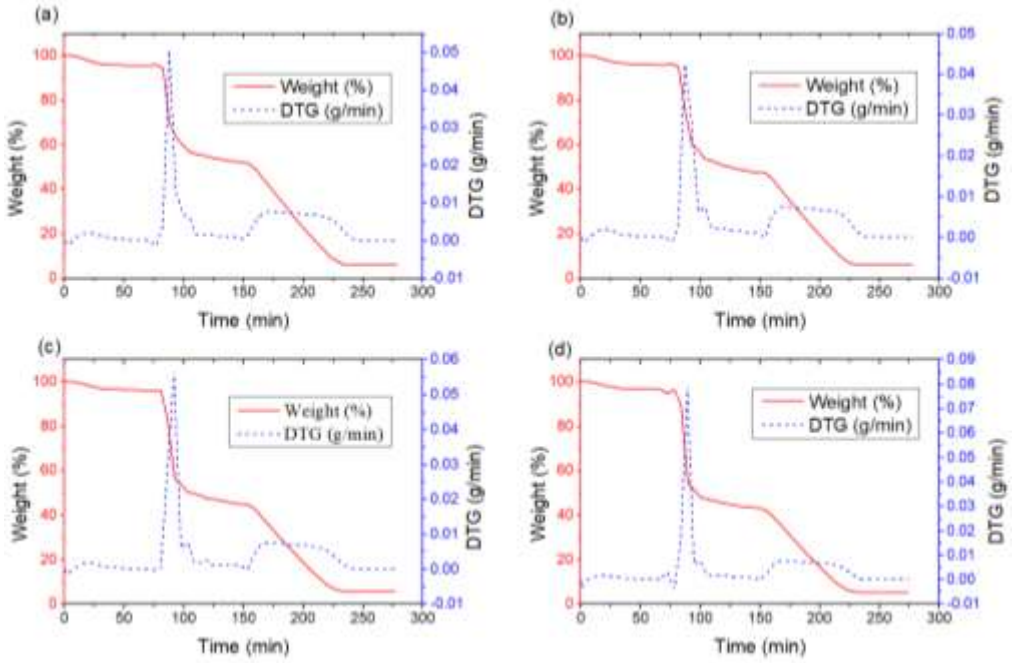

Figure 27: TG and DTG thermograms for briquettes; (a) B25, (b) B30, (c) B35, (d) B40

4.3.2 Proximate Analysis of Briquettes

Proximate analysis results of carbonized briquettes are shown in Tables 5, 6 and Appendix 25. From Table 5, ANOVA showed that there was significant difference between the means of briquette samples for all the properties. From Table 6, for highly volatile matter, LSD showed that the difference of the means was not significant for briquettes B35/B30. For medium volatile matter, LSD showed that there was significant difference between the means for all the briquette samples. The medium volatile matter increased with increasing binder concentration from B25 to B40 as a result of the binder used which contains terpenoids that are highly volatile. For fixed carbon, LSD showed that there was significant difference between the means for all the briquette samples. The amount of fixed carbon decreased with increase in the binder concentration since the binder has no fixed carbon as observed from the proximate analysis results of Table 4. For ash, LSD showed that the difference of the means was not significant for briquettes B30/B25, B35/B25, B35/B30 and B40/B35. The percentage of ash decreased slightly between the binder concentrations since the same amount of charcoal fines was used in all the experiments and the binder used does not contain ash as seen from the proximate analysis results in Table 4 thus, the combustion of the briquettes is only affected by ash from the charcoal fines as reported by Obi (2015).

4.3.3 Ultimate Analysis, Higher Heating Value, and Energy Density of Briquettes

Ultimate analysis, HHV, and energy density results of carbonized briquettes are shown in Tables 5, 6 and Appendices 26-28**.** From Table 5, ANOVA showed that there was significant difference between the means of briquette samples for all the properties except nitrogen. From Table 6, for carbon, LSD showed that the difference of the means was not significant for briquettes B30/B25, B35/B30 and B40/B35. For hydrogen, LSD showed that the difference of the means was not significant for briquettes B30/B25 and B35/B30. The percentage of carbon and hydrogen increased with binder concentration due to the terpenoids that contain a high amount of carbon and hydrogen. The nitrogen found in the briquettes is attributed to the fuel-N found in charcoal fines (Glarborg *et al*., 2003) as well as nitrogen-containing compounds in the *Canarium Schweinfurthii* resin (Ameh, 2018). For oxygen, LSD showed that the difference of the means was not significant for briquettes B30/B25, B35/B25 and B35/B30.

For heating value, LSD showed that the difference of the means was not significant for briquettes B35/B30, B40/B30 and B40/B35. The increase in binder concentration initially led to an increase in the HHV and after it remained constant. The variability in fixed carbon of feedstock has a greater impact on the HHV as compared to variability in other feedstock parameters such as volatile matter and ash content as shown in Table 6 (Samadi *et al.,* 2019). The incoherency in the results of oxygen, and nitrogen could be attributed to manually mixing the binder and charcoal fines and agglomeration of the mixture with increasing binder concentration which could have resulted in the mixture which is not homogeneous. The energy density of the briquettes was 22.83, 27.68, 29.79, 32.04 GJ/m^3 for briquettes B25, B30, B35 and B40. The energy density of the briquettes increased with increase in the binder concentration due to an increase in the bulk density of the briquettes as shown in Fig. 22. Wu *et al*. (2018) reported energy density and HHV (15.3–27.6 GJ/m^3, 17.3-27.9 MJ/kg) for charcoal briquettes prepared from hydrothermal pretreated biomass wastes without binder and these are comparable to the ones (22.83–32.04 GJ/m^3, 29.66-31.56 MJ/kg) obtained in this study. Sotannde *et al.* (2010) produced charcoal briquettes from neem wood residues using starch and gum arabica as binders and the HHV (32.27-33.54 MJ/kg) of the briquettes were close to the ones obtained in this study.

Table 5: One-way ANOVA for proximate analysis, ultimate analysis, and HHV of briquettes

Property	Parameters	DF	Sum of Squares	Mean Square	F-value	P-value
Highly volatile matter	Model	3	1.91	0.64	19.38	5.01E-04[b]
	Error	8	0.26	0.03		
	Total	11	2.17			
medium volatile matter	Model	3	172.36	57.45	346.65	8.33E-09[b]
	Error	8	1.33	0.17		
	Total	11	173.69			
Ash	Model	3	0.62	0.21	4.49	3.98E-02[b]
	Error	8	0.37	0.05		
	Total	11	0.99			
Fixed carbon	Model	3	121.42	40.47	326.09	1.06E-08[b]
	Error	8	0.99	0.12		
	Total	11	122.42			
C	Model	3	48.26	16.09	8.79	6.52E-03[b]
	Error	8	14.64	1.83		
	Total	11	62.90			
H	Model	3	4.12	1.37	15.11	1.17E-03[b]
	Error	8	0.73	0.09		
	Total	11	4.85			
N	Model	3	0.75	0.25	1.45	2.99E-01[a]
	Error	8	1.37	0.17		
	Total	11	2.12			

Property	Parameters	DF	Sum of Squares	Mean Square	F-value	P-value
O	Model	3	6.11	2.04	22.91	2.79E-04[b]
	Error	8	0.71	0.09		
	Total	11	6.82			
HHV	Model	3	6.49	2.16	7.62	9.88E-03[b]
	Error	8	2.27	0.28		
	Total	11	8.76			

[a] Not significant (P> 0.05), [b] significant (P< 0.05)

Table 6: Fishers LSD test for proximate analysis, ultimate analysis, and HHV of briquettes

Briquette	Proximate analysis (wt %, as received)				Ultimate analysis (wt%, db*)					HHV (MJ/kg)
	Highly volatile matter	medium volatile matter	Ash	Fixed carbon	C	H	N	S	O	
B25	4.68[a]	40.46[d]	5.48[a]	49.38[a]	74.62[c]	4.40[c]	2.17[a]	ND*	7.37[a]	29.66[b]
B30	4.24[b]	44.52[c]	5.47[a]	45.77[b]	75.13[bc]	4.87[bc]	1.94[a]	ND*	7.34[a]	31.56[a]
B35	3.94[b]	47.86[b]	5.15[ab]	43.04[c]	77.37[ab]	5.27[b]	2.37[a]	ND*	7.41[a]	31.32[a]
B40	3.59[c]	50.61[a]	4.94[b]	40.86[d]	79.67[a]	6.00[a]	1.70[a]	ND*	5.73[b]	30.92[a]

Means with the same letter(s) in a column for briquette properties are not significantly different (P < 0.05)
*db- dry basis *ND-Not Detected

4.4 Effect of Binder Concentration and Compaction Pressure on Physical Properties of Briquettes

The experimental data for binder concentration (A) and compaction pressure (B) was extracted from Appendices 3 and 4 respectively. The experimental data for bulk density (ρ), impact resistance index (IRI), compressive strength (F), splitting tensile strength (T), and water resistance index (WRI) was extracted from Appendices 12, 13, 16, 17, and 20 respectively and is shown in Table 7.

Table 7: Data for factors and responses analysed in Design Expert

Run	A (%)	B (MPa)	ρ (g/cm^3)	IRI	F (MPa)	T (MPa)	WRI (%)
1	25	8.2	0.788	3.33	1.97	0.09	99.32
2	25	7.6	0.767	3.13	2.53	0.08	99.14
3	25	8.0	0.826	2.50	2.25	0.08	99.24
4	30	7.6	0.858	25.00	3.91	0.19	99.30
5	30	7.8	0.879	11.11	3.80	0.22	99.18
6	30	7.8	0.885	16.67	4.09	0.22	99.18
7	35	6.2	0.954	50.00	8.38	0.31	99.30
8	35	7.0	0.933	50.00	7.42	0.35	99.31
9	35	7.8	0.974	50.00	8.37	0.28	99.27
10	40	5.8	1.025	50.00	9.67	0.42	99.32
11	40	6.0	1.063	50.00	14.23	0.42	99.02
12	40	6.2	1.053	100.00	8.92	0.43	99.45

4.4.1 Development of Model

Based on the experimental data from Table 7, Design Expert developed model equations showing the empirical relationship between factors and responses as described in Equations 149-153. Linear models were developed by Design Expert for bulk density, impact resistance index, compressive strength, and splitting tensile strength. For water resistance index, a model based on the mean was suggested.

$$\boldsymbol{\rho = 0.9150 + 0.1386A + 0.0157B}$$

(149)

$$IRI = 41.74 + 32.52A - 13.46B \quad (150)$$

$$F = 6.39 + 3.96A - 0.6923B \quad (151)$$

$$T = 0.2593 + 0.1652A - 0.0032B \quad (152)$$

$$WRI = 99.25 \quad (153)$$

Table 8 shows the ANOVA for the models. The R^2-values, F-values, and P-values were used to assess the quality of the models. The R^2 is used to compare the experimental and predicted values and models with $R^2 > 0.9$ are considered to exhibit a high correlation (Karungi *et al.*, 2020). The model R^2 values of 0.9670, 0.9253, 0.8747 and 0.9817 respectively for bulk density, impact resistance index, compressive strength and splitting tensile strength, are close to unity. It indicates that the experimental and predicted values are similar, as further illustrated in Appendix 29. For bulk density, the model F-value of 131.95 implies the model is significant. There is only a 0.01% chance that an F-value this large could occur due to noise. Binder concentration was a significant model term with P-value less than 0.0500. Compaction pressure was an insignificant model term with P-value greater than 0.1000. The Lack of Fit F-value of 30.51 implies the Lack of Fit is not significant relative to the pure error. There is a 13.92% chance that a Lack of Fit F-value this large could occur due to noise.

For impact resistance index, the model F-value of 55.72 implies the model is significant. There is only a 0.01% chance that an F-value this large could occur due to noise. Binder concentration was a significant model term with P-value less than 0.0500. Compaction pressure was an insignificant model term with P-value greater than 0.1000. The Lack of Fit F-value of 8.30 implies the Lack of Fit is not significant relative to the pure error. There is a 26.25% chance that a Lack of Fit F-value this large could occur due to noise. For compressive strength, the model F-value of 31.42 implies the model is significant. There is only a 0.01% chance that an F-value this large could occur due to noise. Binder concentration was a significant model term with P-value less than 0.0500. Compaction pressure was an insignificant model term with P-value greater than 0.1000. The Lack of Fit F-value of 59.38 implies the Lack of Fit is not significant relative to the pure error. There is a 10.01% chance that a Lack of Fit F-value this large could occur due to noise.

For splitting tensile strength, the model F-value of 241.15 implies the model is significant. There is only a 0.01% chance that an F-value this large could occur due to noise. Binder concentration was a significant model term with P-value less than 0.0500. Compaction pressure was an insignificant model term with P-value greater than 0.1000. The Lack of Fit F-value of 12.73 implies the Lack of Fit is not significant relative to the pure error. There is a 21.37% chance that a Lack of Fit F-value this large could occur due to noise. For water resistance index, there were no significant model terms. The Lack of Fit F-value of 27601.26 implies the Lack of Fit is significant. There is only a 0.47% chance that a Lack of Fit F-value this large could occur due to noise.

4.4.2 Diagnostics

The developed models were checked to ascertain their validity. For a good model, the residuals should be randomly and normally distributed. To ascertain this, plots of the normal % probability versus externally studentized residuals, externally studentized residuals versus predicted values, and predicted versus actual values of the responses were analysed as shown in Fig. 28-30 respectively. Figure 28a–e shows that the points conform to a straight line, implying normal distribution of the data (Menya *et al.,* 2020).

Figure 29a-d shows that the results do not show any particular pattern, suggesting random distribution of the residuals which is a requirement of a good model (Menya *et al.,* 2020). On the contrary, Fig. 29e shows a particular pattern, thus there was no random distribution of the residuals. This is attributed to the Lack of fit of the data as shown in Table 8. The plots for Fig. 30a-d show minimal divergence of points from the straight line. Thus, the resulting response surface plots can be used to predict the interaction between the factors and responses (Menya *et al.,* 2020). The data for Fig. 30e could not follow a linear trend due to a Lack of Fit of the data.

Table 8: ANOVA for the models of the experimental design

Source	sum of squares	Degrees of freedom	Mean square	F-value	P-value	
(a) Bulk density: R^2=0.9670, Adjusted R^2=0.9597, predicted, R^2= 0.9445						
Model	0.1059	2	0.0529	131.95	<0.0001	significant
A-Binder	0.0312	1	0.0312	77.86	<0.0001	
B-Pressure	0.0004	1	0.0004	0.88	0.3723	
Lack of Fit	0.0036	8	0.0004	30.51	0.1392	not significant
(b) Impact resistance index: R^2=0.9253, Adjusted R^2=0.9087, predicted R^2= 0.8587)						
Model	12884.8692	2	6442.4346	55.72	<0.0001	significant
A-Binder	1718.9940	1	1718.9940	14.87	0.0039	
B-Pressure	259.7978	1	259.7978	2.25	0.1681	
Lack of Fit	1025.0696	8	128.1337	8.30	0.2625	not significant
(c) Compressive strength: R^2=0.8747, Adjusted R^2=0.8469, Predicted, R^2= 0.7547						
Model	137.5046	2	68.7523	31.42	<0.0001	significant
A-Binder	25.5472	1	25.5472	11.67	0.0077	
B-Pressure	0.6871	1	0.6871	0.31	0.5889	
Lack of Fit	19.6529	8	2.4566	59.38	0.1001	not significant
(d) Splitting tensile strength: R^2=0.9817, Adjusted R^2=0.9776, predicted, R^2= 0.9575						
Model	0.1878	2	0.0939	241.15	<0.0001	significant
A-Binder	0.0444	1	0.0444	113.94	<0.0001	
B-Pressure	0.0000	1	0.0000	0.04	0.8506	
Lack of Fit	0.0035	8	0.0004	12.73	0.2137	not significant
(e) Water resistance index: R^2=0.0000, Adjusted R^2=0.0000, predicted, R^2= -0.1901)						
Model	0.0000	0				
Lack of Fit	0.1301	10	0.0130	27601.26	0.0047	significant

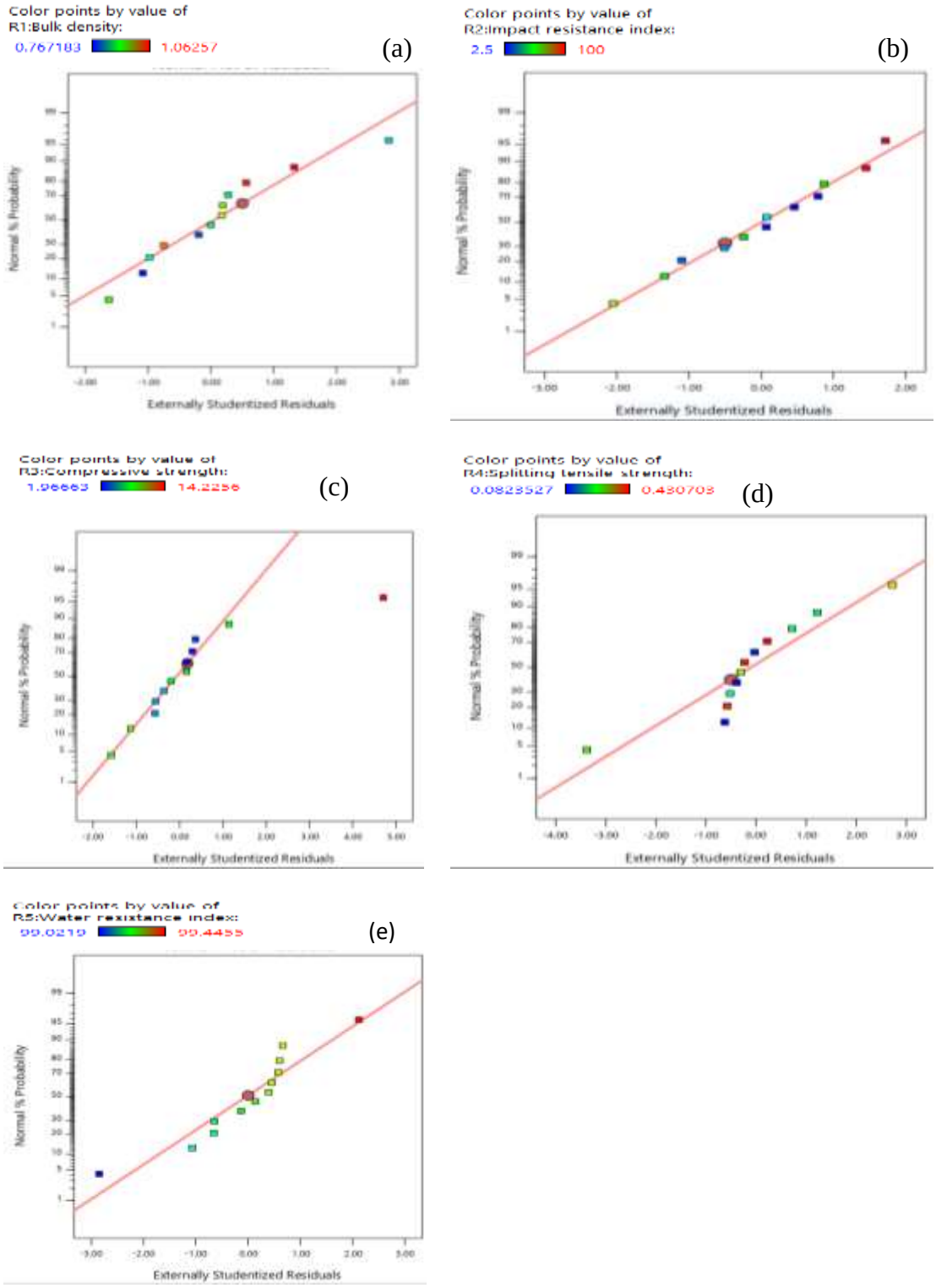

Figure 28: **Normal % probability vs Externally studentized residuals;(a) Bulk density, (b) Impact resistance index, (c) Compressive strength, (d) Splitting tensile strength, (e) Water resistance index**

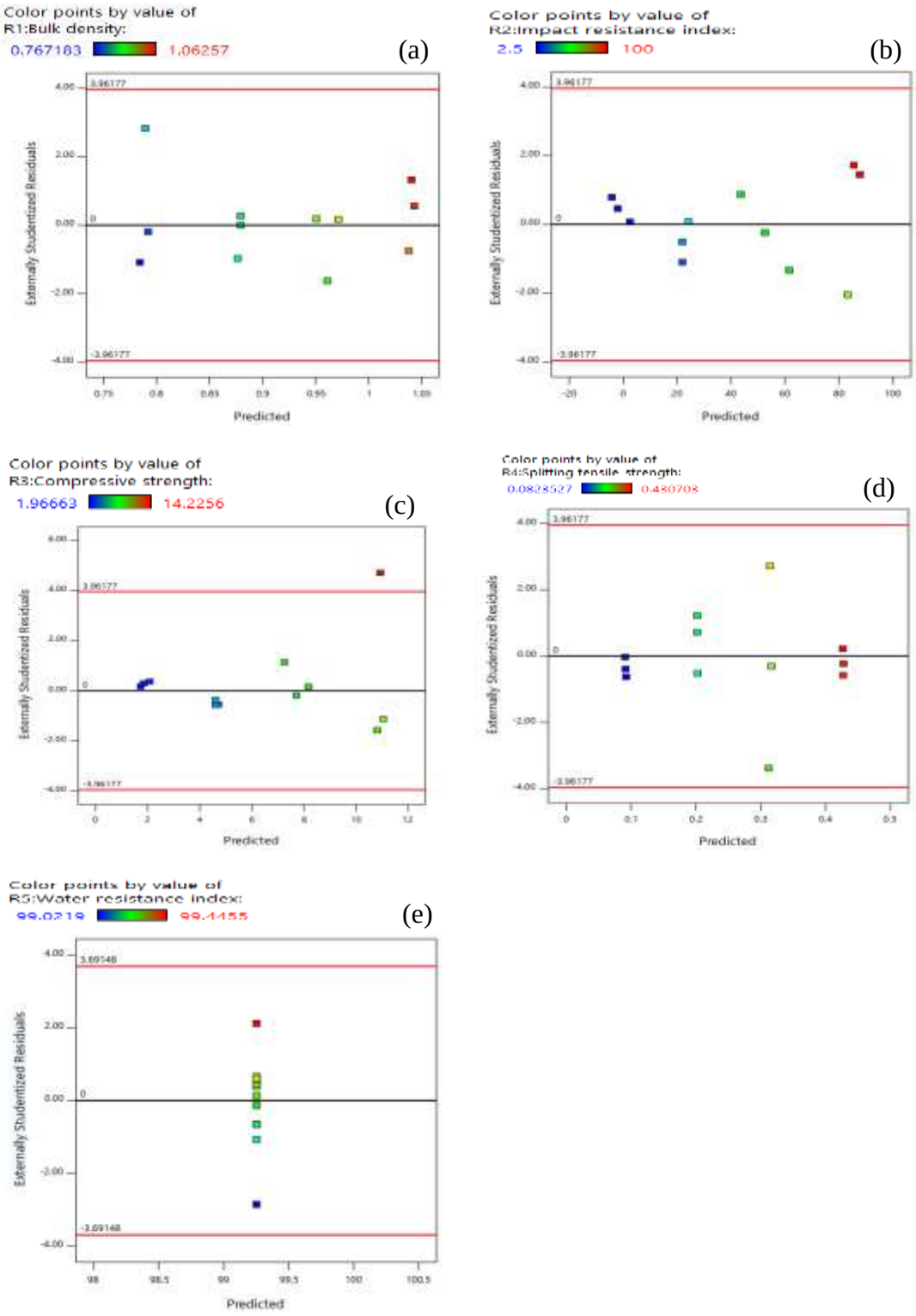

Figure 29: **Externally studentized residuals vs predicted;(a) Bulk density, (b) Impact resistance index, (c) Compressive strength, (d) Splitting tensile strength, (e) Water resistance index**

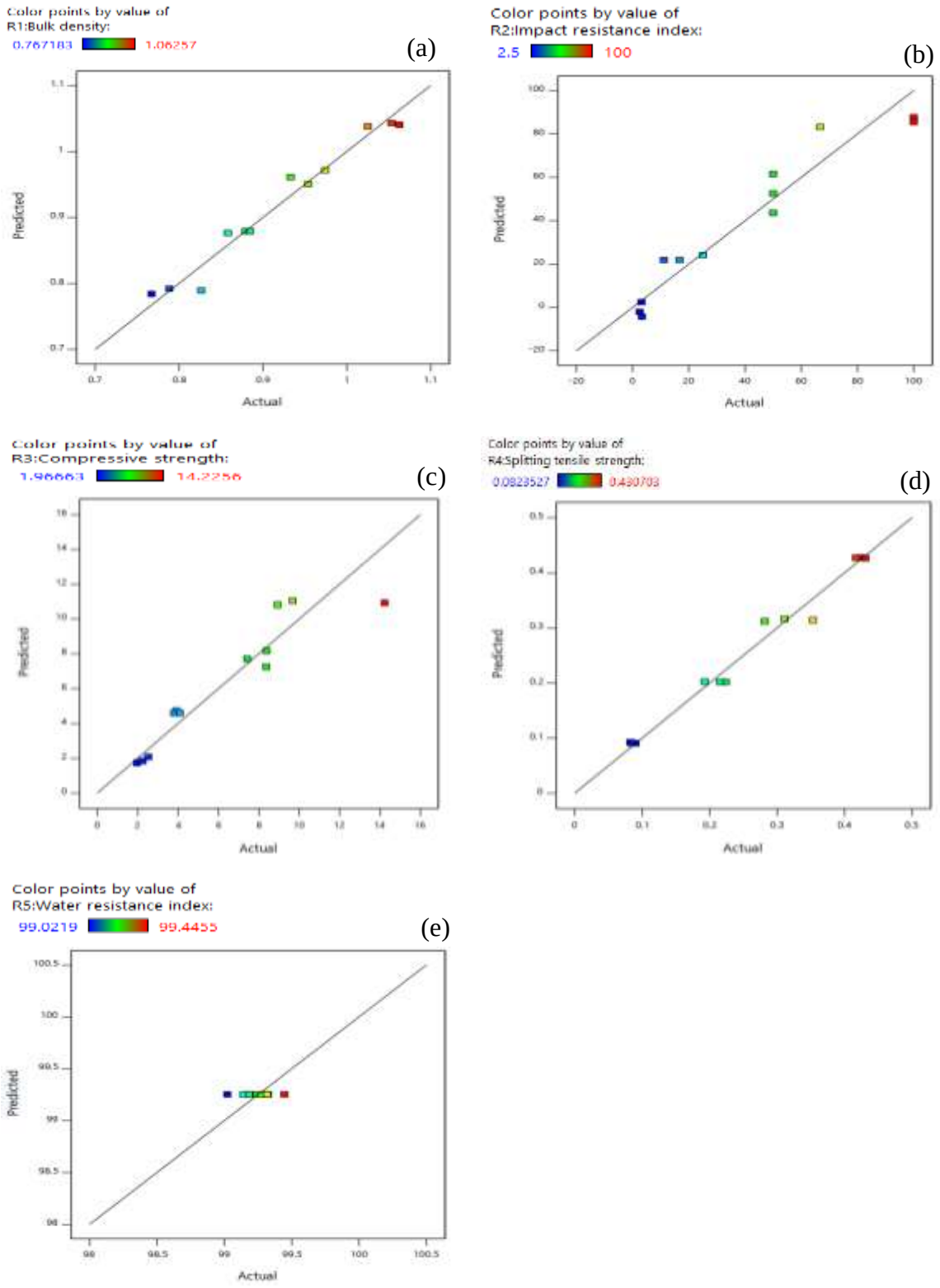

Figure 30: Predicted vs actual;(a) Bulk density, (b) Impact resistance index, (c) Compressive strength, (d) Splitting tensile strength, (e) Water resistance index

4.4.3 Response Surface Plots

Three-dimensional response surface plots were analysed to show the effect of binder concentration and compaction pressure on physical properties of briquettes, as shown in Fig. 31a–e. The response surface plots are useful in the efficient tracking of optimal levels of variables to obtain the best

response range. The shapes of the plots depict the extent of interactions between variables in determining the response (Karungi *et al.*, 2020). Figure 31a shows that for a compaction pressure of 5.8-8.2 MPa, bulk density of the briquettes increases with binder concentration and the optimum bulk density is predicted at a binder concentration of 40% and compaction pressure of 8.2 MPa. Figure 31b shows that for a compaction pressure of 5.8-8.2 MPa the IRI of the briquettes increases with binder concentration and the optimum IRI is predicted at a binder concentration of 40% and compaction pressure of 5.8 MPa.

Figure 31c shows that for compaction pressure of 5.8-8.2 MPa the compressive strength of the briquettes increases with binder concentration and the optimum compressive strength is predicted at a binder concentration of 40% and compaction pressure of 5.8 MPa. Figure 31d shows that for a compaction pressure of 5.8-8.2 MPa splitting tensile strength of the briquettes increases with binder concentration and the optimum splitting tensile strength is predicted at a binder concentration of 40% and compaction pressure of 5.8-8.2 MPa. Figure 31e shows that the water resistance index is independent of binder concentration and compaction pressure. This is attributed to the model using the mean value predicted by Design Expert since there was a Lack of Fit for the experimental data.

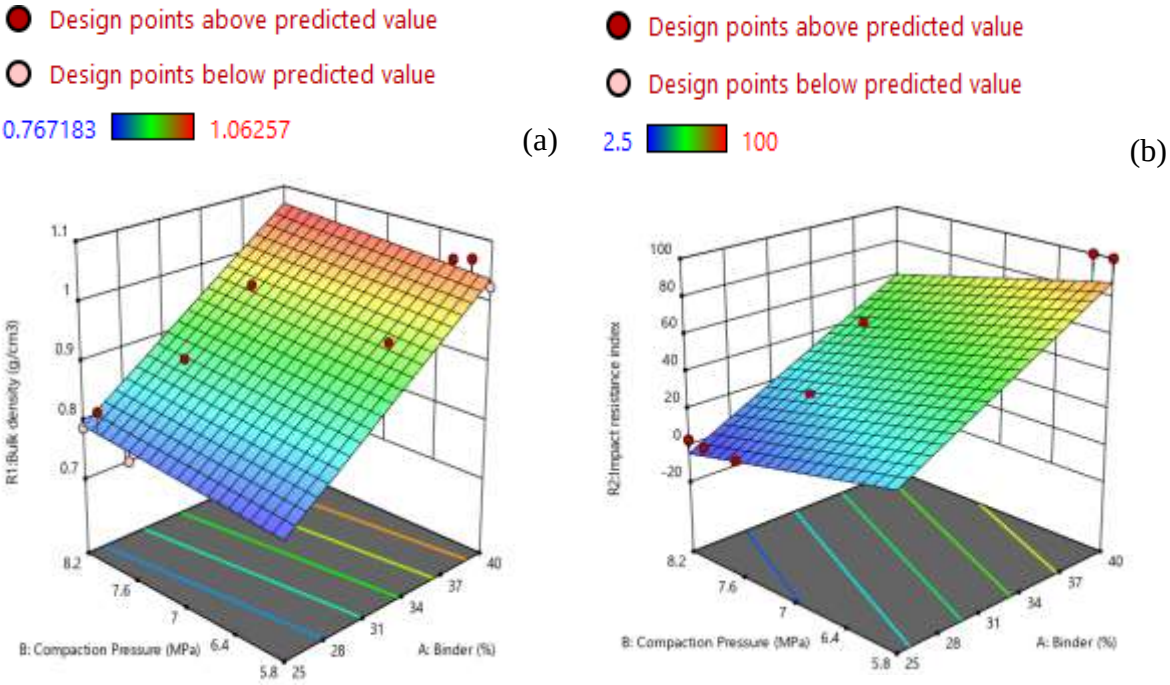

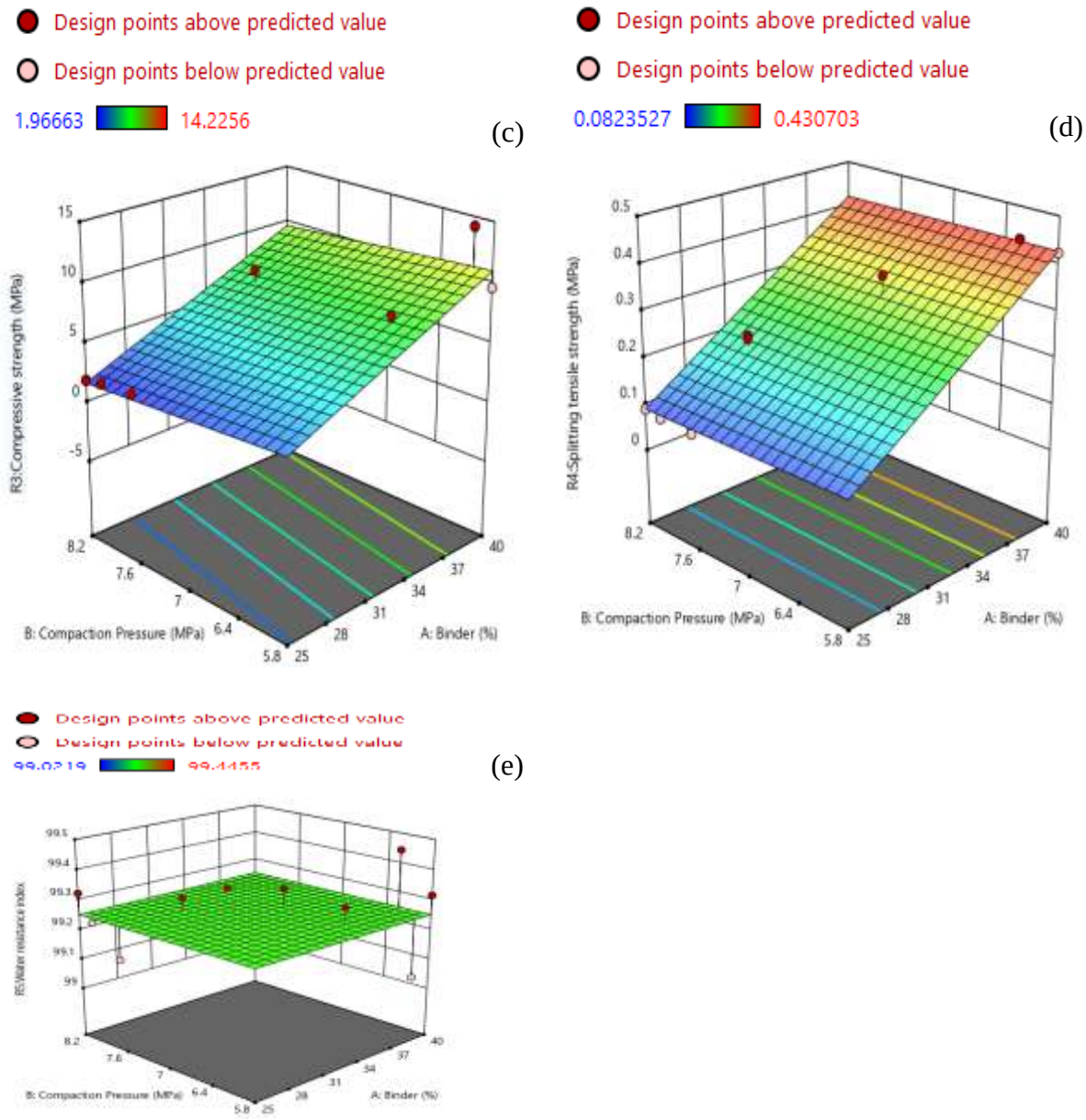

Figure 31: Response surface plots; (a) bulk density, (b) impact resistance index, (c) compressive strength, (d) splitting tensile strength, and (e) water resistance index

4.5 Water Boiling Test of the Carbonized Briquettes

4.5.1 Ignition

Figure 32a-e shows the ignition images. Figure 32a shows the bioethanol gel (CH_3CH_2OH, yellow in colour) before ignition (Balat, 2011). Figure 32b shows the cookstove loaded with the briquettes before ignition. Figure 32c shows that after igniting the bioethanol gel with a match, it burned with a blue flame to provide the ignition energy required to ignite the briquettes. The blue radiation is due to excited CH radicals in the high temperature zone (Turns, 2000). The OH radicals also contribute to visible radiation (Turns, 2000). Figure 32d shows the ignited briquettes burning with a yellow flame due to the highly volatile terpenoids in the binder used. Furthermore, briquette B40

was observed to burn with a more intense yellow flame due to the increase of volatile matter with binder concentration.

The ignition time of the briquettes was 6.47-7.01 min (Appendix 32). Nwabue *et al*. (2017) produced smokeless bio-coal briquettes incorporating plastic waste materials using cassava starch as binder. The briquettes were ignited using a lighter and found that the ignition time was 0.88-2.60 min. The low ignition time was attributed to the added biomass and plastic materials and the results are comparable to the ones obtained in this study. Ormeño *et al*. (2009) reported that at relatively low temperatures and concentrations, liquid terpenes can generate an ignitable mixture, leading to a flame in the presence of an ignition source. The same observation was made in this ignition experiment (Fig. 32d) where the binder containing terpenoids is a solid at room temperature. The formation of the yellow flame can be attributed to the high volatile content of the briquette which is an indication of easy ignition of the briquette and proportionate increase in flame length (Obi, 2015). Blasi (1993) reported that to get a flaming ignition as shown in Fig. 32d, three conditions must be met: (a) the gas phase temperature must attain values sufficiently high to initiate and accelerate the combustion reaction, (b) fuel and oxidizer must be available at a proper level of concentration to give a mixture within the flammability limits, and (c) the extent of the heated zone must be sufficiently large to overcome heat losses. Figure 32e shows the ignited briquette with a red glow in the central hole as well as at the curved surface. Fernandez-Anez *et al*. (2018) studied ignition sensitivity of solid fuel mixtures and one of the criteria to confirm ignition was observation of visible flame or incandescence which are the features observed in Fig. 32 d, e respectively.

Figure 32: Ignition images; (a) Weighing bioethanol gel, (b) Briquettes loaded on the cookstove, (c) Bioethanol gel burning with a blue flame (d) Briquettes burning with a yellow flame, (e) ignited briquette with a red glow

4.5.2 Combustion

Figure 33a-e shows the combustion images. At the start of the CSHP phase, briquette B25 burned with white smoke and no flame as shown in Fig. 33a while briquettes B30, B35 and B40 burned with a yellow flame and soot as shown in Fig. 33b. Briquette B40 burned with a more intense yellow flame and produced the highest amount of soot since it contained more binder. Briquette B25 burned with a yellow flame and soot towards the end of the CSHP phase. The yellow flame and soot are attributed to the binder used that contains volatile terpenoids with a high molecular weight thus, resulting in a rich air/fuel mixture forming soot with its consequent blackbody continuum radiation (Turns, 2000). Although the soot radiation has its maximum intensity in the infrared (Wiens Law), the spectral sensitivity of the human eye causes us to see a bright yellow to dull orange emission depending on the flame temperature (Turns, 2000). Part of the soot was trapped on the pot as shown in Fig. 33b, c. Mitchell *et al*. (2016) reported that the high volatile wood fuels release a high concentration of highly carbonaceous dark smoke during flaming combustion thus, the combustion characteristics of the briquettes is similar to that of wood fuels. Romallosa and Kraft (2017) reported that a hole at the centre of the fuel improves the combustion characteristics of the briquette through rapid drying, easy ignition and highly efficient burning due to the draft and insulated combustion chamber that the hole creates.

During the HSHP and Simmer phases, there was ash formation creating a layer of insulation around the burning briquettes as shown in Fig. 33d, e. Consequently, there was a reduction in the burning rate and the insulation minimised heat transfer to the pot resulting in a long time to boil during HSHP phase. Ash influences heat transfer and diffusion of oxygen to the surface of fuel during combustion (Obi, 2015). There was also a tendency for the briquettes to undergo fragmentation as shown in Fig. 33d but they remained stable until the end of the combustion process.

Figure 33: Combustion images; (a) Briquette B25 burning with white smoke, (b) Briquettes B25, B30, B35, and B40 burning with a yellow flame and soot (d) Briquettes burning without soot and yellow flame (e) Ash formation around the briquettes

4.5.3 Temperature Profiles and Gaseous Emissions

Figures 34a, 35a, 36a, and 37a show temperature profiles while Appendices 33-36 show temperature data during the WBT. The T_{gas} remained relatively constant and close to the $T_{ambient}$ which is important for measuring PM (Clean cooking alliance, 2014). The spikes in the T_{gas} during the ignition phase occurred due to the pot not being placed on the cookstove as the bioethanol gel was allowed to burn to completion. The spikes in the T_{gas} during the HSHP and Simmer phases occurred during weighing of the pot with water. The T_{water} trends are similar to the international WBT reported by Chen *et al*. (2016). At the start of the experiment, the $T_{ambient}$ and T_{water} corresponded to the dry bulb and wet bulb temperatures respectively. The T_{water} was lower than $T_{ambient}$ due to evaporative cooling (Amer *et al*., 2015; Yang *et al*., 2019).

During the CSHP phase, the pot containing water was not covered with a lid as the burning characteristics of the fuel exhibited that of wood fuel and this is in accordance with the WBT 4.2.3 protocol (Clean cooking alliance, 2014). The depression in the T_{water} during the HSHP phase was due to withdrawing of the thermocouple from the hot water to cover the pot with a lid when the yellow flame and soot had stopped and the burning characteristics of the fuel exhibited that of charcoal as shown in Fig. 33d in accordance with the WBT 4.2.2 protocol (Clean cooking alliance, 2013). Moreover, without covering the pot during the HSHP phase, the water would not reach the boiling point. In addition, a high amount of fuel would be required to heat the water to the boiling point and consequently increase the emissions. Quist *et al*. (2020) did a study on influence of variability in testing parameters on cookstove performance metrics based on the WBT and reported that the use of a lid greatly reduced variations in both thermal efficiency associated with heating water and specific consumption metrics even when there were significant variations in the other testing parameters. Quist *et al*. (2020) also reported that, the use of a lid would provide better consistency for cookstove comparisons when using these metrics. The use of a lid reduces the radiation losses with its emissivity of perhaps 0.1, compared to almost 1 for the water surface. Thus, there is more net heat available to heat the water (Hermans, 2012).

Figures 34b, 35b, 36b, and 37b show the profile of gaseous emissions while Appendices 33-36 show the gaseous emissions data during the WBT. Mitchell *et al*. (2016) reported that the route leading to the formation of smoke from biomass involves pyrolysis of the different constituents, cellulose and lignin and can form soot via the HACA (hydrogen abstraction–C_2H_2 addition) route or via aromatic compounds respectively. The concentration of CO_2, C_xH_y, CO, SO_2, and NO_x increased with time during ignition and CSHP phase to a maximum and then decreased during the HSHP and Simmer phases and the peak values are shown in Table 9 along with their Occupational

Safety and Health Administration (OSHA) permitted industrial concentration. The peak emissions of SO_2, NO_2, and CO_2 from the briquettes met this standard. The NO_x found in the briquettes is attributed to the fuel-N found in charcoal fines (Glarborg *et al*., 2003) as well as nitrogen-containing compounds in the *Canarium Schweinfurthii* resin (Ameh, 2018). The SO_2 is attributed to the Sulphur in the charcoal fines (Deac *et al*., 2016). Arora *et al*. (2014) tested CO emissions from ignition materials (wood, kerosene, mustard stalks) in a natural draft cookstove (Philips) and found that the highest amount of CO emission was 1100 ppm generated using mustard stalks and this is higher than the value of 25 ppm obtained in this study during the ignition phase. Oketch *et al*. (2014) did a study on fuel efficiency and emissions comparison from bioethanol gel stoves and detected presence of CO and CO_2. Thus, the bioethanol gel used for ignition in this study contributed to the CO and CO_2 emissions during ignition.

Household coal combustion, even with the cleaner coals and higher quality stoves more commonly used in cities, still produces relatively high levels of emissions of PM, SO_2, and black carbon (World Health Organization [WHO], 2014). Similar emissions are reported for the briquettes in this study. World Health Organization (2014) reported that many products of incomplete combustion components exert a radiative forcing of climate, either because they are greenhouse gases (GHGs) able to trap long-wave heat radiation from the earth (methane, N_2O), they indirectly affect GHGs via chemical processes in the atmosphere (CO, non-methane volatile organic compounds), or because they interfere with short-wave solar radiation and/or they affect climate through impacts on clouds (particulate matter/aerosols – including black carbon). These components (except N_2O) are often referred to as short-lived climate pollutants.

Table 9: Peak concentration (ppm) of the gaseous emissions

Briquette	**CO_2**	**C_xH_y**	**CO**	**SO_2**	**NO_x**
B25	775	325	150	0.325	0.125
B30	950	250	150	2.75	6.25
B35	1650	225	150	2.375	2.375
B40	1500	300	175	3.125	1.375
Permitted industrial concentrations, 15 min peak*	-	-	400	5	5

*(El-Mahallawy & El-Din Habik, 2002)

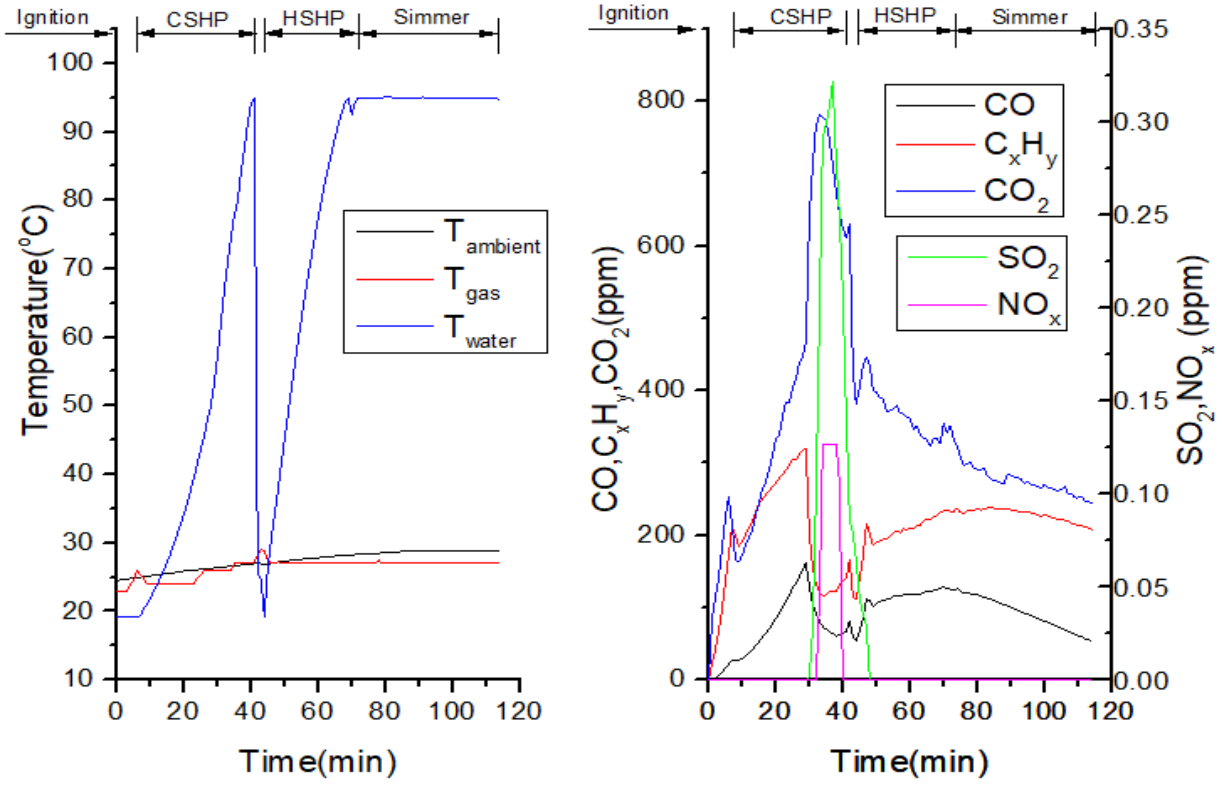

(a) (b)

Figure 34: Briquette B25 during ignition, CSHP, HSHP, and Simmer phases; (a) Temperature profiles, (b) Gaseous emissions

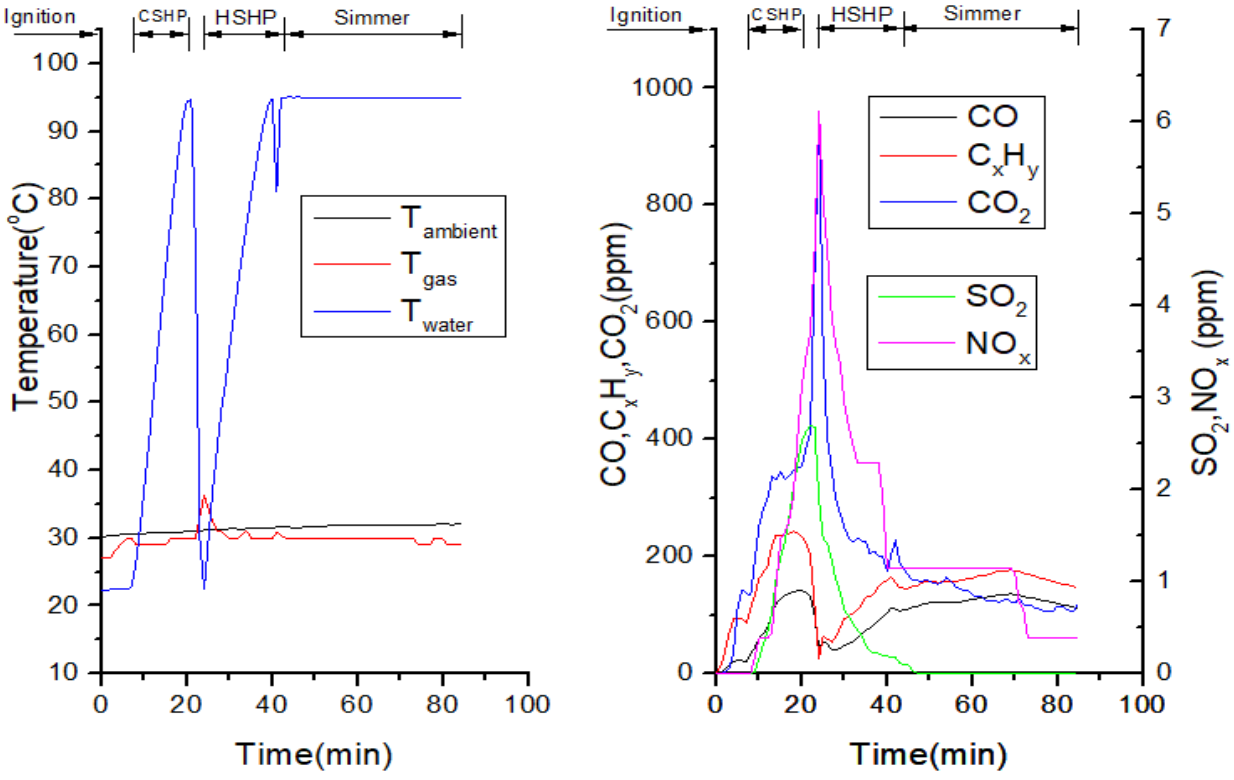

(a) (b)

Figure 35: Briquette B30 during ignition, CSHP, HSHP, and Simmer phases; (a) Temperature profiles, (b) Gaseous emissions

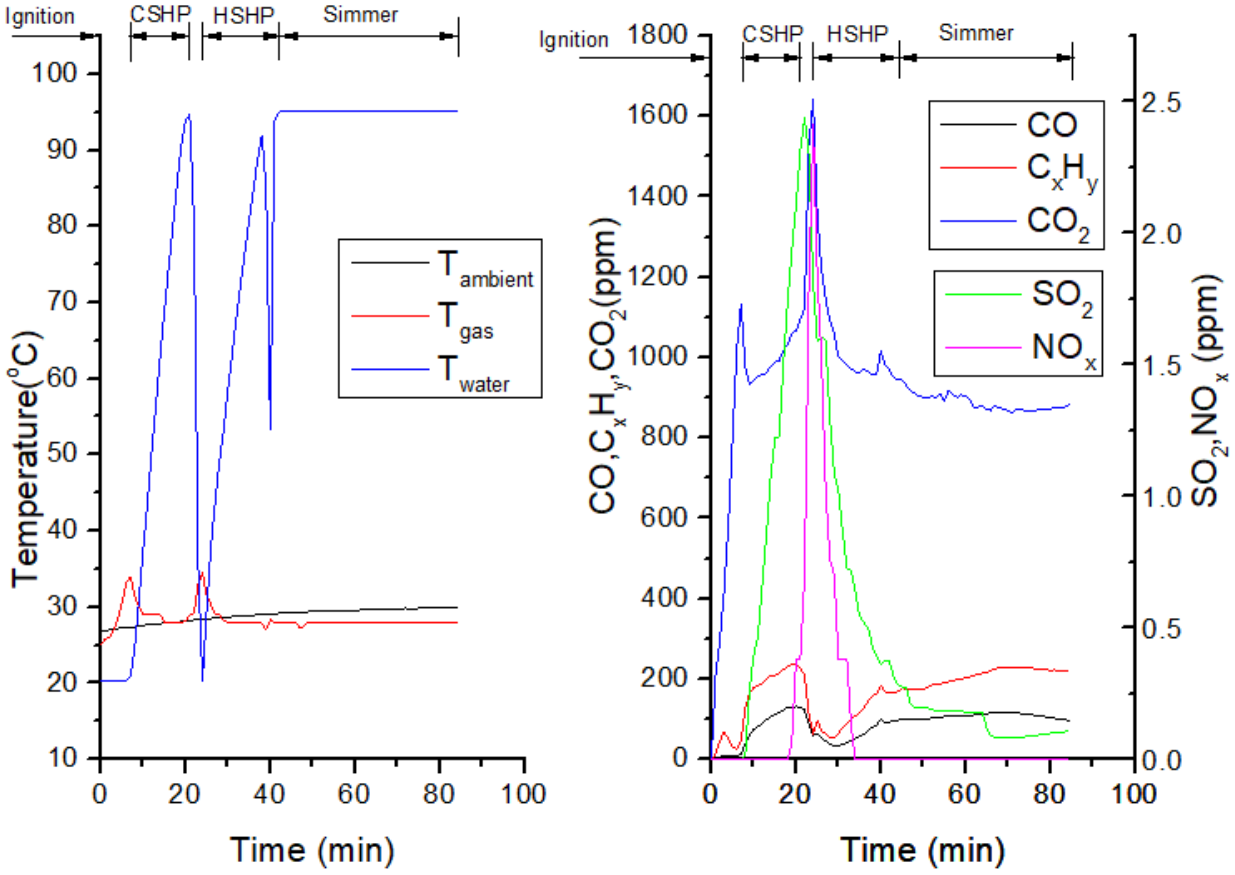

(a) (b)

Figure 36: Briquette B35 during ignition, CSHP, HSHP, and Simmer phases; (a) Temperature profiles, (b) Gaseous emissions

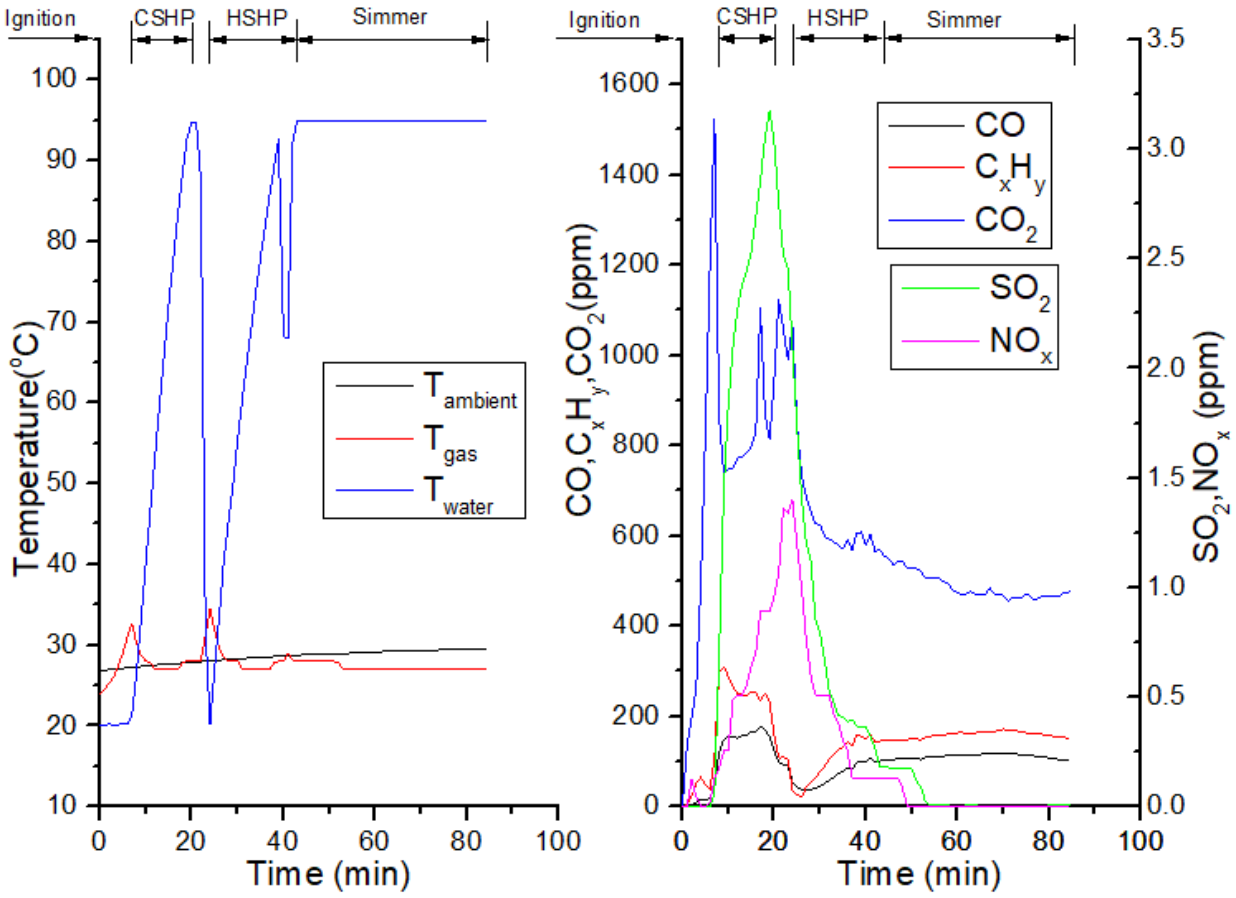

(a) (b)

Figure 37: Briquette B40 during ignition, CSHP, HSHP, and Simmer phases; (a) Temperature profiles, (b) Gaseous emissions

4.5.4 WBT Performance Metrics

Appendix 37 shows results of the WBT performance metrics. Appendix 38 shows images of the filter paper for briquettes B25, B30, B35 and B40 during CSHP, HSHP and Simmer phases.

(i) Time to Boil

Figure 38 shows the results of time to boil. The time to boil during the HSHP phase was shorter than for CSHP phase for all the briquettes since a lid was used during the HSHP phase. During the CSHP phase, briquettes B30, B35 and B40 boiled water faster than briquette B25 due to the exothermic reaction resulting from the flaming combustion of the terpenoids in the binder as shown in Fig. 33b. Furthermore, briquette B40 boiled water in the shortest time during the CSHP and HSHP phases since it contained more binder implying that it generated more heat. On the contrary, briquette B25 took a long time to boil water during the CSHP since it contained the least amount of binder and initially burned with white smoke and no flame for about 23 min as shown in Fig. 33a. The Simmer phase considered the same boiling time of 45 min for all briquette samples (Clean cooking alliance, 2014). The time to boil was 20.3- 41.9 min, 14.7-25.2 min for CSHP and

HSHP phases, respectively. Lask *et al*. (2015) tested an improved charcoal cookstove (EcoRecho) to boil 2.5 L of water and found that the boiling time was 30-50 min implying that the cookstove and briquettes used in this study boiled water faster (14.7-41.9 min) during CSHP and HSHP phases.

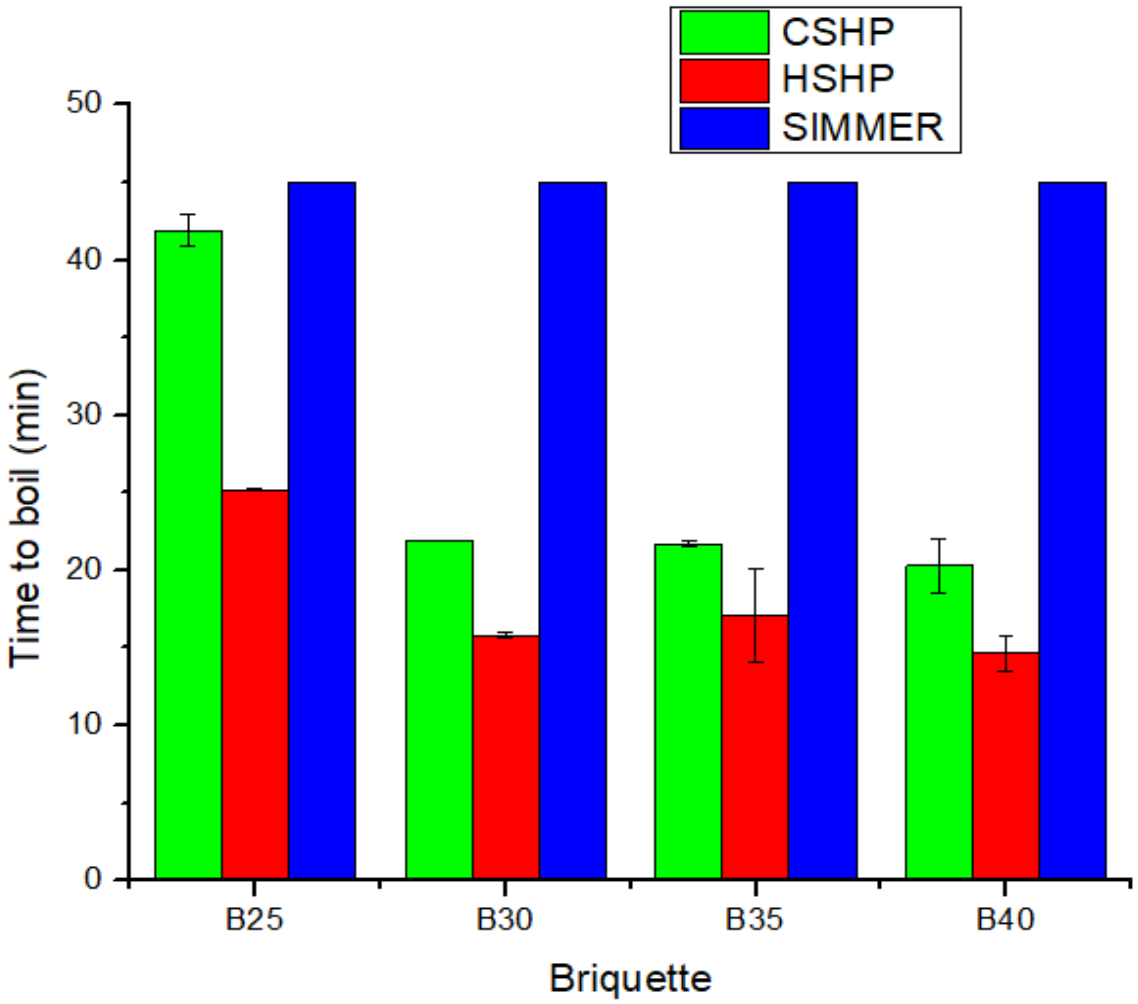

Figure 38: Time to boil

(ii) Burning rate

Figure 39 shows the results of burning rate. During the CSHP and HSHP phases, the burning rate of briquettes increased with the binder concentration as a result of increase in the volatile matter in the binder used. Lubwama and Yiga (2017) reported that high volatile matter eases ignition and enhances combustion due to increased chemical reactivity. During the Simmer phase, the burning rate of briquettes B30, B35 and B40 was higher than that of briquette B25 since the later had taken a long time to boil during the CSHP and HSHP phases thus, the briquette had been covered with ash which minimised heat transfer and limited diffusion of oxygen to the briquette to support combustion. Furthermore, briquettes B30, B35 and B40 had the same burning rate during the Simmer phase since they had a slight difference in time to boil during the CSHP and HSHP phases,

thus could have been covered with the same amount of ash. The burning rate was 3.7-8.2 g/min, 2.1-4.2 g/min,1.1-1.7 g/min for CSHP, HSHP and Simmer phases, respectively. Nwabue *et al*. (2017) obtained a burning rate of 1300-3800 g/min for smokeless bio-coal briquettes incorporating plastic waste materials. This implies that the briquettes used in this study burn slower (1.1-8.2 g/min), thus the cookstove does not have to be loaded with fuel frequently.

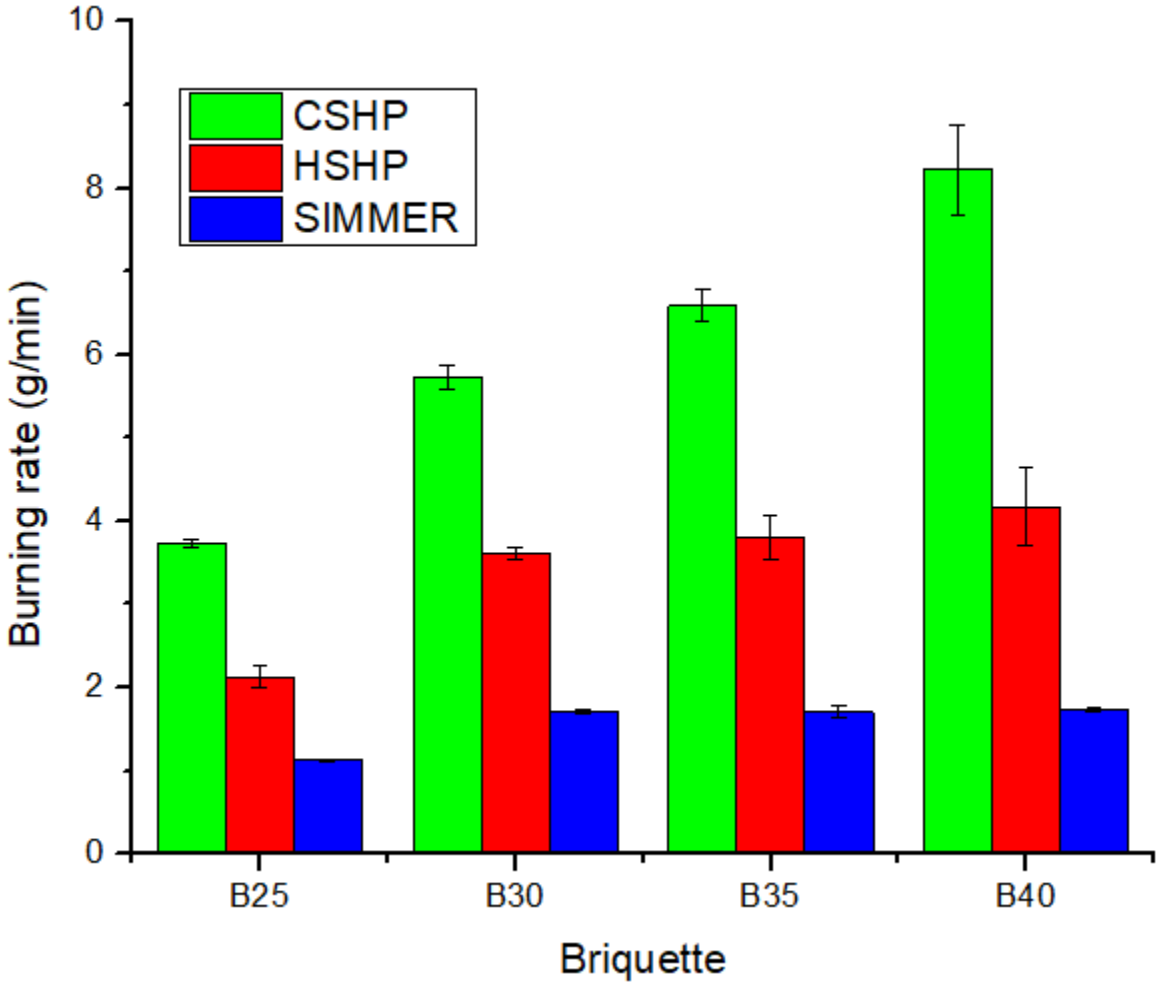

Figure 39: Burning rate

(iii) Thermal Efficiency, Dry Fuel Used, Effective Mass of Water Boiled and Specific Fuel Consumption

Figure 40a-d shows the results of thermal efficiency, dry fuel used, effective mass of water boiled, and specific fuel consumption (SC). The thermal efficiency (Fig. 40a) of the cookstove during the CSHP phase was lower than during the HSHP phase due to covering of the pot with a lid in the later phase which reduced the time to boil and consequently minimised on the amount of dry fuel used (Fig. 40b). During the CSHP and HSHP phases, the thermal efficiency of the cookstove fluctuated with binder concentration as a result of fluctuation in the dry fuel consumed. Considering the CSHP and HSHP phases for each briquette type, there was a slight difference in

the amount of water evaporated as shown in Fig. 40c. Hermans (2012) reported that whether or not there is a lid on the pan, the heat supply to the water remains the same. Except for the (relatively small) heat losses by radiation and conduction, all heat is used for evaporation when approaching boiling point. This means that there should be no difference in the amount of water evaporated, irrespective of the details of condensation and backflow that occur under the lid. The amount of water evaporated during the Simmer phase was higher than that during the CSHP and HSHP phases since the Simmer phase took a long time of 45 min.

Clean cooking alliance (2014) recommends considering SC instead of thermal efficiency, especially during the Simmer phase of the WBT. This is because a stove that is very slow to boil may have a very good-looking thermal efficiency because a great deal of water was evaporated. However, the fuel used per water remaining may be too high since so much water was evaporated and so much time was taken while bringing the pot to a boil. From Fig. 40d, during the Simmer phase, the SC of the cookstove for briquette B25 was lower than that for briquettes B30, B35 and B40 since B25 had the lowest amount of dry fuel consumed and highest amount of effective mass of water boiled (Fig. 40c). Furthermore, briquettes B30, B35 and B40 had approximately the same value of SC since they had approximately the same amount of dry fuel consumed and effective mass of water boiled.

The thermal efficiency was 21.79-30.86%, 44.62-54.61%, 39.14-50.34% during CSHP, HSHP, and Simmer phases, respectively. Lask *et al*. (2015) obtained an average thermal efficiency of 40% using a charcoal cookstove (Prakti) implying that the cookstove and fuel used in this study performed better during the HSHP. The SC was 53.2-70.1 g/L, 21.7-26.1 g/L, 22.8-39.4 g/L during CSHP, HSHP and Simmer phases, respectively. Grimsby *et al*. (2016) obtained SC values for CSHP of 83 and 102 g/L for the traditional charcoal stove (no liner) and improved charcoal stove (jiko bora-ceramic liner), respectively implying that the stove used in this study requires less fuel to boil a litre of water (53.2-70.1 g/L).

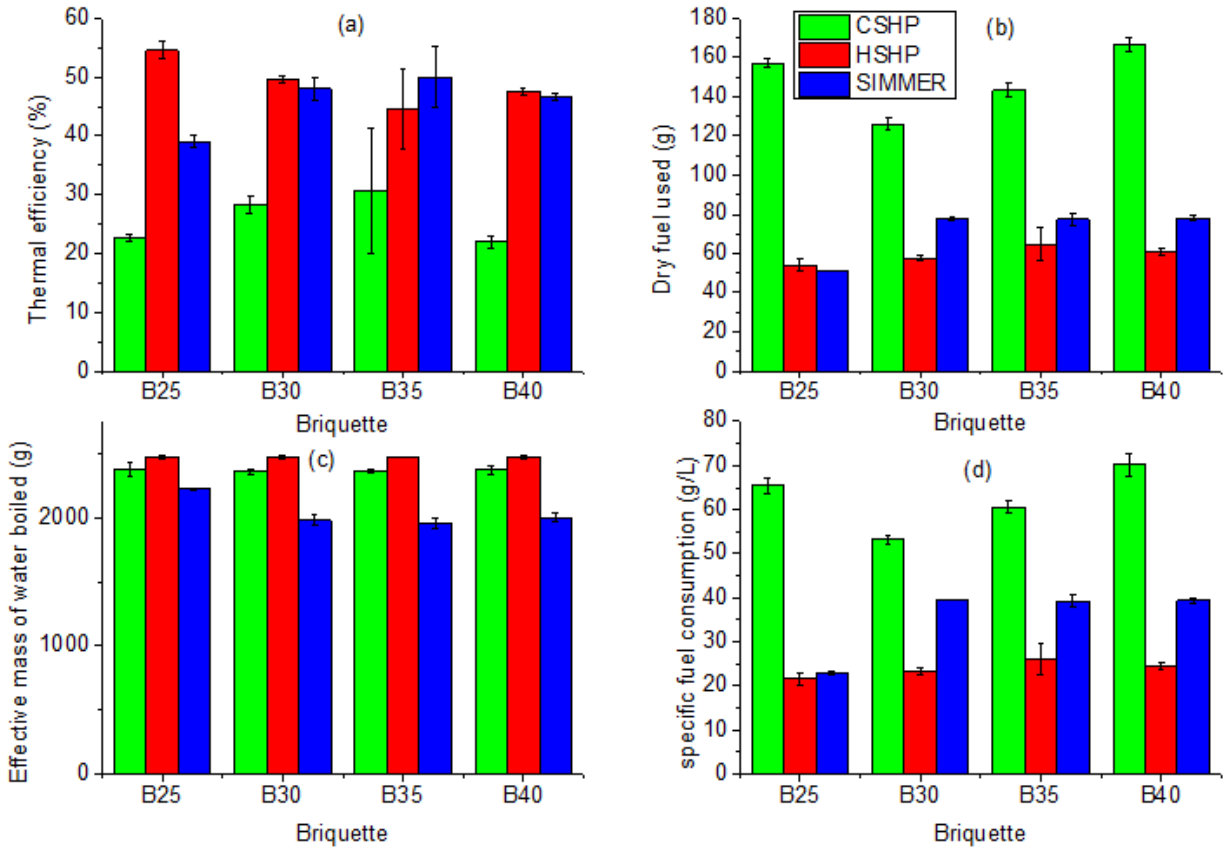

Figure 40: (a) Thermal efficiency, (b) Dry fuel used, (c) Effective mass of water boiled, (d) Specific fuel consumption

(iv) Firepower

Figure 41 shows the results of firepower. The firepower increased with binder concentration during CSHP and HSHP phases for briquettes B25, B30, B35 and B40, respectively. During the Simmer phase, there was negligible difference in the firepower for briquettes B30, B35 and B40 since they had the same time to boil and approximately the same amount of dry fuel used as shown in Fig.38 and Fig. 40b, respectively. However, the firepower for briquettes B30, B35 and B40 was higher than that for briquettes B25 since the later had the lowest amount of dry fuel used. Each briquette type showed a decreasing firepower during CSHP, HSHP and Simmer phases. The firepower was 1775.0-4123.2 W, 1011.5-2091.8 W, 535.9-867.8 W for the CSHP, HSHP and Simmer phases, respectively. Grimsby *et al*. (2016) obtained values of firepower for CSHP of 4200 W and 3000 W for the traditional charcoal stove (no liner) and improved charcoal stove (jiko bora-ceramic liner), respectively which are within the range (535.9-4123.2 W) of the cookstove used in this study.

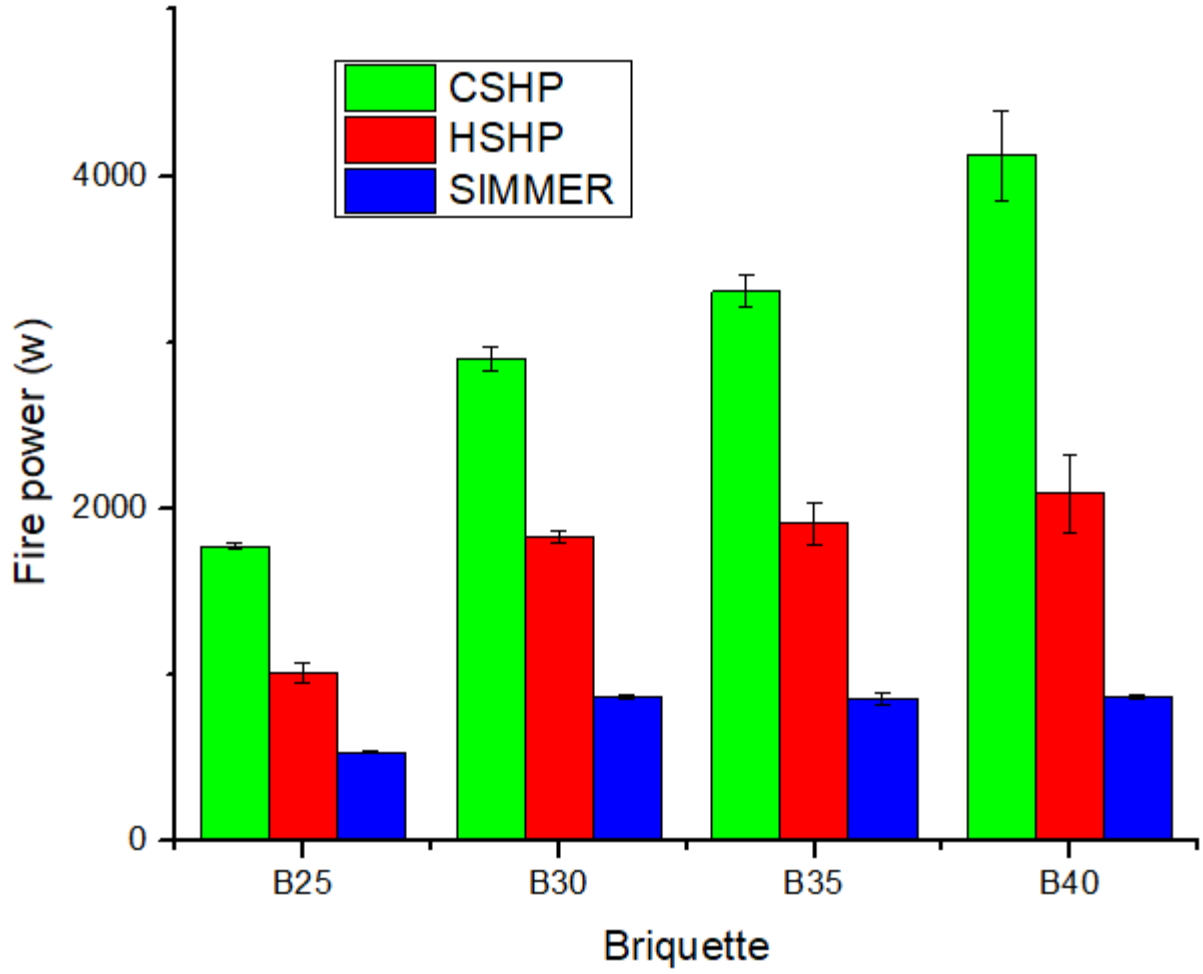

Figure 41: Firepower

(v) Total Emissions

Figure 42 shows the results of total emissions. From Fig. 42a it was observed that generally, the amount of $PM_{2.5}$ increased with binder concentration during CSHP, HSHP, and Simmer phases. Moreover, briquettes B40 produced the highest amount of $PM_{2.5}$ for all the phases since it contained the highest amount of binder. The highest amount of $PM_{2.5}$ was captured during the CSHP phase since the fuel burned with a yellow flame accompanied with emission of soot. During the HSHP and Simmer phases, the soot emission had reduced considerably since most of the binder had been combusted. The total emissions of $PM_{2.5}$ were 10.5-25.5 mg, 0.5-1.9 mg, 0.3-0.8 mg for the CSHP, HSHP, and Simmer phases respectively.

Figure 42b shows that during the CSHP phase, the amount of CO emitted fluctuated with binder concentration for briquettes B25, B30, B35 and B40 since the binder contains terpenoids thus there was not enough air to combust them. During the HSHP phase the amount of CO decreased with binder concentration. During the Simmer phase there was fluctuation of CO for briquettes B25, B30, B35, and B40. Figure 42c shows that generally, during the CSHP phase, the amount of CO_2 increased with binder concentration for briquettes B25, B30, B35, and B40. During the HSHP

phase there was fluctuation in the amount of CO_2. During the Simmer phase, the amount of CO_2 increased with binder concentration. Briquette B40 produced the greatest amount of CO_2 since it contained more binder.

From Fig. 34b, 35b, 36b and 37b, a significant level of hydrocarbons was still detectable in the fuel during the HSHP phase and this could explain the high amount of CO and CO_2 measured during this phase. The total emissions of CO and CO_2 during the Simmer phase was higher than during the CSHP and HSHP phases due to the fact that the Simmer phase takes a long time of 45 min. The total emissions of CO were 21.0-28.9 g, 9.3-28.9 g and 44.5-58.0 g for the CSHP, HSHP, and Simmer phases, respectively. The total emissions of CO_2 were 104.2-172.4 g, 92.4-110.1 g and 123.5-173.3 g for the CSHP, HSHP, and Simmer phases, respectively. Mitchell *et al*. (2016) reported that the level of CO emitted depends on the time-temperature history above the burning bed and this agrees with the results of the Simmer phase considering the time taken. Furthermore, the carbon monoxide in the exhaust could be attributed to dissociation of the carbon dioxide formed during combustion (Turns, 2000).

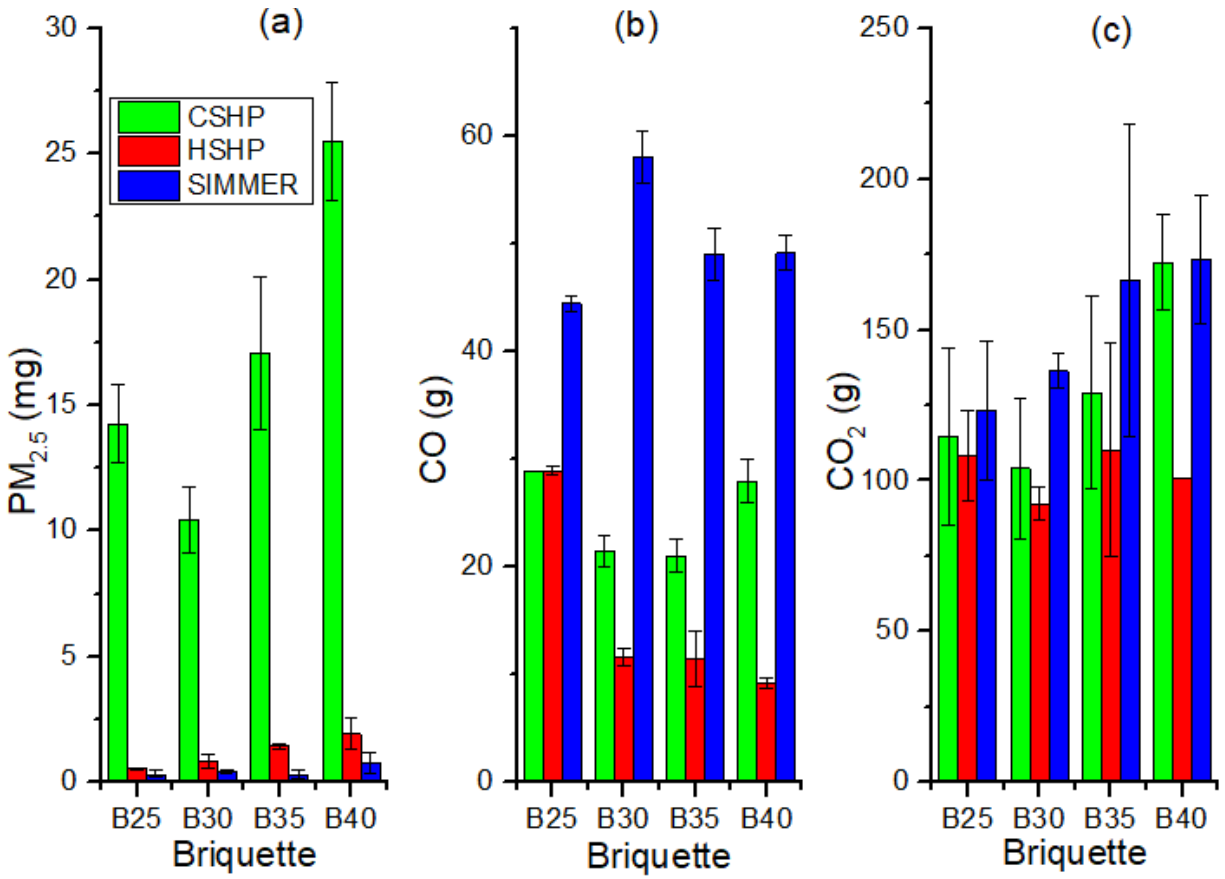

Figure 42: Total Emissions; (a) $PM_{2.5}$, (b) CO, (c) CO_2

(vi) Emissions per MJ

Figure 43a-c shows the results of emissions per MJ delivered to the cooking pot. From Fig. 43a it was observed that the emissions per MJ for $PM_{2.5}$ fluctuated with binder concentration during CSHP phase and increased with binder concentration during HSHP phase. During the Simmer phase the emissions per MJ for $PM_{2.5}$ of briquettes B25, B30 B35, and B40 fluctuated with binder concentration. Moreover, briquettes B40 produced the highest emissions per MJ for $PM_{2.5}$ for all the phases since it contained the highest amount of binder. The highest emissions per MJ for $PM_{2.5}$ was captured during the CSHP phase since the fuel burned with a yellow flame accompanied with emission of soot. The emissions per MJ for $PM_{2.5}$ were 9.6-23.6 mg/MJ, 0.7-2.2 mg/MJ, 0.3-0.7 mg/MJ for the CSHP, HSHP and Simmer phases, respectively. Mitchell *et al*. (2016) obtained total particulate matter ($PM_{2.5}$ and PM_{10}) values of 15-47.5 mg/MJ during flaming and smouldering after combustion of torrefied wood briquettes in a fixed bed domestic stove. Thus, the PM was quite higher than the one (0.3-23.6 mg/MJ) obtained in this study.

From Fig. 43b, c it was observed that generally, during the CSHP phase, the emissions per MJ for CO and CO_2 fluctuated with binder concentration for briquettes B25, B30, B35 and B40. During the HSHP phase, the emissions per MJ of CO decreased while that of CO_2 fluctuated with binder concentration. During the Simmer phase, the emissions per MJ for CO and CO_2 fluctuated with binder concentration. The emissions per MJ for CO were 16.8-28.8 g/MJ, 10.7-34.7 g/MJ, 42.4-78.6 g/MJ for the CSHP, HSHP and Simmer phases, respectively. The emissions per MJ for CO_2 were 95.5-160.4 g/MJ, 107.0-129.3 g/MJ, 121.2-218.4 g/MJ for the CSHP, HSHP and Simmer phases, respectively. Mitchell *et al*. (2016) obtained CO values of 500-7000 mg/MJ during ignition, flaming and smouldering after combustion of torrefied wood briquettes in a fixed bed domestic stove. Thus, the CO was quite higher than the one (10.7- 78.6 mg/MJ) obtained in this study.

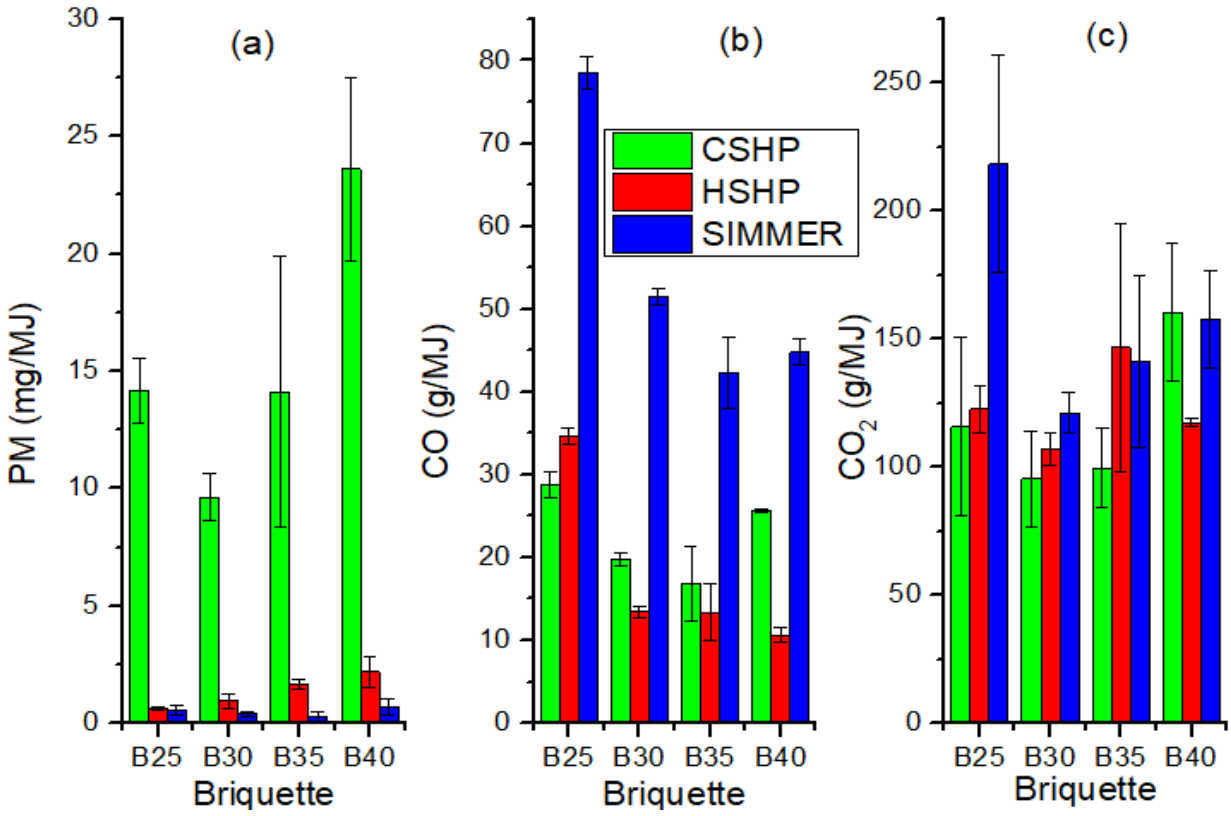

Figure 43: Emissions per MJ; (a) $PM_{2.5}$, (b) CO and (c) CO_2

(vii) Specific Emissions and Emission Rate

The results of specific emissions and emission rate of $PM_{2.5}$, CO, and CO_2 are summarized in Table 10. Grimsby *et al*. (2016) did a study on multiple biomass fuels and improved cookstoves from Tanzania assessed with the WBT and used concentrations of CO and PM as values for comparing cleanliness of cooking options. Other researchers have also considered $PM_{2.5}$, CO, and CO_2 (Chen *et al*., 2016; Lask *et al*., 2015; Medina *et al*., 2016). Burnett *et al*. (2014) did a study on an integrated risk function for estimating the global burden of disease attributable to ambient fine PM exposure and one of the diseases modelled was lung cancer by comparing the predicted and relative risk (RR) vs Log $PM_{2.5}$ (µg/m^3). The results showed that below 5 µg/m^3, the predicted and RR is about 1 thus, the specific emissions results of the Log $PM_{2.5}$ (µg/m^3) from the current study show limited risk to development of lung cancer.

World Health Organization (2014) recommends an annual interim target-1 (IT-1) of 35-75 µg/m^3 $PM_{2.5}$ thus, the results of specific emissions obtained in this study were above the standard for CSHP, HSHP and Simmer phases. In comparison to cooking with kerosene for both wick and pressurized stoves, studies of kitchen and personal exposure levels found respirable PM in the range of 340 µg/m^3 to more than 1000 µg/m^3 (WHO, 2014). These results are similar to the ones (422.1- 1034.9 µg/m^3) obtained in this study for the Simmer phase. The WHO (annual average)

air quality guidelines IT-1 for $PM_{2.5}$ (vented) is 0.80 mg/min (WHO, 2014). From the results of the emissions rate, briquettes B25, B30, and B35 met this standard during the CSHP, HSHP and Simmer phases while B40 achieved the same during HSHP and Simmer phases. The 24-hour average air quality guideline for CO (vented) is 0.59 g/min (WHO, 2014). From the results of the emissions rate, briquette B25 was close to this standard during the CSHP phase while briquettes B30, B35 and B40 were close to this standard during the HSHP phase. World Health Organization (2014) reported that CO_2 emissions from non-sustainable use of biomass fuel affects the climate, but does not directly impact health.

Table 10: Specific emissions and emissions rate of $PM_{2.5}$, CO, and CO_2

	Unit	B25	B30	B35	B40
Specific Emissions					
CSHP phase					
CO	g/L	12.0	9.1	8.9	11.8
CO_2	g/L	47.7	44.3	54.7	72.8
$PM_{2.5}$	µg/m^3	19 904.9	28 337.9	47 265.8	76 692.9
Log ($PM_{2.5}$)	µg/m^3	4.3	4.4	4.7	4.9
HSHP phase					
CO	g/L	11.7	4.7	4.6	3.8
CO_2	g/L	43.7	37.5	44.5	40.9
$PM_{2.5}$	µg/m^3	1288.3	3050.1	5071.4	7857.4
Log ($PM_{2.5}$)	µg/m^3	3.1	3.5	3.7	3.9
simmer phase					
CO	g/L	20.0	29.6	25.1	24.8
CO_2	g/L	55.6	69.5	85.4	87.6
$PM_{2.5}$	µg/m^3	422.1	570.6	404.8	1034.9
Log ($PM_{2.5}$)	µg/m^3	2.6	2.8	2.6	3.0
Emissions Rate					
CSHP phase					
CO	g/min	0.7	1.0	1.0	1.4
CO_2	g/min	2.8	4.8	5.9	8.6
$PM_{2.5}$	mg/min	0.34	0.48	0.79	1.26
HSHP phase					
CO	g/min	1.1	0.7	0.7	0.6
CO_2	g/min	4.3	5.8	6.4	6.9
$PM_{2.5}$	mg/min	0.02	0.05	0.09	0.14
simmer phase					
CO	g/min	1.0	1.3	1.1	1.1
CO_2	g/min	2.7	3.0	3.7	3.8
$PM_{2.5}$	mg/min	0.01	0.010	0.01	0.02

4.6 Ash

Figure 44 shows the XRD results for ash and charcoal fines. The properties of wood ash depend on various factors; type of plant, part of plant combusted (bark, wood, leaves), type of waste

(wood, pulp or paper residue), combination with other fuel sources, type of soil, climate, conditions of combustion, collection and of storage (Demeyer *et al*., 2001; Pitman, 2006). Steenari *et al*. (1999) reported that Ca and Si are the most dominant elements in wood ash, but significant amounts of other important nutrients, such as Mg, K, P and Mn, are also present. The ash contained mainly $CaCO_3$ (76.6 wt%) followed by CaO (13.1 wt%) and the remainder was the amorphous compounds (10.3 wt%). Steenari and Lindqvist (1997) reported that calcium in wood ash is present mainly in a $CaCO_3$ form which agrees with the results in this study. Misra *et al*. (1993) did a study on wood ash composition as a function of furnace temperature and considered temperatures of 600 and 1300℃. At a temperature of 600℃ the XRD analysis of the wood ash showed a relative intensity of the strongest peaks as 100% for $CaCO_3$ and this is similar to the results obtained in this study.

The charcoal fines contained $CaCO_3$ (70%) and the remainder was the amorphous compounds (30 wt%). Tongpoothorn *et al*. (2011) did a study on preparation of activated carbon derived from Jatropha curcas fruit shell and the XRD analysis of the activated carbon exhibited broad peaks and absence of a sharp peak that revealed predominantly amorphous structure. Thus, the disappearance of peaks for CaO could be attributed to the high percentage of amorphous carbon in the charcoal fines. Etiégni and Campbell (1991) did a study on physical and chemical characteristics of wood ash from Lodgepole pine saw dust and found that ash yield and chemical composition changed with temperature. In addition, XRD analysis of a dry sample as well as a sample hydrated and air dried for 24 h showed that the most probable major components of the wood ash were lime (CaO), calcite ($CaCO_3$), portlandite ($Ca(OH)_2$) and calcium silicate (Ca_2SiO_4). The $Ca(OH)_2$ could have formed as a result of the hydration reaction between CaO and water as reported by Steenari *et al*. (1999). Steenari *et al*. (1999) reported that combustion temperatures of 1000-1200℃ result in the formation of calcium silicates thus Ca_2SiO_4 reported by Etiégni and Campbell (1991) could have formed as a result of heating the samples between 538-1093℃.

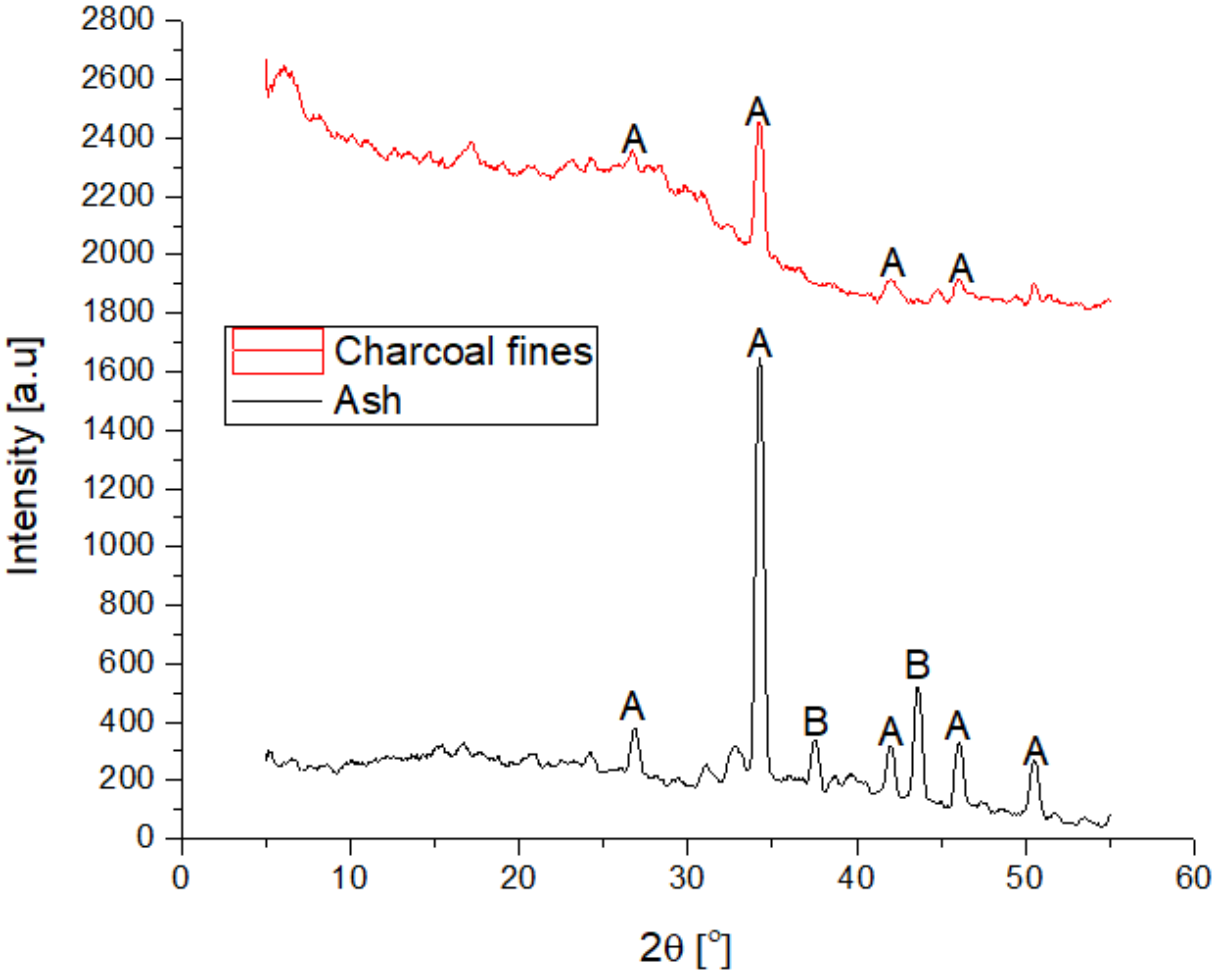

Figure 44: XRD analysis of ash and charcoal fines; A-Calcite ($CaCO_3$), B- lime *(CaO)*

CHAPTER FIVE

CONCLUSION AND RECOMMENDATIONS

5.1 Conclusion

The study showed that *Canarium Schweinfurthii* resin is a suitable binder for production of carbonized briquettes using charcoal fines as feedstock. Alternatively, biomass waste can be carbonized to provide the char which can supplement the charcoal fines. The charcoal fines contained medium volatile matter as a result of the inefficient local methods of carbonization of wood to produce charcoal. In addition, the binder does not contain ash which interferes with the combustion of the briquettes. The heating value of the binder was higher than that of the charcoal fines and hence improved the higher heating value of the briquettes in addition to acting as binder.

The briquettes were found to cure instantly since the binder used is a solid at room temperature and does not need water in its preparation thus, the briquettes can be used as soon as they are ejected from the die. The increased strength and density of the briquettes with binder concentration implies that they can easily be stored and transported. The increased density of the briquettes with binder concentration implies that briquettes burn longer thus, reducing the loading time of the cookstove. For compressive strength, all the briquettes met the recommended minimum value of 0.375 MPa reported for commercial charcoal briquettes. The high WRI showed that the briquettes are impervious to water which would cause easy disintegration as well as difficulty during ignition of the briquettes.

Since the binder is combustible, it contributes to the heat energy from the briquettes as observed by the flaming combustion during ignition and CSHP phases. The briquettes were found to ignite easily and burned with white smoke, yellow flame and soot during CSHP phase and later burned without a yellow flame and soot during the HSHP and Simmer phases. Briquettes B40 were found to boil water faster during CSHP and HSHP phase though they also contribute the highest emissions in terms of $PM_{2.5}$. The sulphur in the charcoal fines as well as the nitrogen in the charcoal fines and binder contributed to the SO_2 and NO_x emissions respectively. During the WBT, the terpenoids in the binder contributed to the high amount of soot, hydrocarbons, CO and CO_2 during ignition and combustion of the briquettes.

5.2 Recommendations

Briquettes B35 and B40 passed the recommended IRI value of 50. To mitigate the emission of $PM_{2.5}$, briquettes B25 and B30 with a lower binder concentration are recommended. The briquettes

can be used as an alternative source of fuel to firewood since they exhibit similar combustion behaviour. To improve indoor air quality when using the developed briquettes, it is recommended that a chimney should be installed on the kitchen to vent outdoor these pollutant emissions during cooking. Furthermore, individuals involved in cooking are advised to stay away from the kitchen especially during the CSHP phase to avoid exposure to the pollutant emissions. This would however, be practical only when cooking food that does not require close attention to be near the cookstove such as boiling water. The ash can be a potential fertilizer to replenish the soil thus, increasing harvests and neutralising soil acidity**.**

Due to scarcity of the resin, its synthesis in the laboratory should be investigated to ensure sustainability. During mixing of binder and charcoal fines, there was agglomeration of the mixture and this can be avoided by using deflocculants which need to be studied. In addition, techno-economic and life-cycle assessment should be done. The effect of soot on heat transfer to the pot should also be investigated. The gas analyser (Ametek Land, lancom 4) could not identify the exact species of the hydrocarbons from the combustion products thus their chemical formulae could not be determined. Analysis of the gaseous emissions to identify these species using more sophisticated equipment is recommended. Further research to understand the chemical composition and more binding properties (softening point, quinoline insoluble, toluene insoluble; physicochemical and rheological properties i.e. colour, odour, taste, pH, solubility (in hot water, cold water, acetone, chloroform, ethanol), intrinsic viscosity, protein, percentage yield, swelling capacity, melting temperature, tannin content, total soluble fibre) of the resin is suggested. Thus, this study has shown that *Canarium Schweinfurthii* resin can be used as a binder for converting of waste material such as charcoal fines to energy through the production of briquettes.

REFERENCES

Ameh, P. O. (2018). Electrochemical and computational study of gum exudates from Canarium schweinfurthii as green corrosion inhibitor for mild steel in HCl solution . *Journal of Taibah University for Science*, *12*(6), 783–795. https://doi.org/10.1080/16583655.2018.1514147

Amer, O., Boukhanouf, R., & Ibrahim, H. G. (2015). A review of evaporative cooling technologies. *International Journal of Environmental Science and Development*, *6*(2), 111–117. https://doi.org/10.7763/ijesd.2015.v6.571

Aprovecho Research Center. (2018). *Instructions for use of the Laboratory Emissions Monitoring System*. https://www.google.com

Aprovecho Research Center. (2020). *Sensor Box Processing WBT 4.2.3 apr.28.20.xls* (4.2.3). http://aprovecho.org/software/

Arora, P., Das, P., Jain, S., & Kishore, V. V. N. (2014). A laboratory based comparative study of Indian biomass cookstove testing protocol and water boiling test. *Energy for Sustainable Development*, *21*, 81–88. https://doi.org/10.1016/j.esd.2014.06.001

ASTM. (2011). *Standard Test Method for Splitting Tensile Strength of Cylindrical Concrete Specimens*. https://doi.org/10.1520/C0496_C0496M-11

ASTM. (2013). *Standard Test Method for Gross Calorific Value of Coal and Coke*. https://doi.org/10.1520/D5865-13

ASTM. (2014a). *Standard Test Method for Compositional Analysis By Thermogravimetry*. https://doi.org/10.1520/E1131-08R14

ASTM. (2014b). *Standard Test Methods for Density and Specific Gravity (Relative Density) of Wood And Wood-Based Materials*. https://doi.org/10.1520/D2395-14

ASTM. (2015). *Standard Practice for Ultimate Analysis of Coal and Coke*. https://doi.org/10.1520/D3176-15

ASTM. (2017). *Standard Test Method for Compressive Strength of Cylindrical Concrete Specimens*. https://doi.org/10.1520/C0039_C0039M-17B

Balat, M. (2011). Production of bioethanol from lignocellulosic materials via the biochemical pathway: A review. *Energy Conversion and Management*, *52*(2), 858–875.

https://doi.org/10.1016/j.enconman.2010.08.013

Bazargan, A., Rough, S. L., & McKay, G. (2014). Compaction of palm kernel shell biochars for application as solid fuel. *Biomass and Bioenergy*, *70*, 489–497. https:// doi. org/ 10. 1016/j. biombioe.08.015

Benk, A. (2010). Utilisation of the binders prepared from coal tar pitch and phenolic resins for the production metallurgical quality briquettes from coke breeze and the study of their high temperature carbonization behaviour. *Fuel Processing Technology*, *91*(9), 1152–1161. https://doi.org/10.1016/j.fuproc.2010.03.030

Bhattacharya, S. C., Sett, S., & Shrestha, R. M. (1989). State of the art for biomass densification. *Energy Sources*, *11*(3), 161–182. https://doi.org/10.1080/00908318908908952

Blasi, C. D. (1993). Modeling and simulation of combustion processes of charring and non-charring solid fuels. *Progress in Energy and Combustion Science*, *19*(1), 71–104. https://doi.org/10.1016/0360-1285(93)90022-7

Blesa, M. J., Fierro, V., Miranda, J. L., Moliner, R., & Palacios, J. M. (2001). Effect of the pyrolysis process on the physicochemical and mechanical properties of smokeless fuel briquettes. *Fuel Processing Technology*, *74*(1), 1–17. https://doi.org/10.1016/S0378-3820(01)00209-0

Burnett, R. T., Arden, P. C., Ezzati, M., Olives, C., Lim, S. S., Mehta, S., Shin, H. H., Singh, G., Hubbell, B., Brauer, M., Ross Anderson, H., Smith, K. R., Balmes, J. R., Bruce, N. G., Kan, H., Laden, F., Prüss-Ustün, A., Turner, M. C., Gapstur, S. M., … Cohen, A. (2014). An integrated risk function for estimating the global burden of disease attributable to ambient fine particulate matter exposure. *Environmental Health Perspectives*, *122*(4), 397–403. https://doi.org/10.1289/ehp.1307049

Carnaje, N. P., Talagon, R. B., Peralta, J. P., Shah, K., & Paz-Ferreiro, J. (2018). Development and characterisation of charcoal briquettes from water hyacinth (*Eichhornia crassipes*)-molasses blend. *PloS One*, 13(11), e0207135.

Chen, Y., Shen, G., Su, S., Du, W., Huangfu, Y., Liu, G., Wang, X., Xing, B., Smith, K. R., & Tao, S. (2016). Efficiencies and pollutant emissions from forced-draft biomass-pellet semi-gasifier stoves: Comparison of International and Chinese water boiling test protocols. *Energy for Sustainable Development*, *32*, 22–30. https://doi.org/10.1016/j.esd.2016.02.008

Chirchir, D. K ., Nyaanga , D. M., & Githeko, J. M. (2013). Effect of binder types and amount on physical and combustion characterisitics. *International Journal of Engineering Research and Science and Technology*, *2*(1), 12–20.

Clean cooking alliance. (2013). *Guidelines for Testing Charcoal Stoves with WBT 4.2.2*. http://cleancookingalliance.org/binary-data/document/file/000/000/401-1.pdf

Clean cooking alliance. (2014). *The Water Boiling Test version 4.2.3*. https://www.cleancookingalliance.org/technology-and-fuels/testing/protocols.html

Da Silva Rodrigues-Corrêa, K. C., De Lima, J. C., & Fett-Neto, A. G. (2013). Oleoresins from pine: Production and industrial uses. *Natural Products*,136, 4037-4060.

Deac, T., Fechete-tutunaru, L., & Gaspar, F. (2016). Environmental impact of sawdust briquettes use - experimental approach. *Energy Procedia*, *85*, 178–183.

Demeyer, A., Voundi Nkana, J. C., & Verloo, M. G. (2001). Characteristics of wood ash and influence on soil properties and nutrient uptake: An overview. *Bioresource Technology*, *77*(3), 287–295. https://doi.org/10.1016/S0960-8524(00)00043-2

Drobíková, K., Plachá, D., Motyka, O., Gabor, R., Kutláková, K. M., Vallová, S., & Seidlerová, J. (2015). Recycling of blast furnace sludge by briquetting with starch binder: Waste gas from thermal treatment utilizable as a fuel. *Waste Management*, *48*, 471–477.

El-Mahallawy, F., & El-Din Habik, S. (2002). *Fundamentals and Technology of Combustion* (V. *Thame (1st Ed.)* Elsevier. https://www.google.com

Etiégni, L., & Campbell, A. G. (1991). Physical and chemical characteristics of wood ash. *Bioresource Technology*, *37*(2), 173–178. https://doi.org/10.1016/0960-8524(91)90207-Z

Fadhil, A. B. (2020). Production and characterization of liquid biofuels from locally available nonedible feedstocks. *Asia-Pacific Journal of Chemical Engineering*, *16*(1), 1–21. https://doi.org/10.1002/apj.2572

Fagbemi, E., Ayeke, P., Omonigho, B., Udokpo, N., Iseru, E., Akpovwovwo, T., & Awolola, E. (2014). Determination of physical and mechanical properties of briquettes produced from carbonized rubber seed shell using local binder. *American Journal of Materials Research*, *1*(3), 44–47. http://www.aascit.org/journal/ajmr

Ferguson, H. (2012). *Briquette Businesses in Uganda; The potential for briquette enterprises to*

address the sustainability of the Ugandan biomass fuel market. www. gvepinternational. org%0A

Fernandez-Anez, N., Slatter, D. J. F., Saeed, M. A., Phylaktou, H. N., Andrews, G. E., & Garcia-Torrent, J. (2018). Ignition sensitivity of solid fuel mixtures. *Fuel*, *223*, 451–461. https://doi.org/10.1016/j.fuel.2018.02.106

Fichan, I., Larroche, C., & Gros, J. B. (1999). Water solubility, vapor pressure, and activity coefficients of terpenes and terpenoids. *Journal of Chemical and Engineering Data*, *44*(1), 56–62. https://doi.org/10.1021/je980070+

Gani, A., & Naruse, I. (2007). Effect of cellulose and lignin content on pyrolysis and combustion characteristics for several types of biomass. *Renewable Energy*, *32*(4), 649–661. https://doi.org/10.1016/j.renene.2006.02.017

Gesase, L. E., King'ondu, C. K., & Jande, Y. A. C. (2019). Manihot glaziovii-Bonded and Bioethanol-Infused Charcoal Dust Briquettes: A New Route of Addressing Sustainability, Ignition, and Food Security Issues in Briquette Production. *Bioenergy Research*, *13*, 378–386. https://doi.org/10.1007/s12155-019-10076-9

Gilvari, H., De Jong, W., & Schott, D. L. (2019). Quality parameters relevant for densification of bio-materials: Measuring methods and affecting factors: A review. *Biomass and Bioenergy*, *120*, 117–134. https://doi.org/10.1016/j.biombioe.2018.11.013

Glarborg, P., Jensen, A. D., & Johnsson, J. E. (2003). Fuel nitrogen conversion in solid fuel fired systems. *Progress in Energy and Combustion Science*, *29*(2), 89–113.

Grimsby, L. K., Rajabu, H. M., & Treiber, M. U. (2016). Multiple biomass fuels and improved cook stoves from Tanzania assessed with the water boiling test. *Sustaninable Energy Technologies and Assessments*, *14*, 63–73. https://doi.org/10.1016/j.seta.2016.01.004

Grover, P. D., & Mishra, S. K. (1996). *Biomass Briquetting: Technology and Pratices.* (No.46). FAO Regional Wood Energy Development Programme in Asia. https://www.google.com

Haykiri-Acma, H., Yaman, S., & Kucukbayrak, S. (2013). Production of biobriquettes from carbonized brown seaweed. *Fuel Processing Technology*, *106*, 33–40.

Heinimö, J., & Junginger, M. (2009). Production and trading of biomass for energy: An overview of the global status. *Biomass and Bioenergy*, *33*(9), 1310–1320.

Hermans, L. J. F. (2012). Boiling water. *Europhysics News*, *43*(2), 13–13.

Hu, Q., Shao, J., Yang, H., Yao, D., Wang, X., & Chen, H. (2015). Effects of binders on the properties of bio-char pellets. *Applied Energy*, *157*, 508–516.

Huang, G., & Hao, Y. (2012). Preparation and principle of Shenmu bituminous coal gasification briquette. *China Coal*, *38*, 83–90.

Idris, J., Shirai, Y., Andou, Y., Ali, A. A. M., Othman, M. R., Ibrahim, I., & Hassan, M. A. (2015). Self-sustained carbonization of oil palm biomass produced an acceptable heating value charcoal with low gaseous emission. *Journal of Cleaner Production*, *89*, 257–261. https://doi.org/10.1016/j.jclepro.2014.11.016

ISO. (2018). *Clean cookstoves and clean cooking solutions: Harmonized laboratory test protocols: Part 1: Standard test sequence for emissions and performance, safety and durability*. https://www.google.com

Kambo, H. S., & Dutta, A. (2014). Strength, storage, and combustion characteristics of densified lignocellulosic biomass produced via torrefaction and hydrothermal carbonization. *Applied Energy*, *135*, 182–191. https://doi.org/10.1016/j.apenergy.2014.08.094

Karungi, A., Pogrebnoi, A., & Kivevele, T. (2020). Optimization of microwave-assisted alkali pretreatment followed by acid hydrolysis of sugarcane straw for production of acetone-butanol-ethanol. *Energy Sources, Part A: Recovery, Utilization and Environmental Effects*, 2020, 1–17. https://doi.org/10.1080/15567036.2020.1760404

Khlifi, S., Lajili, M., Tabet, F., Boushaki, T., & Sarh, B. (2019). Investigation of the combustion characteristics of briquettes prepared from olive mill solid waste blended with and without a natural binder in a fixed bed reactor. *Biomass Conversion and Biorefinery*, *10*, 535–544. https://doi.org/10.1007/s13399-019-00449-7

Kivevele, T. T., & Huan, Z. (2013). Effects of antioxidants on the cetane number, viscosity, oxidation stability, and thermal properties of biodiesel produced from nonedible oils. *Energy Technology*, *1*(9), 537–543. https://doi.org/10.1002/ente.201300072

Kpalo, S. Y., Zainuddin, M. F., Manaf, L. A., & Roslan, A. M. (2020a). A review of technical and economic aspects of biomass briquetting. *Sustainability*, *12*(11), 4609. https://doi.org/10.3390/su12114609

Kpalo, S. Y., Zainuddin, M. F., Manaf, L. A., & Roslan, A. M. (2020b). Production and characterization of hybrid briquettes from corncobs and oil palm trunk bark under a low pressure densification technique. *Sustainability, 12*(6), 2468.

Kuete, V. (2017). *Canarium schweinfurthii*. https://doi.org/10.1016/B978-0-12-809286-6.00016-9

Lackner, M. (2011). *Combustion: Ullmann's Encyclopedia of Industrial Chemistry*. Wiley-VCH. https://doi.org/10.1002/14356007.b03

Lask, K., Booker, K., Han, T., Granderson, J., Yang, N., Ceballos, C., & Gadgil, A. (2015). Performance comparison of charcoal cookstoves for Haiti: laboratory testing with water boiling and controlled cooking tests. *Energy for Sustainable Development*, *26*, 79–86. https://doi.org/10.1016/j.esd.2015.02.002

Lubwama, M., & Yiga, V. A. (2017). Development of groundnut shells and bagasse briquettes as sustainable fuel sources for domestic cooking applications in Uganda. *Renewable Energy*, *111*, 532–542. https://doi.org/10.1016/j.renene.2017.04.041

Lubwama, M., Yiga, V. A., & Lubwama, H. N. (2020). Effects and interactions of the agricultural waste residues and binder type on physical properties and calorific values of carbonized briquettes. *Biomass Conversion and Biorefinery*, 2020, 1-21.

Medina, P., Berrueta, V., Martínez, M., Ruiz, V., Edwards, R. D., & Masera, O. (2016). Comparative performance of five Mexican plancha-type cookstoves using water boiling tests. *Development Engineering*, *2*, 20–28. https://doi.org/10.1016/j.deveng.2016.06.001

Menya, E., Olupot, P. W., Storz, H., Lubwama, M., Kiros, Y., & John, M. J. (2020). Optimization of pyrolysis conditions for char production from rice husks and its characterization as a precursor for production of activated carbon. *Biomass Conversion and Biorefinery*, *10*(1), 57–72. https://doi.org/10.1007/s13399-019-00399-0

Misra, M. K., Ragland, K. W., & Baker, A. J. (1993). Wood ash composition as a function of furnace temperature. *Biomass and Bioenergy, 4*(2), 103–116.

Mitchell, E. J. S., Lea-Langton, A. R., Jones, J. M., Williams, A., Layden, P., & Johnson, R. (2016). The impact of fuel properties on the emissions from the combustion of biomass and other solid fuels in a fixed bed domestic stove. *Fuel Processing Technology*, *142*, 115–123. https://doi.org/10.1016/j.fuproc.2015.09.031

Moqbel, S., Reinhart, D., & Chen, R. H. (2010). Factors influencing spontaneous combustion of solid waste. *Waste Management*, *30*(8–9), 1600–1607.

Nagawa, C., Böhmdorfer, S., & Rosenau, T. (2015). Chemical composition and anti-termitic activity of essential oil from Canarium schweinfurthii Engl. *Industrial Crops and Products*, *71*, 75–79. https://doi.org/10.1016/j.indcrop.2015.03.078

Nwabue, F. I., Unah, U., & Itumoh, E. J. (2017). Production and characterisation of smokeless bio-coal briquettes incorporating plastic waste materials. *Environmental Technology and Innovation*, *8*, 233–245. https://doi.org/10.1016/j.eti.2017.02.008

Obi, O. F. (2015). Evaluation of the effect of palm oil mill sludge on the properties of sawdust briquette. *Renewable and Sustainable Energy Reviews*, *52*, 1749–1758.

Oketch, P. O., Ndiritu, H. M., & Gathitu, B. B. (2014). Experimental study of fuel efficiency and emissions comparison from bio-ethanol gel Stoves. *European International Journal of Science and Technology*, *3*(7), 328–339.

Okot, D. K., Bilsborrow, P. E., & Phan, A. N. (2018). Effects of operating parameters on maize cob briquette quality. *Biomass and Bioenergy*, *112*, 61–72.

Onchieku, J. M., Chikamai, B. N., & Rao, M. S. (2012). Optimum Parameters for the Formulation of Charcoal Briquettes Using Bagasse and Clay as Binder. *European Journal of Sustainable Development*, *1*(3), 477–492. https://doi.org/10.14207/ejsd.2012.v1i3p477

Onuegbu, T. U., Ekpunobi, U. E., Ogbu, I. M., Ekeoma, M. O., & Obumselu, F. O. (2011). Comparative studies of ignition time and water boiling test of coal and biomass briquettes blend. *International Journal of Recent Research and Applied Studies*, 7(2), 153-159.

Onuegbu, Theresa Uzoma, Ogbu, I. M., & Ilochi, N. O. (2010). Enhancing the Properties of Coal Briquette Using Spear Grass (Imperata Cylindrica). *Leonardo Journal of Sciences*, *17*(2), 47–58. http://ljs.academicdirect.org

Ormeño, E., Céspedes, B., Sánchez, I. A., Velasco-García, A., Moreno, J. M., Fernandez, C., & Baldy, V. (2009). The relationship between terpenes and flammability of leaf litter. *Forest Ecology and Management*, *257*(2), 471–482. https://doi.org/10.1016/j.foreco.2008.09.019

Pandey, S., & Dhakal, R. P. (2013). Pine Needle Briquettes: A Renewable Source of Energy. *International Journal of Energy Science*, *3*(3), 254–260.

Pereira, B. L. C., Oliveira, A. C., Carvalho, A. M. M. L., Carneiro, A. D. C. O., Santos, L. C., & Vital, B. R. (2012). Quality of wood and charcoal from Eucalyptus clones for ironmaster use. *International Journal of Forestry Research*, 2012, 1-9.

Pitman, R. M. (2006). Wood ash use in forestry: A review of the environmental impacts. *Forestry*, *79*(5), 563–588. https://doi.org/10.1093/forestry/cpl041

Prasityousil, J., & Muenjina, A. (2013). Properties of solid fuel briquettes produced from rejected material of municipal waste composting. *Procedia Environmental Sciences*, *17*, 603–610. https://doi.org/10.1016/j.proenv.2013.02.076

Quist, C. M., Jones, M. R., & Lewis, R. S. (2020). Influence of variability in testing parameters on cookstove performance metrics based on the water boiling test. *Energy for Sustainable Development*, *58*, 112–118. https://doi.org/10.1016/j.esd.2020.07.006

Raju, A. I. C., Jyothi, R. K., Satya, M., & Praveena, U. (2014). Studies on development of fuel briquettes for household and industrial purpose. *International Journal of Research in Engineering and Technology*, *3*(2), 54–63.

Rezzi, S., Bighelli, A., Castola, V., & Casanova, J. (2005). Composition and chemical variability of the oleoresin of Pinus nigra ssp. laricio from Corsica. *Industrial Crops and Products*, *21*(1), 71–79. https://doi.org/10.1016/j.indcrop.2003.12.008

Romallosa, A. R. D., & Kraft, E. (2017). Feasibility of biomass briquette production from municipal waste streams by integrating the informal sector in the philippines. *Resources*, *6*(12), 1–19. https://doi.org/10.3390/resources6010012

Rotich, K. P. (1998). *Carbonization and Briquetting of Sawdust for Use in Domestic Cookers*. University of Nairobi. https://www.google.com

Rousset, P., Caldeira-Pires, A., Sablowski, A., & Rodrigues, T. (2011). LCA of eucalyptus wood charcoal briquettes. *Journal of Cleaner Production*, *19*(14), 1647–1653. https://doi.org/10.1016/j.jclepro.2011.05.015

Samadi, S. H., Ghobadian, B., & Nosrati, M. (2019). Prediction of higher heating value of biomass materials based on proximate analysis using gradient boosted regression trees method. *Energy Sources, Part A: Recovery, Utilization and Environmental Effects*, *0*(0), 1–10.

Sen, R., Wiwatpanyaporn, S., & Annachhatre, A. P. (2016). Influence of binders on physical

properties of fuel briquettes produced from cassava rhizome waste. *International Journal of Environment and Waste Management*, *17*(2), 158–175.

Šiler, B., & Mišić, D. (2016). Biologically active compounds from the genus Centaurium sl (Gentianaceae): current knowledge and future prospects in medicine. *Studies in Natural Products Chemistry*, 49, 363-397.

Sotannde, O. A., Oluyege, A. O., & Abah, G. B. (2010). Physical and combustion properties of charcoal briquettes from neem wood residues. *International Agrophysics*, *24*(2), 189–194.

Sotannde, O. A., Oluyege, A. O., & Abah, G. B. (2016). Physical and combustion properties of briquettes from sawdust of Azadirachta indica. *International Agrophysics*, *21*(1), 63–67. https://doi.org/10.1007/s11676-010-0010-6

Steenari, B. M., Karlsson, L. G., & Lindqvist, O. (1999). Evaluation of the leaching characteristics of wood ash and the influence of ash agglomeration. *Biomass and Bioenergy*, *16*(2), 119–136. https://doi.org/10.1016/S0961-9534(98)00070-1

Steenari, B. M., & Lindqvist, O. (1997). Stabilization of biofuel ashes for recycling to forest soil. *Biomass and Bioenergy*, *13*(1–2), 39–50.

Sugumaran, P., & Seshadri, S. (2010). *Biomass Charcoal Briquetting, Technology for Alternative Energy Based Income Generation in Rural Areas*. www.amm-mcrc.org

Suhartini, S., Hidayat, N., & Wijaya, S. (2011). Physical properties characterization of fuel briquette made from spent bleaching earth. *Biomass and Bioenergy*, *35*(10), 4209–4214. https://doi.org/10.1016/j.biombioe.2011.07.002

Teixeira, S. R., Pena, A. F. V., & Miguel, A. G. (2010). Briquetting of charcoal from sugar-cane bagasse fly ash (scbfa) as an alternative fuel. *Waste Management*, 30(5), 804-807.

Thermopedia. (2011). *Steam Tables: A-to-Z Guide to Thermodynamics, Heat & Mass Transfer, and Fluids Engineering*. https://doi.org/10.1615/AtoZ.s.steam_tables

Thoms, L. J., Snape, C. E., & Taylor, D. (1999). Physical characteristics of cold cured anthracite/coke breeze briquettes prepared from a coal tar acid resin. *Fuel*, *78*(14), 1691–1695. https://doi.org/10.1016/S0016-2361(99)00116-7

Tilli, A. (2003). *Bioenergy*. https://www.google.com

Tongpoothorn, W., Sriuttha, M., Homchan, P., Chanthai, S., & Ruangviriyachai, C. (2011). Preparation of activated carbon derived from Jatropha curcas fruit shell by simple thermo-chemical activation and characterization of their physico-chemical properties. *Chemical Engineering Research and Design*, *89*(3), 335–340.

Turns, S. R. (2000). *An introduction to combustion;concepts and applications* (2nd Ed.). McGraw-Hill. https://www.google.com

Ward, B. J., Yacob, T. W., & Montoya, L. D. (2014). Evaluation of solid fuel char briquettes from human waste. *Environmental Science and Technology*, *48*(16), 9852–9858. https://doi.org/doi.org/10.1021/es500197h

WHO. (2014). *WHO Guidelines for Indoor Air Quality: Household Fuel Combustion*. WHO Document Production Services. https://www.google.com

Wikipedia. (2021). *Makerere*. https://en.wikipedia.org/wiki/Makerere

Wu, S., Zhang, S., Wang, C., Mu, C., & Huang, X. (2018). High-strength charcoal briquette preparation from hydrothermal pretreated biomass wastes. *Fuel Processing Technology*, *171*, 293–300. https://doi.org/10.1016/j.fuproc.2017.11.025

Yadav, N., Yadav, R., & Goyal, A. (2014). Chemistry of terpenoids. *International Journal of Pharmaceutical Sciences Review and Research*, *27*(2), 272–278.

Yang, Y., Cui, G., & Lan, C. Q. (2019). Developments in evaporative cooling and enhanced evaporative cooling: A review. *Renewable and Sustainable Energy Reviews, 113,* 1–10. https://doi.org/10.1016/j.rser.2019.06.037

Yousuf, S., Kamdem, R. S. T., Ngadjui, B. T., Wafo, P., & Fun, H. K. (2011). 3a-Hydroxytirucalla-8,24-dien-21-oic acid. *Acta Crystallographica*, *67*(4), o937–o938.

Zhang, G., Sun, Y., & Xu, Y. (2018). Review of briquette binders and briquetting mechanism. *Renewable and Sustainable Energy Reviews*, *82*(Part 1), 477–487.

Zhao, F. J., Shu, L. F., & Wang, Q. H. (2012). Terpenoid emissions from heated needles of Pinus sylvestris and their potential influences on forest fires. *Acta Ecologica Sinica*, *32*(1), 33–37. https://doi.org/10.1016/j.chnaes.2011.06.002

Zhu, P., Quan, S., Lei, Z., & Zhang, J. (2019). Structural and pyrolysis behaviors analysis of coal pretreated with a weak acid. *Energy Sources, Part A: Recovery, Utilization and*

Environmental Effects, *43*(6), 660–671. https://doi.org/10.1080/15567036.2019.1630520

APPENDICES

Appendix 1: Boiling point of the binder

Sample	Top	Middle	Bottom	AVG	STD
1	98	100	275	158	101
2	107	112	284	168	100
3	102	108	279	163	100
				163	

Appendix 2: Equipment used for characterization: (a)Elemental (CHNSO) analyser, (b)Thermogravimetric analyser (c)Bomb Calorimeter, (d) SEM

(a)

(b)

(c)

(d)

Appendix 3: Pouring temperature of the mixture (charcoal fines and binder)

*Briquette	1	2	3	AVG (°C)	STD
B25	135	123	116	125	10
B30	125	143	112	127	16
B35	128	136	131	132	4
B40	140	123	138	134	9

*Briquette; B25-25 wt% binder, B30-30 wt% binder, B35-35 wt% binder, B40-40 wt% binder

Appendix 4: Compaction pressure of the briquettes

Briquette	Compaction pressure (MPa)					AVG (MPa)	STD
B25	8.2	7.6	8	8	8	7.96	0.22
B30	7.6	7.8	7.8	8	7.8	7.80	0.14
B35	6.2	7	7.8	7.6	7	7.12	0.63
B40	5.8	5.8	5.8	6	6.2	5.92	0.18

Appendix 5: LEMS hood, ducting and gravimetric assembly (Aprovecho Research Centre, 2018)

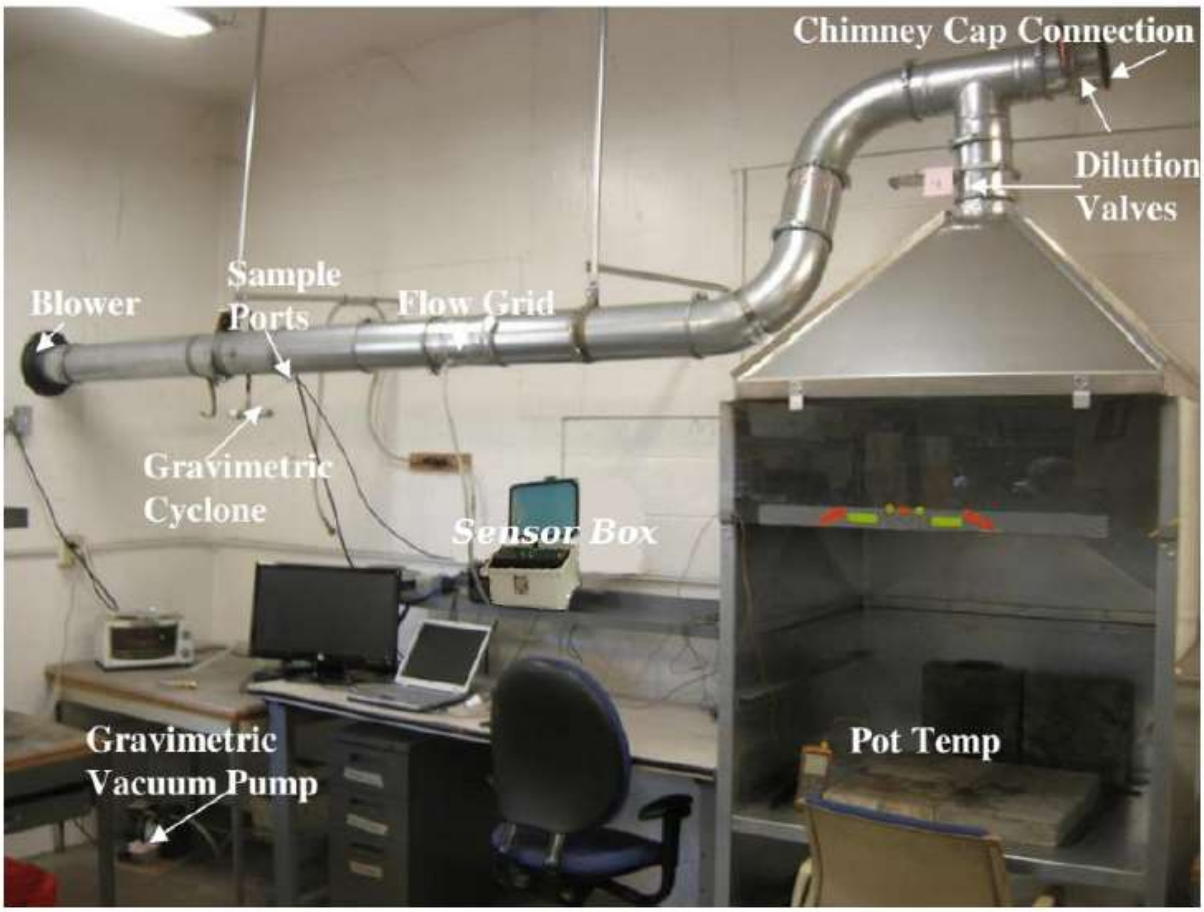

Appendix 6: WBT 4.2.3 Data Calculation Sheet

(a) Sample data Import sheet

Data Import Sheet

Aprovecho Advanced Studies in Appropriate Technology
Sensor Box -- For PEMS and LEMS
Software Version 4.2.3 for all Sensor Boxes
Updated Dec. 20, 2018 - Final

Sensor Box Number: 2029

Data file name (without .csv or .txt): 20201212_WBT_25g_01

Process Data

Enter PEMS # and data file name

Then Click "Process Data" Button and proceed to "WBT" sheet entry.

Fuel carbon fraction	50%	Wood is about 50%, other fuels differ.
Charcoal carbon fracti	90%	50 - 90%

Flow Data	Magnahelic Inch Water	Screen Reading	
Zero Flow	0	10606	Fan on @: 1.6 minutes
Full Flow	0.4	39184	Fan should be turned on between 1 and 4 r

Background (before lighting fire)

Start time	8:08:57	Verify these times
End time	8:47:31	But do not change unless in error
Start row	120	
End row	1277	
CO background concentration	-0.004165983	
PM background concentration	-18.44494721	

	Phase 1 (Cold Start)	*Phase 2 (Hot Start)*	*Phase 3 (Simmer)*	*Entire Measured Period*
Start time	08:49:31	09:33:11	09:59:10	
End time	09:30:23	09:58:26	10:44:10	
Test length (min)	40.9	25.3	45.0	
Start row	1337	2647	3427	
End row	2563	3405	4777	

Total consumption/emission

	Phase 1	*Phase 2*	*Phase 3*

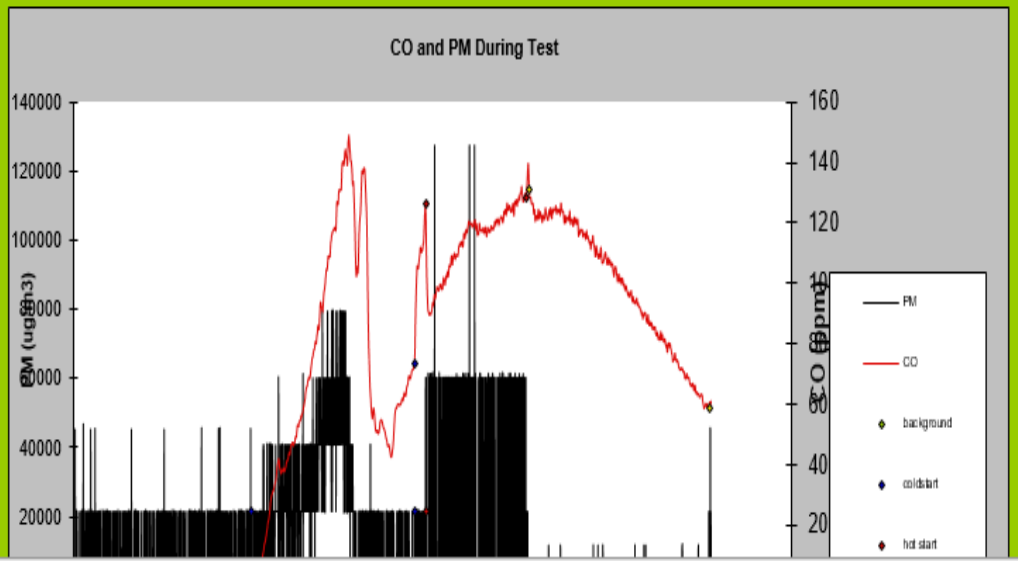

(b) Sample WBT sheet

SHELL FOUNDATION HEH PROJECT WATER BOILING TEST

DATA AND CALCULATION FORM (the form can be used with stoves that cook between one and four pots)*

Shaded cells require user input; unshaded cells automatically display outputs

Qualitative data

Name(s) of Tester(s)	Derrick
Test Number	1
Date	12.12.2020
Stove type/model	Burn
Location	Creec
Fuel species	25% Binder
Wind conditions	No wind

the data entry places in the simmering test for pots other than the primary pot are left blank intentionally because the simmering test can not account for pots other than the primary pot.

Magnahelic

Full Flow: 0.40 inches H20

Initial Test Conditions

Data	value	units	label	Data	value	units	label
Air temp	19.9	°C		Dry weight of Pot # 1 (grams)	198	g	P1
Average dimensions of fuel		cm x cm x cm		Dry weight of Pot # 2 (grams)		g	P2
Gross calorific value (dry fuel)	29,700	kJ/kg	HHV	Dry weight of Pot # 3 (grams)		g	P3
Net calorific value (dry fuel)	28,500	kJ/kg	LHV	Dry weight of Pot # 4 (grams)		g	P4
Wood moisture content (% - wet basis)	4.7%	%	MC	(grams)	-	g	k
the fuel)	27,046	kJ/kg	EHV	Local boiling point	94.9	°C	T_b
Net calorific value charcoal (dry fuel)		kJ/kg	LHV				
Fuel type (enter "W","K","G",or "C")	c	W = wood, K = kerosene, G = LPG, C = coal and charcoal					

	Black Carbon	Gravimetric
Description of stove and other comments:	Enter filter info for each phase	Enter filter info for each phase

		HIGH POWER TEST (COLD START			
		Start		Finish: whe Pot #1 boil	
Measurements	Units	data	label	data	la
Time	hh:mm:ss	08:49	t_{ci}	09:30:23	t
Weight of fuel	g	3293	f_{ci}	3130	f
Water temperature, Pot # 1	°C	19.1	$T1_{ci}$	94.9	T
Water temperature, Pot # 2	°C		$T2_{ci}$		T
Water temperature, Pot # 3	°C		$T3_{ci}$		T
Water temperature, Pot # 4	°C		$T4_{ci}$		T
Weight of Pot # 1 with water	g	2698	$P1_{ci}$	2627	P
Weight of Pot # 2 with water	g		$P2_{ci}$		P
Weight of Pot # 3 with water	g		$P3_{ci}$		P
Weight of Pot # 4 with water	g		$P4_{ci}$		P
Fire-starting materials (if any)	--				
Weight of charcoal+container	g				

		COLD START		HOT START	
Calculations/Results	Units	data	label	data	la
Fuel consumed (moist)	g	163	f_{cm}	60	f
Net change in char during test	g	-	Dc_c	-	D
Equivalent dry wood consumed	g	155	f_{cd}	57	f
Water vaporized from all pots	g	71	w_{cv}	32	w
Effective mass of water boiled	g	2,429	w_{cr}	2,471	w

(c) Sample results sheet

		Burn
Stove type/model		
Location		Creec
Fuel species		25% Binder
Date		12.12.2020

IWA Performance Metrics	units	Value
High Power Thermal Efficiency	%	37.5%
Low Power Specific Consumption Rate	MJ/min/L	0.015
High Power CO	g/MJ	32.02
Low Power CO	g/min/L	0.45
High Power PM	mg/MJ	3740.4
Low Power PM	mg/min/L	0.92
Indoor Emissions CO	g/min	1.01
Indoor Emissions PM	mg/min	88.9
Safety	Index	

	Tier
High Power Thermal Efficiency	3.2
Low Power Specific Consumption Rate	4.1
High Power CO	0.4
Low Power CO	0.4
High Power PM	0.2
Low Power PM	4.0
Indoor Emissions CO	0.9
Indoor Emissions PM	0.4
Safety	0.0

Standard Performance Measures		
Fuel to Cook 5L (850/1500)	g	330.0
CO to Cook 5L (20)	g	161.3
PM to Cook 5L (1500)	mg	7518.4
Energy to Cook 5L (15,000/25,000)	kJ	9,406
Time to Boil	min	32.7

Summarized Data is found at the bottom of this sheet

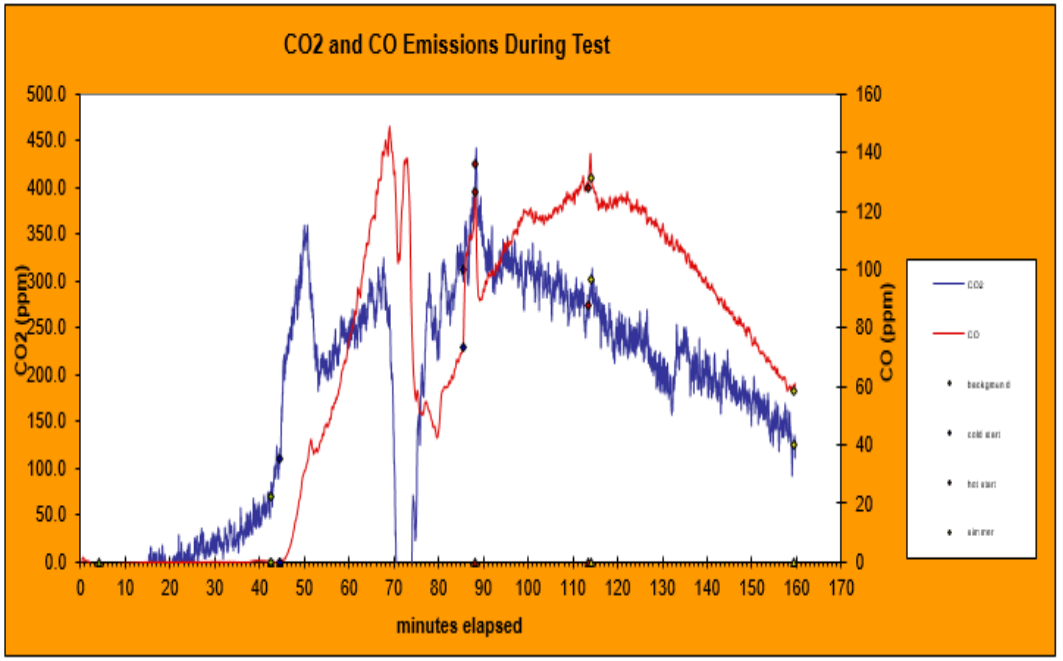

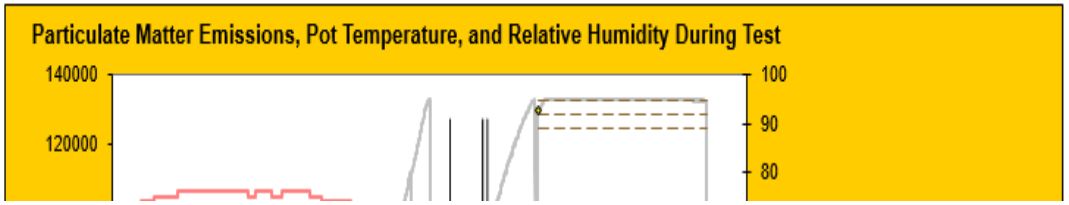

IWA VITA WBT Tie
High Power Therm
Low Power Speci
High Power CO
Low Power CO
High Power PM
Low Power PM
Indoor Emissions (
Indoor Emissions P
Safety

(d) Sample logger data sheet

Background--->			4046.6		0.0	0.1			114.6	4.7		
Time			PM						CO			
Seconds Elapsed	Minutes Elapsed	Clock	PM scat coef (1 / Mm)	Zeroed PM scat coef (1 /Mm)	PM (ug/m3)	PM Flow (ug/sec)	PM Flow (mg/min)	Integrated PM (ug)	CO (logunits)	CO (ppm)	Zeroed CO (ppm)	CO (mg
1	0.0	8:04:58	4048	1	-2490.103	-8.0	-0.5	0	-97	-4	-9	
3	0.1	8:05:00	4048	1	-2490.103	0.0	0.0	0	-23	-1	-6	
5	0.1	8:05:02	4061	14	-26321.01	-116.9	-7.0	-233.71725	40	2	-3	
7	0.1	8:05:04	4048	1	-2490.103	-11.7	-0.7	-257.10979	83	3	-1	
9	0.2	8:05:06	4061	14	-26321.01	0.0	0.0	-257.10979	112	5	0	
11	0.2	8:05:08	4048	1	-2490.103	-7.0	-0.4	-271.15558	135	6	1	
13	0.2	8:05:10	4061	14	-26321.01	-114.5	-6.9	-500.18037	143	6	1	
15	0.3	8:05:12	4061	14	-26321.01	0.0	0.0	-500.18037	150	6	1	
17	0.3	8:05:14	4048	1	-2490.103	-9.9	-0.6	-519.97187	151	6	2	
19	0.3	8:05:16	4048	1	-2490.103	0.0	0.0	-519.97187	159	7	2	

(e) Sample raw data sheet

#	12/12/2020							
#	8:04:57							
##	##							
#0	0.041394	0.00384	4.27	1	0.00384	0.1	1	1
seconds	CO	GasTemp	PM	Flow	FlueTemp	TC	CO2	PM_RH
1	-97	5605	316	10619	5748	195	533	65
3	-23	5601	316	10572	5745	195	539	66
5	40	5601	317	10631	5746	195	537	66
7	83	5600	316	10634	5746	195	545	67
9	112	5601	317	10589	5747	195	543	67
11	135	5600	316	10616	5746	195	539	67
13	143	5601	317	10630	5747	195	531	68
15	150	5603	317	10600	5748	195	527	68
17	151	5605	316	10626	5749	195	527	68
19	159	5606	316	10602	5747	195	519	68
21	157	5607	316	10591	5747	195	514	68
23	153	5608	316	10605	5747	195	516	69
25	156	5608	314	10590	5747	195	512	69
27	152	5608	316	10627	5747	195	510	69
29	153	5610	317	10591	5749	195	505	69
31	153	5611	316	10598	5746	195	503	69
33	144	5612	315	10622	5749	195	503	69
35	143	5613	316	10620	5749	195	498	69
37	142	5614	316	10610	5749	195	490	69
39	142	5613	316	10584	5748	195	490	69
41	138	5616	317	10609	5749	195	490	69
43	137	5618	316	10587	5748	195	494	70

(f) Sample assumptions sheet

Worksheet to read real-time data & calculate performance

Tami Bond (UIUC), Nordica MacCarty (Aprovecho), and Ryan Thompson (Aprovecho)

Assumptions:				
Carbon fraction of fuel	50%	PM Coefficient	4	(ug/m3)/logunit
Scattering cross-section (m2/g)	3			
Ambient pressure (Pa)	101325			
Altitude (m)	0			
		Delay Time		minutes
		CO2 Maximum ppm		
		CO Calibration	0.041394	ppm/logunit
		Flue Temp Calibration	0.00384	degC/logunit
		CO2 Calibration	1	ppm/logunit
File locations		Thermocouple Calibration	0.1	degC/logunit
Raw data files	C:\Emissions-Output			
Output files	C:\Emissions-Output			
Sample Pump Flow Rate	4.4 LPM			
Gravimetric Flow Rate (actual)	16.67 LPM			
Black Carbon Filter Area	cm2			
Black Carbon Flow Rate	LPM			

(g) Sample calorific values sheet

	Tree species	Tree species	Common name(s)	Calorific value (kcal/kg			kJ/kg
				low	high	average	
1	(Select from list)	(select from list or use defalut value of 20,000 MJ/kg)					
2	LPG						48,000
3	Kerosene						43,300
4	Charcoal						29,400
5	Coal						24,700
6	Crop residues						14,700
7	Dung						13,600
	Ethanol						26,800
8	Average Hardwood	Average Hardwood					19,734
9	Average Softwood (Conifer)	Average Softwood (conifer)					20,817
10	Abies Balsamea (Balsam Fir)	Abies Balsamea	balsam fir				18,916
11	Acacia Auriculiformis (Ear-Leaf Acacia, Ear-Pod Wattle)	Acacia Auriculiformis	ear-leaf acacia, ear-pod wattle	4800	4900	4850	20,370
12	Acacia Decurrens (King Wattle, Green Wattle, Sydney Black Wattle)	Acacia Decurrens	king wattle, green wattle, Sydney black wattle				18,700
13	Acacia Farnesiana (Sweet Acacia, Sweet Wattle)	Acacia Farnesiana	sweet acacia, sweet wattle				19,200
14	Acacia Leucophloea (Kikar, Kuteeera Gum)	Acacia Leucophloea	kikar, kuteeera gum				21,800
15	Acacia Mearnsi (Black Wattle)	Acacia Mearnsi	black wattle	4650		4650	19,530
16	Acacia Nilotica (Egyptian Thorn, Babul (India), Babar (Pakistan))	Acacia Nilotica	egyptian thorn, babul (India), babar (P	4800	4950	4875	20,475
17	Acacia Tortilis (Umbrella Thorn)	Acacia Tortilis	umbrella thorn	4400		4400	18,480
18	Acer Rubrum (Red Maple)	Acer Rubrum	red maple				18,545
19	Albizia Falcataria (Batai, Malucca Albizia, ,Placata)	Albizia Falcataria	batai, malucca albizia, ,placata				18,100
20	Albizia Lebbek (Lebbek, East Indian Walnut Tree)	Albizia Lebbek	lebbek, East Indian walnut tree;	5200		5200	21,840
21	Albizia Procera (Albicia, Silver Bark Rain Tree)	Albizia Procera	albicia, silver bark rain tree				19,700
22	Alnus Nepalensis (Nepal Alder)	Alnus Nepalensis	Nepal alder				17,150
23	Alnus Rubra (Red Alder)	Alnus Rubra	red alder	4600		4600	19,320
24	Alnus Rubra (Red Alder)	Alnus Rubra	red alder				18,545

(h) Sample change log sheet

Fixed an error so that thermocouple calibratiion is correctly read for all sensor boxes
39. Sensor Box WBT 4.2.3 Feb.3.2015 no catalog
Fixed framework of single grav filter for whole test. Further documentation is provided in "Single filter spreadsheet development feb 3.docx"
40. Sensor Box WBT 4.2.3 Jun.18.2015
More inputs for the GACC stove performance catalog were provided in the results tab.
41. Sensor Box WBT 4.2.3 Aug.31.2015
Fixed charcoal remaining catalog entry
Added weight of charcoal container to catalog entries
42. Sensor Box WBT 4.2.3 Sep.28.2015
The macro was fixed to work with SB < 2008
42. Sensor Box WBT 4.2.3 Nov.10.2015
Added support for BC system
43. made PM light scattering results be totally overridded by grav measurements. Realtime graphs are still dependent on the background
44. sensor box processing wbt 4.2.3 Dec.5.2016
removed the gravimetric altitude correction after experiments showed that it was not nessary
45. sensor box processing wbt 4.2.3 Nov. 11. 2017
added support for 3XXX series sensor box
46. sensor box processing wbt 4.2.3 Jan 31. 2018

Appendix 7: TG and DTG results for the charcoal fines

Time (min)	Temperature (°C)	Original weight (g)	Final weight (g)	Weight (%)	ΔT (min)	Weight loss (g)	DTG (g/min)
0.0	24.1	1.2054	1.2054	100.0	0	0	0
4.6	86.3	1.2054	1.2081	100.2	4.6	-0.0027	-0.000586232
10.2	104.1	1.2054	1.2016	99.7	5.6	0.0065	0.0011533
15.9	105.0	1.2054	1.1887	98.6	5.6	0.0129	0.002298124
21.5	104.9	1.2054	1.1738	97.4	5.6	0.0149	0.002651536
27.1	105.4	1.2054	1.1610	96.3	5.6	0.0128	0.002293942
32.7	105.4	1.2054	1.1515	95.5	5.6	0.0095	0.001681657
38.3	104.9	1.2054	1.1451	95.0	5.6	0.0064	0.001144807
43.9	105.0	1.2054	1.1410	94.7	5.6	0.0041	0.000735044
49.6	104.8	1.2054	1.1382	94.4	5.6	0.0028	0.000492095
55.2	104.7	1.2054	1.1364	94.3	5.6	0.0018	0.000325444
60.8	104.6	1.2054	1.1350	94.2	5.6	0.0014	0.00024273
66.4	105.0	1.2054	1.1341	94.1	5.6	0.0009	0.000154014
72.0	105.7	1.2054	1.1333	94.0	5.6	0.0008	0.000143569
77.7	276.3	1.2054	1.1389	94.5	5.7	-0.0055	-0.00097076
83.3	456.6	1.2054	1.1150	92.5	5.6	0.0239	0.004275149
88.9	615.0	1.2054	1.0529	87.3	5.6	0.0620	0.011111642
94.5	719.5	1.2054	0.9853	81.7	5.6	0.0676	0.012076786
100.1	827.8	1.2054	0.9270	76.9	5.6	0.0583	0.010415476
105.7	903.7	1.2054	0.8903	73.9	5.6	0.0367	0.006550595
111.3	915.5	1.2054	0.8801	73.0	5.6	0.0102	0.001823857
116.8	915.1	1.2054	0.8709	72.2	5.6	0.0092	0.001653134
122.5	898.7	1.2054	0.8603	71.4	5.7	0.0106	0.001869863
128.1	864.7	1.2054	0.8526	70.7	5.6	0.0076	0.001368432
133.6	832.7	1.2054	0.8458	70.2	5.6	0.0069	0.001239
139.2	803.0	1.2054	0.8399	69.7	5.6	0.0058	0.001044179
144.8	775.0	1.2054	0.8348	69.2	5.6	0.0052	0.000928144
150.4	748.2	1.2054	0.8335	69.1	5.6	0.0013	0.000225519
156.2	749.9	1.2054	0.8285	68.7	5.8	0.0050	0.000875362
161.8	749.6	1.2054	0.7910	65.6	5.6	0.0375	0.006690476
167.4	749.9	1.2054	0.7450	61.8	5.6	0.0460	0.008183383
173.0	750.1	1.2054	0.6978	57.9	5.6	0.0473	0.00842495
178.6	749.7	1.2054	0.6508	54.0	5.6	0.0470	0.008359091
Time (min)	Temperature (°C)	Original weight (g)	Final weight (g)	Weight (%)	ΔT (min)	Weight loss (g)	DTG (g/min)

Time (min)	Temperature (ºC)	Original weight (g)	Final weight (g)	Weight (%)	ΔT (min)	Weight loss (g)	DTG (g/min)
184.2	749.7	1.2054	0.6044	50.1	5.6	0.0464	0.008285714
189.8	749.7	1.2054	0.5588	46.4	5.6	0.0456	0.008142262
195.4	749.7	1.2054	0.5138	42.6	5.6	0.0449	0.008000593
201.0	749.7	1.2054	0.4699	39.0	5.6	0.0440	0.007873433
206.6	749.7	1.2054	0.4264	35.4	5.6	0.0434	0.00771767
212.2	750.1	1.2054	0.3842	31.9	5.6	0.0422	0.007572311
217.8	750.0	1.2054	0.3426	28.4	5.6	0.0416	0.007452789
223.4	750.0	1.2054	0.3015	25.0	5.6	0.0411	0.007346574
229.0	750.1	1.2054	0.2607	21.6	5.6	0.0408	0.007300199
234.5	750.2	1.2054	0.2208	18.3	5.6	0.0399	0.0071886
240.1	750.2	1.2054	0.1823	15.1	5.6	0.0385	0.006859941
245.7	750.2	1.2054	0.1497	12.4	5.6	0.0325	0.005803766
251.4	750.1	1.2054	0.1241	10.3	5.6	0.0257	0.004578791
257.0	750.0	1.2054	0.1099	9.1	5.6	0.0141	0.002524405
262.5	750.0	1.2054	0.1020	8.5	5.6	0.0079	0.001420299
268.1	750.0	1.2054	0.0983	8.2	5.6	0.0037	0.000654113
273.8	749.9	1.2054	0.0978	8.1	5.6	0.0005	9.5549E-05
279.4	749.9	1.2054	0.0975	8.1	5.6	0.0003	5.85222E-05

Appendix 8: TG and DTG results for the binder

Time (min)	Temperature (°C)	Original weight (g)	Final weight (g)	Weight (%)	Weight loss (g)	ΔT (min)	DTG (g/min)
0.0	24.1	1.1763	1.1763	100.0	0	0.0	0
5.3	90.5	1.1763	1.1772	100.1	-0.0009	5.3	-0.0001683
10.9	104.1	1.1763	1.1747	99.9	0.0025	5.6	0.0004467
16.6	105.3	1.1763	1.1712	99.6	0.0034	5.6	0.0006115
22.2	105.4	1.1763	1.1676	99.3	0.0037	5.6	0.0006537
27.8	104.9	1.1763	1.1644	99.0	0.0032	5.6	0.0005727
33.4	105.3	1.1763	1.1603	98.6	0.0040	5.6	0.0007169
39.0	105.3	1.1763	1.1565	98.3	0.0039	5.6	0.0006855
44.6	105.3	1.1763	1.1527	98.0	0.0038	5.6	0.0006706
50.3	105.1	1.1763	1.1481	97.6	0.0046	5.6	0.0008216
55.9	104.7	1.1763	1.1444	97.3	0.0037	5.6	0.0006636
61.5	104.6	1.1763	1.1392	96.8	0.0051	5.6	0.000911
67.1	105.8	1.1763	1.1346	96.5	0.0046	5.6	0.0008269
72.7	105.0	1.1763	1.1309	96.1	0.0037	5.6	0.0006678
78.4	304.8	1.1763	1.1381	96.8	-0.0072	5.7	-0.0012623
84.0	476.4	1.1763	1.0512	89.4	0.0868	5.6	0.0155543
89.6	630.6	1.1763	0.0165	1.4	1.0347	5.6	0.1853257
95.2	732.2	1.1763	0.0118	1.0	0.0047	5.6	0.0008452
100.8	840.8	1.1763	0.0086	0.7	0.0032	5.6	0.0005655
106.4	907.5	1.1763	0.0083	0.7	0.0003	5.6	5.991E-05
112.0	915.5	1.1763	0.0088	0.7	-0.0005	5.6	-8.571E-05
117.5	914.9	1.1763	0.0084	0.7	0.0004	5.6	7.164E-05
123.2	894.1	1.1763	0.0069	0.6	0.0014	5.7	0.0002532
128.8	860.4	1.1763	0.0069	0.6	0.0000	5.6	-1.796E-06
134.3	828.6	1.1763	0.0067	0.6	0.0002	5.6	4.054E-05
139.9	799.3	1.1763	0.0068	0.6	-0.0001	5.6	-2.593E-05
145.5	771.5	1.1763	0.0065	0.5	0.0004	5.6	7.096E-05
151.1	744.9	1.1763	0.0076	0.6	-0.0012	5.6	-0.0002044
156.9	749.3	1.1763	0.0048	0.4	0.0028	5.8	0.0004878
162.5	749.3	1.1763	0.0048	0.4	-0.0001	5.6	-8.929E-06
168.1	749.2	1.1763	0.0048	0.4	0.0000	5.6	0
173.7	749.3	1.1763	0.0048	0.4	0.0000	5.6	0
179.3	748.9	1.1763	0.0048	0.4	0.0001	5.6	8.902E-06
Time (min)	Temperature (°C)	Original weight (g)	Final weight (g)	Weight (%)	Weight loss (g)	ΔT (min)	DTG (g/min)

Time (min)	Temperature (ºC)	Original weight (g)	Final weight (g)	Weight (%)	Weight loss (g)	ΔT (min)	DTG (g/min)
184.9	749.0	1.1763	0.0047	0.4	0.0000	5.6	8.902E-06
190.5	749.0	1.1763	0.0048	0.4	0.0000	5.6	-8.929E-06
196.1	749.0	1.1763	0.0048	0.4	-0.0001	5.6	-8.902E-06
201.7	749.0	1.1763	0.0049	0.4	0.0000	5.6	-8.955E-06
207.3	748.9	1.1763	0.0048	0.4	0.0000	5.6	8.915E-06
212.9	749.2	1.1763	0.0048	0.4	0.0000	5.6	0
218.5	749.2	1.1763	0.0049	0.4	0.0000	5.6	-8.969E-06
224.1	749.2	1.1763	0.0047	0.4	0.0002	5.6	3.571E-05
229.7	749.3	1.1763	0.0048	0.4	-0.0002	5.6	-2.683E-05
235.2	749.5	1.1763	0.0048	0.4	0.0000	5.6	0
240.8	750.0	1.1763	0.0048	0.4	0.0000	5.6	0
246.4	749.7	1.1763	0.0048	0.4	0.0000	5.6	0
252.1	749.6	1.1763	0.0048	0.4	0.0000	5.6	0
257.7	749.5	1.1763	0.0050	0.4	-0.0001	5.6	-2.675E-05
263.2	750.0	1.1763	0.0049	0.4	0.0001	5.6	1.791E-05
268.8	749.9	1.1763	0.0049	0.4	0.0000	5.6	0
274.5	750.0	1.1763	0.0048	0.4	0.0000	5.6	8.902E-06
280.1	749.9	1.1763	0.0049	0.4	0.0000	5.6	-8.876E-06

Appendix 9: Proximate analysis of charcoal fines (C), and binder (B)

Sample	Weight (g)	Highly volatile matter (%)	Medium volatile matter (%)	Ash (%)	Fixed carbon (%)
			Charcoal fines		
C1	1.328	6.03	22.13	7.72	64.12
C2	1.1282	6.07	21.78	7.70	64.44
C3	1.1601	6.07	21.94	7.66	64.33
AVG		6.06	21.95	7.69	64.30
STD		0.02	0.18	0.03	0.17
			Binder		
B1	1.1266	4.05	95.93	0.04	-0.02
B2	1.1667	5.05	95.01	-0.09	0.03
B3	1.1834	5.04	94.96	-0.02	0.01
AVG		4.71	95.30	-0.03	0.01
STD		0.58	0.54	0.06	0.02

Appendix 10: Ultimate analysis of charcoal fines (C), and binder (B)

Sample	Weight (mg)	Nitrogen (N)	Carbon (C)	Hydrogen (H)	Oxygen (O)
			Binder		
BI	2.5	1.04	70.83	9.57	6.82
B2	2.6	1.20	84.53	11.53	6.47
B3	2.8	1.07	83.56	11.43	5.59
B4	2.5	1.00	91.92	9.57	
B5	2.4	1.06	79.30	11.53	
B6	2.7	1.30	76.08	11.43	
AVG		1.11	81.04	10.84	6.29
STD		0.11	7.33	0.99	0.63
			Charcoal fines		
C1	2.1	1.95	73.39	2.06	7.19
C2	2.8	1.67	75.97	2.13	6.98
C3	2.8	1.63	67.57	1.93	6.55
C4	2.7	1.68	70.50	2.26	
C5	2.3	1.69	68.57	2.25	
C6	2.6	1.71	74.39	2.41	
AVG		1.72	71.73	2.17	6.91
STD		0.11	3.36	0.17	0.33

Appendix 11: Higher heating value of charcoal fines (C), and binder (B)

Sample	m±0.0001 g	HHV (MJ/kg)
	Charcoal fines	
C1	0.7955	27.9
C2	0.8244	27.9
C3	0.6123	28.2
C4	0.6635	28.2
C5	0.7823	28.3
AVG		28.1
STD		0.2
	Binder	
B1	0.6238	40.2
B2	0.6022	39.9
B3	0.539	40.5
B4	0.7336	39.9
B5	0.6561	40.4
AVG		40.2
STD		0.3

Appendix 12: Outside diameter (d_1), inside diameter (d_2), height (h), mass (m), volume (V), and density (ρ) of the briquettes

Briquette	d_1±0.005cm	d_2±0.005cm	h±0.005cm	V, cm^3	m±0.0001gm	ρ, g/cm^3
B25	5.47	2	4.36	88.72	64.5046	0.727
B25	5.5	1.94	4.565	94.91	70.2795	0.740
B25	5.41	1.9	3.7	74.52	58.7551	0.788
B25	5.55	2.1	4.435	91.88	70.4925	0.767
B25	5.45	2.2	4.645	90.66	74.9162	0.826
AVG	5.476	2.028	4.341	88.14	67.78958	0.770
STD	0.053	0.122	0.375	7.937	6.259	0.039
B30	5.5	1.94	4.45	92.52	79.3883	0.858
B30	5.5	1.96	4.43	91.84	80.735	0.879
B30	5.435	2	4.51	90.42	79.9786	0.885
B30	5.49	2	4.4	90.29	80.2153	0.888
B30	5.485	1.995	4.465	91.50	80.005	0.874
AVG	5.482	1.979	4.451	91.31	80.06444	0.877
STD	0.027	0.027	0.041	0.952	0.485	0.012
B35	5.49	1.95	4.43	91.59	87.3779	0.954
B35	5.475	1.985	4.52	92.38	86.1845	0.933
B35	5.45	1.985	4.41	89.19	86.8743	0.974
B35	5.505	2	4.535	93.65	86.717	0.926
B35	5.51	2	4.425	91.57	88.6533	0.968
AVG	5.486	1.984	4.464	91.67	87.1614	0.951
STD	0.024	0.020	0.059	1.628	0.936	0.021
B40	5.46	1.99	4.545	92.23	94.5426	1.025
B40	5.48	1.98	4.355	89.26	94.8467	1.063
B40	5.47	1.985	4.35	88.72	93.4495	1.053
B40	5.49	1.97	4.45	91.73	93.6252	1.021
B40	5.48	1.99	4.35	89.02	90.8448	1.020
AVG	5.476	1.983	4.410	90.19	93.46176	1.036
STD	0.011	0.008	0.087	1.654	1.578	0.020

Appendix 13: Impact resistance index (IRI) of the briquettes

Briquette	Drops, n_d	Pieces, n_p	IRI
B25	1	30	3.33
B25	1	32	3.13
B25	1	40	2.50
B25	1	35	2.86
B25	1	37	2.70
AVG			2.90
STD			0.33
B30	1	4	25.00
B30	1	9	11.11
B30	2	12	16.67
B30	1	6	16.67
B30	2	13	15.38
AVG			16.97
STD			5.04
B35	1	2	50.00
B35	1	2	50.00
B35	2	4	50.00
B35	4	4	100.00
B35	2	4	50.00
AVG			60.00
STD			22.36
B40	1	2	50.00
B40	1	2	50.00
B40	2	2	100.00
B40	2	2	100.00
B40	2	3	66.67
AVG			73.33
STD			25.28

Appendix 14: **Testing compressive strength of briquettes; (a)flat surface of briquette placed between horizontal metal plates, (b)beginning of experiment, (c) end of experiment**

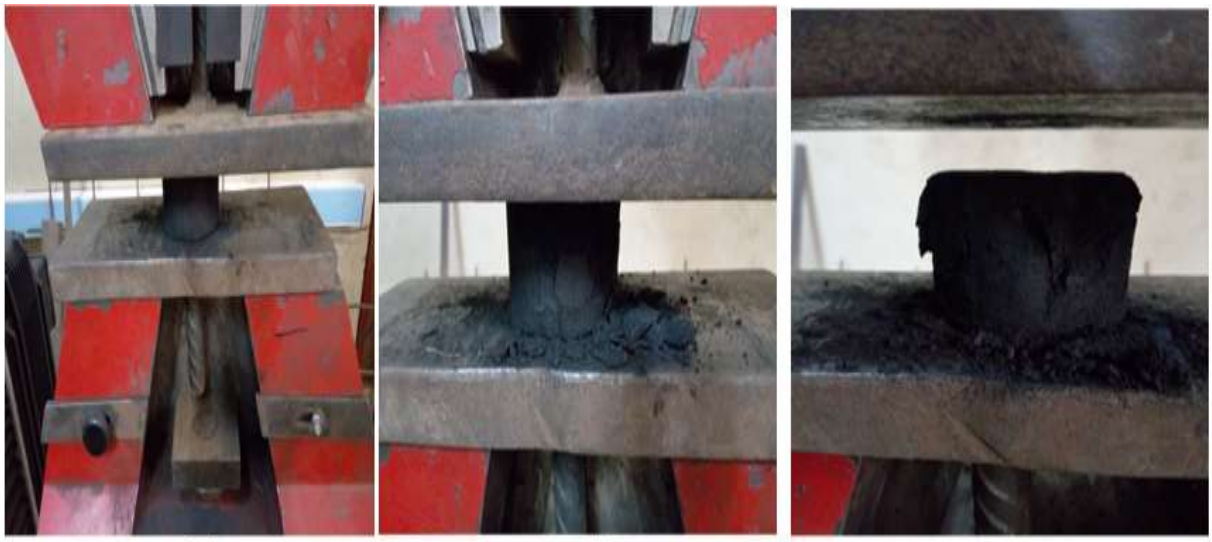

(a) (b) (c)

Appendix 15: Testing splitting tensile strength of briquettes; (a) &(b) curved surface of briquette placed between horizontal metal plates

(a) (b)

Appendix 16: Compressive strength of briquettes

Briquette	Outside diameter, d_1±0.05mm	Inside diameter, d_2±0.05mm	Height, h±0.05mm	Area, mm^2	Force at break, F_b (N)	Force at peak, F_p (N)	Stress at break, S_b (N/mm^2)	Stress at peak , S_p (N/mm^2)
B25	55.35	19.95	43.1	2094.44	3176	4119	1.52	1.97
B25	54.8	20	42	2045.27	3738	5169	1.83	2.53
B25	54.95	20	42	2058.21	2789	5888	1.36	2.25
AVG								2.25
STD								0.28
B30	54.5	19.9	43.65	2022.64	7221	7915	3.57	3.91
B30	55	20	41.1	2062.53	6889	7837	3.34	3.80
B30	54.9	20	41.4	2053.89	6787	8395	3.30	4.09
AVG								3.93
STD								0.14
B35	54.65	20	44.55	2032.37	15351	17032	7.55	8.38
B35	55	20.2	41.45	2056.21	14639	15257	7.12	7.42
B35	55	19.9	43.35	2065.66	16917.999	17283.001	8.19	8.37
AVG								8.06
STD								0.55
B40	54.6	20	42.45	2028.08	19005	19617	9.37	9.67
B40	54.6	19.95	42.42	2029.65	28687	28873	14.13	14.23
B40	54.9	20	43.3	2053.89	18269	18324	8.89	8.92
AVG								10.94
STD								2.87

Appendix 17: Splitting tensile strength of briquettes

Briquette	Outside diameter, d_1±0.05mm	Inside diameter, d_2±0.05mm	Height, h±0.05mm	Area, mm^2	Force at peak, F_p (N)	Stress at peak, S_p (N/mm^2)
B25	54.9	19.9	42.55	3667.51	331	0.09
B25	54.5	19.9	43	3679.30	303	0.08
B25	55	19.8	43.5	3756.23	317	0.08
AVG						0.09
STD						0.00
B30	55	19.95	43.5	3756.23	723	0.19
B30	54.8	19.6	41.6	3579.10	801	0.22
B30	54.6	19.9	41.62	3567.75	769	0.22
AVG						0.21
STD						0.02
B35	54.8	20	43.15	3712.45	1155	0.31
B35	55	20	42.35	3656.92	1291	0.35
B35	54.5	20	42.7	3653.63	1029	0.28
AVG						0.32
STD						0.04
B40	54.45	20	42.35	3620.35	1534	0.42
B40	54.6	20	42	3600.32	1501	0.42
B40	54.45	20	41.5	3547.69	1528	0.43
AVG						0.42
STD						0.01

Appendix 18: Sample results from the materials testing machine (Testometric, FS300AT)

a) Compressive strength test results for briquettes B25

Testometric
materials testing machines

winTest™
Analysis

25%binder

SPECIEN 1

Sample : 1
Height : 42
Outer Diameter : 54.95
Inner Diameter : 20

Machine No. : 0300-02032
Test Name : Compression For Briquettes
Test Type : Compression
Test Date : 23/01/2020 09:41
Test Speed : 0.500 mm/min
Preload : Off
Sample Height : 42.000 mm

Test No	Area (m²)	Force @ Break (N)	EN826 Comp. Modulus of Elasticity (N/mm²)	Def. @ Break (mm)	Force @ Peak (N)	Energy to Break (J)	Measured Volume (m³)
1	0.002	2789.000	79.172	5.607	5888.000	10.456	0.000

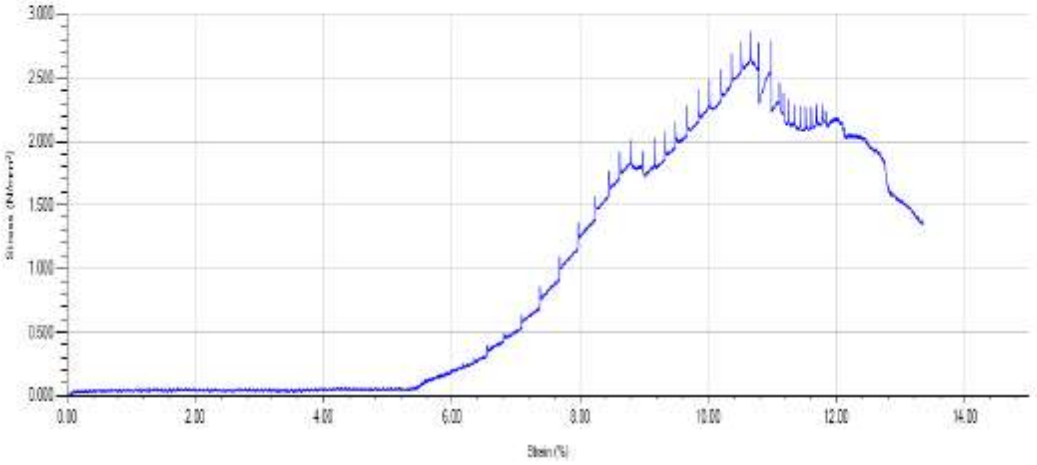

b) Compressive strength test results for briquettes B30

Testometric
materials testing machines

winTest™ Analysis

30% Binder

Briquette Sample1

Sample : 1
Height : 41.1
Outer Diameter : 55
Inner Diameter : 20

Machine No. : 0300-02032
Test Name : Compression For Briquettes
Test Type : Compression
Test Date : 23/01/2020 16:22
Test Speed : 0.500 mm/min
Preload : Off
Sample Height : 41.100 mm

Test No	Area (m^2)	Force @ Break (N)	EN826 Comp. Modulus of Elasticity (N/mm^2)	Def. @ Break (mm)	Force @ Peak (N)	Energy to Break (J)	Measured Volume (m^3)
1	0.002	6889.000	107.820	5.250	7837.000	24.730	0.000

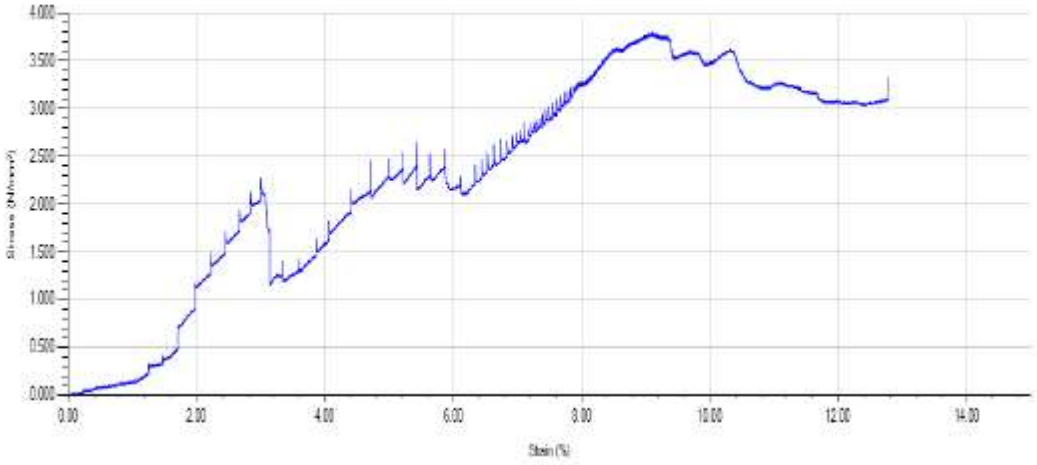

c) Compressive strength test results for briquettes B35

Testometric
materials testing machines

winTest™ Analysis

35% Binder

Briquette Sample1

Sample : 1
Height : 41.45
Outer Diameter : 55
Inner Diameter : 20.2

Machine No. : 0300-02032
Test Name : Compression For Briquettes
Test Type : Compression
Test Date : 23/01/2020 15:47
Test Speed : 0.500 mm/min
Preload : Off
Sample Height : 41.450 mm

Test No	Area (m²)	Force @ Break (N)	EN826 Comp. Modulus of Elasticity (N/mm²)	Def. @ Break (mm)	Force @ Peak (N)	Energy to Break (J)	Measured Volume (m³)
1	0.002	14639.000	180.479	4.972	15257.000	19.410	0.000

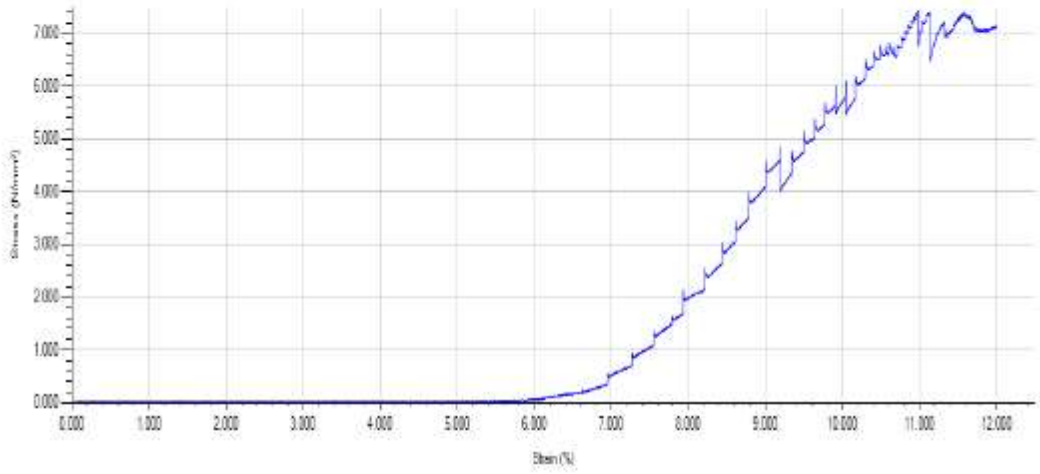

d) Compressive strength test results for briquettes B40

Testometric
materials testing machines

winTest™ Analysis

40% Binder

Briquette Sample1

Sample : 2
Height : 42.45
Outer Diameter : 54.60
Inner Diameter : 20

Machine No. : 0300-02032
Test Name : Compression For Briquettes
Test Type : Compression
Test Date : 23/01/2020 15:06
Test Speed : 0.500 mm/min
Preload : Off
Sample Height : 42.450 mm

Test No	Area (m²)	Force @ Break (N)	EN826 Comp. Modulus of Elasticity (N/mm²)	Def. @ Break (mm)	Force @ Peak (N)	Energy to Break (J)	Measured Volume (m³)
1	0.002	19004.999	323.636	1.941	19617.001	12.453	0.000

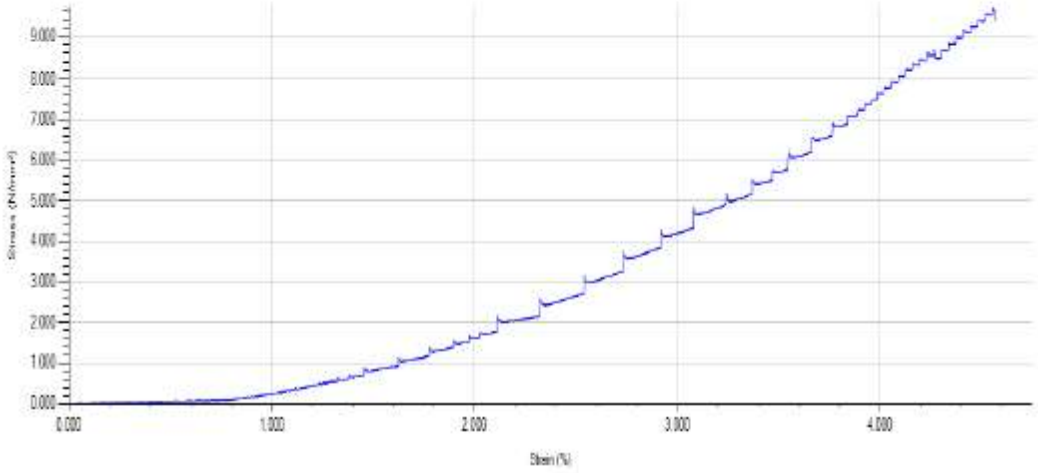

Appendix 19: Sample results from the materials testing machine (Testometric, M500-25)

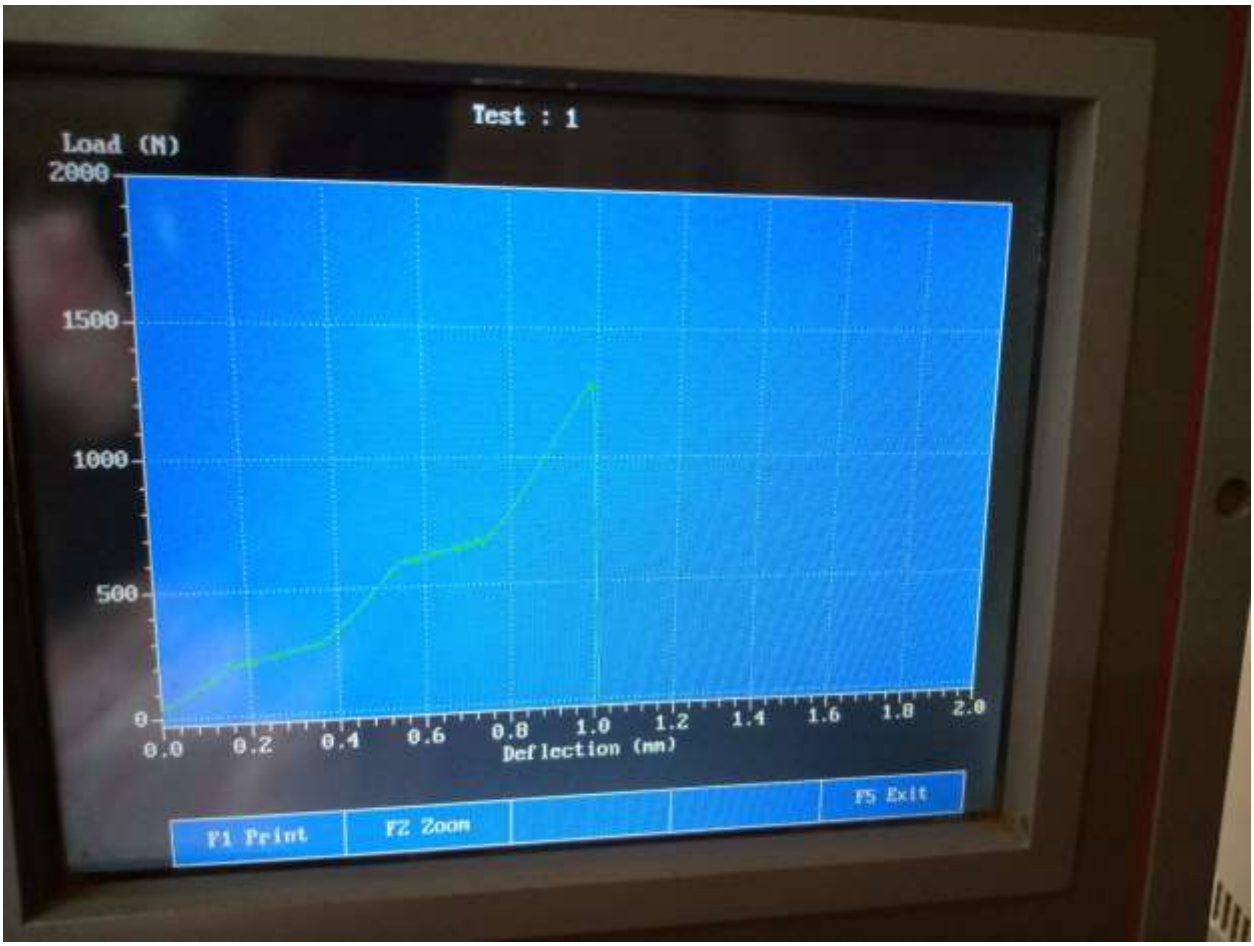

Appendix 20: Water resistance index (WRI) of the briquettes

Briquette	Weight of briquette before, w_1±0.0001 g	Weight of briquette after, w_2±0.0001 g	Percentage of water absorbed, (%)	WRI (%)
B25	70.4905	70.967	0.68	99.32
B25	60.2395	60.756	0.86	99.14
B25	67.758	68.274	0.76	99.24
B25	67.425	67.872	0.66	99.34
B25	64.512	64.987	0.74	99.26
AVG				99.26
STD				0.08
B30	77.676	78.223	0.70	99.30
B30	78.8515	79.495	0.82	99.18
B30	78.819	79.463	0.82	99.18
B30	76.5746	77.132	0.73	99.27
B30	74.3089	74.798	0.66	99.34
AVG				99.26
STD				0.07
B35	88.993	89.614	0.70	99.30
B35	88.2008	88.805	0.69	99.31
B35	88.022	88.666	0.73	99.27
B35	88.287	88.918	0.71	99.29
B35	90.9385	91.685	0.82	99.18
AVG				99.27
STD				0.05
B40	91.0731	91.6945	0.68	99.32
B40	91.505	92.4	0.98	99.02
B40	90.5797	91.082	0.55	99.45
B40	92.6403	93.315	0.73	99.27
B40	90.5175	91.05	0.59	99.41
AVG				99.29
STD				0.17

Appendix 21: TG and DTG results for briquette B25

Time (min)	Temperature (°C)	Original weight (g)	Final weight (g)	Weight (%)	weight loss (g)	ΔT (min)	DTG (g/min)
0.0	24.1	1.1340	1.1340	100.0	0	0	0.000000
3.8	83.8	1.1340	1.1379	100.3	-0.0039	3.8	-0.001045
9.4	104.2	1.1340	1.1329	99.9	0.0050	5.6	0.000887
15.0	104.6	1.1340	1.1227	99.0	0.0102	5.6	0.001816
20.6	104.8	1.1340	1.1105	97.9	0.0122	5.6	0.002179
26.2	105.0	1.1340	1.1008	97.1	0.0097	5.6	0.001735
31.9	104.8	1.1340	1.0942	96.5	0.0066	5.6	0.001175
37.5	104.5	1.1340	1.0901	96.1	0.0040	5.6	0.000719
43.1	104.9	1.1340	1.0875	95.9	0.0027	5.6	0.000475
48.7	105.3	1.1340	1.0856	95.7	0.0019	5.6	0.000332
54.4	104.8	1.1340	1.0843	95.6	0.0013	5.6	0.000237
60.0	104.7	1.1340	1.0833	95.5	0.0009	5.6	0.000166
65.6	104.6	1.1340	1.0826	95.5	0.0007	5.6	0.000130
71.2	105.9	1.1340	1.0819	95.4	0.0007	5.6	0.000125
76.9	237.7	1.1340	1.0900	96.1	-0.0081	5.7	-0.001428
82.4	434.7	1.1340	1.0692	94.3	0.0208	5.6	0.003715
88.0	594.7	1.1340	0.7873	69.4	0.2819	5.6	0.050538
93.6	703.6	1.1340	0.7177	63.3	0.0696	5.6	0.012448
99.2	811.5	1.1340	0.6781	59.8	0.0396	5.6	0.007057
104.8	896.7	1.1340	0.6438	56.8	0.0344	5.6	0.006142
110.4	915.6	1.1340	0.6352	56.0	0.0085	5.6	0.001526
116.0	915.0	1.1340	0.6272	55.3	0.0081	5.6	0.001445
121.7	904.2	1.134	0.6172	54.4	0.0100	5.7	0.001753
127.3	869.7	1.134	0.6109	53.9	0.0063	5.6	0.001124
132.8	837.4	1.134	0.6047	53.3	0.0063	5.5	0.001133
138.4	807.0	1.134	0.5993	52.8	0.0054	5.6	0.000963
144.0	779.1	1.134	0.5945	52.4	0.0048	5.6	0.000859
149.6	751.9	1.134	0.5923	52.2	0.0022	5.6	0.000398
155.3	749.3	1.134	0.5807	51.2	0.0116	5.7	0.002011
160.9	750.1	1.134	0.5493	48.4	0.0314	5.6	0.005605
166.5	749.6	1.134	0.5064	44.7	0.0429	5.6	0.007610
172.2	749.7	1.134	0.4635	40.9	0.0429	5.6	0.007645
177.8	749.6	1.134	0.4211	37.1	0.0425	5.6	0.007584
183.4	749.5	1.134	0.3791	33.4	0.0420	5.6	0.007493
189.0	749.6	1.134	0.3377	29.8	0.0414	5.6	0.007386

Time (min)	Temperature (ºC)	Original weight (g)	Final weight (g)	Weight (%)	weight loss (g)	ΔT (min)	DTG (g/min)
194.6	749.6	1.134	0.2971	26.2	0.0406	5.6	0.007222
200.2	749.6	1.134	0.2573	22.7	0.0398	5.6	0.007114
205.8	749.7	1.134	0.2183	19.2	0.0390	5.6	0.006956
211.4	749.4	1.134	0.1806	15.9	0.0377	5.6	0.006739
217.0	749.8	1.134	0.1445	12.7	0.0361	5.6	0.006479
222.5	749.7	1.134	0.1111	9.8	0.0334	5.6	0.005982
228.1	750.0	1.134	0.0860	7.6	0.0251	5.6	0.004490
233.7	750.2	1.134	0.0719	6.3	0.0141	5.6	0.002532
239.3	750.0	1.134	0.0683	6.0	0.0036	5.6	0.000642
244.9	750.1	1.134	0.0681	6.0	0.0002	5.6	0.000030
250.5	750.1	1.134	0.0679	6.0	0.0002	5.6	0.000036
256.1	750.1	1.134	0.0676	6.0	0.0003	5.6	0.000047
261.7	749.9	1.134	0.0674	5.9	0.0002	5.6	0.000041
267.3	749.9	1.134	0.0672	5.9	0.0002	5.6	0.000036
272.9	750.0	1.134	0.0670	5.9	0.0002	5.6	0.000030
278.6	750.0	1.134	0.0669	5.9	0.0001	5.6	0.000018

Appendix 22: TG and DTG results for briquette B30

Time (min)	Temperature (°C)	Original weight (g)	Final weight (g)	Weight (%)	Weight loss (g)	ΔT (min)	DTG (g/min)
0.0	24.1	1.1417	1.1417	100.0	0	0	0.000000
2.9	72.6	1.1417	1.1451	100.3	-0.0034	2.9	-0.001169
8.6	105.6	1.1417	1.1424	100.1	0.0027	5.6	0.000487
14.2	105.7	1.1417	1.1334	99.3	0.0090	5.6	0.001597
19.8	105.4	1.1417	1.1220	98.3	0.0114	5.6	0.002034
25.4	105.1	1.1417	1.1124	97.4	0.0095	5.6	0.001701
31.0	105.0	1.1417	1.1060	96.9	0.0064	5.6	0.001143
36.6	105.3	1.1417	1.1020	96.5	0.0040	5.6	0.000712
42.3	105.4	1.1417	1.0994	96.3	0.0026	5.6	0.000457
47.9	105.4	1.1417	1.0977	96.2	0.0017	5.6	0.000303
53.5	104.8	1.1417	1.0965	96.0	0.0012	5.6	0.000219
59.1	105.0	1.1417	1.0955	96.0	0.0010	5.6	0.000178
64.7	104.6	1.1417	1.0947	95.9	0.0008	5.6	0.000137
70.3	105.3	1.1417	1.0942	95.8	0.0006	5.6	0.000102
76.0	193.9	1.1417	1.1006	96.4	-0.0064	5.7	-0.001127
81.6	410.9	1.1417	1.0882	95.3	0.0124	5.6	0.002213
87.2	573.5	1.1417	0.8507	74.5	0.2375	5.6	0.042489
92.8	688.3	1.1417	0.6907	60.5	0.1600	5.6	0.028630
98.4	794.9	1.1417	0.6554	57.4	0.0354	5.6	0.006294
104.0	887.9	1.1417	0.6135	53.7	0.0419	5.6	0.007496
109.6	917.4	1.1417	0.6014	52.7	0.0120	5.6	0.002155
115.2	915.0	1.1417	0.5905	51.7	0.0110	5.6	0.001960
120.8	909.6	1.1417	0.5771	50.5	0.0134	5.7	0.002354
126.4	874.7	1.1417	0.5688	49.8	0.0083	5.6	0.001484
132.0	842.0	1.1417	0.5602	49.1	0.0086	5.6	0.001556
137.5	811.5	1.1417	0.5529	48.4	0.0073	5.6	0.001315
143.1	783.3	1.1417	0.5464	47.9	0.0065	5.6	0.001168
148.7	755.9	1.1417	0.5409	47.4	0.0055	5.6	0.000983
154.4	749.1	1.1417	0.5406	47.3	0.0003	5.6	0.000052
160.1	749.8	1.1417	0.5088	44.6	0.0318	5.7	0.005552
165.7	750.1	1.1417	0.4677	41.0	0.0410	5.6	0.007298
171.3	749.5	1.1417	0.4261	37.3	0.0416	5.6	0.007435
176.9	749.9	1.1417	0.3848	33.7	0.0413	5.6	0.007375
182.5	749.7	1.1417	0.3440	30.1	0.0408	5.6	0.007265
188.1	749.8	1.1417	0.3039	26.6	0.0401	5.6	0.007139
193.7	749.8	1.1417	0.2646	23.2	0.0393	5.6	0.007017
199.3	749.8	1.1417	0.2263	19.8	0.0383	5.6	0.006833
204.9	749.8	1.1417	0.1890	16.6	0.0373	5.6	0.006661
210.5	749.6	1.1417	0.1530	13.4	0.0360	5.6	0.006429
216.1	749.8	1.1417	0.1187	10.4	0.0343	5.6	0.006150
221.7	750.0	1.1417	0.0907	7.9	0.0280	5.6	0.005021
227.3	750.1	1.1417	0.0748	6.6	0.0159	5.6	0.002839
232.9	750.2	1.1417	0.0690	6.0	0.0058	5.6	0.001042
238.5	750.2	1.1417	0.0686	6.0	0.0004	5.6	0.000072

Time (min)	Temperature (ºC)	Original weight (g)	Final weight (g)	Weight (%)	Weight loss (g)	ΔT (min)	DTG (g/min)
244.1	750.0	1.1417	0.0683	6.0	0.0003	5.6	0.000060
249.7	749.8	1.1417	0.0680	6.0	0.0003	5.6	0.000048
255.3	749.9	1.1417	0.0678	5.9	0.0002	5.6	0.000036
260.9	750.0	1.1417	0.0676	5.9	0.0002	5.6	0.000035
266.5	750.0	1.1417	0.0674	5.9	0.0002	5.6	0.000042
272.1	750.0	1.1417	0.0672	5.9	0.0001	5.6	0.000024
277.7	750.0	1.1417	0.0671	5.9	0.0001	5.6	0.000018

Appendix 23: TG and DTG results for briquette B35

Time (min)	Temperature (°C)	Original weight (g)	Final weight (g)	Weight loss (%)	Weight loss (g)	ΔT (min)	DTG (g/min)
0.0	24.1	1.2117	1.2117	100.0	0.0000	0.0000	0.000000
2.1	52.8	1.2117	1.2144	100.2	-0.0027	2.1	-0.001294
7.7	107.1	1.2117	1.2132	100.1	0.0012	5.6	0.000214
13.3	105.1	1.2117	1.2054	99.5	0.0078	5.6	0.001380
19.0	105.3	1.2117	1.1943	98.6	0.0111	5.6	0.001975
24.6	105.3	1.2117	1.1845	97.8	0.0098	5.6	0.001743
30.2	105.6	1.2117	1.1777	97.2	0.0068	5.6	0.001217
35.8	105.3	1.2117	1.1734	96.8	0.0043	5.6	0.000760
41.4	105.0	1.2117	1.1706	96.6	0.0028	5.6	0.000503
47.0	104.7	1.2117	1.1687	96.5	0.0019	5.6	0.000337
52.7	104.8	1.2117	1.1673	96.3	0.0014	5.6	0.000249
58.3	105.6	1.2117	1.1663	96.3	0.0010	5.6	0.000179
63.9	104.6	1.2117	1.1654	96.2	0.0009	5.6	0.000154
69.5	104.8	1.2117	1.1648	96.1	0.0006	5.6	0.000108
75.2	146.7	1.2117	1.1662	96.3	-0.0014	5.7	-0.000246
80.8	386.4	1.2117	1.1638	96.0	0.0025	5.6	0.000441
86.4	548.7	1.2117	1.0060	83.0	0.1577	5.6	0.028222
91.9	673.6	1.2117	0.6914	57.1	0.3146	5.6	0.056457
97.6	778.1	1.2117	0.6567	54.2	0.0347	5.6	0.006179
103.1	877.6	1.2117	0.6131	50.6	0.0436	5.6	0.007815
108.7	920.6	1.2117	0.6019	49.7	0.0112	5.6	0.001996
114.3	915.2	1.2117	0.5913	48.8	0.0106	5.6	0.001900
120.0	913.8	1.2117	0.5762	47.6	0.0151	5.7	0.002662
125.6	879.5	1.2117	0.5715	47.2	0.0047	5.6	0.000839
131.1	846.7	1.2117	0.5637	46.5	0.0078	5.5	0.001407
136.7	815.9	1.2117	0.5569	46.0	0.0068	5.6	0.001216
142.3	787.4	1.2117	0.5510	45.5	0.0059	5.6	0.001058
147.9	760.0	1.2117	0.5458	45.0	0.0053	5.6	0.000943
153.5	745.3	1.2117	0.5456	45.0	0.0001	5.6	0.000022
159.2	749.9	1.2117	0.5207	43.0	0.0249	5.7	0.004343
164.9	750.4	1.2117	0.4795	39.6	0.0412	5.6	0.007335
170.5	750.9	1.2117	0.4376	36.1	0.0420	5.6	0.007487
176.1	750.9	1.2117	0.3960	32.7	0.0415	5.6	0.007409
181.7	750.9	1.2117	0.3550	29.3	0.0411	5.6	0.007305
187.3	750.9	1.2117	0.3148	26.0	0.0402	5.6	0.007173

Time (min)	Temperature (ºC)	Original weight (g)	Final weight (g)	Weight loss (%)	Weight loss (g)	ΔT (min)	DTG (g/min)
192.9	750.9	1.2117	0.2755	22.7	0.0393	5.6	0.007017
198.5	750.9	1.2117	0.2372	19.6	0.0383	5.6	0.006834
204.1	750.9	1.2117	0.1998	16.5	0.0375	5.6	0.006684
209.7	751.2	1.2117	0.1636	13.5	0.0362	5.6	0.006470
215.3	750.7	1.2117	0.1293	10.7	0.0342	5.6	0.006126
220.9	750.7	1.2117	0.1009	8.3	0.0284	5.6	0.005082
226.5	750.6	1.2117	0.0817	6.7	0.0192	5.6	0.003422
232.0	750.3	1.2117	0.0719	5.9	0.0098	5.6	0.001760
237.6	750.2	1.2117	0.0685	5.7	0.0034	5.6	0.000610
243.2	750.2	1.2117	0.0683	5.6	0.0003	5.6	0.000047
248.8	750.1	1.2117	0.0680	5.6	0.0003	5.6	0.000053
254.4	749.9	1.2117	0.0678	5.6	0.0002	5.6	0.000036
260.0	749.9	1.2117	0.0675	5.6	0.0002	5.6	0.000042
265.6	749.9	1.2117	0.0674	5.6	0.0001	5.6	0.000018
271.2	750.0	1.2117	0.0672	5.5	0.0002	5.6	0.000036
276.9	750.0	1.2117	0.0672	5.5	0.0001	5.6	0.000012

Appendix 24: TG and DTG results for briquette B40

Time (min)	Temperature (ºC)	Original weight (g)	Final weight (g)	Weight loss (%)	Weight loss (g)	ΔT (min)	DTG (g/min)
0.0	24.11	1.2456	1.24560	100.0	0	0	0.000000
0.7	33.34	1.2456	1.24768	100.2	-0.00208	0.7	-0.002858
5.0	106.41	1.2456	1.24876	100.3	-0.00108	4.3	-0.000254
10.6	104.14	1.2456	1.24226	99.7	0.00650	5.6	0.001157
16.2	105.24	1.2456	1.23230	98.9	0.00997	5.6	0.001769
21.8	104.91	1.2456	1.22270	98.2	0.00960	5.6	0.001716
27.5	105.11	1.2456	1.21579	97.6	0.00690	5.6	0.001229
33.1	104.95	1.2456	1.21123	97.2	0.00457	5.6	0.000812
38.7	104.57	1.2456	1.20819	97.0	0.00303	5.6	0.000540
44.3	104.54	1.2456	1.20606	96.8	0.00213	5.6	0.000379
49.9	105.29	1.2456	1.20456	96.7	0.00150	5.6	0.000267
55.6	105.66	1.2456	1.20339	96.6	0.00117	5.6	0.000207
61.2	104.60	1.2456	1.20243	96.5	0.00096	5.6	0.000171
66.8	105.09	1.2456	1.20173	96.5	0.00070	5.6	0.000126
72.4	110.25	1.2456	1.18215	94.9	0.01958	5.6	0.003469
78.1	359.56	1.2456	1.20332	96.6	-0.02117	5.6	-0.003759
83.7	521.30	1.2456	1.11720	89.7	0.08612	5.6	0.015409
89.2	659.15	1.2456	0.67727	54.4	0.43994	5.6	0.078795
94.8	761.35	1.2456	0.64206	51.5	0.03520	5.6	0.006293
100.4	866.21	1.2456	0.59860	48.1	0.04347	5.6	0.007754
106.0	920.66	1.2456	0.58893	47.3	0.00967	5.6	0.001724
111.6	914.99	1.2456	0.57916	46.5	0.00977	5.6	0.001750
117.2	915.34	1.2456	0.57129	45.9	0.00787	5.6	0.001408
122.9	884.34	1.2456	0.56192	45.1	0.00937	5.6	0.001660
128.5	851.41	1.2456	0.55520	44.6	0.00672	5.6	0.001203
134.0	820.20	1.2456	0.54918	44.1	0.00602	5.6	0.001083
139.6	791.48	1.2456	0.54424	43.7	0.00494	5.6	0.000886
145.2	763.94	1.2456	0.53997	43.4	0.00427	5.6	0.000765
150.8	740.84	1.2456	0.53920	43.3	0.00077	5.6	0.000138
156.5	750.14	1.2456	0.52193	41.9	0.01727	5.7	0.003033
162.1	750.41	1.2456	0.48196	38.7	0.03997	5.6	0.007074
167.8	750.98	1.2456	0.44019	35.3	0.04177	5.6	0.007429
173.4	750.83	1.2456	0.39873	32.0	0.04146	5.6	0.007404
179.0	751.24	1.2456	0.35756	28.7	0.04116	5.6	0.007343
184.6	751.13	1.2456	0.31719	25.5	0.04037	5.6	0.007202
190.2	751.16	1.2456	0.27743	22.3	0.03976	5.6	0.007094

Time (min)	Temperature (ºC)	Original weight (g)	Final weight (g)	Weight loss (%)	Weight loss (g)	ΔT (min)	DTG (g/min)
195.8	751.02	1.2456	0.23853	19.1	0.03890	5.6	0.006940
201.4	751.07	1.2456	0.20049	16.1	0.03804	5.6	0.006779
207.0	751.01	1.2456	0.16359	13.1	0.03690	5.6	0.006589
212.6	750.85	1.2456	0.12836	10.3	0.03523	5.6	0.006298
218.2	750.64	1.2456	0.09836	7.9	0.03000	5.6	0.005373
223.8	750.31	1.2456	0.07780	6.2	0.02057	5.6	0.003684
229.3	750.12	1.2456	0.06856	5.5	0.00924	5.6	0.001654
234.9	750.13	1.2456	0.06746	5.4	0.00110	5.6	0.000197
240.5	750.09	1.2456	0.06713	5.4	0.00033	5.6	0.000059
246.1	750.18	1.2456	0.06689	5.4	0.00024	5.6	0.000042
251.7	750.12	1.2456	0.06670	5.4	0.00020	5.6	0.000035
257.3	750.05	1.2456	0.06653	5.3	0.00017	5.6	0.000030
262.9	750.01	1.2456	0.06639	5.3	0.00013	5.6	0.000024
268.5	749.94	1.2456	0.06629	5.3	0.00010	5.6	0.000018
274.1	749.97	1.2456	0.06623	5.3	0.00007	5.6	0.000012

Appendix 25: Proximate analysis of briquettes

Sample	Weight (g)	Highly volatile matter (%)	Medium volatile matter (%)	Ash (%)	Fixed carbon (%)
			Briquettes		
B25	1.1384	4.45	40.39	5.69	49.46
B25	1.1558	4.50	40.02	5.74	49.75
B25	1.1078	5.08	40.99	5.02	48.91
AVG		4.68	40.46	5.48	49.38
STD		0.35	0.49	0.40	0.42
B30	1.1405	4.24	43.86	5.59	46.31
B30	1.1204	4.28	44.82	5.52	45.38
B30	1.1641	4.19	44.87	5.31	45.63
AVG		4.24	44.52	5.47	45.77
STD		0.05	0.57	0.14	0.48
B35	1.134	4.01	47.97	5.11	42.91
B35	1.3147	3.90	47.62	5.19	43.29
B35	1.1863	3.91	47.99	5.17	42.93
AVG		3.94	47.86	5.15	43.04
STD		0.06	0.20	0.04	0.21
B40	1.1821	3.55	50.89	4.93	40.63
B40	1.2341	3.57	50.49	4.97	40.97
B40	1.3206	3.65	50.45	4.92	40.98
AVG		3.59	50.61	4.94	40.86
STD		0.05	0.24	0.02	0.20

Appendix 26: Ultimate analysis of briquettes

Sample	Weight (mg)	Nitrogen (N)	Carbon (C)	Hydrogen (H)	Oxygen (O)
B25	2.7	2.74	73.43	4.18	7.36
B25	2.2	2.14	75.64	4.63	7.46
B25	2.8	1.64	74.79	4.40	7.30
AVG		2.17	74.62	4.40	7.37
STD		0.55	1.11	0.23	0.08
B30	2.1	1.95	75.55	5.40	7.32
B30	2.6	1.78	76.13	4.69	7.44
B30	2.6	2.10	73.70	4.51	7.26
AVG		1.94	75.13	4.87	7.34
STD		0.16	1.27	0.47	0.09
B35	2.6	1.69	77.18	5.19	7.35
B35	2.5	2.81	76.23	5.40	7.28
B35	3	2.61	78.69	5.22	7.59
AVG		2.37	77.37	5.27	7.41
STD		0.60	1.24	0.11	0.16
B40	2.6	1.72	78.14	5.98	5.90
B40	2.8	1.67	79.36	5.73	5.10
B40	2.5	1.72	81.52	6.29	6.18
AVG		1.70	79.67	6.00	5.73
STD		0.03	1.71	0.28	0.56

Appendix 27: Higher heating value of briquettes

Sample	m±0.0001 g	HHV (MJ/kg)
B25	0.8932	30.5
B25	0.6524	29.4
B25	0.5783	29.0
AVG		29.7
STD		0.7
B30	0.7972	32.0
B30	0.6428	31.5
B30	0.8791	31.2
AVG		31.6
STD		0.4
B35	0.5327	31.5
B35	0.7328	31.6
B35	0.9794	30.9
AVG		31.3
STD		0.4
B40	0.5922	31.3
B40	0.5528	30.9
B40	0.5794	30.5
AVG		30.9
STD		0.4

Appendix 28: Higher heating value (HHV), density and energy density of briquettes

Briquette	HHV (MJ/kg)	Density (g/cm^3)	Density (kg/m^3)	Energy density (MJ/m^3)	Energy density (GJ/m^3)
B25	29.7	0.770	770	22832	22.83
B30	31.6	0.877	877	27678	27.68
B35	31.3	0.951	951	29791	29.79
B40	30.9	1.036	1036	32050	32.05

Appendix 29: Statistical analysis- ANOVA

Property	Briquette	N Analysis	N missing	*Mean	Standard deviation	SE of Mean
Highly VM	B25	3	0	4.67823	0.35049	0.20236
	B30	3	0	4.24003	0.04617	0.02665
	B35	3	0	3.94187	0.06117	0.03532
	B40	3	0	3.59213	0.05107	0.02948
medium VM	B25	3	0	40.46407	0.48883	0.28222
	B30	3	0	44.51513	0.56838	0.32815
	B35	3	0	47.85963	0.20423	0.11791
	B40	3	0	50.60663	0.24340	0.14053
Ash	B25	3	0	5.48250	0.40201	0.23210
	B30	3	0	5.47000	0.14385	0.08305
	B35	3	0	5.15353	0.04255	0.02457
	B40	3	0	4.94037	0.02376	0.01372
FC	B25	3	0	49.37517	0.42451	0.24509
	B30	3	0	45.77487	0.48157	0.27804
	B35	3	0	43.04497	0.20931	0.12085
	B40	3	0	40.86087	0.20138	0.11627
C	B25	3	0	74.62000	1.11476	0.64361
	B30	3	0	75.12667	1.26911	0.73272
	B35	3	0	77.36667	1.24058	0.71625
	B40	3	0	79.67333	1.71165	0.98822
H	B25	3	0	4.40333	0.22502	0.12991
	B30	3	0	4.86667	0.47057	0.27168
	B35	3	0	5.27000	0.11358	0.06557
	B40	3	0	6.00000	0.28054	0.16197
N	B25	3	0	2.17333	0.55076	0.31798
	B30	3	0	1.94333	0.16010	0.09244
	B35	3	0	2.37000	0.59733	0.34487
	B40	3	0	1.70333	0.02887	0.01667
O	B25	3	0	7.37333	0.08083	0.04667
	B30	3	0	7.34000	0.09165	0.05292
	B35	3	0	7.40667	0.16258	0.09387
	B40	3	0	5.72667	0.56048	0.32359
HHV	B25	3	0	29.65600	0.79673	0.45999
	B30	3	0	31.56333	0.43054	0.24857
	B35	3	0	31.32467	0.40915	0.23622
	B40	3	0	30.92433	0.38501	0.22228

*Null Hypothesis: The means of all levels are equal

*Alternative Hypothesis: The means of one or more levels are different

*At the 0.05 level, the population means are significantly different.

Appendix 30: Statistical analysis-Fisher's LSD

Property	Briquette	Mean Diff	SEM	t Value	Prob	Alpha	Sign	LCL	UCL
Highly VM	B30- B25	-0.4382	0.14795	-2.96189	0.01809	0.05	1	-0.77936	-0.09704
	B35- B25	-0.73637	0.14795	-4.97727	0.00108	0.05	1	-1.07753	-0.3952
	B35- B30	-0.29817	0.14795	-2.01538	0.07862	0.05	0	-0.63933	0.043
	B40-B25	-1.0861	0.14795	-7.3412	0.00008	0.05	1	-1.42726	-0.74494
	B40-B30	-0.6479	0.14795	-4.37931	0.00235	0.05	1	-0.98906	-0.30674
	B40-B35	-0.34973	0.14795	-2.36393	0.04568	0.05	1	-0.6909	-0.00857
medium VM	B30-B25	4.05107	0.3324	12.18716	0.00000	0.05	1	3.28454	4.81759
	B35-B25	7.39557	0.3324	22.2487	0.00000	0.05	1	6.62904	8.16209
	B35-B30	3.3445	0.3324	10.06154	0.00001	0.05	1	2.57797	4.11103
	B40-B25	10.14257	0.3324	30.51273	0.00000	0.05	1	9.37604	10.9091
	B40-B30	6.0915	0.3324	18.32557	0.00000	0.05	1	5.32497	6.85803
	B40-B35	2.747	0.3324	8.26403	0.00003	0.05	1	1.98047	3.51353
Ash	B30-B25	-0.0125	0.17544	-0.07125	0.94495	0.05	0	-0.41707	0.39207
	B35-B25	-0.32897	0.17544	-1.87508	0.09764	0.05	0	-0.73354	0.0756
	B35-B30	-0.31647	0.17544	-1.80383	0.10891	0.05	0	-0.72104	0.0881
	B40-B25	-0.54213	0.17544	-3.0901	0.01489	0.05	1	-0.9467	-0.13756
	B40-B30	-0.52963	0.17544	-3.01885	0.01659	0.05	1	-0.9342	-0.12506
	B40-B35	-0.21317	0.17544	-1.21503	0.25899	0.05	0	-0.61774	0.1914
FC	B30-B25	-3.6003	0.28766	-12.51585	0.00000	0.05	1	-4.26364	-2.93696
	B35-B25	-6.3302	0.28766	-22.0059	0.00000	0.05	1	-6.99354	-5.66686
	B35-B30	-2.7299	0.28766	-9.49005	0.00001	0.05	1	-3.39324	-2.06656
	B40-B25	-8.5143	0.28766	-29.59857	0.00000	0.05	1	-9.17764	-7.85096
	B40-B30	-4.914	0.28766	-17.08272	0.00000	0.05	1	-5.57734	-4.25066
	B40-B35	-2.1841	0.28766	-7.59267	0.00006	0.05	1	-2.84744	-1.52076
C	B30-B25	0.50667	1.10469	0.45865	0.65869	0.05	0	-2.04076	3.0541
	B35-B25	2.74667	1.10469	2.48636	0.03774	0.05	1	0.19924	5.2941
	B35-B30	2.24	1.10469	2.02771	0.07713	0.05	0	-0.30743	4.78743
	B40-B25	5.05333	1.10469	4.57442	0.00182	0.05	1	2.5059	7.60076
	B40-B30	4.54667	1.10469	4.11577	0.00336	0.05	1	1.99924	7.0941
	B40-B35	2.30667	1.10469	2.08806	0.07023	0.05	0	-0.24076	4.8541
H	B30-B25	0.46333	0.24619	1.88199	0.09661	0.05	0	-0.10439	1.03106
	B35-B25	0.86667	0.24619	3.52027	0.00784	0.05	1	0.29894	1.43439
	B35-B30	0.40333	0.24619	1.63828	0.14000	0.05	0	-0.16439	0.97106
	B40-B25	1.59667	0.24619	6.48542	0.00019	0.05	1	1.02894	2.16439
	B40-B30	1.13333	0.24619	4.60343	0.00175	0.05	1	0.56561	1.70106
	B40-B35	0.73	0.24619	2.96515	0.01800	0.05	1	0.16228	1.29772
N	B30-B25	-0.23	0.33828	-0.67991	0.51575	0.05	0	-1.01007	0.55007
	B35-B25	0.19667	0.33828	0.58137	0.57700	0.05	0	-0.58341	0.97674
	B35-B30	0.42667	0.33828	1.26128	0.24274	0.05	0	-0.35341	1.20674
	B40-B25	-0.47	0.33828	-1.38938	0.20216	0.05	0	-1.25007	0.31007
	B40-B30	-0.24	0.33828	-0.70947	0.49818	0.05	0	-1.02007	0.54007
	B40-B35	-0.66667	0.33828	-1.97075	0.08424	0.05	0	-1.44674	0.11341
O	B30-B25	-0.03333	0.24341	-0.13694	0.89446	0.05	0	-0.59464	0.52798
	B35-B25	0.03333	0.24341	0.13694	0.89446	0.05	0	-0.52798	0.59464
	B35-B30	0.06667	0.24341	0.27388	0.79111	0.05	0	-0.49464	0.62798
	B40-B25	-1.64667	0.24341	-6.7649	0.00014	0.05	1	-2.20798	-1.08536

Property	Briquette	Mean Diff	SEM	t Value	Prob	Alpha	Sign	LCL	UCL
	B40-B30	-1.61333	0.24341	-6.62796	0.00016	0.05	1	-2.17464	-1.05202
	B40-B35	-1.68	0.24341	-6.90184	0.00012	0.05	1	-2.24131	-1.11869
HHV	B30-B25	1.90733	0.43508	4.38386	0.00234	0.05	1	0.90404	2.91063
	B35-B25	1.66867	0.43508	3.83531	0.00498	0.05	1	0.66537	2.67196
	B35-B30	-0.23867	0.43508	-0.54856	0.59828	0.05	0	-1.24196	0.76463
	B40-B25	1.26833	0.43508	2.91517	0.01943	0.05	1	0.26504	2.27163
	B40-B30	-0.639	0.43508	-1.46869	0.18010	0.05	0	-1.6423	0.3643
	B40-B35	-0.40033	0.43508	-0.92014	0.38441	0.05	0	-1.40363	0.60296

*Sign equals 1 indicates that the difference of the means is significant at the 0.05 level.

*Sign equals 0 indicates that the difference of the means is not significant at the 0.05 level.

Appendix 31: Experimental (Exp), predicted (pred) and deviation (dev) values of the responses

Run	Exp	Pred	Dev	Exp	Pred	Dev	Exp	Pred	Dev	Exp	Pred	Dev	Exp	Pred	Dev
		Density			IRI			F			T		WRI		
1	0.788	0.792	-0.004	3.33	-4.25	7.582	1.97	1.73	0.234	0.090	0.091	-0.001	99.32	99.25	0.071
2	0.767	0.784	-0.017	3.13	2.48	0.642	2.53	2.08	0.448	0.082	0.092	-0.010	99.14	99.25	-0.111
3	0.826	0.789	0.037	2.50	-2.00	4.505	2.25	1.85	0.399	0.084	0.091	-0.007	99.24	99.25	-0.015
4	0.858	0.877	-0.019	25.00	24.16	0.836	3.91	4.72	-0.809	0.192	0.203	-0.010	99.30	99.25	0.043
5	0.879	0.879	0.000	11.11	21.92	-10.809	3.80	4.61	-0.807	0.224	0.202	0.022	99.18	99.25	-0.069
6	0.885	0.879	0.005	16.67	21.92	-5.254	4.09	4.61	-0.520	0.216	0.202	0.013	99.18	99.25	-0.070
7	0.954	0.951	0.003	50.00	61.55	-11.553	8.38	8.17	0.207	0.311	0.316	-0.005	99.30	99.25	0.049
8	0.933	0.961	-0.028	50.00	52.58	-2.578	7.42	7.71	-0.292	0.353	0.314	0.039	99.31	99.25	0.062
9	0.974	0.972	0.002	50.00	43.60	6.398	8.37	7.25	1.117	0.282	0.312	-0.031	99.27	99.25	0.015
10	1.025	1.038	-0.013	100.00	87.72	12.278	9.67	11.05	-1.375	0.424	0.428	-0.004	99.32	99.25	0.064
11	1.063	1.041	0.022	100.00	85.48	14.521	14.23	10.93	3.294	0.417	0.427	-0.010	99.02	99.25	-0.231
12	1.053	1.043	0.010	66.67	83.23	-16.568	8.92	10.82	-1.895	0.431	0.427	0.004	99.45	99.25	0.192

Appendix 32: Ignition time of the briquettes

Sample	B25	B30	B35	B40
1	7.12	6.32	6.75	6.2
2	7.22	6.67	6.15	6.76
3	6.68	6.43	7.08	6.53
AVG	7.01	6.47	6.66	6.50
STD	0.29	0.18	0.47	0.28

Appendix 33: Temperature profiles and gaseous emissions during the WBT (B25)

Time (min)	$T_{ambient}$ (°C)	T_{gas} (°C)	T_{water} (°C)	CO (ppm)	SO_2 (ppm)	C_xH_y (ppm)	CO_2 (ppm)	NO_x (ppm)
0	24.5	23.0	19.20	0.00	0.0000	0.00	0.00	0.0000
1	24.6	23.0	19.20	0.37	0.0000	22.51	83.89	0.0000
2	24.7	23.0	19.20	2.22	0.0000	40.93	113.89	0.0000
3	24.8	23.0	19.20	6.17	0.0000	66.67	139.44	0.0000
4	24.8	24.0	19.20	10.62	0.0000	96.42	182.22	0.0000
5	24.9	24.3	19.20	17.02	0.0000	137.04	224.44	0.0000
6	25.0	26.0	19.20	21.77	0.0000	172.51	253.33	0.0000
7	25.0	25.3	19.36	26.48	0.0000	212.67	215.56	0.0000
8	25.1	25.0	20.30	26.67	0.0000	199.63	166.67	0.0000
9	25.1	24.0	21.08	26.63	0.0000	185.09	162.78	0.0000
10	25.2	24.0	21.94	29.78	0.0000	192.06	172.22	0.0000
11	25.3	24.0	22.99	32.96	0.0000	201.08	186.11	0.0000
12	25.4	24.0	23.94	37.10	0.0000	210.46	196.67	0.0000
13	25.4	24.0	24.93	41.30	0.0000	219.61	205.56	0.0000
14	25.5	24.0	25.97	47.08	0.0000	232.20	228.33	0.0000
15	25.5	24.0	27.14	53.02	0.0000	243.18	243.33	0.0000
16	25.6	24.0	28.40	58.97	0.0000	250.05	263.89	0.0000
17	25.6	24.0	29.80	64.44	0.0000	256.11	273.33	0.0000
18	25.8	24.0	31.32	70.66	0.0000	261.61	289.44	0.0000
19	25.8	24.0	32.68	77.39	0.0000	266.41	308.33	0.0000
20	25.9	24.0	34.17	84.58	0.0000	271.79	333.33	0.0000
21	25.9	24.0	35.80	92.79	0.0000	278.88	338.89	0.0000
22	25.9	24.0	37.65	100.25	0.0000	283.57	363.33	0.0000
23	26.0	24.0	39.50	107.94	0.0000	289.87	383.89	0.0000
24	26.1	24.8	41.49	117.01	0.0000	295.59	383.33	0.0000
25	26.2	25.3	43.55	127.28	0.0000	305.31	402.78	0.0000
26	26.2	26.0	45.61	133.96	0.0000	303.94	415.56	0.0000
27	26.2	26.0	47.86	142.68	0.0000	311.49	437.22	0.0000
28	26.3	26.0	50.00	152.62	0.0000	316.98	445.56	0.0000
29	26.4	26.0	52.96	161.46	0.0000	320.30	466.67	0.0000
30	26.4	26.0	57.19	129.16	0.0018	201.99	638.33	0.0000
31	26.5	26.0	61.86	105.54	0.0266	156.91	712.22	0.0000
32	26.5	26.0	66.74	91.88	0.1007	133.23	765.56	0.0000
33	26.6	26.0	70.70	81.43	0.1964	120.76	781.11	0.0422
34	26.6	26.0	74.27	73.92	0.2916	116.87	778.33	0.1267
35	26.7	27.0	77.79	70.11	0.2993	117.67	773.89	0.1267

Time (min)	$T_{ambient}$ (℃)	T_{gas} (℃)	T_{water} (℃)	CO (ppm)	SO_2 (ppm)	C_xH_y (ppm)	CO_2 (ppm)	NO_x (ppm)
36	26.7	27.0	79.90	66.83	0.3081	122.71	745.56	0.1267
37	26.8	27.0	83.98	64.02	0.3221	123.39	713.33	0.1267
38	26.8	27.0	87.39	61.18	0.2777	122.02	673.89	0.1267
39	26.9	27.0	91.22	63.31	0.2496	132.09	645.00	0.1056
40	26.9	27.0	94.11	65.21	0.2081	137.35	625.00	0.0000
41	27.0	27.2	94.89	67.07	0.1398	141.01	611.11	0.0000
42	27.1	28.3	25.75	81.58	0.0853	166.99	630.00	0.0000
43	27.0	29.0	24.57	58.96	0.0791	114.81	427.78	0.0000
44	26.9	28.8	19.20	54.33	0.0648	111.72	381.67	0.0000
45	26.9	27.5	26.28	66.84	0.0429	139.41	405.56	0.0000
46	27.0	27.0	30.50	86.48	0.0356	170.87	436.11	0.0000
47	27.1	27.0	33.91	111.76	0.0293	216.18	445.56	0.0000
48	27.2	27.3	37.63	110.50	0.0000	203.37	435.56	0.0000
49	27.3	27.0	41.40	102.30	0.0000	185.98	401.11	0.0000
50	27.4	27.0	45.16	105.91	0.0000	190.32	397.78	0.0000
51	27.4	27.0	48.82	108.20	0.0000	192.96	388.89	0.0000
52	27.5	27.0	52.41	110.31	0.0000	194.67	389.44	0.0000
53	27.6	27.0	56.01	111.35	0.0000	195.82	370.56	0.0000
54	27.6	27.0	59.24	112.30	0.0000	199.02	372.22	0.0000
55	27.6	27.0	62.71	115.48	0.0000	204.17	375.00	0.0000
56	27.7	27.0	65.93	117.52	0.0000	206.23	380.00	0.0000
57	27.7	27.0	68.91	116.17	0.0000	203.60	369.44	0.0000
58	27.8	27.0	71.83	117.91	0.0000	208.63	368.33	0.0000
59	27.8	27.0	74.61	117.60	0.0000	208.29	363.89	0.0000
60	27.9	27.0	77.43	117.61	0.0000	210.23	361.11	0.0000
61	27.9	27.0	80.09	118.39	0.0000	210.35	346.67	0.0000
62	27.9	27.0	82.58	119.13	0.0000	212.86	351.67	0.0000
63	28.0	27.0	84.75	118.94	0.0000	214.35	338.33	0.0000
64	28.0	27.0	86.96	120.52	0.0000	219.04	335.56	0.0000
65	28.1	27.0	89.09	123.47	0.0000	222.59	331.67	0.0000
66	28.1	27.0	91.08	122.43	0.0000	221.67	322.78	0.0000
67	28.1	27.0	92.75	124.08	0.0000	225.22	334.44	0.0000
68	28.2	27.0	94.22	124.75	0.0000	227.28	334.44	0.0000
69	28.2	27.0	94.98	127.18	0.0000	231.40	326.67	0.0000
70	28.2	27.0	92.54	128.16	0.0000	233.91	355.00	0.0000
71	28.3	27.0	94.36	125.74	0.0000	233.77	342.22	0.0000
72	28.3	27.0	95.02	125.58	0.0000	233.65	351.67	0.0000

Time (min)	$T_{ambient}$ (℃)	T_{gas} (℃)	T_{water} (℃)	CO (ppm)	SO_2 (ppm)	C_xH_y (ppm)	CO_2 (ppm)	NO_x (ppm)
73	28.3	27.0	95.01	123.65	0.0000	232.62	333.33	0.0000
74	28.4	27.0	95.00	126.37	0.0000	237.77	323.89	0.0000
75	28.4	27.0	95.00	122.10	0.0000	231.48	308.33	0.0000
76	28.5	27.0	95.00	120.36	0.0000	231.14	296.11	0.0000
77	28.5	27.0	95.02	119.93	0.0000	233.42	299.44	0.0000
78	28.5	27.5	95.01	119.56	0.0000	235.14	301.11	0.0000
79	28.6	27.0	95.02	118.14	0.0000	235.14	293.89	0.0000
80	28.6	27.0	95.03	118.02	0.0000	236.28	291.11	0.0000
81	28.6	27.0	95.06	115.61	0.0000	235.25	289.44	0.0000
82	28.7	27.0	95.03	114.68	0.0000	237.08	293.33	0.0000
83	28.7	27.0	95.03	112.86	0.0000	237.54	282.22	0.0000
84	28.7	27.0	95.01	112.05	0.0000	240.17	278.89	0.0000
85	28.8	27.0	95.01	109.70	0.0000	236.74	276.11	0.0000
86	28.8	27.0	95.01	108.22	0.0000	236.74	275.00	0.0000
87	28.8	27.0	95.01	105.37	0.0000	235.94	272.78	0.0000
88	28.8	27.0	95.01	103.99	0.0000	235.48	270.56	0.0000
89	28.8	27.0	95.00	103.08	0.0000	236.97	285.00	0.0000
90	28.8	27.0	95.00	101.01	0.0000	235.03	282.78	0.0000
91	28.8	27.0	95.05	99.07	0.0000	234.80	281.11	0.0000
92	28.8	27.0	95.01	96.92	0.0000	233.54	279.44	0.0000
93	28.8	27.0	95.00	94.45	0.0000	232.39	277.78	0.0000
94	28.8	27.0	95.00	92.17	0.0000	231.94	271.67	0.0000
95	28.8	27.0	95.00	91.09	0.0000	232.62	273.89	0.0000
96	28.8	27.0	95.01	88.67	0.0000	230.91	269.44	0.0000
97	28.8	27.0	95.00	87.11	0.0000	230.11	269.44	0.0000
98	28.8	27.0	95.00	84.61	0.0000	227.82	267.22	0.0000
99	28.8	27.0	95.00	82.61	0.0000	226.90	265.00	0.0000
100	28.8	27.0	95.00	81.29	0.0000	227.47	271.11	0.0000
101	28.8	27.0	95.00	79.86	0.0000	227.47	266.11	0.0000
102	28.8	27.0	95.00	77.98	0.0000	225.19	265.56	0.0000
103	28.8	27.0	95.00	75.96	0.0000	223.36	263.33	0.0000
104	28.8	27.0	95.00	73.20	0.0000	222.10	262.22	0.0000
105	28.8	27.0	95.01	72.12	0.0000	222.33	262.78	0.0000
106	28.8	27.0	95.00	69.66	0.0000	221.18	267.78	0.0000
107	28.8	27.0	95.00	67.99	0.0000	219.81	257.78	0.0000
108	28.8	27.0	95.00	65.27	0.0000	217.06	257.78	0.0000
109	28.8	27.0	94.98	63.22	0.0000	215.23	252.78	0.0000

Time (min)	$T_{ambient}$ (℃)	T_{gas} (℃)	T_{water} (℃)	CO (ppm)	SO_2 (ppm)	C_xH_y (ppm)	CO_2 (ppm)	NO_x (ppm)
110	28.8	27.0	94.98	60.82	0.0000	214.09	251.67	0.0000
111	28.8	27.0	94.90	59.70	0.0000	214.20	253.89	0.0000
112	28.8	27.0	94.91	57.49	0.0000	211.69	247.22	0.0000
113	28.8	27.0	94.86	55.91	0.0000	210.54	246.11	0.0000
114	28.8	27.0	94.76	53.54	0.0000	207.68	245.56	0.0000
114.2	28.8	27.0	94.75	51.25	0.0000	205.85	242.22	0.0000

Appendix 34: Temperature profiles and gaseous emissions during the WBT (B30)

Time (min)	$T_{ambient}$ (℃)	T_{gas} (℃)	T_{water} (℃)	CO (ppm)	SO_2 (ppm)	C_xH_y (ppm)	CO_2 (ppm)	NO_x (ppm)
0	30.2	27.0	22.4	0.00	0.0000	0.00	0.00	0.0000
1	30.3	27.0	22.4	2.53	0.0000	13.04	0.00	0.0000
2	30.4	27.0	22.4	8.04	0.0000	37.87	3.33	0.0000
3	30.4	28.0	22.4	14.41	0.0000	69.68	10.00	0.0000
4	30.5	28.8	22.4	20.28	0.0000	93.59	37.22	0.0000
5	30.6	29.3	22.4	22.85	0.0000	94.05	113.33	0.0000
6	30.6	30.0	22.4	22.19	0.0000	94.51	143.89	0.0000
7	30.6	30.0	22.8	18.93	0.0000	85.58	136.67	0.0000
8	30.6	29.0	26.4	34.13	0.0000	113.39	135.00	0.0000
9	30.7	29.0	31.6	44.94	0.0160	134.44	194.44	0.1911
10	30.7	29.0	37.4	60.42	0.1717	162.24	253.33	0.3822
11	30.8	29.0	43.8	68.86	0.3234	173.57	281.67	0.3822
12	30.7	29.0	50.3	79.51	0.4626	183.75	298.89	0.3822
13	30.7	29.0	57.1	102.62	0.6693	220.25	337.22	0.4459
14	30.8	29.0	63.4	119.39	1.0287	236.61	332.22	0.9555
15	30.8	29.0	69.9	126.73	1.2727	235.24	344.44	1.4651
16	30.9	29.8	76.0	133.30	1.4222	235.46	332.22	1.5288
17	30.9	30.0	81.6	136.67	1.6876	240.27	338.33	1.6562
18	30.9	30.0	87.0	139.21	2.0096	243.13	346.11	1.9110
19	30.9	30.0	91.7	141.86	2.2768	240.84	351.11	2.5480
20	31.0	30.0	94.4	142.08	2.5217	234.09	353.89	3.1213
21	31.0	30.0	94.7	138.88	2.6376	222.08	386.11	3.4398
22	31.1	30.0	71.3	132.20	2.6929	202.74	411.11	3.6946
23	31.1	33.3	29.7	99.39	2.6797	115.33	685.00	4.5864
24	31.2	36.3	22.4	44.14	1.8969	26.09	948.33	6.1152
25	31.2	34.3	29.7	55.18	1.4654	65.33	556.11	5.1597
26	31.2	32.5	36.8	51.68	1.4177	59.61	401.67	4.5864
27	31.2	31.2	43.0	40.49	1.2369	53.89	348.89	3.8857
28	31.2	31.0	48.8	39.55	1.0212	61.67	297.78	3.5672
29	31.3	30.3	53.0	43.96	0.8888	80.21	273.33	3.3761
30	31.4	30.0	58.2	48.56	0.6880	93.71	249.44	2.9302
31	31.4	30.0	63.0	51.73	0.6266	99.09	231.67	2.6754
32	31.3	30.0	67.7	55.41	0.5509	102.63	223.89	2.4843
33	31.3	30.7	72.2	60.23	0.4723	108.47	232.22	2.2932
34	31.4	31.0	76.4	66.28	0.4187	117.16	227.22	2.2932
35	31.4	30.0	80.4	73.66	0.3077	129.98	226.11	2.2932

Time (min)	$T_{ambient}$ (℃)	T_{gas} (℃)	T_{water} (℃)	CO (ppm)	SO_2 (ppm)	C_xH_y (ppm)	CO_2 (ppm)	NO_x (ppm)
36	31.4	30.0	84.4	78.85	0.2421	132.15	204.44	2.2932
37	31.4	30.0	88.0	83.88	0.2313	136.50	209.44	2.2932
38	31.5	30.0	91.3	90.44	0.2172	148.63	201.11	2.2932
39	31.5	30.0	93.9	97.67	0.2019	154.92	198.89	1.9110
40	31.5	30.0	94.8	104.41	0.1889	159.84	174.44	1.1466
41	31.6	30.8	81.0	113.50	0.1749	164.76	203.89	1.1466
42	31.6	30.5	94.9	109.90	0.1756	155.83	228.33	1.1466
43	31.6	30.0	95.0	106.52	0.1149	146.22	188.33	1.1466
44	31.6	30.0	95.0	109.04	0.0959	146.22	177.78	1.1466
45	31.6	30.0	95.0	110.46	0.0929	145.77	167.78	1.1466
46	31.5	30.0	95.0	113.66	0.0346	149.66	160.00	1.1466
47	31.6	30.0	95.0	115.12	0.0052	150.00	159.44	1.1466
48	31.7	30.0	95.0	118.15	0.0007	155.49	157.22	1.1466
49	31.8	30.0	95.0	120.21	0.0006	157.09	159.44	1.1466
50	31.8	30.0	95.0	120.98	0.0002	157.55	158.33	1.1466
51	31.7	30.0	95.0	122.39	0.0012	157.32	155.00	1.1466
52	31.8	30.0	95.0	121.52	0.0015	155.72	152.22	1.1466
53	31.8	30.0	95.0	122.16	0.0008	157.09	157.78	1.1466
54	31.8	30.0	95.0	122.44	0.0014	157.67	165.00	1.1466
55	31.8	30.0	95.0	122.65	0.0012	157.32	157.78	1.1466
56	31.8	30.0	95.0	122.51	0.0016	157.44	148.89	1.1466
57	31.8	30.0	95.0	122.89	0.0011	158.92	145.00	1.1466
58	31.9	30.0	95.0	123.81	0.0006	160.18	141.11	1.1466
59	31.9	30.0	95.0	125.69	0.0007	162.47	141.67	1.1466
60	31.8	30.0	95.0	126.06	0.0009	162.59	135.56	1.1466
61	31.8	30.0	95.0	128.36	0.0000	166.13	131.11	1.1466
62	31.8	30.0	95.0	128.41	0.0006	166.70	131.67	1.1466
63	31.8	30.0	95.0	130.58	0.0000	168.08	126.11	1.1466
64	31.8	30.0	95.0	131.44	0.0000	169.68	123.89	1.1466
65	31.8	30.0	95.0	132.97	0.0000	171.85	125.00	1.1466
66	31.9	30.0	95.0	134.34	0.0000	175.06	122.78	1.1466
67	31.9	30.0	95.0	135.35	0.0000	176.20	123.33	1.1466
68	31.9	30.0	95.0	135.29	0.0000	175.74	127.78	1.1466
69	31.9	30.0	95.0	136.63	0.0000	177.35	122.78	1.1466
70	31.9	30.0	95.0	134.96	0.0000	175.29	121.11	1.0829
71	32.0	30.0	95.0	134.79	0.0000	175.40	128.89	0.7644
72	32.0	30.0	95.0	131.24	0.0000	171.05	117.78	0.7007

Time (min)	$T_{ambient}$ (℃)	T_{gas} (℃)	T_{water} (℃)	CO (ppm)	SO_2 (ppm)	C_xH_y (ppm)	CO_2 (ppm)	NO_x (ppm)
73	32.0	30.0	95.0	130.62	0.0000	169.68	117.22	0.3822
74	32.0	29.2	95.0	130.36	0.0000	168.54	115.56	0.3822
75	32.0	29.0	95.0	127.71	0.0000	165.68	111.67	0.3822
76	32.0	29.0	94.9	125.35	0.0000	161.79	110.00	0.3822
77	32.0	29.0	94.9	123.91	0.0000	161.21	106.11	0.3822
78	32.0	30.0	94.9	123.23	0.0000	159.73	107.22	0.3822
79	32.1	30.0	94.9	121.44	0.0000	157.41	107.22	0.3822
80	32.0	29.8	94.9	119.51	0.0000	155.23	115.56	0.3822
81	32.1	29.0	94.9	117.35	0.0002	153.17	115.00	0.3822
82	32.0	29.0	94.9	116.08	0.0001	151.79	110.00	0.3822
83	32.1	29.0	94.9	114.96	0.0006	150.42	106.11	0.3822
84	32.1	29.0	94.9	112.39	0.0024	148.36	108.33	0.3822
84.5	32.2	29.0	94.9	110.61	0.0021	148.13	118.33	0.3822

Appendix 35: Temperature profiles and gaseous emissions during the WBT (B35)

Time (min)	$T_{ambient}$ (°C)	T_{gas} (°C)	T_{water} (°C)	CO (ppm)	SO_2 (ppm)	C_xH_y (ppm)	CO_2 (ppm)	NO_x (ppm)
0	26.9	25.0	20.3	0.00	0.0000	0.00	0.00	0.0000
1	26.9	25.8	20.3	0.81	0.0000	12.67	206.11	0.0000
2	27.1	26.0	20.3	5.49	0.0000	45.85	296.67	0.0000
3	27.1	27.0	20.3	10.92	0.0000	68.28	417.22	0.0000
4	27.2	28.3	20.3	10.20	0.0000	52.72	581.11	0.0000
5	27.3	30.5	20.3	6.98	0.0000	30.75	798.33	0.0000
6	27.3	33.2	20.3	7.02	0.0000	25.60	1022.22	0.0000
7	27.4	34.0	20.8	13.41	0.0000	45.28	1132.22	0.0000
8	27.4	31.3	24.8	38.11	0.0163	130.64	975.56	0.0000
9	27.5	30.2	31.1	60.37	0.2650	163.23	931.11	0.0000
10	27.6	29.0	37.4	74.70	0.3960	179.01	943.89	0.0000
11	27.7	29.0	43.6	82.00	0.4664	183.59	955.56	0.0000
12	27.8	29.0	50.2	89.38	0.6553	189.31	956.11	0.0000
13	27.8	29.0	56.6	98.46	0.8542	200.06	962.78	0.0000
14	27.9	29.0	62.9	105.29	1.0719	208.19	977.78	0.0000
15	27.9	28.0	69.0	111.87	1.2216	209.33	988.89	0.0000
16	27.9	28.0	74.6	116.05	1.2264	213.11	991.11	0.0000
17	28.0	28.0	79.8	122.83	1.4982	222.95	1017.78	0.0000
18	28.0	28.0	85.5	128.97	1.7446	233.24	1031.67	0.0000
19	28.1	28.0	90.6	130.31	1.9324	235.99	1060.56	0.0634
20	28.2	28.2	93.9	131.07	2.1082	234.50	1066.67	0.3801
21	28.3	29.0	94.7	130.15	2.3147	226.15	1095.00	0.3801
22	28.3	29.2	79.9	123.07	2.4389	208.99	1121.67	0.6986
23	28.3	33.0	35.0	89.05	2.3056	114.71	1526.67	1.7805
24	28.4	34.5	20.3	59.13	1.8108	63.22	1642.78	2.4164
25	28.5	31.5	29.6	65.82	1.5911	97.17	1354.44	1.8431
26	28.5	30.3	37.8	52.19	1.6067	70.40	1217.22	1.5246
27	28.6	29.2	43.9	46.80	1.5909	65.72	1145.56	1.0171
28	28.6	29.0	49.1	37.91	1.2962	53.93	1091.11	0.7623
29	28.7	28.2	53.3	32.95	1.0884	51.87	1058.33	0.6986
30	28.7	28.0	58.6	33.18	1.0198	65.84	1001.11	0.3801
31	28.8	28.0	63.3	37.62	0.8604	79.10	990.00	0.3801
32	28.8	28.0	68.0	42.43	0.7273	90.98	981.11	0.3801
33	28.8	28.0	72.5	46.72	0.7184	98.76	972.22	0.1267
34	28.8	28.0	76.6	52.27	0.6384	108.38	963.33	0.0000
35	28.9	28.0	80.8	57.22	0.5459	115.70	963.89	0.0000

Time (min)	$T_{ambient}$ (℃)	T_{gas} (℃)	T_{water} (℃)	CO (ppm)	SO_2 (ppm)	C_xH_y (ppm)	CO_2 (ppm)	NO_x (ppm)
36	29.0	28.0	84.7	63.45	0.5192	127.71	973.33	0.0000
37	29.0	28.0	88.7	72.20	0.5006	144.07	964.44	0.0000
38	29.0	27.8	92.0	79.70	0.4301	157.92	958.33	0.0000
39	29.1	27.0	85.2	85.64	0.3902	163.75	958.33	0.0000
40	29.1	28.3	53.2	99.94	0.3604	184.81	1016.67	0.0000
41	29.1	28.0	93.8	92.50	0.3755	168.67	981.11	0.0000
42	29.2	28.0	95.0	93.38	0.3736	167.76	969.44	0.0000
43	29.2	28.0	95.1	94.75	0.3162	167.30	951.67	0.0000
44	29.2	28.0	95.1	96.63	0.2851	168.67	943.33	0.0000
45	29.2	28.0	95.1	101.64	0.2743	177.94	945.56	0.0000
46	29.2	28.0	95.1	101.35	0.2746	176.00	931.11	0.0000
47	29.3	27.2	95.1	100.02	0.2095	173.37	918.33	0.0000
48	29.4	27.5	95.1	100.40	0.1951	173.02	910.00	0.0000
49	29.4	28.0	95.1	100.44	0.1947	174.40	903.33	0.0000
50	29.4	28.0	95.1	100.27	0.1951	175.20	901.67	0.0000
51	29.4	28.0	95.1	100.43	0.1951	177.60	897.22	0.0000
52	29.4	28.0	95.1	103.79	0.1881	185.15	904.44	0.0000
53	29.5	28.0	95.1	104.50	0.1872	187.10	898.89	0.0000
54	29.5	28.0	95.1	104.90	0.1873	188.13	908.89	0.0000
55	29.5	28.0	95.1	106.24	0.1858	191.21	892.22	0.0000
56	29.5	28.0	95.1	106.64	0.1856	193.85	918.89	0.0000
57	29.5	28.0	95.1	107.43	0.1843	196.36	906.67	0.0000
58	29.6	28.0	95.1	107.72	0.1838	198.08	901.11	0.0000
59	29.6	28.0	95.1	107.82	0.1817	200.25	906.67	0.0000
60	29.6	28.0	95.0	108.13	0.1812	202.89	905.00	0.0000
61	29.6	28.0	95.1	108.75	0.1803	205.06	894.44	0.0000
62	29.7	28.0	95.1	110.42	0.1783	208.72	874.44	0.0000
63	29.7	28.0	95.1	112.01	0.1764	211.70	877.78	0.0000
64	29.7	28.0	95.1	112.69	0.1761	213.98	878.89	0.0000
65	29.7	28.0	95.1	113.99	0.1193	216.84	870.56	0.0000
66	29.7	28.0	95.1	115.25	0.0894	221.19	868.89	0.0000
67	29.7	28.0	95.1	116.84	0.0851	224.74	881.11	0.0000
68	29.7	28.0	95.1	117.89	0.0827	227.94	874.44	0.0000
69	29.7	28.0	95.1	117.93	0.0809	228.40	871.11	0.0000
70	29.8	28.0	95.1	117.76	0.0803	230.00	867.22	0.0000
71	29.8	28.0	95.1	116.93	0.0803	230.35	860.56	0.0000
72	29.9	28.0	95.1	115.52	0.0828	230.09	871.67	0.0000

Time (min)	$T_{ambient}$ (℃)	T_{gas} (℃)	T_{water} (℃)	CO (ppm)	SO_2 (ppm)	C_xH_y (ppm)	CO_2 (ppm)	NO_x (ppm)
73	29.8	28.0	95.1	114.20	0.0846	228.71	871.67	0.0000
74	29.8	28.0	95.1	112.88	0.0859	226.99	867.78	0.0000
75	29.8	28.0	95.1	112.05	0.0874	227.79	868.33	0.0000
76	29.9	28.0	95.1	110.36	0.0893	226.31	866.67	0.0000
77	29.9	28.0	95.1	108.53	0.0921	225.16	870.00	0.0000
78	29.9	28.0	95.1	107.07	0.0942	223.90	868.89	0.0000
79	30.0	28.0	95.1	106.06	0.0947	223.68	872.22	0.0000
80	30.0	28.0	95.1	103.17	0.0990	221.73	872.78	0.0000
81	30.0	28.0	95.1	102.29	0.0999	222.74	874.44	0.0000
82	30.0	28.0	95.1	100.74	0.1029	221.58	875.56	0.0000
83	30.0	28.0	95.1	99.13	0.1041	220.67	872.78	0.0000
84	30.0	28.0	95.1	97.62	0.1069	219.87	880.00	0.0000
84.5	30.0	28.0	95.1	97.20	0.1079	220.89	885.56	0.0000

Appendix 36: Temperature profiles and gaseous emissions during the WBT (B40)

Time (min)	$T_{ambient}$ (°C)	T_{gas} (°C)	T_{water} (°C)	CO (ppm)	SO_2 (ppm)	C_xH_y (ppm)	CO_2 (ppm)	NO_x (ppm)
0	26.1	23.7	20.5	0.00	0.0000	0.00	0.00	0.0000
1	26.1	23.9	13.8	0.87	0.0000	3.32	133.33	0.0000
2	26.2	24.4	20.5	4.40	0.0000	23.00	196.67	0.1275
3	26.3	25.0	20.5	9.92	0.0000	50.69	260.00	0.0425
4	26.4	26.9	20.5	15.98	0.0000	65.22	493.89	0.0000
5	26.4	29.7	20.6	15.12	0.0000	46.91	823.33	0.0000
6	26.5	33.3	20.6	18.84	0.0000	36.96	1205.00	0.0212
7	26.5	35.2	22.5	52.02	0.0658	112.02	1523.89	0.1274
8	26.6	31.3	28.4	120.65	0.6716	295.90	866.67	0.1699
9	26.6	29.0	35.2	148.02	1.4458	310.77	736.67	0.2548
10	26.6	28.0	42.4	154.80	1.8266	289.37	748.89	0.2548
11	26.7	27.6	49.5	154.30	2.1006	266.83	750.56	0.4884
12	26.7	27.6	58.6	151.98	2.2692	250.93	772.78	0.5096
13	26.8	27.3	65.1	156.89	2.3818	246.46	773.33	0.5096
14	26.8	27.3	71.5	159.34	2.4446	244.63	784.44	0.5521
15	26.9	27.3	77.3	165.00	2.5282	255.85	797.78	0.6370
16	26.9	27.7	83.0	166.39	2.6889	252.99	829.44	0.7007
17	26.9	28.9	88.3	178.04	2.8556	233.19	1104.44	0.8918
18	27.0	28.4	80.7	169.14	3.0507	251.96	870.00	0.8918
19	27.0	28.2	73.6	154.36	3.1773	231.25	813.33	0.8918
20	27.1	29.1	67.7	124.34	3.0366	160.76	942.22	0.9555
21	27.1	30.8	53.0	98.19	2.7506	108.13	1122.78	1.0617
22	27.2	30.4	50.9	93.28	2.5168	109.16	1060.56	1.3589
23	27.2	29.8	36.9	89.42	2.4558	104.35	990.00	1.3377
24	27.3	30.3	39.7	54.73	2.0933	36.62	1066.67	1.4014
25	27.3	29.2	43.9	44.60	1.7197	26.66	837.22	1.1891
26	27.3	28.2	48.5	36.40	1.4093	21.51	735.56	0.9980
27	27.4	27.5	54.2	36.25	1.2056	42.91	686.11	0.7644
28	27.4	27.3	59.4	38.19	1.1193	55.61	654.44	0.5945
29	27.5	27.3	64.0	40.48	0.8555	64.08	626.67	0.5096
30	27.5	27.3	69.1	45.64	0.7898	76.55	625.56	0.5096
31	27.5	27.0	73.3	51.14	0.6692	89.71	598.89	0.5096
32	27.6	27.0	77.3	58.46	0.5310	104.12	592.78	0.5096
33	27.6	27.0	81.3	66.02	0.4737	116.37	587.22	0.4247
34	27.6	26.9	81.1	72.76	0.4182	127.01	579.44	0.3822
35	27.7	26.7	68.6	78.07	0.4072	132.39	571.67	0.2973

Time (min)	$T_{ambient}$ (℃)	T_{gas} (℃)	T_{water} (℃)	CO (ppm)	SO_2 (ppm)	C_xH_y (ppm)	CO_2 (ppm)	NO_x (ppm)
36	27.7	26.6	88.7	87.01	0.3882	144.17	591.11	0.2548
37	27.7	26.7	87.9	82.40	0.3987	135.02	568.33	0.1274
38	27.8	27.3	73.3	98.27	0.3656	159.14	605.56	0.1274
39	27.8	27.4	93.2	99.87	0.3614	154.89	608.33	0.1274
40	27.8	27.3	85.9	97.80	0.3652	149.40	578.89	0.1274
41	27.9	27.7	86.0	107.32	0.3177	160.15	602.78	0.1274
42	27.9	27.4	94.1	98.19	0.2659	143.45	565.56	0.1274
43	27.9	27.0	95.1	100.96	0.1797	145.62	569.44	0.1274
44	27.9	27.0	95.0	102.88	0.1786	146.42	556.67	0.1274
45	28.0	27.0	95.0	103.80	0.1782	147.34	548.33	0.1274
46	28.0	27.0	95.0	104.63	0.1766	147.34	536.11	0.1274
47	28.0	27.0	95.0	105.85	0.1735	147.80	544.44	0.1274
48	28.0	27.0	95.0	106.08	0.1732	147.80	542.78	0.0849
49	28.1	27.0	95.0	106.31	0.1731	148.83	527.78	0.0000
50	28.1	27.0	95.0	107.09	0.1735	151.23	528.33	0.0000
51	28.1	27.0	95.0	108.42	0.1188	151.69	528.89	0.0000
52	28.1	26.9	95.0	104.12	0.0903	145.85	521.67	0.0000
53	28.2	26.7	95.0	109.84	0.0202	155.46	506.11	0.0000
54	28.2	26.7	95.0	109.81	0.0068	156.15	507.78	0.0000
55	28.2	26.7	95.0	111.31	0.0062	157.29	507.78	0.0000
56	28.2	26.7	95.0	111.84	0.0050	158.09	505.56	0.0000
57	28.3	26.7	95.0	112.02	0.0057	158.67	498.89	0.0000
58	28.3	26.6	95.0	112.88	0.0054	161.30	492.78	0.0000
59	28.3	26.3	95.0	113.74	0.0033	162.90	480.56	0.0000
60	28.3	26.3	95.0	114.45	0.0035	163.81	472.78	0.0000
61	28.4	26.3	95.0	114.37	0.0039	163.81	470.00	0.0000
62	28.4	26.3	95.0	114.25	0.0049	163.47	471.67	0.0000
63	28.4	26.1	95.0	114.49	0.0058	163.36	477.22	0.0000
64	28.4	26.0	95.0	114.55	0.0049	163.13	468.89	0.0000
65	28.4	26.0	95.0	115.94	0.0044	165.53	468.33	0.0000
66	28.4	26.0	94.9	116.70	0.0032	166.79	470.00	0.0000
67	28.4	26.0	94.9	116.98	0.0027	167.46	484.44	0.0000
68	28.5	26.0	94.9	116.18	0.0030	166.75	471.11	0.0000
69	28.5	26.0	94.9	116.78	0.0023	169.50	472.22	0.0000
70	28.5	26.0	94.9	119.12	0.0006	171.44	467.78	0.0000
71	28.5	26.0	94.9	118.77	0.0004	169.95	456.11	0.0000
72	28.5	26.0	94.9	117.31	0.0016	167.89	463.89	0.0000

Time (min)	$T_{ambient}$ (℃)	T_{gas} (℃)	T_{water} (℃)	CO (ppm)	SO_2 (ppm)	C_xH_y (ppm)	CO_2 (ppm)	NO_x (ppm)
73	28.6	26.0	94.9	116.40	0.0016	167.55	461.67	0.0000
74	28.6	26.0	94.9	115.34	0.0023	167.09	462.22	0.0000
75	28.6	26.1	94.9	113.92	0.0037	163.55	472.22	0.0000
76	28.6	26.3	94.9	113.22	0.0022	162.40	463.89	0.0000
77	28.7	26.4	94.9	111.97	0.0021	162.63	458.33	0.0000
78	28.7	26.7	94.9	110.15	0.0032	160.91	464.44	0.0000
79	28.7	26.7	94.9	109.01	0.0038	159.54	468.33	0.0000
80	28.7	26.7	94.9	107.97	0.0053	158.28	465.56	0.0000
81	28.7	26.7	94.9	105.89	0.0053	155.77	464.44	0.0000
82	28.8	26.7	94.9	104.73	0.0053	154.39	464.44	0.0000
83	28.8	26.7	94.9	103.72	0.0053	153.94	472.78	0.0000
84	28.8	26.7	94.9	102.62	0.0053	151.99	474.44	0.0000
84.5	28.8	26.7	94.9	102.51	0.0053	151.86	479.26	0.0000

Appendix 37: Water Boiling Test performance metrics

Basic Operation	units	B25	B30	B35	B40
COLD START HIGH POWER PHASE					
Time to boil	min	41.9	21.9	21.7	20.3
Burning rate	g/min	3.7	5.7	6.6	8.2
Thermal efficiency	%	22.52	28.50	30.86	21.79
Specific fuel consumption	g/L	65.4	53.2	60.5	70.1
Temp-corrected specific consumption	g/L	66.7	54.4	60.6	70.7
Firepower	W	1775.0	2900.1	3305.8	4123.2
Equivalent Dry Fuel Consumed	g	156.6	125.5	142.9	165.8
HOT START HIGH POWER PHASE					
Time to boil	min	25.2	15.8	17.0	14.7
Burning rate	g/min	2.1	3.6	3.8	4.2
Thermal efficiency	%	54.61	49.63	44.62	47.72
Specific fuel consumption	g/L	21.7	23.3	26.1	24.5
Temp-corrected specific consumption	g/L	22.1	23.8	26.2	24.7
Firepower	W	1011.5	1833.2	1908.8	2091.8
Equivalent Dry Fuel Consumed	g	53.6	57.2	64.5	60.5
SIMMER PHASE					
Burning rate	g/min	1.1	1.7	1.7	1.7
Thermal efficiency	%	39.14	47.96	50.34	46.87
Specific fuel consumption 45 min	g/L	22.8	39.4	39.3	39.3
Firepower	W	535.9	870.1	857.3	867.8
Turn down ratio		2.6	2.7	3.0	3.6
Equivalent Dry Fuel Consumed	g	50.8	77.3	76.9	77.8
Energy Consumption					
Net Calorific Value (dry)	kJ/kg	28500.0	30400.0	30100.0	30100.0
Moisture Content	%	4.68	4.24	3.94	3.59
COLD START HIGH POWER PHASE					
Temp-Corrected Time to Boil	min	42.8	22.4	21.7	20.4
Energy Consumption Rate	kJ/min	106.5	174.0	198.3	247.4
Temp-Corrected Specific Energy Consumption	kJ/L	1901.8	1655.0	1825.2	2128.1
Specific Energy Consumption Rate	MJ/min/L	0.0	0.1	0.1	0.1
Dry Fuel Consumed	g	157.3	125.9	143.4	166.3

Basic Operation	units	B25	B30	B35	B40
Total Energy Consumed	kJ	4482.4	3828.1	4317.8	5005.8
	units	B25	B30	B35	B40
Energy Delivered to the Cooking Pot	MJ	1.0	1.1	1.3	1.1
Average Cooking Power	kW	0.4	0.8	1.0	0.9
HOT START HIGH POWER PHASE					
Temp-Corrected Time to Boil	min	25.7	16.2	17.1	14.8
Energy Consumption Rate	kJ/min	60.7	110.0	114.5	125.5
Temp-Corrected Specific Energy Consumption	kJ/L	628.4	723.8	787.6	744.2
Specific Energy Consumption Rate	MJ/min/L	0.0	0.0	0.0	0.1
Dry Fuel Consumed	g	53.9	57.5	64.7	60.7
Total Energy Consumed	kJ	1534.9	1746.7	1946.9	1828.2
Energy Delivered to the Cooking Pot	MJ	0.8	0.9	0.9	0.9
Average Cooking Power	kW	0.5	0.9	0.9	1.0
SIMMER PHASE					
Energy Consumption Rate	kJ/min	32.2	52.2	51.4	52.1
Time-Corrected Specific Energy Consumption	kJ/L	650.9	1198.6	1182.7	1183.8
Specific Energy Consumption Rate	MJ/min/L	0.0	0.0	0.0	0.0
Dry Fuel Consumed	g	51.0	77.6	77.2	78.1
Total Energy Consumed	kJ	1453.4	2358.0	2322.8	2350.6
Energy Delivered to the Cooking Pot	MJ	0.6	1.1	1.2	1.1
Average Cooking Power	kW	0.2	0.4	0.4	0.4
Total Emissions					
COLD START HIGH POWER PHASE					
CO	g	28.9	21.4	21.0	28.0
CO_2	g	114.6	104.2	129.1	172.4
$PM_{2.5}$	mg	14.3	10.5	17.1	25.5
HOT START HIGH POWER PHASE					
CO	g	28.9	11.6	11.4	9.3
CO_2	g	108.2	92.4	110.1	101.0
$PM_{2.5}$	mg	0.5	0.8	1.4	1.9
SIMMER PHASE					
CO	g	44.5	58.0	49.0	49.2
CO_2	g	123.5	136.3	166.4	173.2

Basic Operation	units	B25	B30	B35	B40
$PM_{2.5}$	mg	0.3	0.4	0.3	0.8
Emissions per MJ Delivered to the Cooking Pot					
COLD START HIGH POWER PHASE					
	units	B25	B30	B35	B40
CO	g/MJ	28.8	19.7	16.8	25.7
CO_2	g/MJ	115.8	95.5	99.7	160.4
$PM_{2.5}$	mg/MJ	14.2	9.6	14.1	23.6
HOT START HIGH POWER PHASE					
CO	g/MJ	34.7	13.4	13.4	10.7
CO_2	g/MJ	129.3	107.0	129.5	116.2
$PM_{2.5}$	mg/MJ	0.7	0.9	1.7	2.2
SIMMER PHASE					
CO	g/MJ	78.6	51.5	42.4	44.8
CO_2	g/MJ	218.4	121.2	141.4	157.7
$PM_{2.5}$	mg/MJ	0.6	0.4	0.3	0.7
Specific Emissions					
COLD START HIGH POWER PHASE					
CO	g/L	12.0	9.1	8.9	11.8
CO_2	g/L	47.7	44.3	54.7	72.8
$PM_{2.5}$	$\mu g/m^3$	19904.9	28337.9	47265.8	76692.9
Log ($PM_{2.5}$)	$\mu g/m^3$	4.3	4.4	4.7	4.9
HOT START HIGH POWER PHASE					
CO	g/L	11.7	4.7	4.6	3.8
CO_2	g/L	43.7	37.5	44.5	40.9
$PM_{2.5}$	$\mu g/m^3$	1288.3	3050.1	5071.4	7857.4
Log ($PM_{2.5}$)	$\mu g/m^3$	3.1	3.5	3.7	3.9
SIMMER PHASE					
CO	g/L	20.0	29.6	25.1	24.8
CO_2	g/L	55.6	69.5	85.4	87.6
$PM_{2.5}$	$\mu g/m^3$	422.1	570.6	404.8	1034.9
Log ($PM_{2.5}$)	$\mu g/m^3$	2.6	2.8	2.6	3.0
Specific Emissions Rate					
COLD START HIGH POWER PHASE					
CO	g/min/L	0.287	0.415	0.409	0.584
CO_2	g/min/L	1.145	2.021	2.518	3.639

Basic Operation	units	B25	B30	B35	B40
$PM_{2.5}$	mg/min/ L	0.143	0.202	0.334	0.530
HOT START HIGH POWER PHASE					
CO	g/min/L	0.464	0.298	0.269	0.257
CO_2	g/min/L	1.736	2.372	2.577	2.810
	units	B25	B30	B35	B40
$PM_{2.5}$	mg/min/ L	0.009	0.021	0.034	0.055
SIMMER PHASE					
CO	g/min/L	0.445	0.658	0.557	0.552
CO_2	g/min/L	1.235	1.545	1.897	1.946
$PM_{2.5}$	mg/min/ L	0.003	0.005	0.003	0.009
Emissions Rate					
COLD START HIGH POWER PHASE					
CO	g/min	0.7	1.0	1.0	1.4
CO_2	g/min	2.8	4.8	5.9	8.6
$PM_{2.5}$	mg/min	0.34	0.48	0.79	1.26
HOT START HIGH POWER PHASE					
CO	g/min	1.1	0.7	0.7	0.6
CO_2	g/min	4.3	5.8	6.4	6.9
$PM_{2.5}$	mg/min	0.02	0.05	0.09	0.14
SIMMER PHASE					
CO	g/min	1.0	1.3	1.1	1.1
CO_2	g/min	2.7	3.0	3.7	3.8
$PM_{2.5}$	mg/min	0.01	0.010	0.01	0.02
Emission per kg Fuel					
COLD START HIGH POWER PHASE					
g CO/kg dry fuel consumed	g/kg	183.5	170.6	146.4	167.9
g CO_2/kg dry fuel consumed	g/kg	730.9	833.0	903.7	1038.8
g $PM_{2.5}$/kg dry fuel consumed	g/kg	0.09	0.083	0.1	0.154
HOT START HIGH POWER PHASE					
g CO/kg dry fuel consumed	g/kg	538.2	202.0	175.3	152.9
g CO_2/kg dry fuel consumed	g/kg	1999.6	1607.0	1675.0	1663.9
g $PM_{2.5}$/kg dry fuel consumed	g/kg	0.010	0.014	0.022	0.031
SIMMER PHASE					
g CO/kg dry fuel consumed	g/kg	872.1	748.3	636.5	629.9

Basic Operation	units	B25	B30	B35	B40
g CO_2/kg dry fuel consumed	g/kg	2417.3	1756.7	2170.1	2214.8
g $PM_{2.5}$/kg dry fuel consumed	g/kg	0.006	0.006	0.004	0.010

Appendix 38: Images of the filter paper for briquettes B25, B30, B35, B40; (a) CSHP phase (b) HSHP phase, (c) Simmer phase

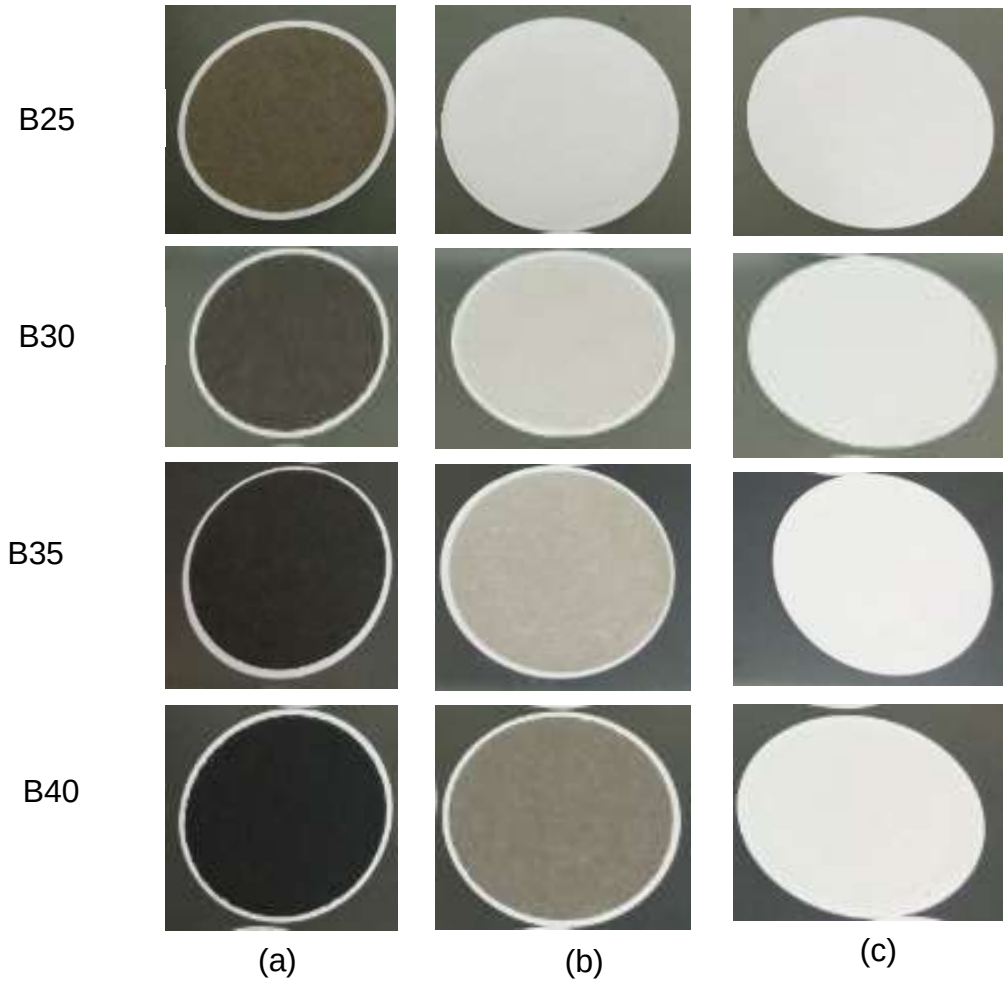

RESEARCH OUTPUTS

(i) Publication

Kivumbi, B., Jande, Y. A. C., Kirabira, J. B., & Kivevele, T. T. (2021a). Production of carbonized briquettes from charcoal fines using African Elemi (Canarium *schweinfurthii*) resin as an organic binder. *Energy Sources, Part A: Recovery, Utilization, and Environmental Effects*, 2021, 1–17. https://doi.org/10.1080/15567036.2021.1977870

Kivumbi, B., Jande, Y. A. C., Kirabira, J. B., & Kivevele, T. T. (2021b). Water Boiling Test of carbonized briquettes produced from charcoal fines using African Elemi (Canarium schweinfurthii) resin as an organic binder. *Biomass Conversion and Biorefinery*, 202, 1-16. https://doi.org/10.1007/s13399-021-02000-z

(ii) Poster Presentation